Modifying TiO2 Nanoparticles by Atomic Layer Deposition for Enhanced Photocatalytic Water Purification

Benz, D.

DOI
10.4233/uuid:b463325f-e22c-48e5-b665-ab487e7eff77

Publication date
2020

Document Version
Final published version

Citation (APA)
Benz, D. (2020). *Modifying TiO2 Nanoparticles by Atomic Layer Deposition for Enhanced Photocatalytic Water Purification*. [Dissertation (TU Delft), Delft University of Technology].
https://doi.org/10.4233/uuid:b463325f-e22c-48e5-b665-ab487e7eff77

Important note
To cite this publication, please use the final published version (if applicable).
Please check the document version above.

Modifying TiO_2 Nanoparticles by Atomic Layer Deposition for Enhanced Photocatalytic Water Purification

Dissertation

for the purpose of obtaining the degree of doctor
at Delft University of Technology
by the authority of the Rector Magnificus, prof. dr. ir. T.H.J.J. van der Hagen
Chair of the Board of Doctorates

To be defended publicly on
4th September, 2020 at 12:30

By

Dominik BENZ
Master of Science in Molecular Science,
Friedrich-Alexander University of Erlangen-Nuremberg, Germany
Born in Roth, Germany

This dissertation has been approved by the promotors.

Composition of the doctoral committee:

Rector Magnificus,	chairperson
Prof. Dr. ir. J. R. van Ommen	Delft University of Technology, promotor
Prof. Dr. ir. M. T. Kreutzer	Delft University of Technology, promotor
Dr. H. T. J. M. Hintzen	Delft University of Technology, copromotor

Independent members:

Prof. Dr. ir. L. C. Rietveld	Delft University of Technology
Prof. Dr. B. Dam	Delft University of Technology
Prof. Dr. ir. S. Verbruggen	University of Antwerp
Prof. Dr. J. Bachmann	Friedrich-Alexander University of Erlangen-Nuremberg

TU Delft | Global Initiative

Science for the benefit of people. All people. Worldwide.

This research was supported by the TU Delft | Global Initiative, a program of the Delft University of Technology to boost Science and Technology for Global Development.

Keywords: photocatalysis, water cleaning, TiO_2, nanoparticles, atomic layer deposition

Printed by: Ipskamp Printing

Cover: Dominik Benz/ Chéron Huskens

ISBN 978-94-028-2143-7

An electronic version of this dissertation is available at
https://repository.tudelft.nl/

TABLE OF CONTENTS

1 Introduction

1

1.1. THE WATER PROBLEM IN DEVELOPING COUNTRIES

Water – the most abundant resource on earth yet freshwater is so scarce. Billions of people are condemned to only have access to polluted water sources, which causes diseases and death. [1] Many scientists and politicians predict that future wars will not be fought over land or oil but over clean water, which indicates the high importance of this topic. [2-3] Clean drinking water is one of the significant challenges humankind is facing nowadays all around the world and is therefore legitimately represented as one of the UN sustainable development goals (SDG 6: Clean Drinking water and sanitation). The specific target 6.1 describes the aim to provide universal and equitable access to safe and affordable drinking water for all by 2030. [1]

Figure 1.1: Pollution in the River Sông Nhuệ in Hanoi, Vietnam; photo taken during a research stay in Vietnam (Sept. 2019).

Especially the situation in developing countries is alarming where access to clean drinking water is a luxury, and water bodies are often used as an easy cheap solution for waste discharge resulting in massive contamination of both solids and dissolved contaminants. However, conventional water treatment technologies require complex infrastructure and significant financial investments. Especially in more remote areas, this is not feasible, and other solutions might be better suitable for the needs. Ideally, in those cases, a treatment technology can be operated with little reliance on the power grid and is reliable in remote areas. That means that maintenance should be limited and easily manageable.

Conventional water treatment technologies rely on multistep treatments where sieving, filtration, and bacterial treatment for very polluted sources is applied to ensure high-quality drinking water. Those conventional steps to clean water are cost and equipment intensive technologies. Especially adsorption technology to filter micropollutants from

the water only binds the pollutants on the active surface to separate it from the water, which makes refurbishing of the filters needed after they reached their maximum capacity. A cheaper technology, which does not separate but degrades the pollutants from the water into non-toxic compounds, would be therefore preferred.

1.2. HETEROGENEOUS PHOTOCATALYSIS FOR WATER TREATMENT

As an alternative approach to conventional water treatment, photocatalysis has developed over the last decades as a promising technology that uses the light, e.g., sunlight or artificial light sources, to generate active species which are able to degrade the organic pollutants in the water. [4-6]

1.2.1. Fundamentals

In heterogeneous photocatalysis, a solid material serves as a catalytic surface to transform chemicals into degradation products. Different from conventional thermal catalysis, the material is activated by light, which provides the energy to convert chemicals into other compounds. [7] For water treatment, organic molecules are degraded via redox reactions ideally to CO_2 and H_2O, leaving little trace behind in the water. Photocatalytic materials are usually semiconductors having a bandgap that separates the valence band (VB), which in the ground state is filled with electrons, and the empty conduction band (CB).

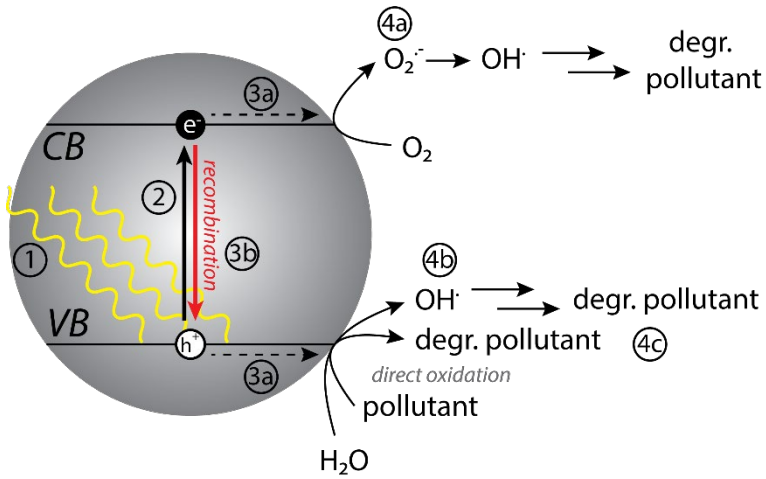

Figure 1.2: Scheme of the photocatalytic mechanisms to degrade organic pollutants in water. [8]

In particular, as illustrated in Figure 1.2, upon light excitation (1), an electron (e^-) is transferred from the VB to the CB (2), gaining the energy of the absorbed photon. After excitation, the generated electrons and holes (h^+) will transfer to the surface (3a) or

suffer undesired charge recombination losing the potential to facilitate relevant redox reactions. Possible charge recombination (3b) can be minimized by electron-hole pair separation (e.g., by combing with a second material). If the band level of the CB is higher than the reduction potential of O_2 the high energy electron in the CB is able to reduce dissolved oxygen in the water (4a) to a superoxide radical (O_2^{*-}) which subsequently reacts to a hydroxyl radical (OH^*) degrading the organic pollutant. On the other hand, upon excitation of an electron, a hole resides in the VB. This hole can contribute in two ways to pollutant degradation: firstly, the hole can react with water to form OH^* radicals, which subsequently degrade the organic pollutant (4b) or, secondly, with the pollutant, oxidizing it directly resulting in the degradation of the molecule (4c). This gives three different pathways to degrade organic pollutants: 1) via OH^* radicals formed from superoxide O_2^{*-} radicals by excited electrons in the CB pathway, 2) via OH^* radicals generated by the hole, and 3) direct oxidation of the pollutant by the hole both in the VB pathway. Often the generation of radicals from electrons or holes is summarized as the generation of reactive oxygen species (ROS).

1.2.2. Parameters influencing the photocatalytic activity

Despite the enormous potential of using sunlight to degrade organic pollutants, the development of photocatalysis has not reached a state yet to implement this technology on an industrial scale. After decades of research, photocatalysis is still facing challenges caused by low efficiencies in catalyst materials. [9] [6]

Table 1.1: Influence of a) process parameters and b) material properties on the photocatalytic activity, "positive" indicates with increase of the parameter/property the activity increases, "negative" " indicates with increase of the parameter/property the activity decreases, "optimal" indicates this parameter has an optimal value for the highest photocatalytic activity.

a) Process parameters	Influence on activity
Temperature	Negligible [4, 10]
Dissolved Oxygen	Positive [11-12]
Catalyst concentration	Optimal [13-14]
Mixing	Positive [13]
Pollutant concentration	Negative [15]
pH	Dependent on catalyst [16]
Light intensity	Positive [17-18]
b) Material properties	**Influence on activity**
Surface area	Positive [19]
Surface charge	Pollutant dependent [20-21]
Bandgap	Negative [22-23] (also dependent band levels and radiation source)
Charge carrier lifetime	Positive [24-25]
Surface reactivity	Positive [26-27]

Many different parameters are influencing the photocatalytic activity of a material. [5, 9] On the one hand, process parameters such as temperature, dissolved oxygen concentration, catalyst concentration, mixing (mass transfer), pollutant concentration, pH, and light intensity generally affect the photocatalytic activity (Table 1.1a).

However, external process parameters are usually predefined for a particular environment and need to be taken into account for the catalyst development. On the other hand, material properties (Table 1.1b) such as surface area, bandgap, charge carrier kinetics and surface functionalities for ROS generation give the intrinsic activity of the catalyst material that is directly related to the prevalent mechanistic steps during the photocatalytic degradation:

1) Adsorption of reactants (pollutant or ROS educts)
2) Light absorption resulting in electron-hole pairs
3) Generation of active species by oxidation/reduction reactions
4) Desorption of reactants (degraded pollutants or ROS)

1.2.3. TiO_2 (P25) as benchmark photocatalyst

TiO_2 is one of the most often used photocatalysts and often serves as a benchmark for new developments because of its stability, non-toxicity, low costs, and good performance. [9, 28] A particular type of TiO_2 is P25. This purely TiO_2 based material consists of nanoparticles (mean primary particle size approx. 21 nm) [29] with mixed crystalline phases of anatase (~80 %) and rutile (~20 %). With a large bandgap of about 3.0 eV for the rutile and 3.2 eV for anatase phase, P25 absorbs light with a wavelength lower than 410 nm. [7] However, due to this large bandgap, P25 suffers poor sunlight absorption just in the UV range, which hampers the application under solar light. Additionally, mechanistic insights state that rapid charge recombination keeps the efficiency too low for implementation in real water treatment using solar light. [6] Therefore, from the discovery of TiO_2 as a photocatalyst, a lot of effort was dedicated to improving the photocatalytic efficiency using modifications.

1.2.4. Modification and improvement possibilities

Several strategies arise to modify a catalytic material in order to improve the activity by reducing limiting factors for the catalyst in the photocatalytic mechanism. Each of the above-mentioned steps of the photocatalytic pathway may be subject to improvement, starting from the light absorption and charge separation to then generation of radical oxygen species (ROS). Furthermore, the adsorption of reactants, both pollutants, and precursors for the ROS generation, may increase the overall activity of the photocatalyst as it increases the local concentration close to the catalyst surface. Apart from those intrinsic photocatalytic properties, especially the surface area

and for powders additionally the dispersibility, which influences the accessible surface area due to agglomeration, are essential parameters.

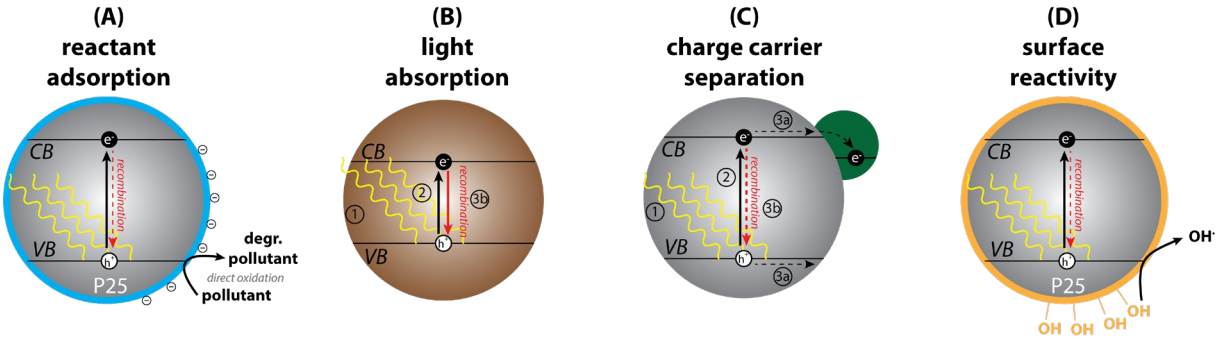

Figure 1.3: Modification possibilities of base photocatalysts to improve the overall reaction rate: A) optimizing the reactant adsorption by modifying the surface charge with the deposition of a thin layer, B) improving the light absorption by decreasing the bandgap employing bulk doping, C) modifying the surface by adding clusters of a second material on the surface to enhance the charge separation in order to prevent charge recombination, D) modifying the surface by depositing a thin layer of a second material to enhance the reactivity on the surface.

In principle, three strategies arise to modify the intrinsic activity of a catalyst – 1) bulk doping, incorporating heteroatom in the structure of the material, 2) surface modification, adding functionalities on the surface, and 3) modification of the surface morphology/crystal structure.

In order to improve the light absorption, usually, bulk doping is applied to influence the band structure shifting the light absorption to longer wavelength (Fig. 1.3 b). [22-23] Minute surface modifications, on the other hand, can give an improvement in the reactant adsorption [21], charge carrier kinetics [25], and surface reactivity (Fig. 1.3) [26]. In order to enhance the adsorption of the reactants, the surface properties may be changed by adding a thin layer of material to modify the surface charge (Fig 1.3 a). Furthermore, charge recombination is an important factor limiting the photocatalytic activity. Adding different materials can facilitate charge separation, where the distinct band levels allow spatial separation of an electron from the hole (Fig. 1.3 c). [24-25] This increases the lifetime of the electron and hole, enabling an efficient transfer to the reactants and more probable reaction. In order to improve the surface reactivity, materials with a high number of functional groups, i.e. M–OH groups, may be deposited to increase the ROS generation (Fig. 1.3 d). [26-27] Thirdly, modifying the crystal structure or surface morphology will influence these parameters and are commonly used to improve the photocatalytic activity. However, the aim to improve the photocatalytic activity of an already prepared crystalline material such as TiO_2 (P25) nanoparticles only make modifications at the surface feasible and accessible. This approach of surface modification excludes, therefore, modifying the bandgap but enables the changes in the reactant adsorption, charge carrier separation, and surface reactivity. In recent years reseach efforts have been mainly focused on the reduction of the

charge recobination and the development of visible light absorbing photocatalysts. Substantial steps have been made to improve the photocatalytic activity. Despite these improvements in photocatalytic activity especially by tuning visible light activity and suppression of charge recombination, the lack of implementation into real applications shows that the technology of cleaning water using photocatalysis still faces challenges both on a fundamental and application level. [30]

1.3. SURFACE MODIFICATION OF PHOTOCATALYSTS BY ATOMIC LAYER DEPOSITION

1.3.1. Fundamentals

Atomic Layer Deposition (ALD) belongs to the family of chemical vapor deposition techniques where vaporized chemicals react at the surface to build-up materials. ALD relies on the principle of self-limiting surface reaction, where two or more reactants are introduced to the surface separately. Figure 1.4 describes a detailed scheme on the four general ALD steps on the example of the growth of SiO_2 layers on the TiO_2 surface.

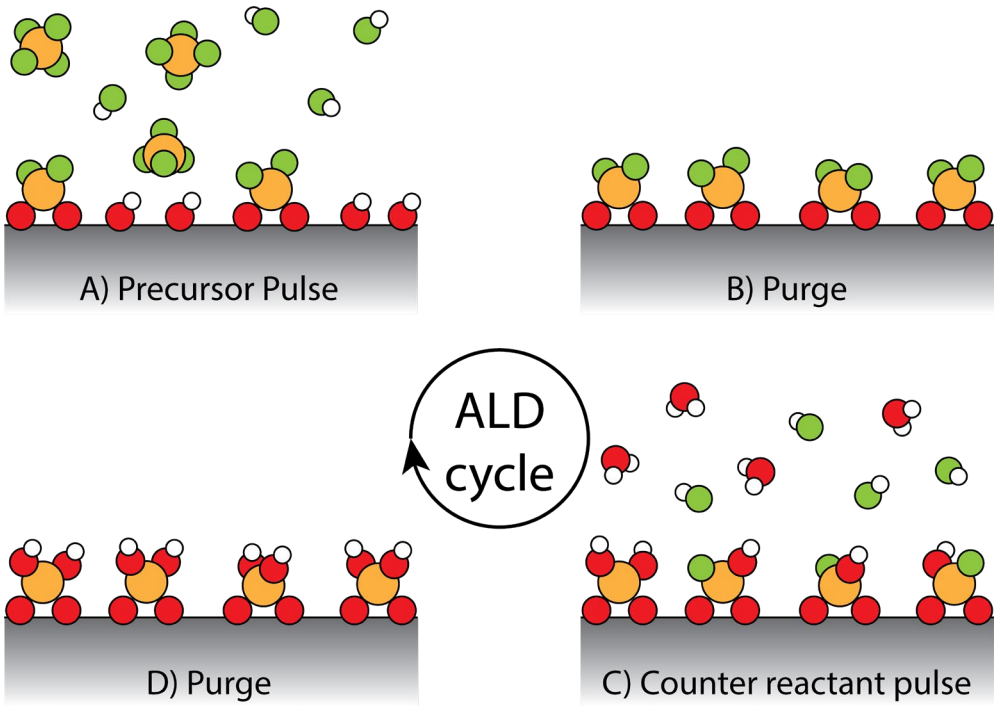

Figure 1.4: Scheme of the four steps of an ALD cycle to deposit layers of, e.g. SiO_2 on a metal oxide surface, A) Precursor pulse $SiCl_4$, B) Purge with inert gas, C) Oxidizer pulse H_2O, D) Purge with inert gas. (Si = orange sphere, Cl = green sphere, O = red sphere, H = white sphere).

In detail, in the first step, $SiCl_4$ reacts with the M-OH groups commonly present at the metal oxide surface, resulting in a chemisorbed Si-Cl group until no OH group remains on the surface or is not accessible anymore due to steric hindrance. In a second step, the excess precursor (i.e., $SiCl_4$) and formed by-products (i.e., HCl) are purged out of the reaction chamber by an inert gas. In order to refresh the surface with –OH groups, the counter-reactant (i.e., H_2O) is introduced to the reaction chamber to react with the terminal Si-Cl groups resulting in the terminal Si-OH groups. The counter-reactant pulse is again followed by a purging step to flush left-over precursor and by-products out of the system. This last purging step concludes one ALD cycle. Adding various cycles ideally changes the amount of material proportionally. The deposition of metals using ALD usually occurs via the combustion of the ligands by strong oxidizers such as O_3. [31-32]

Dependent on the surface properties of the substrate and the molecule affinity towards the surface, different structures may arise – a high affinity of the deposited material towards the surface leads to full coverage of the substrate resulting in layers or a low affinity/high surface energy of the deposited material leads to the formation of particles. The versatility of ALD gives the opportunity to deposit many different materials, which establishes it as a powerful tool for surface modification and (photo)catalyst development concisely reviewed by O'Neill et al. [33]

1.3.2. Benefits of ALD for photocatalyst development

Catalytic activity strongly depends on various structural factors in a material – crystallinity [20], surface area & morphology [19, 34] of a material and especially even minute addition of material both as overcoating [35] and as nanoclusters [36]. This implies that in order to meet those requirements of precise surface tunability, ALD serves as a very suitable technique. Especially for the addition of material while sustaining the photocatalytic activity of the base materials, only very subtle modifications may be induced to the surface, such as deposition of very thin/porous layers or nanoclusters. The self-limiting behavior allows depositing materials on a substrate in a very defined manner being able to tune the material properties precisely. It further allows (dependent on the substrate and the deposited material's surface energy) to either overcoat a material [37] or deposit nanoclusters [38] on the surface, which gives an additional degree of surface modification. Dependent on the process parameters such as deposition temperature or pulse time also the cluster size and size distribution can accurately be tuned as shown in previous research [39], which significantly influences the catalytic properties [40-41]. Furthermore, as a gas phase deposition, the use of solvents is redundant. Apart from the environmental factor, the degree of contamination due to a solvent can be minimized. Last but certainly not least, the scalable approach using ALD in a fluidized bed at atmospheric pressure gives additionally the chance to produce more copious amounts [42] to meet eventual needs for the implementation in a photoreactor.

1.4. FRAMEWORK OF THIS THESIS AND RESEARCH QUESTIONS

This project was initiated in the framework of the Delft | Global Initiative, a program that supports global development by tackling rising problems in developing countries. In that regard, this project was aiming at the combination of catalyst design with reactor engineering to develop a smart solution for water purification in low resource countries.

For the development of a photocatalytic system to purify water, several steps need to be tackled. An efficient catalyst needs to be developed by smart modification of the surface combined with carefully analyzing the mechanisms behind the improved photocatalytic activity. This analysis will set the framework on the working conditions of the catalyst. The working conditions greatly influence the design of the photoreactor where mass transport, light distribution, and kinetic reaction rate limitations need to be optimized. It is crucial to iterate between catalyst design and reactor design since, e.g. an improvement in the activity of the catalyst would be redundant if the mass transfer would limit the efficiency of the system. Therefore, only after developing a photocatalyst in agreement with a suitable reactor, a next step can be taken towards implementation. The relationships between these different aspects are schematically represented in Fig. 1.5.

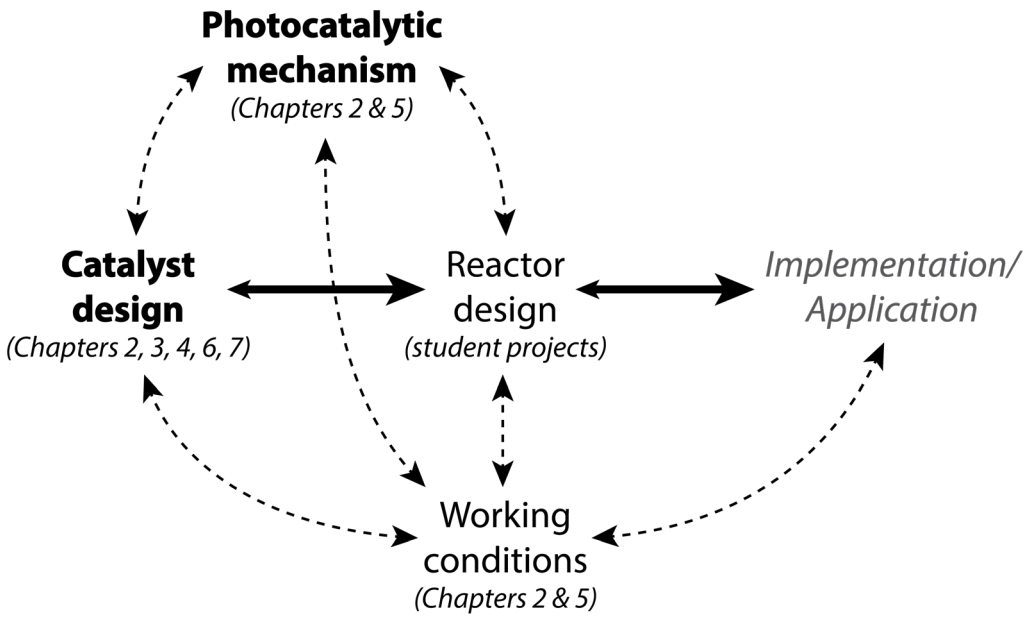

Figure 1.5: Framework of this thesis in the picture of the development and application of a photoreactor to clean water. Arrows indicate relationships between the main topics covered in this thesis (bold characters), topics excluded from this thesis but accessible in various student theses from our group on related topics (regular characters), research not addressed in this thesis (italic characters). Dashed arrows represent the subjects influencing the primary steps towards implementation, catalyst design, and reactor design.

Specifically, the primary goal of this research was to improve the photocatalytic activity of TiO_2 nanopowder (P25) by surface modification using atomic layer deposition and secondly to design a suitable reactor for the cleaning of water. However, after an initial assessment of this project proposal, the focus shifted to material improvement combined with mechanistic studies rather than the complete path to implementation in a photoreactor.

Therefore, this thesis will deal with the main research question,

How can we modify the surface of TiO_2 (P25) using ALD to improve its photocatalytic activity to purify water?

and the following sub-questions:

1) Is it possible to use cheaper materials than the commonly used noble metals to improve the photocatalytic activity of TiO_2 (P25)?
2) How do ALD surface modifications affect the photocatalytic mechanism of the modified material compared to TiO_2 (P25)?
3) Using the understanding of how surface modifications improve the photocatalytic activity of TiO_2 (P25), is it possible to combine multiple modifications in one material to design better multicomponent photocatalysts?

1.5. OUTLINE

In this thesis, six experimental chapters (Chapter 2 - 7) are accompanied by an introduction to photocatalysis for water treatment and atomic layer deposition (Chapter 1), and a conclusion chapter with an outlook on the approach investigated in this Ph.D. thesis and future feasibility of applying photocatalysis for water purification as a low-cost technology to provide clean drinking water (Chapter 8). All scientific chapters are (or will be) submitted to peer-reviewed international journals.

Chapter 2 tackles the unresolved mechanism of the improvement due to Pt clusters on TiO_2 (P25) in the photocatalytic activity of dye degradation. The combination of several characterization methods looking into both the physical and the photochemical properties of Pt:TiO_2(P25) gives a broad picture of the processes during the photocatalytic degradation. Especially the degradation under different atmospheres reveals the importance of dissolved O_2 for the different materials – TiO_2(P25) and Pt:TiO_2(P25).

Chapter 3 describes the new development of depositing Cu_2O clusters on TiO_2(P25) using atomic layer deposition in a fluidized bed at atmospheric pressure. The Cu_2O:TiO_2(P25) system was chosen to enhance the charge separation due to the

beneficial band level arrangements of Cu_2O with TiO_2 (P25). This system demonstrated low loadings of Cu_2O enhance the photocatalytic activity for various pollutants.

Chapter 4 deals with the deposition of ultrathin SiO_2 layers on TiO_2 (P25) nanoparticles using ALD. Layers of various thicknesses were deposited, which showed an optimum in the photocatalytic degradation of Rhodamine B. The mechanism for this improvement is further investigated in the following chapter.

Chapter 5 investigates how ultrathin SiO_2 layers on TiO_2 (P25) improve the photocatalytic activity by revealing the photocatalytic mechanism of this low-cost modification with SiO_2 on TiO_2 (P25). Various characterization techniques, including scavenging agents, were used to evaluate the contribution of different steps in the photocatalytic mechanism of degradation of two dyes with opposite charge. The results indicate a change of the mechanism from direct oxidation for TiO_2 (P25) to a more hydroxyl radical based degradation.

Chapter 6 takes the results of Chapters 2, 4, and 5 to design a photocatalyst that uses both improvement strategies into one material. SiO_2 is deposited in layers first on TiO_2 (P25) particles, followed by the deposition of Pt clusters. This Pt:SiO_2:TiO_2 combination exceeds the photocatalytic activity of both single modified materials SiO_2:TiO_2(P25) and Pt:TiO_2(P25) indicating a smart catalyst design leads to an even further improved photocatalytic activity.

Chapter 7 shows the first time deposition of Au clusters via ALD in a fluidized bed at atmospheric pressure onto TiO_2 (P25) particles. We could show that different ALD parameters such as cycle number, but more importantly, pulse time influence the particle size distribution. Both the loading and the especially the Au particle size strongly influence the photocatalytic activity for the degradation of Acid Blue 9, where specifically smaller Au clusters improve the photocatalytic degradation.

1

REFERENCES

1. Nations, U. *Synthesis Report 2018 on Water and Sanitation*; New York, 2018.
2. Whigham, N. Researchers use AI to predict outbreak of water wars in the future. https://www.news.com.au/technology/environment/researchers-use-ai-to-predict-outbreak-of-water-wars-in-the-future/news-story/f1d91a6ba462aba9b94886b9a1112dfb (accessed 03-03-2020).
3. Khan, Z. Future Water Wars. https://dailytimes.com.pk/344521/future-water-wars/ (accessed 03-03-2020).
4. Gaya, U. I., *Heterogeneous Photocatalysis Using Inorganic Semiconductor Solids*. Springer: 2014.
5. Ahmed, S.; Rasul, M. G.; Martens, W. N.; Brown, R.; Hashib, M. A., Advances in Heterogeneous Photocatalytic Degradation of Phenols and Dyes in Wastewater: A Review. *Water, Air, & Soil Pollution* **2010,** *215* (1-4), 3-29.
6. Loeb, S. K.; Alvarez, P. J. J.; Brame, J. A.; Cates, E. L.; Choi, W.; Crittenden, J.; Dionysiou, D. D.; Li, Q.; Li-Puma, G.; Quan, X.; Sedlak, D. L.; David Waite, T.; Westerhoff, P.; Kim, J. H., The Technology Horizon for Photocatalytic Water Treatment: Sunrise or Sunset? *Environ Sci Technol* **2019,** *53* (6), 2937-2947.
7. Gaya, U. I., Principles of Heterogeneous Photocatalysis. In *Heterogeneous Photocatalysis Using Inorganic Semiconductor Solids*, Springer Netherlands: Dordrecht, 2014; pp 1-41.
8. Gaya, U. I., Mechanistic Principles of Photocatalytic Reaction. In *Heterogeneous Photocatalysis Using Inorganic Semiconductor Solids*, Gaya, U. I., Ed. Springer Netherlands: Dordrecht, 2014; pp 73-89.
9. Anwer, H.; Mahmood, A.; Lee, J.; Kim, K.-H.; Park, J.-W.; Yip, A. C. K., Photocatalysts for degradation of dyes in industrial effluents: Opportunities and challenges. *Nano Research* **2019,** *12* (5), 955-972.
10. Evgenidou, E.; Fytianos, K.; Poulios, I., Semiconductor-sensitized photodegradation of dichlorvos in water using TiO_2 and ZnO as catalysts. *Applied Catalysis B: Environmental* **2005,** *59* (1), 81-89.
11. Muhich, C. L.; Zhou, Y.; Holder, A. M.; Weimer, A. W.; Musgrave, C. B., Effect of Surface Deposited Pt on the Photoactivity of TiO_2. *The Journal of Physical Chemistry C* **2012,** *116* (18), 10138-10149.
12. Liang, H.-c.; Li, X.-z.; Yang, Y.-h.; Sze, K.-h., Effects of dissolved oxygen, pH, and anions on the 2,3-dichlorophenol degradation by photocatalytic reaction with anodic TiO_2 nanotube films. *Chemosphere* **2008,** *73* (5), 805-812.
13. Mehrotra, K.; Yablonsky, G. S.; Ray, A. K., Kinetic Studies of Photocatalytic Degradation in a TiO2 Slurry System: Distinguishing Working Regimes and Determining Rate Dependences. *Ind. Eng. Chem. Res.* **2003,** *42* (11), 2273-2281.
14. Daneshvar, N.; Salari, D.; Khataee, A. R., Photocatalytic degradation of azo dye acid red 14 in water on ZnO as an alternative catalyst to TiO2. *Journal of Photochemistry and Photobiology A: Chemistry* **2004,** *162* (2), 317-322.
15. Zhang, A.-Y.; Wang, W.-K.; Pei, D.-N.; Yu, H.-Q., Degradation of refractory pollutants under solar light irradiation by a robust and self-protected ZnO/CdS/TiO_2 hybrid photocatalyst. *Water Research* **2016,** *92*, 78-86.
16. Sun, J.; Wang, X.; Sun, J.; Sun, R.; Sun, S.; Qiao, L., Photocatalytic degradation and kinetics of Orange G using nano-sized Sn(IV)/TiO2/AC photocatalyst. *Journal of Molecular Catalysis A: Chemical* **2006,** *260* (1), 241-246.
17. Herrmann, J.-M., Heterogeneous photocatalysis: fundamentals and applications to the removal of various types of aqueous pollutants. *Catalysis Today* **1999,** *53* (1), 115-129.
18. Motegh, M.; Cen, J.; Appel, P. W.; van Ommen, J. R.; Kreutzer, M. T., Photocatalytic-reactor efficiencies and simplified expressions to assess their relevance in kinetic experiments. *Chemical Engineering Journal* **2012,** *207-208*, 607-615.
19. Cheng, H.; Wang, J.; Zhao, Y.; Han, X., Effect of phase composition, morphology, and specific surface area on the photocatalytic activity of TiO_2 nanomaterials. *RSC Advances* **2014,** *4* (87), 47031-47038.
20. Bahnemann, W.; Muneer, M.; Haque, M. M., Titanium dioxide-mediated photocatalysed degradation of few selected organic pollutants in aqueous suspensions. *Catalysis Today* **2007,** *124* (3), 133-148.

21. Azeez, F.; Al-Hetlani, E.; Arafa, M.; Abdelmonem, Y.; Nazeer, A. A.; Amin, M. O.; Madkour, M., The effect of surface charge on photocatalytic degradation of methylene blue dye using chargeable titania nanoparticles. *Sci Rep* **2018,** *8* (1), 7104.
22. Wilke, K.; Breuer, H. D., The influence of transition metal doping on the physical and photocatalytic properties of titania. *Journal of Photochemistry and Photobiology A: Chemistry* **1999,** *121* (1), 49-53.
23. Kisch, H.; Sakthivel, S.; Janczarek, M.; Mitoraj, D., A Low-Band Gap, Nitrogen-Modified Titania Visible-Light Photocatalyst. *The Journal of Physical Chemistry C* **2007,** *111* (30), 11445-11449.
24. Wang, Z.; Guan, W.; Sun, Y.; Dong, F.; Zhou, Y.; Ho, W.-K., Water-assisted production of honeycomb-like g-C_3N_4 with ultralong carrier lifetime and outstanding photocatalytic activity. *Nanoscale* **2015,** *7* (6), 2471-2479.
25. Varma, R. S.; Thorat, N.; Fernandes, R.; Kothari, D. C.; Patel, N.; Miotello, A., Dependence of photocatalysis on charge carrier separation in Ag-doped and decorated TiO_2 nanocomposites. *Catalysis Science & Technology* **2016,** *6* (24), 8428-8440.
26. Simonsen, M. E.; Li, Z.; Søgaard, E. G., Influence of the OH groups on the photocatalytic activity and photoinduced hydrophilicity of microwave assisted sol–gel TiO_2 film. *Applied Surface Science* **2009,** *255* (18), 8054-8062.
27. Vorontsov, A. V.; Kabachkov, E. N.; Balikhin, I. L.; Kurkin, E. N.; Troitskii, V. N.; Smirniotis, P. G., Correlation of Surface Area with Photocatalytic Activity of TiO_2. *Journal of Advanced Oxidation Technologies* **2018,** *21* (1), 127-137.
28. Hoffmann, M. R.; Martin, S. T.; Choi, W.; Bahnemann, D. W., Environmental Applications of Semiconductor Photocatalysis. *Chemical Reviews* **1995,** *95* (1), 69-96.
29. Industries, E. AEROXIDE®, AERODISP® and AEROPERL® Titanium Dioxide as Photocatalyst Technical Information 1243. https://www.aerosil.com/sites/lists/RE/DocumentsSI/TI-1243-Titanium-Dioxide-as-Photocatalyst-EN.pdf (accessed 21-02-2020).
30. Loeb, S. K.; Alvarez, P. J. J.; Brame, J. A.; Cates, E. L.; Choi, W.; Crittenden, J.; Dionysiou, D. D.; Li, Q.; Li-Puma, G.; Quan, X.; Sedlak, D. L.; David Waite, T.; Westerhoff, P.; Kim, J.-H., The Technology Horizon for Photocatalytic Water Treatment: Sunrise or Sunset? *Environmental Science & Technology* **2019,** *53* (6), 2937-2947.
31. Richey, N. E.; Paula, C. d.; Bent, S. F., Understanding chemical and physical mechanisms in atomic layer deposition. *The Journal of Chemical Physics* **2020,** *152* (4), 040902.
32. Knapas, K.; Ritala, M., In Situ Studies on Reaction Mechanisms in Atomic Layer Deposition. *Critical Reviews in Solid State and Materials Sciences* **2013,** *38* (3), 167-202.
33. O'Neill, B. J.; Jackson, D. H. K.; Lee, J.; Canlas, C.; Stair, P. C.; Marshall, C. L.; Elam, J. W.; Kuech, T. F.; Dumesic, J. A.; Huber, G. W., Catalyst Design with Atomic Layer Deposition. *ACS Catalysis* **2015,** *5* (3), 1804-1825.
34. Das, A.; S.K, N.; Nair, R. G., Influence of surface morphology on photocatalytic performance of zinc oxide: A review. *Nano-Structures & Nano-Objects* **2019,** *19*, 100353.
35. Wang, X.; Patel, Rajankumar L.; Liang, X., Significant improvement in TiO2 photocatalytic activity through controllable ZrO2 deposition. *RSC Advances* **2018,** *8* (45), 25829-25834.
36. Gould, T. D.; Lubers, A. M.; Corpuz, A. R.; Weimer, A. W.; Falconer, J. L.; Medlin, J. W., Controlling Nanoscale Properties of Supported Platinum Catalysts through Atomic Layer Deposition. *ACS Catalysis* **2015,** *5* (2), 1344-1352.
37. Zhao, X.-R.; Cao, Y.-Q.; Chen, J.; Zhu, L.; Qian, X.; Li, A.-D.; Wu, D., Photocatalytic Properties of Co_3O_4-Coated TiO_2 Powders Prepared by Plasma-Enhanced Atomic Layer Deposition. *Nanoscale Research Letters* **2017,** *12* (1), 497.
38. Christensen, S. T.; Feng, H.; Libera, J. L.; Guo, N.; Miller, J. T.; Stair, P. C.; Elam, J. W., Supported Ru−Pt Bimetallic Nanoparticle Catalysts Prepared by Atomic Layer Deposition. *Nano Letters* **2010,** *10* (8), 3047-3051.
39. Grillo, F.; Van Bui, H.; Moulijn, J. A.; Kreutzer, M. T.; van Ommen, J. R., Understanding and Controlling the Aggregative Growth of Platinum Nanoparticles in Atomic Layer Deposition: An Avenue to Size Selection. *The Journal of Physical Chemistry Letters* **2017,** *8* (5), 975-983.
40. Feng, H.; Elam, J. W.; Libera, J. A.; Setthapun, W.; Stair, P. C., Palladium Catalysts Synthesized by Atomic Layer Deposition for Methanol Decomposition. *Chemistry of Materials* **2010,** *22* (10), 3133-3142.
41. King, J. S.; Wittstock, A.; Biener, J.; Kucheyev, S. O.; Wang, Y. M.; Baumann, T. F.; Giri, S. K.; Hamza, A. V.; Baeumer, M.; Bent, S. F., Ultralow Loading Pt Nanocatalysts Prepared by Atomic Layer Deposition on Carbon Aerogels. *Nano Letters* **2008,** *8* (8), 2405-2409.
42. van Ommen, J. R.; Goulas, A., Atomic layer deposition on particulate materials. *Materials Today Chemistry* **2019,** *14*, 100183.

Assessing the role of Pt clusters on TiO_2 (P25) on the photocatalytic degradation of Acid Blue 9 and Rhodamine B

2

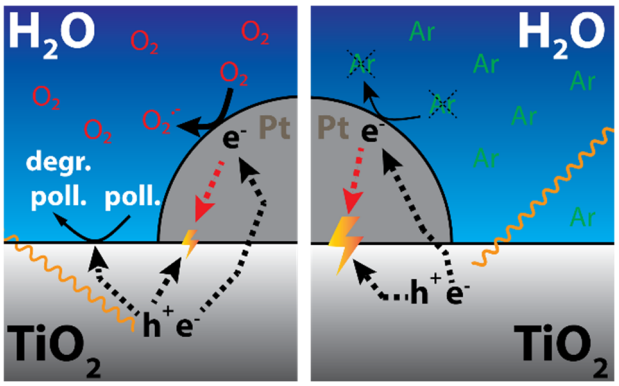

The role of Pt on photocatalytic substrates such as TiO_2 (P25) for the decomposition of organic pollutants is still controversial in the scientific community. The well-observed behavior of an optimum catalytic activity as a function of the Pt loading is usually explained by the shift from charge separation to charge recombination behavior of Pt clusters. However, experiments supporting this explanation are still lacking to give a concise understanding of the effect of Pt on the photocatalytic activity. Here, we present an experimental study that tries to discriminate the different effects influencing the photocatalytic activity. Using atomic layer deposition (ALD) in a fluidized bed reactor, we prepared TiO_2 (P25) samples with Pt loadings ranging from 0.04 wt. % to around 3 wt. %. In order to reveal the mechanism behind the photocatalytic behavior of Pt on TiO_2 (P25)*, we investigated the different aspects (i.e., surface area, reactant adsorption, light absorption, charge transfer, reaction pathway) of heterogeneous photocatalysis individually. In contrast to the often proposed prolonged life-time of charge carriers in Pt loaded TiO_2 , we found that after collecting the excited electrons, Pt acts more as a recombination center independent of the amount of Pt deposited. Only when dissolved O_2 is present in the solution, charge recombination is suppressed by the subsequential consumption of electrons at the surface of the Pt clusters with the dissolved O_2 benefited by the improved O_2 adsorption on the Pt surface.*

Published in Journal of Physical Chemistry C

Dominik Benz, Kevin M. Felter, Jan Köser, Jorg Thöming, Guido Mul, Ferdinand C. Grozema, Hubertus T. Hintzen, Michiel T. Kreutzer, J. Ruud van Ommen

2.1. INTRODUCTION

Photocatalysis to clean water is a promising technology for tackling the rising problem of water pollution, especially in low resource countries. Using materials such as TiO_2 and sunlight, many reports have shown the degradation of a range of pollutants in water. [1-6] However, the implementation in real-life remains challenging because of a lack of efficiency. Getting insight into the working principles of the developed catalyst will especially help further developments such as combining materials in order to make even more active catalysts. In order to degrade organic pollutants using photocatalysis, generally, four steps take place: [7-8]

1) Adsorption of the reactants (pollutant, O_2, H_2O) on the surface
2) Light absorption and generation of charge carriers (e^-/h^+)
3) Redox reaction on the surface creating hydroxyl radicals, superoxide radicals or directly oxidizing the pollutant
4) Desorption of products from the surface

Upon light excitation of the photocatalysts, an electron (e^-) is excited to the conduction band (CB), leaving a hole (h^+) in the valence band (VB). Those excited charges generate reactive oxygen species (ROS) such as superoxide radicals (O_2^{-*}) from e^-_{CB} and hydroxyl radicals (OH^*) from h^+_{VB}. However, excited electrons are prone to recombine with holes, if not harvested efficiently, losing the potential for the preferred redox reaction to degrade organic pollutants.

According to this mechanism for the photocatalytic degradation of organic pollutants, three different events lead to the degradation of the pollutant [4, 9]:

1) The creation of superoxide radicals (O_2^{*-}) from the CB electrons and dissolved oxygen leads to the formation of OH^* radicals which oxidize the pollutant subsequently to CO_2 and H_2O:
   $e^-_{CB} + O_2 \rightarrow O_2^{*-} \rightarrow\rightarrow OH^*$
   $OH^* + \textit{pollutant} \rightarrow\rightarrow \textit{decomposed pollutant}$ (Eq. 1)
2) The creation of OH^* radicals from the reaction of H_2O or –OH groups at the surface with the VB holes which subsequently oxidize the pollutant:
   $H_2O + h^+_{VB} \rightarrow OH^* + H^+$ (Eq. 2)
   $–OH + h^+_{VB} \rightarrow OH^*$ (Eq. 3)
   $OH^* + \textit{pollutant} \rightarrow\rightarrow \textit{decomposed pollutant}$ (Eq. 4)
3) Generated holes in the VB directly oxidize the pollutant:
   $\textit{pollutant} + h^+_{VB} \rightarrow \textit{pollutant}^{+*} \rightarrow \textit{decomposed pollutant}$ (Eq. 5)

In order to improve the performance of a photocatalyst, several approaches are generally proposed: 1) enhance the affinity of the reactants towards the catalyst surface to improve proximity to ROS and therefore degradation probability; 2) enhance the amount of light absorbed by the catalyst which results in more electron-hole pair generation; 3) enhance the quantum yield by preventing charge recombination; or 4) improving the desorption of the products from the surface.

Many publications claim to have found a better catalyst because of the improvement of one or more of those aspects, while a complete description of the materials' properties is generally lacking. Especially for photocatalysts, many properties influence the overall activity, which makes a complete analysis of the relationship to the final photocatalytic activity challenging. Apart from experimental design parameters such as catalyst concentration in the slurry, irradiation area, light intensity, and pollutant concentration, the materials' properties are the key to improve the intrinsic photocatalytic activity. Accessible reaction surface area, light absorption/bandgap, extrinsic quantum yield (how many separated charge carriers are created from the incident light and that further react with the contaminant or generate ROS), and the affinity of the pollutants towards the surface play important roles and are related to the intrinsic material properties. In order to have insight into the difference in activity between various materials, all relevant properties should be taken into consideration and compared to enable the elaboration of the structure-activity relationships, which requires numerous characterization tools and analyses. For getting a complete picture of the prepared material, it is ubiquitous to address all these questions simultaneously.

The lack of insight often leads to discussions on what is the real reason for enhancement or suppression in photocatalytic performance for the degradation of dyes as a function of the surface modification. Pt decorated TiO_2 nanoparticles demonstrated in earlier studies, an improved activity for dye degradation [10-12]. However, there exist still different theories why a low amount of platinum clusters onto TiO_2 (P25) enhances the photocatalytic activity. The explanations include enhanced charge separation [13-16], improved light absorption [17], and better O_2 adsorption [18-22]. On the other hand, especially for higher Pt loadings, the photocatalytic activity drops as proposed in earlier research due to charge recombination. [18, 23-25] However, this explanation seems contradictory since a change from charge separation to charge recombination purely based on Pt loading does not seem likely. With their purely theoretical approach, Muhich et al. provided a reasonable explanation stating that Pt serves as a recombination center independent of the loading, where electrons and holes recombine in the Pt cluster. On the other hand, they advocate the importance of dissolved O_2 in solution, which adsorbs on the surface of Pt. [18] The objective of this chapter is to substantiate Muhich's et al. theoretical approach by an experimental study elaborating on the different effects Pt clusters can have on the surface of TiO_2 (P25) focused on the charge carrier kinetics and to investigate the importance of dissolved oxygen.

2.1. EXPERIMENTAL SECTION

2.1.1. Materials

TiO_2 nanoparticles (P25, mean diameter ~21 nm, BET surface area of ~54 m^2g^{-1}, information from supplier) were purchased from Evonik Industries (Hanau, Germany). Trimethyl(methylcyclopentadienyl)-platinum(IV) ($MeCpPtMe_3$) was obtained from Strem Chemicals and used as received. Acid Blue 9 (Brilliant Blue FCF) and Rhodamine B were purchased from Sigma Aldrich and were used without further purification.

2.1.2. Deposition

Prior to the deposition, the TiO_2 powder was sieved with a 250 µm mesh to break and exclude larger agglomerates. Platinum was deposited on TiO_2 (P25) using a homebuilt ALD setup in a fluidized bed under atmospheric pressure [26-27]. In brief, the powder was placed in a quartz glass column (diameter 26 mm, height 500 mm), which was then placed on a vertical vibration table (Paja 40/40-24) to assist fluidization. $(MeCp)PtMe_3$ was used as the Pt precursor, and oxygen gas was used as a counter reactant. For the ALD reactions, the Pt precursor was contained in a stainless-steel bubbler heated to 70 °C and the stainless steel lines, connecting both the Pt precursor and O_2 (Grade 5.0) individually to the reactor, were heated to 90 °C to avoid precursor condensation. The glass reactor was heated to 100 °C throughout the experiment using an infrared lamp, which was placed parallel to the column, with feedback control. For every experiment, 1.5 g of TiO_2(P25) powder was placed in the reactor column. Nitrogen (Grade 5.0), serving as a carrier gas for the precursor, was introduced through a distributor plate at the bottom of the column with a flow of 0.5 l/min resulting in a superficial gas velocity of 1.6 cm s^{-1} to ensure proper fluidization and distribution of the precursor. The deposition process consisted of sequential exposures of the powders to the Pt precursor (20 sec – 5 min) and oxygen (5 min), separated by a purging step (5 min) using nitrogen as an inert gas.

After deposition, the powders were treated under an atmosphere of 5 % H_2 in nitrogen (v/v) in the fixed bed reactor with a flow of 100 ml/min. The temperature was ramped up from room temperature to 200 °C with a rate of 2 °C/min and then was held constant for 5 min after which the powder was allowed to cool down to room temperature.

2.1.3. Characterization

For the inductively coupled plasma - optical emission spectrometry (ICP-OES) analysis, approximately 30 mg of sample was digested in 4.5 ml 30 % HCl + 1.5 ml 65% HNO_3 + 0.2 ml 40 % HF acid mixture using a microwave. The digestion duration

in the microwave was 60 min. After the digestion, the samples were diluted to 50 ml with MQ water and analyzed with ICP-OES 5300DV. The samples were also diluted 20 times for Ti.

Transmission electron microscopy (TEM) pictures were acquired from a JEOL JEM1400 transmission electron microscope at 120 kV. As-deposited Pt:TiO_2(P25) nanoparticles were suspended in ethanol and transferred to Cu transmission electron microscopy grids (3.05 mm in diameter, Quantifoil).

X-ray photoelectron spectra (XPS) were recorded on a ThermoFisher K-Alpha system using Al Kα radiation with a photon energy of 1486.7 eV. A sufficient amount of powders was immobilized on copper tape before loading into the XPS chamber. Scans were acquired using a 400 μm spot size, 55 eV pass energy, and 0.1 eV/step with charge neutralization. The peaks positions were analyzed using the Thermo Avantage software after *SMART* type background subtraction and calibrating the measurements by taking the C 1s peak as a reference at 284.8 eV.

The Brunauer-Emmett-Teller (BET) surface area was measured on a Micromeritics Tristar II 3020. The samples were degassed overnight at 150 °C to remove adsorbed water on the surface.

Measurements of the mean agglomerate diameter (z-average) in dispersion and the zeta-potential have been carried out at a Beckmann-Coulter DelsaNanoC (Krefeld, Germany). Prior to the measurement, 15 mg of powder in 15 ml (MilliQ water) was dispersed by a sequence of 15 min stirring followed by sonication treatment for 20 s and an amplitude of 100 % (200 W) using a Bandelin Sonopuls HD 3100 sonicator (Berlin, Germany). Afterward, the dispersion was stirred for another 15 min. The mean particle size (z-average diameter) was measured using the cumulant analysis by averaging ten measurements with the detector configuration at an angle of 165° respective to the incident light beam. Three independent samples were measured for each material. The zeta-potential measurements were executed using the correlating flow cell of the same instrument using the same dispersion protocol. The pH of the dispersions was measured after 5 min of submerging the pH electrode (Voltcraft pH-100ATC, Hirschau, Germany) into the freshly dispersed powder.

For adsorption measurements, the catalyst (2 g/l) was dispersed in a solution of Acid Blue 9 (16 mg/l_{aq}) or Rhodamine B (12 mg/l_{aq}) under vigorous stirring. After distinct time intervals, a liquid sample was analyzed using UV/Vis spectroscopy to measure the remaining concentration of the corresponding dye in solution.

UV/VIS-DRS measurements were performed using a PerkinElmer-Lambda 900 spectrometer equipped with an integrating sphere device scanning from 200 nm to 800 nm. The reflectance for various samples was measured where Barium sulfate served as a reference for 100 % reflection over the measured wavelength range.

The photoconductive behavior of the samples was measured with the time-resolved microwave conductivity technique (TRMC) on a custom-built setup described elsewhere. [28] The TRMC technique allows the measurement of the intrinsic photoconductivity of a sample without the need for external electrical contacts. A thin film sample was prepared on a quartz slide from a concentrated dispersion in ethanol by doctor blade coating and then dried at 80°C for 30 min and placed in a microwave cavity cell. The sample was continuously exposed to continuous X-band microwaves at an approximate resonance frequency of 8.5 GHz that were generated by a Gunn diode. Photoexcitation of the sample occurred with 3.5 ns full width half maximum laser pulses of tunable wavelength (240-2200 nm) using an *EKSPLA NT342B SH/SFG-10-AW Nd:YAG laser*. Upon photoexcitation, free and mobile charge carriers were generated, i.e. electrons and holes that absorb part of the incident microwave power expressed as: $\Delta P(t)/P$. The change in microwave power is proportional to a change in the photoconductance $\Delta G(t)$ as

$$\Delta P(t)/P = - K\Delta G(t).$$

Here K is a frequency-dependent sensitivity factor ($40 \cdot 10^3$ S^{-1}) that follows from the resonance properties of the setup and the properties of the dielectric media present. The half-life of the transient photoconductance was used as a measure for charge transfer from TiO2 to the Pt clusters on the hundred to microsecond timescale.

2.1.4. Photocatalytic testing

Photocatalytic testing under saturated Ar and O_2 atmosphere was done in a 30 ml custom made quartz reactor with 15 mg of powder and a 30 ml solution of Acid Blue 9 (16 mg/l) or Rhodamine B (12 mg/l). For better dispersion and degassing, the powder was put into the solution of Acid Blue 9 or Rhodamine B and sonicated in an ultrasonic bath (Ultrasonic Cleaner, USC–TH, VWR) for 10 min. For the experiments under an inert atmosphere, the solution was transferred into the reactor vessel in an N_2 glovebox to avoid exposure to the oxygen in the air. Afterward, the dispersion was stirred for 30 minutes under bubbling of Ar or O_2 gas in order to reach the desired atmosphere – inert vs. saturated solution of dissolved O_2. The samples were irradiated using a 500 W Deep UV Mercury lamp from Ushio (25.4 mW/cm^2; see Appendix for light spectrum) and after distinct times samples of 0.5 ml were taken, filtered through a 0.45 µm PTFE filter and the filtrate was then analyzed using a UV/Vis spectrometer (Hach-Lange, DR5000, Düsseldorf, Germany) in a quartz glass cuvette with a thickness of 1 cm. A blank spectrum of water as the reaction medium was measured as a reference and automatically subtracted. The absorption was measured at 629 nm and 554 nm for Acid Blue 9 and Rhodamine B, respectively. According to quasi first-order kinetics, $\ln(C_0/C_t)$ was plotted vs. the time, and the slope of a linear regression represents the kinetic constant.

2.2. RESULTS AND DISCUSSION

2.2.1. Material synthesis and characterization

Changing the pulse times of the Pt precursor from 20 sec to 5 minutes, we could achieve loadings of Pt ranging from 0.04 wt% to about 0.7 wt% at a reaction temperature of 100 °C. We were able to precisely control the loading, which increases with pulse time (Fig. S2.1). Higher loadings (up to 3.13 wt % Pt) were achieved by applying up to four ALD cycles of $Pt(Me_3)(MeCp)$ and O_2 at pulse times of five minutes each. After annealing in an H_2/N_2 atmosphere, the Pt clusters were converted to their more active metallic state [29], which has been confirmed by XPS with peaks arising at 71.28 eV ($Pt5f_{7/2}$) and 74.28 eV ($Pt5f_{5/2}$) (Fig. S2.2). TEM pictures confirmed the homogeneously distributed deposition of Pt clusters on the surface of TiO_2 with an average particle size of about 1.4 nm (Fig. 2.1).

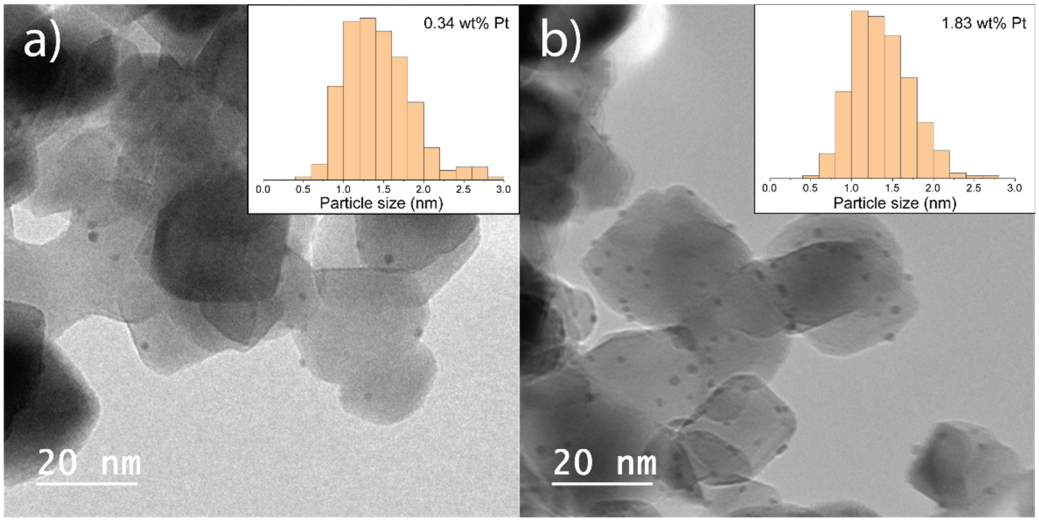

Figure 2.1: a) TEM image of Pt clusters deposited on TiO_2 (P25) (0.34 wt % Pt), the bigger particles represent the TiO_2 particles, small black dots on the surface of TiO_2 indicate the Pt clusters, b) TEM image of Pt clusters deposited on TiO_2 (P25) (1.83. wt % Pt), insets: Particle size distribution of Pt clusters of corresponding samples.

2.2.2. Photocatalytic degradation of Acid Blue 9 and Rhodamine B

The photocatalytic activity was evaluated by decolorization of the two differently charged dyes, Acid Blue 9, which is solely negatively charged in natural conditions and Rhodamine B, a positively charged to zwitterionic molecule (pK_a = 3.7). [30] Both demonstrated a drastic increase in the photocatalytic activity for the loading of 0.34 wt % Pt as compared to TiO_2 (P25) for both Acid Blue 9 and Rhodamine B, followed by an activity drop to even lower values than the intrinsic value of TiO_2 (P25)for

higher Pt loadings (>1.8 wt % Pt) (Fig. 2.2, Fig. S2.3). The initial slight decrease in activity for very low loadings around 0.1 wt % Pt observed for both dyes is likely caused by the deposition process. Despite the annealing in a hydrogen atmosphere to convert the Pt into its metallic state, residues from the organic ligands might still be present at the surface of TiO_2 and have a negative effect on the photocatalytic activity.[11] This is very apparent, especially for the very low loaded samples, where the contamination may overpower the positive effect of the Pt deposition.

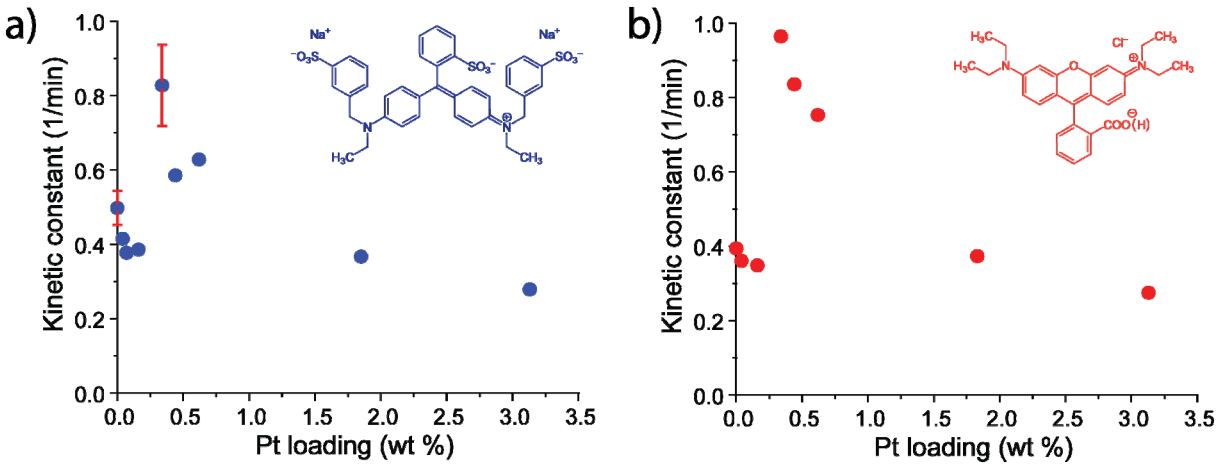

Figure 2.2: Kinetic constants for the degradation of a) Acid Blue 9 and b) Rhodamine B for various laodings of Pt on the surface of TiO_2 (P25).

Despite the well-established behavior of Pt on TiO_2 as a photocatalyst for dye degradation of showing an optimum [31-33], it still gives rise to the question what is the mechanism behind this initial increase and especially the subsequent drop to a lower activity as compared to pure TiO_2 (P25) for higher Pt loadings. It has been proposed in earlier studies that Pt on TiO_2 acts as an electron collector, making the lifetime of the separated electron and hole longer [13] allowing those to react with the pollutant or water to create radicals enabling the degradation of the pollutants. This would explain the initial positive effect of the Pt but not why the activity drops to lower than TiO_2 (P25) for higher Pt loadings. Logically there must be at least two mechanisms behind – at least one positive and one negative – which gives this optimal loading behavior, as discussed in the introduction.

Since many parameters can affect the photocatalytic activity, Table 2.1 gives an indication which factors might be influential to the overall photocatalytic activity:

Table 2.1: Overview of the main (photo-)catalytic parameters as related to various material properties and factors influenced by them, and the corresponding analysis tools.

	Material Property	Affects	Analysis tool
General catalytic parameter	Surface area	Number of reaction sites	BET
	Accessible surface area in solution/agglomeration of catalyst particles	Diffusion/mass transfer	DLS
	Surface charge	Reactant adsorption	1) Zeta-potential 2) Amount of adsorbed dye on the surface
Photocatalytic parameter	Bandgap	Light absorption	UV/Vis-DRS
	Charge carrier kinetics	Lifetime charge carriers	TRMC
	Reactivity	Number of generated ROS (OH^*, O_2^{-*})	Catalytic testing under Ar and O_2 atmosphere

In the following, we will elaborate on each material property individually in order to check in a systematic way the role of Pt on TiO_2 (P25) as a photocatalyst:

1) Surface area

For heterogeneous photocatalysis, the available surface area is an important parameter to describe the activity of a catalyst. Since the reaction takes place in dispersion, it should be described both by the overall surface, which is measured by BET analysis, and the available surface for the reaction where surface coverage of materials or agglomeration of catalyst particles can be a reducing factor. BET analysis yields a surface area of 54.75 m^2/g for Pt:TiO_2(P25) (0.34 wt% Pt), equal to TiO_2 (P25) (from supplier, see Exp. Section), demonstrating that the deposited Pt clusters have only an insignificant effect on the BET surface area. However, since photocatalytic testing takes place in a dispersion of water, a change in the agglomerate size might influence the mass transfer of reactants to the inner surface of agglomerates and, therefore, the overall photocatalytic activity [34]. Dynamic light scattering (DLS) showed a slight increase in the agglomerate size (z-average diameter) from 312 ± 24 nm (P25) to 408 ± 64 nm upon deposition of Pt clusters (0.34 wt% Pt) (Fig. 2.3a). The additional agglomeration is likely caused due to the deposition process where reactions of molecules on the surface might act as a “glue” between particles. However, the additional agglomeration is independent of the Pt loading and therefore acts more as a constant negative effect rather than as a dependency on the Pt loading. The reduced accessible surface due to stronger agglomeration might contribute to the small drop in

activity for very low loadings up to 0.1 wt % Pt. [34] Furthermore, Pt, itself acting as a co-catalyst on the surface of TiO_2 (P25), may reduce the active TiO_2 surface area for reactants. Taking into account the average Pt cluster size deposited on the TiO_2 surface of 1 – 2 nm, the surface coverage with Pt clusters only shows a limited decrease of less than 5 % of the TiO_2 surface, with increasing Pt cluster size, especially for low loadings (Fig. 2.3b). This indicates that the surface coverage of Pt on TiO_2 (P25) also should not be an influential factor on the photocatalytic activity.

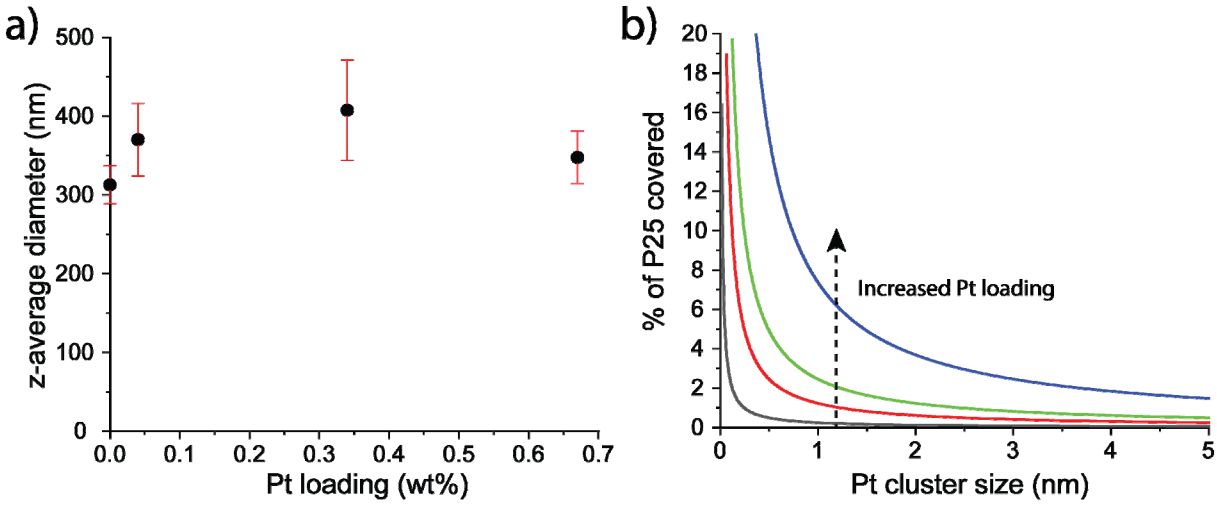

Figure 2.3: a) Z-average diameter from DLS measurements of P25 and differently loaded Pt:TiO_2 (P25) catalysts, b) Calculated coverage of Pt on the TiO_2 (P25) surface as a function of the Pt cluster size for four different Pt loadings: 0.1 wt% (black), 0.5 wt% (red), 1 wt% (blue), 3 wt% (green).

2) Reactant adsorption

Dependent on the predominant reaction mechanism, the adsorption of the reactants plays an essential role in heterogeneous photocatalysis i.e. direct oxidation of the dye at the surface. The surface charge majorly influences the attraction or repulsion of differently charged molecules. The zeta potential often serves as an indication for the relative amount and the nature of charge present at the surface. Upon deposition of Pt, the zeta potential of the catalyst particles remains positive and at about + 30 mV (Fig. 2.4a) measured at a pH of 7.7 ± 0.3. Positive charges are present at the surface of both TiO_2 (P25) and Pt:TiO_2(P25)due to the protonated –OH groups. Dye adsorption measurements (measured at a high powder concentration, see Exp. Section) of the negatively charged dye Acid Blue 9 and differently charged dye Rhodamine B are in agreement with the positive zeta potential. As expected, Acid Blue 9 strongly adsorbs on the surface of both TiO_2 (P25) and Pt:TiO_2(P25), whereas Rhodamine B shows limited adsorption due to only weak interaction with the TiO_2 surface (Fig. 2.4b). The Acid Blue 9 adsorption decreases for higher Pt loadings, while Rhodamine B adsorbs accordingly slightly better to the surface Indicating that the zeta potential slightly decreases for higher Pt loadings. Despite the opposite adsorption behavior of

Rhodamine B and Acid Blue 9, the photocatalytic activity to degrade Acid Blue 9 and Rhodamine B shows similar optimal behavior as a function of the Pt loading. This demonstrates that differences in dye adsorption have no impact on the general photocatalytic behavior of Pt:TiO_2(P25)vs. pure TiO_2 (P25).

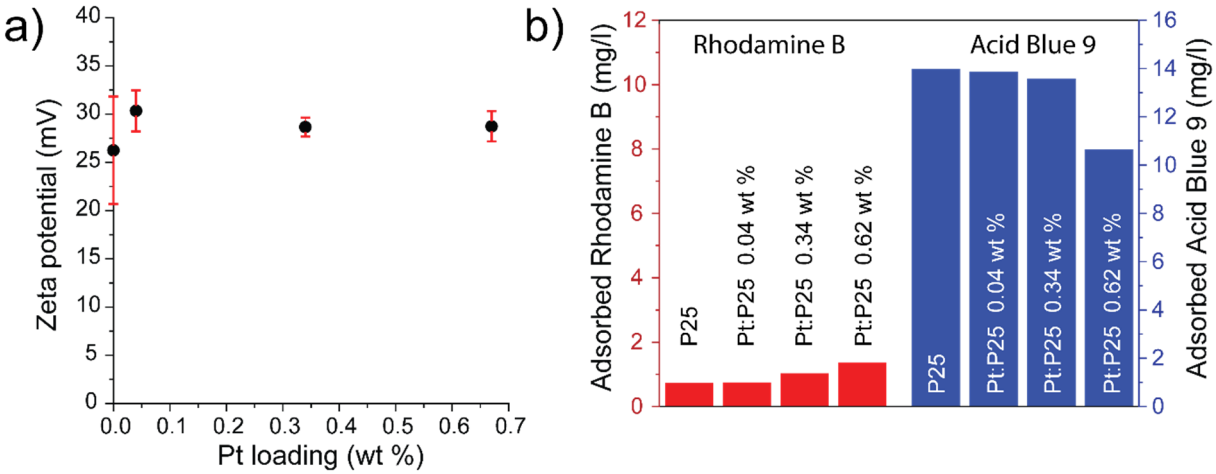

Figure 2.4: a) Zeta-potential of various Pt loaded TiO_2 (P25) samples; b) Dye adsorption studies with a catalyst concentration of 2 g/l. Red bars indicate the amount of adsorbed Rhodamine B on the surface of various loaded Pt:TiO_2(P25), blue bars indicate the adsorption of Acid Blue 9 on the surface of Pt:TiO_2(P25). Samples were taken after 30 min of stirring in the dark.

Summarizing the external effects of surface area and pollutant adsorption of Pt:TiO_2 (P25) compared to TiO_2 (P25), we can conclude that both properties play if at all only a minor role on the dependence of the photocatalytic activity on Pt loading. Both the surface area measured by BET and the calculated actual free TiO_2 surface area from the surface coverage of Pt clusters only show a minor decrease. The agglomerate size instead generally increases for the Pt:TiO_2(P25) which is due to the deposition process rather than related to the loading. Furthermore, the adsorption studies of different pollutants demonstrated the independence of the general photocatalytic behavior on the pollutant adsorption since for both cases of high and low reactant adsorption – dependent on the charge of the dye – Pt:TiO_2(P25) shows the same trend in photocatalytic activity as a function of the Pt loading.

After discussing the influence of the external parameters, we now will look more into the *photo*-catalytic parameters, i.e. light absorption, charge carrier kinetics, and reactivity.

3) Light absorption and charge carrier dynamics

A common approach in photocatalyst development is to reduce the bandgap of the material in order to increase the photon absorption of the solar spectrum. This approach usually requires the incorporation of heteroatoms into the crystal lattice of the base material. In contrast, our deposition of Pt clusters on the TiO_2 surface is not expected to change the bandgap of TiO_2. However, Pt clusters may absorb light of all

wavelengths as a result of the metallic character. The UV/VIS-DRS spectra show increased absorption in the visible at higher Pt loadings (Fig. 2.5a), which is caused by metallic Pt clusters.[12, 35] On the other hand, the presence of Pt clusters do not change the absorption edge which indicates the bandgap of TiO_2 remains unaffected disregarding possible band bending near a junction to Pt. This is also expected because Pt(0) clusters are deposited on the surface and Pt is not incorporated in the TiO_2 lattice. Additionally, it indicates that possible other valencies (i.e. Pt(II) and Pt(IV)of Pt) were reduced to Pt(0) by H_2 post-treatment and are not affecting the band structure of TiO_2.

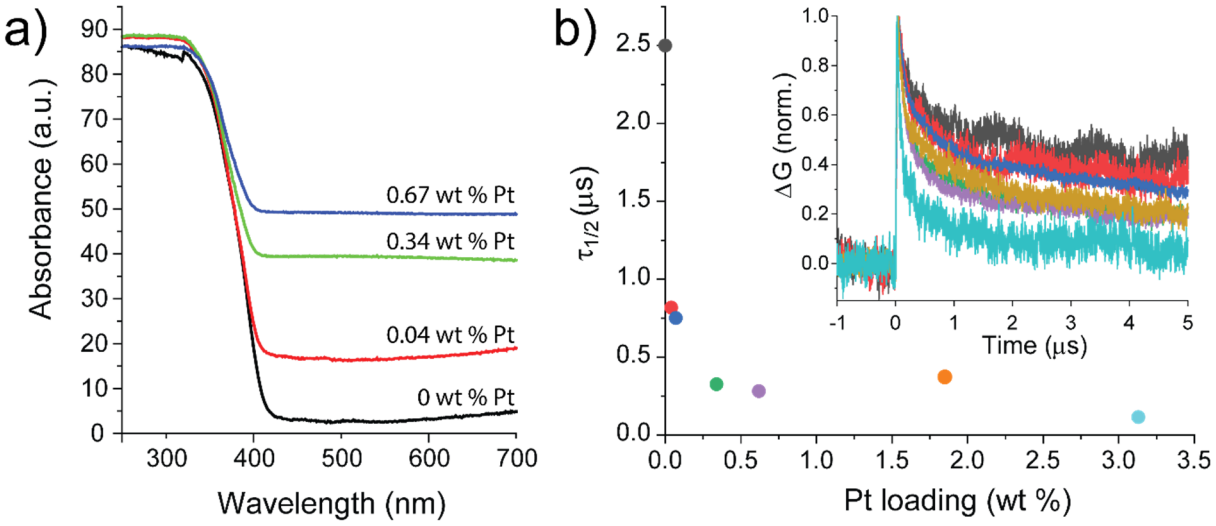

Figure 2.5: a) Absorption spectrum UV/Vis DRS spectra for different loaded Pt:TiO_2(P25), b) Half time ($\tau_{1/2}$) of the mobile charge carriers measured by TRMC, Inset: Transient decay of the mobile charge carrier.

Light absorption by the TiO_2 leads to the creation of mobile electrons and holes. The mobile electrons may transfer into the Pt clusters that allow redox reactions to occur. The electrons that transfer into the Pt clusters become immobile. With the microwave conductivity technique, the decrease in TiO_2 photoconductance is probed owing to the loss of free and mobile electrons in the TiO_2 resulting from charge transfer to the Pt. As the electrons in small noble metal clusters are immobile, no photoconductivity can come from these transferred electrons.[36] As such, the kinetics of the photoconductance transients provide a value for the charge transfer to Pt on the nanosecond to microsecond timescale. The half-life ($\tau_{1/2}$) of the free electrons in the TiO_2 decreases with increasing Pt loadings (Fig. 2.5b), which clearly indicates that the charge carrier dynamics are affected by the presence of Pt at the TiO_2 nanocrystal surface. Even at very low Pt loadings of 0.04 wt.%, the effect is very pronounced. This shows that electron transfer from TiO_2 to Pt is energetically favorable and therefore supports charge separation. The transferred electrons in the Pt clusters may support different reactions determining the fate of the electrons. Pt is not only well known as an H_2 evolution catalyst by reducing H^+ with the collected electrons [37-38] but is also shown to

readily adsorb O_2 on its surface [18, 20]. The reduction of adsorbed O_2 to O_2^{-*} superoxide radical by the collected electrons would positively influence the photocatalytic activity for pollutant degradation, improving the generation of ROS. [9] Therefore, photocatalytic degradation experiments using different environments, such as dispersions saturated with O_2 and Ar atmosphere, would give insight into the influence of adsorbed O_2 on the photocatalytic activity of Pt:TiO_2(P25). Excluding O_2 form the reaction medium will block the generation of superoxide O_2^{*-} radicals via the consumption of the conduction band electrons. The photocatalytic activities for various Pt loadings under saturated O_2 and Ar atmosphere are displayed in Figure 2.6:

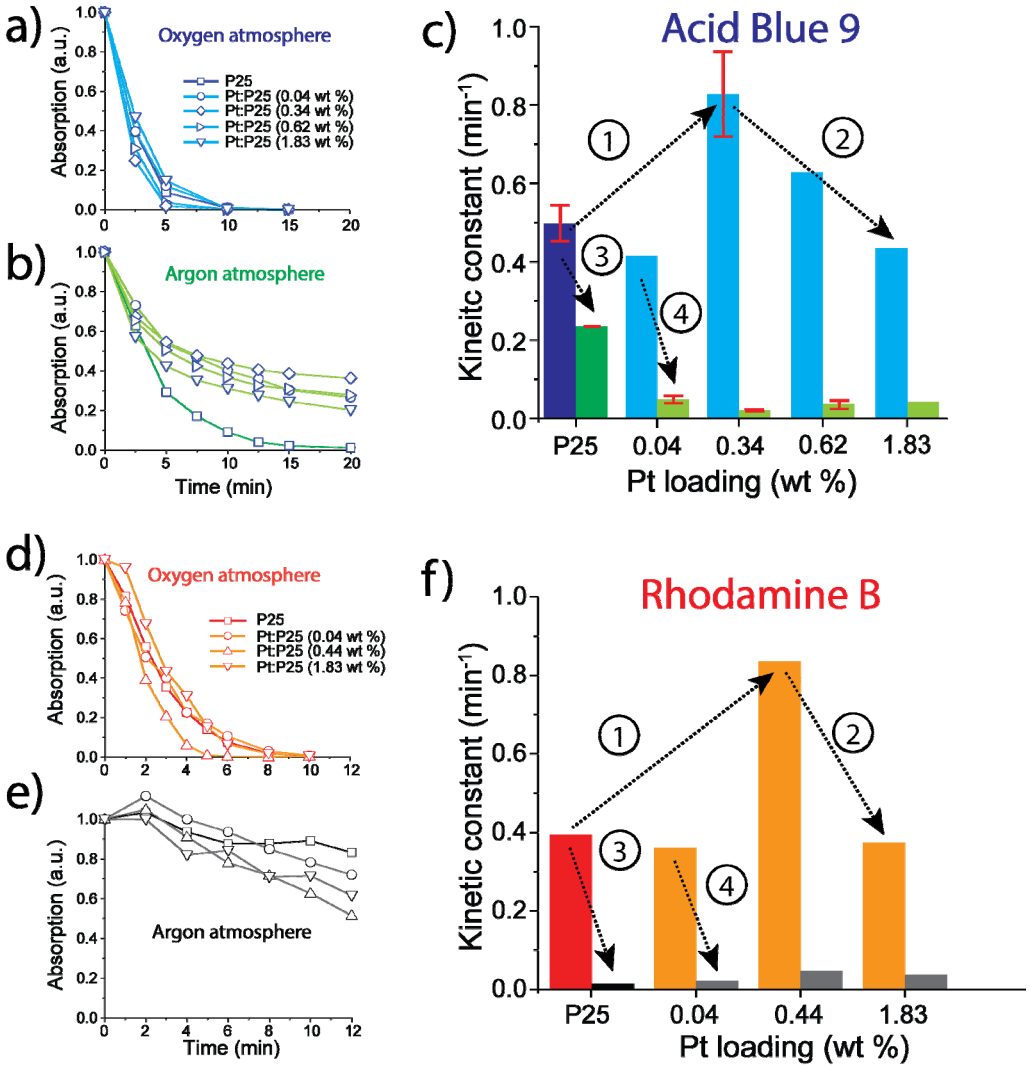

Figure 2.6: Degradation of different dyes in Ar and Oxygen atmosphere: a) Time dependent absorption of dissolved Acid Blue 9 in solutions of TiO_2 (P25) with various Pt catalyst loadings in an O_2 atmosphere and b) in an Ar atmosphere. c) Kinetic constants for the conversion of Acid Blue 9 at different Pt catalyst loadings in an O_2 (blue, 0 – 5 min, more information see SI Fig. S2.4) and Ar atmosphere (green, 10 – 20 min, more information see SI Fig. S2.4). d) Time dependent absorption of dissolved Rhodamine B in dispersions of TiO_2 (P25) with various Pt catalyst loadings in an O_2 and e) Ar atmosphere. f) Kinetic constants for the conversion of Rhodamine B at different Pt catalyst loadings under O_2 atmosphere (red) and Ar atmosphere (black).

Interestingly, we can observe 4 different effects (indicated by the numbers in Fig. 2.6c) and f)):

1) Under O_2 atmosphere, the photocatalytic activity increases to the maximum at 0.34 wt% Pt for both dyes (see also Fig. 2.2).
2) Further increase in the loading of Pt decreases the photocatalytic activity to even lower values than TiO_2 (P25) for both dyes (see also Fig. 2.2).
3) Photoactivity only halves for TiO_2 (P25) in Ar atmosphere for Acid Blue 9 but significantly diminishes for the degradation of Rhodamine B.
4) For both dyes, the photocatalytic activity drops drastically in Ar atmosphere for all Pt:TiO_2(P25)samples.

The degradation of Rhodamine B in inert atmosphere results in a strong suppression of the photocatalytic activity for both TiO_2 (P25) and Pt:TiO_2(P25) (Fig. 2.6f). For Acid Blue 9, the behavior is different. While the argon atmosphere hampers the activity of Pt:TiO_2(P25)drastically, especially in the later stage of the reaction, a significantly higher activity remains for TiO_2(P25) compared to Pt:TiO_2(P25) (Fig. 2.5a-c). These results show that dissolved O_2 is a crucial factor in the degradation of both dyes. Without O_2 dissolved in the water, Pt:TiO_2 (P25) is a worse catalyst than pure TiO_2 (P25) for the degradation of Acid Blue 9. Since the electron transfer within materials is usually not influenced by conditions in the solution, the photo-generated electrons will transfer in both cases (O_2 and Ar atmosphere) to the Pt clusters raising the question about the fate of the electrons in the Pt clusters. Two options can be proposed: 1) the electrons are harvested from the surface of the Pt cluster to generate ROS, 2) in case no electron harvesting at the surface is possible, additional photo-generated electrons will charge up the Pt cluster, increasing the probability of charge recombination at the Pt-TiO_2 interface.

In an oxygen atmosphere, the dissolved O_2 will adsorb on the surface of Pt and subsequently consume the electrons available in the Pt cluster to generate superoxide (O_2^{-*}) radicals, which will degrade the dyes in the water. In the case of an Ar atmosphere, the electrons cannot react with O_2 and, therefore, won't be able to assist this photocatalytic degradation route. Nevertheless, that would still allow the holes in the TiO_2 to react on the surface to generate OH radicals or degrade the dye directly. However, the activity drops drastically for Pt:TiO_2(P25) which demonstrates that not only neither of the degradation pathways (via direct oxidation, via hydroxyl or superoxide radical formation) but also other sacrificial reactions such as H_2 evolution (which could harvest the electrons form the Pt clusters and allow degradation pathway via the valence band) are not very active under these conditions of argon atmosphere. This behavior suggests to be caused by the intrinsic behavior of Pt. Theoretical calculations from Muhich et al. [18] indicate that Pt (in addition to an electron collector) also acts as an electron-hole recombination center, where electrons and holes recombine in the Pt cluster, and this affects the activity more predominantly when the electrons cannot be harvested by O_2 leading to a worse photocatalytic activity compared to TiO_2. On the other hand, according to Muhich's calculations, Pt clusters

on the surface of TiO_2 will improve the adsorption of O_2 with respect to the intrinsic TiO_2 surface, improving the ROS formation to degrade organic pollutants faster. [18] From our results, it becomes clear that for low Pt loadings, O_2 can easily consume all the electrons from the few Pt clusters because the surface of Pt is supplied with enough O_2 so that the benefit of electron consumption by adsorbed O_2 is stronger than the recombination of electrons with holes. As soon there is too much Pt on the surface, insufficient O_2 can be provided for the consumption of all electrons provided by the Pt-surface due to diffusion limiting the transport of O_2 to the Pt-surface, which leads to a more pronounced electron-hole recombination at the Pt-TiO_2 interface becoming the rate-limiting step in the reaction mechanism. This interaction between a beneficial (O_2 adsorption and electron consumption) effect and a disadvantageous (electron-hole recombination) effect explains why an optimal Pt loading for the photocatalytic degradation of dyes by TiO_2-Pt is observed. In this context, it is expected that not only the Pt loading but also the Pt cluster size and morphology will play an essential role [39-40] in the O_2 adsorption versus charge recombination mechanism due to the difference in surface to volume ratio, which would be a relevant property to investigate in future research.

The degradation of Rhodamine B under an argon atmosphere is majorly obstructed for both TiO_2 (P25) and Pt:TiO_2(P25) (Fig. 2.6d-f). The difference to Acid Blue 9 is the charge and the related adsorption on the surface. The zwitterionic Rhodamine B molecule does not adsorb on the surface due to only weak electrostatic interactions (Fig 2.4b). This means that a direct degradation of dyes via holes in the TiO_2 valence band is unlikely. Similarly, dye degradation via surface generated OH^* has no substantial contribution. Without both, this degradation mechanism and the dominance of the consumption of the conduction band electrons by O_2, the photocatalytic activity drops to a minimum as a result of the charge recombination. In contrast, TiO_2 (P25) readily degrades Acid Blue 9 in an Ar atmosphere. This is caused by the degradation reaction of free holes in the TiO_2 with absorbed Acid Blue 9. However, the fate of excited electrons in the CB remains unclear from our present experiments. One possibility is that electrons may be harvested by either other sacrificial reactions such as reduction of water or the adsorbed dye molecules, but this investigation is beyond the scope of this study. This finding substantiates that direct oxidation has a high significance in the degradation pathway of Acid Blue 9 using TiO_2 (P25).

In the case of the Pt:TiO_2(P25) samples, the activity changes for Acid Blue 9 degradation in Ar atmosphere throughout the experiment from an initial higher value (0 – 10 min) , which about 50 % lower than that of TiO_2 (P25), to a very low activity after 10 min (Figs. S2.3, S4.4). Despite that difference in activity according to 1st order kinetics, applying those kinetics gives a chance to still compare both cases. The higher activity in the beginning (0 – 10 min), indicating a deviation from pure quasi 1st order kinetics during the whole course of the reaction, could have two reasons. Since Acid Blue 9 adsorbs on the surface the degradation on Pt:TiO_2(P25) occurs via the generated holes from the TiO_2. The electrons will transfer to the Pt clusters, where the harvesting of electrons due to a lack of O_2 is not possible, which leads to a charge up

of the Pt increasing the recombination rate with the holes in the TiO_2. Secondly, Pt is often used as an oxygen reduction catalyst [39] and readily adsorbs oxygen at its surface. Even with extensive degassing via sonication while purging with Ar and a continuous Ar flow prior to the reaction, the Pt nanoclusters might be able due to strong interaction with O_2 to bind oxygen at its surface. This limited amount of oxygen, bound on the Pt surface, is consumed in the first stages of the irradiation to harvest the electrons in the Pt, leading to decomposition of the adsorbed Acid Blue 9 with a high reaction rate. After depletion of the remained dissolved and adsorbed O_2, the kinetic constant further drops due to the increasing probability of charge recombination of the electrons in the Pt clusters with the holes in the TiO_2. However, this behavior of an initial higher kinetic constant is not observed for the degradation of Rhodamine B in Ar atmosphere, drawing the importance towards the adsorption of the pollutant. Therefore, it is more likely that the direct oxidation due to adsorption of Acid Blue 9 is the determining factor for this behavior.

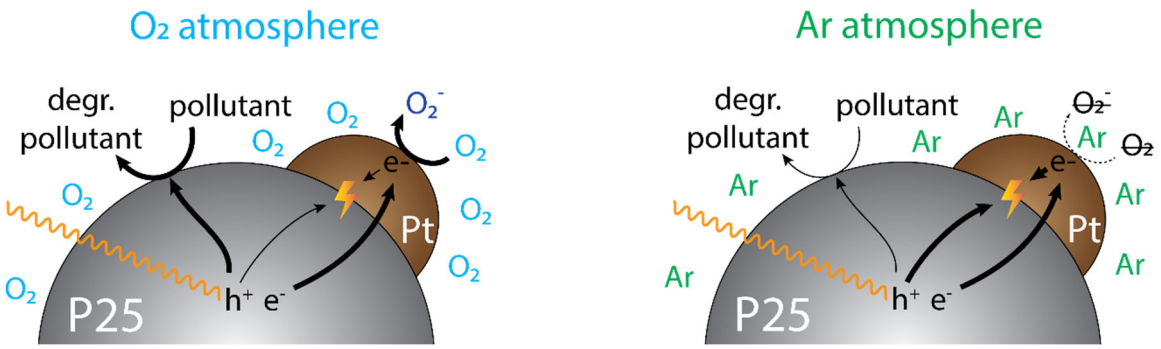

Figure 2.7: Proposed mechanism of photocatalytic dye decomposition for Pt:TiO_2(P25) in O_2 (left) and Ar (right) atmosphere, the thickness of the arrows indicates the probability of the events.

Summarizing the photocatalytic properties, Pt clusters on TiO_2 (P25) nanoparticles don't affect the creation of charge carriers by light absorption in TiO_2, observing only an absorption increase in the range of visible light caused by the metallic state of Pt itself but no change in the UV-absorption properties of TiO_2. However, with higher loading, the Pt clusters themselves will absorb and consequently block light reaching the TiO_2 surface with a possible negative influence on the photocatalytic activity. The fate of charge carriers is strongly determined by the deposition of Pt clusters. Photogenerated electrons are separated from the holes by transferring to the Pt clusters and will react further in the presence of O_2 to generate reactive oxygen species. On the other hand, in case no O_2 is present, electrons will not be consumed by sacrificial redox reactions, but easily recombine with the holes in TiO_2 inhibiting the photocatalytic activity (Fig. 2.7). This makes the presence of sufficient O_2 the crucial factor determining the efficiency of the photocatalytic degradation of dyes using Pt:TiO_2(P25) because dissolved O_2 will harvest the separated electrons in the Pt cluster, preventing the electron-hole recombination independent on the pollutant.

This detailed insight into the photocatalytic dye-degradation mechanism using Pt:TiO_2(P25) gives the opportunity to smartly design photocatalytic materials that optimize different parts of the photocatalysis mechanism, such as the improvement of light absorption or the efficient generation of ROS via electrons in the conduction band. Furthermore, understanding the behavior in different atmospheres is especially valuable for later developments of bringing the Pt:TiO_2(P25) photocatalyst into practice where contaminated water sources might suffer a lack of oxygen due to external influences such as algae growth.

2.3. CONCLUSIONS

Using an atomic layer deposition, we deposited Pt clusters on TiO_2 (P25) nanoparticles at a temperature as low as 100 °C. Depositing various loadings of Pt (0.04 wt % to 3.13 wt % Pt) gave us the opportunity to investigate the role of Pt on TiO_2 (P25) for a range of Pt loadings on the photocatalytic degradation of Acid Blue 9 and Rhodamine B. The synthesized Pt:P25 catalysts exhibited an optimal photocatalytic activity at very low loadings (i.e. 0.36 wt. % Pt) for the degradation of Acid Blue 9 and Rhodamine B under ambient conditions. However, experiments under Ar versus O_2 atmosphere demonstrated the importance of O_2 dissolved in the reactor suspension. Testing the degradation of two different pollutants under inert conditions (Ar atmosphere) the Pt:TiO_2(P25) catalyst showed a tremendous decrease in activity compared to the reaction under O_2 atmosphere, independent on the Pt loading, whereas TiO_2 (P25) remained partly active for the degradation of Acid Blue 9. It can be concluded that O_2 is the critical factor to efficiently harvest the at the TiO_2-Pt interface separated electrons, which are transferred to the Pt clusters. Without the consumption of electrons by O_2 at the Pt surface, the recombination of electrons in the Pt and holes at the Pt-TiO_2 interface dominates the reaction mechanism leading to a poor photocatalytic activity. In an O_2 atmosphere, for low loadings of Pt, the consumption of electrons by oxygen adsorbed on the Pt surface plays the predominant role in enhancing the photocatalytic activity. At higher Pt loadings, the disadvantageous charge recombination properties of Pt exceed the positive effects of O_2 adsorption and the overall photocatalytic efficiency drops even below the initial value of TiO_2 (P25). These findings add experimental proof to the theoretically proposed reaction mechanism by Muhich et al. [18]

APPENDIX

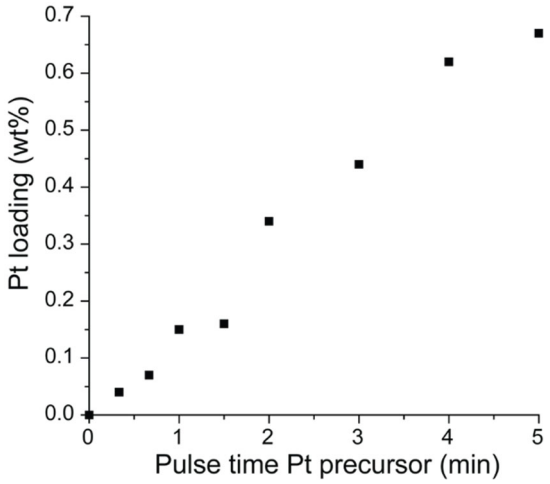

Figure S2.1: Loading from ICP-OES of Platinum on P25 particles (Pt/Ti, wt/wt%).

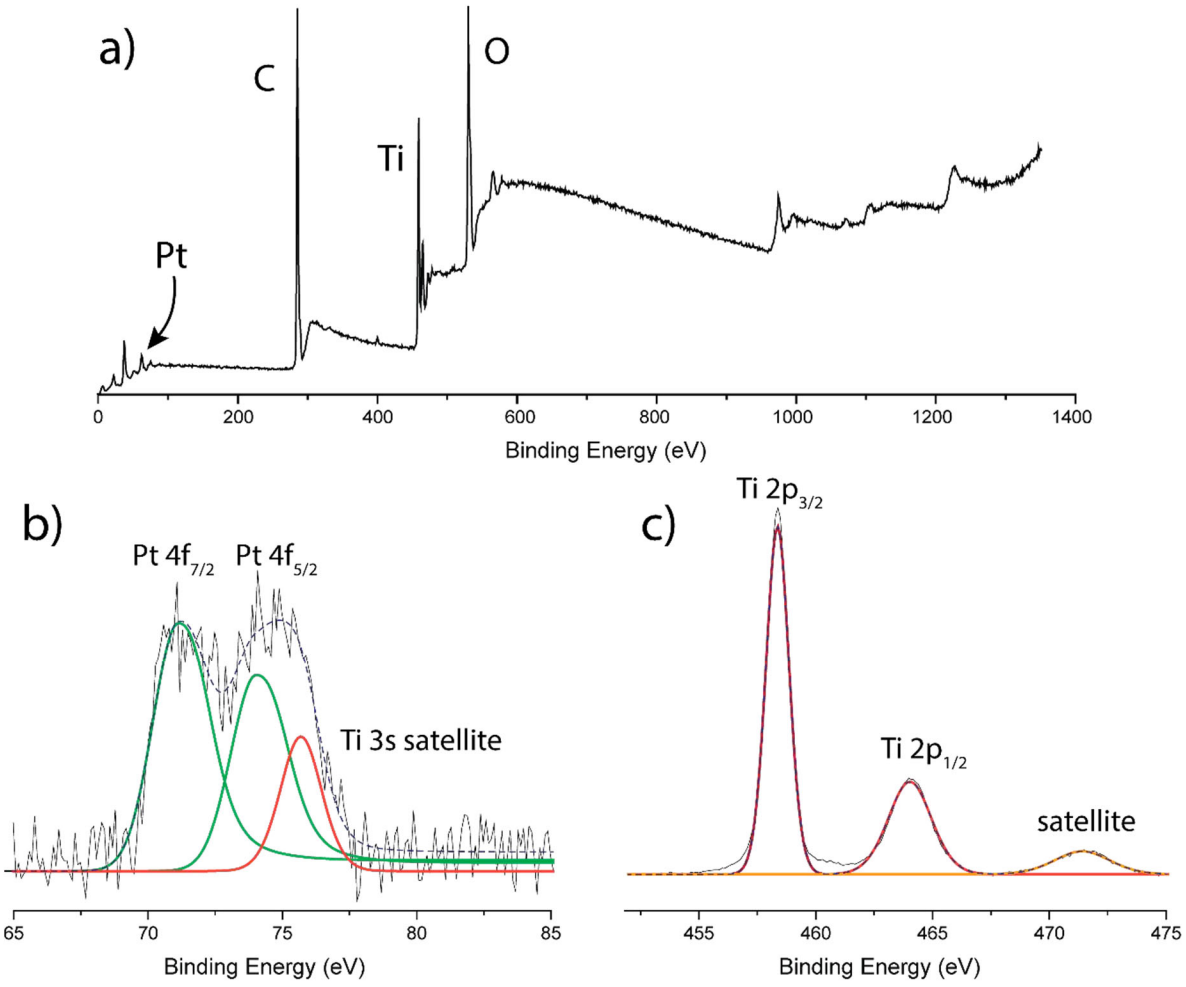

Figure S2.2: a) XPS spectrum for Pt:P25 (0.62 wt %), b) HRXPS spectrum in Pt4f region, c) HRXPS spectrum in Ti2p region.

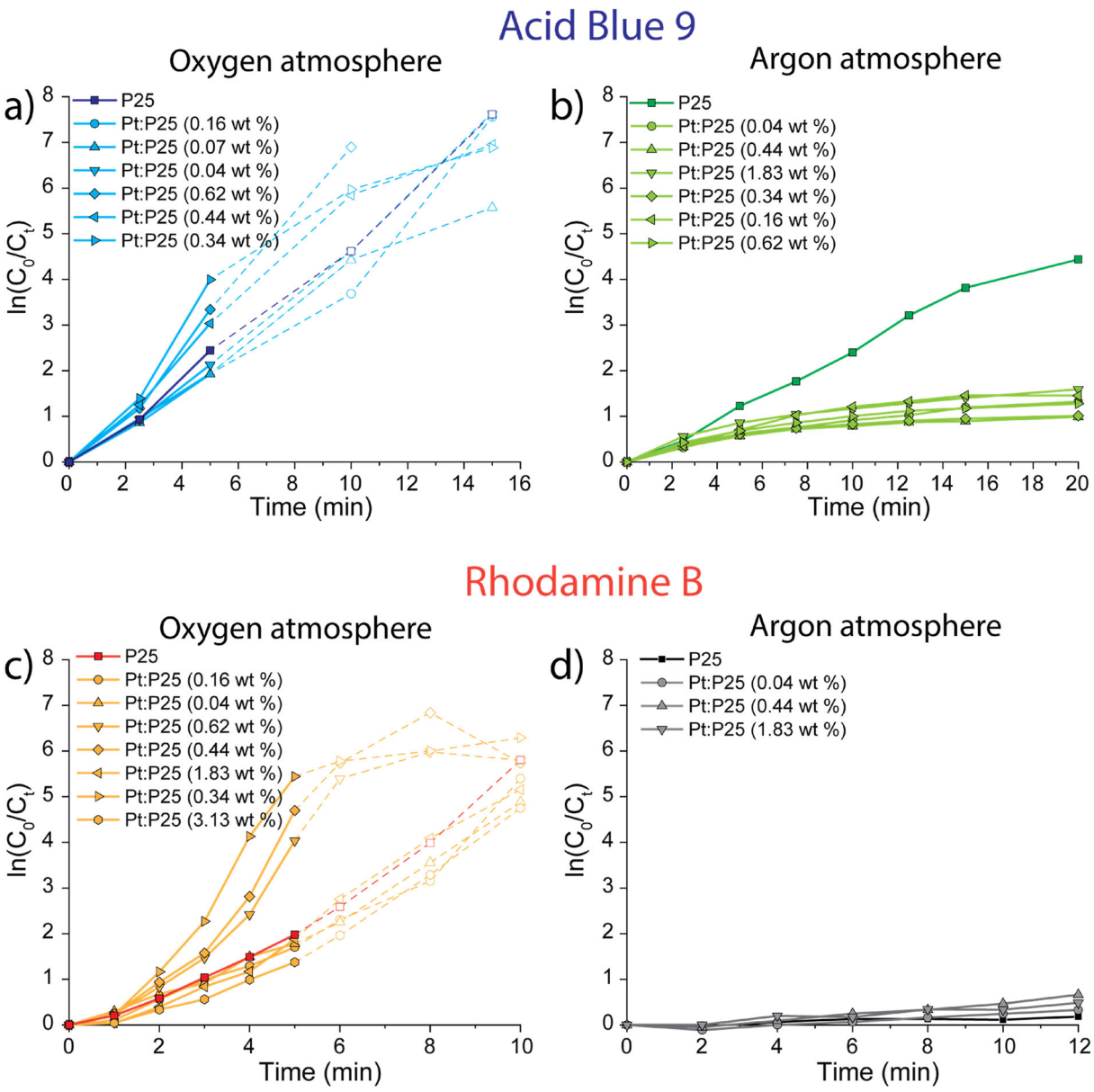

Figure S2.3: Plots of the degradation of Acid Blue 9 and Rhodamine B according to 1st order kinetics; a) Acid Blue 9 in O_2 atmosphere, b) Acid Blue 9 in Ar atmosphere, c) Rhodamine B in O_2 atmosphere, d) Rhodamine B in Ar atmosphere. For the calculation of the kinetic constants, values originated from a too low concentration were excluded. Due to the dependency on the natural logarithm, the error would increase, leading to unreliable results. Furthermore, at the end of the reaction, 1st order kinetics are not valid anymore due to a lack of reactant.

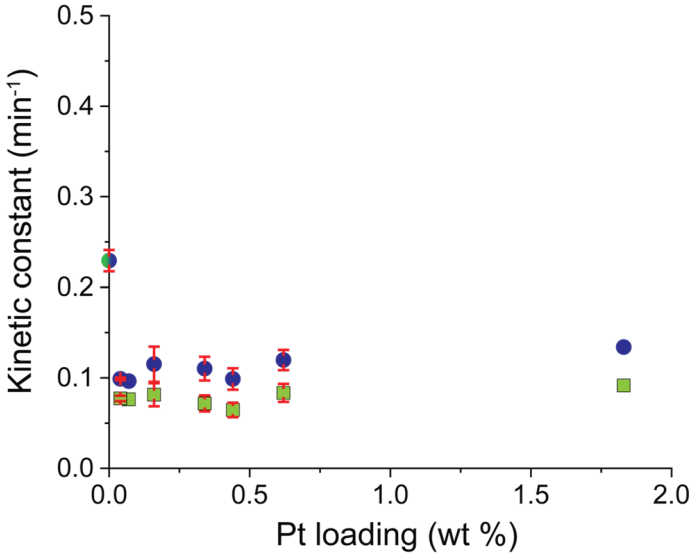

Figure S2.4: Kinetic constants for the degradation of Acid Blue 9 in Ar atmosphere (Fig. S3b). The calculation of the kinetic constant is divided into two reaction regimes. Blue circles represent the kinetic constant calculated using the values form 0 – 10 min. Green squares represent the kinetic constant using the values 10 – 20 min. For P25, no change in kinetics could be observed. Therefore, the kinetic constant was calculated using all values from 0 – 20 min.

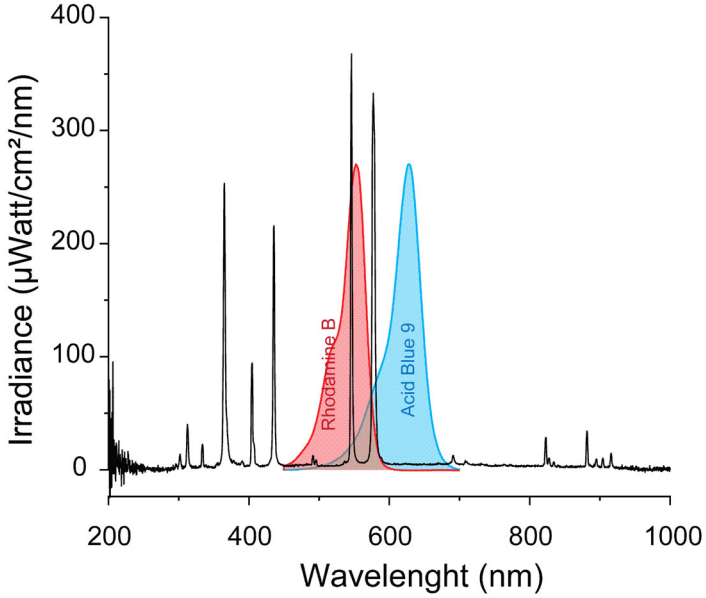

Figure S2.5: Irradicance spectrum (black) from Deep UV Mercury lamp used to irradiate photocatalysts. Since the sample was irradiated from the side, this spectrum represents the light which reached inside the reactor. As insets are the absorption spectra from Acid Blue 9 (blue) and Rhodamine B (red) depicted in the range of 450 to 700 nm.

REFERENCES

1. Zhang, J.; Nosaka, Y., Mechanism of the OH Radical Generation in Photocatalysis with TiO_2 of Different Crystalline Types. *The Journal of Physical Chemistry C* **2014,** *118* (20), 10824-10832.
2. Linsebigler, A. L.; Lu, G.; Yates, J. T., Photocatalysis on TiO_2 Surfaces: Principles, Mechanisms, and Selected Results. *Chemical Reviews* **1995,** *95* (3), 735-758.
3. Mortazavian, S.; Saber, A.; James, D. E., Optimization of Photocatalytic Degradation of Acid Blue 113 and Acid Red 88 Textile Dyes in a UV-C/TiO_2 Suspension System: Application of Response Surface Methodology (RSM). *Catalysts* **2019,** *9* (4).
4. Ahmed, S.; Rasul, M. G.; Martens, W. N.; Brown, R.; Hashib, M. A., Advances in Heterogeneous Photocatalytic Degradation of Phenols and Dyes in Wastewater: A Review. *Water, Air, & Soil Pollution* **2010,** *215* (1-4), 3-29.
5. Reza, K. M.; Kurny, A. S. W.; Gulshan, F., Parameters affecting the photocatalytic degradation of dyes using TiO_2: a review. *Applied Water Science* **2015,** *7* (4), 1569-1578.
6. Motegh, M.; van Ommen, J. R.; Appel, P. W.; Kreutzer, M. T., Scale-Up Study of a Multiphase Photocatalytic Reactor-Degradation of Cyanide in Water over TiO_2. *Environmental Science & Technology* **2014,** *48* (3), 1574-1581.
7. Gaya, U. I., Mechanistic Principles of Photocatalytic Reaction. In *Heterogeneous Photocatalysis Using Inorganic Semiconductor Solids*, Gaya, U. I., Ed. Springer Netherlands: Dordrecht, 2014; pp 73-89.
8. Hoffmann, M. R.; Martin, S. T.; Choi, W.; Bahnemann, D. W., Environmental Applications of Semiconductor Photocatalysis. *Chemical Reviews* **1995,** *95* (1), 69-96.
9. Gaya, U. I., Principles of Heterogeneous Photocatalysis. In *Heterogeneous Photocatalysis Using Inorganic Semiconductor Solids*, Springer Netherlands: Dordrecht, 2014; pp 1-41.
10. Goulas, A.; van Ommen, J. R., Atomic layer deposition of platinum clusters on titania nanoparticles at atmospheric pressure. *Journal of Materials Chemistry A* **2013,** *1* (15), 4647-4650.
11. Zhou, Y.; King, D. M.; Liang, X.; Li, J.; Weimer, A. W., Optimal preparation of Pt/TiO_2 photocatalysts using atomic layer deposition. *Applied Catalysis B: Environmental* **2010,** *101* (1-2), 54-60.
12. Driessen, M. D.; Grassian, V. H., Photooxidation of Trichloroethylene on Pt/TiO_2. *The Journal of Physical Chemistry B* **1998,** *102* (8), 1418-1423.
13. Nasr, O.; Mohamed, O.; Al-Shirbini, A.-S.; Abdel-Wahab, A.-M., Photocatalytic degradation of acetaminophen over Ag, Au and Pt loaded TiO_2 using solar light. *Journal of Photochemistry and Photobiology A: Chemistry* **2019,** *374*, 185-193.
14. Vaiano, V.; Iervolino, G.; Sannino, D.; Murcia, J. J.; Hidalgo, M. C.; Ciambelli, P.; Navío, J. A., Photocatalytic removal of patent blue V dye on Au-TiO_2 and Pt-TiO_2 catalysts. *Applied Catalysis B: Environmental* **2016,** *188*, 134-146.
15. Ofiarska, A.; Pieczyńska, A.; Fiszka Borzyszkowska, A.; Stepnowski, P.; Siedlecka, E. M., Pt–TiO2-assisted photocatalytic degradation of the cytostatic drugs ifosfamide and cyclophosphamide under artificial sunlight. *Chemical Engineering Journal* **2016,** *285*, 417-427.
16. Kryukova, G. N.; Zenkovets, G. A.; Shutilov, A. A.; Wilde, M.; Günther, K.; Fassler, D.; Richter, K., Structural peculiarities of TiO_2 and Pt/TiO_2 catalysts for the photocatalytic oxidation of aqueous solution of Acid Orange 7 Dye upon ultraviolet light. *Applied Catalysis B: Environmental* **2007,** *71* (3), 169-176.
17. Dorothy, A. A.; Subramaniam, N. G.; Panigrahi, P., Tuning electronic and optical properties of TiO2 with Pt/Ag doping to a prospective photocatalyst: a first principles DFT study. *Materials Research Express* **2019,** *6* (4).
18. Muhich, C. L.; Zhou, Y.; Holder, A. M.; Weimer, A. W.; Musgrave, C. B., Effect of Surface Deposited Pt on the Photoactivity of TiO_2. *The Journal of Physical Chemistry C* **2012,** *116* (18), 10138-10149.
19. Saputera, W. H.; Scott, J. A.; Friedmann, D.; Amal, R., Revealing the key oxidative species generated by Pt-loaded metal oxides under dark and light conditions. *Applied Catalysis B: Environmental* **2018,** *223*, 216-227.
20. Saputera, W. H.; Scott, J.; Ganda, N.; Low, G. K. C.; Amal, R., The role of adsorbed oxygen in formic acid oxidation by Pt/TiO_2 facilitated by light pre-treatment. *Catalysis Science & Technology* **2016,** *6* (17), 6679-6687.
21. Pepin, P. A.; Lee, J. D.; Foucher, A. C.; Murray, C. B.; Stach, E. A.; Vohs, J. M., The Influence of Surface Platinum Deposits on the Photocatalytic Activity of Anatase TiO_2 Nanocrystals. *The Journal of Physical Chemistry C* **2019,** *123* (16), 10477-10486.

22. Hu, X. F.; Ji, H. H.; Wu, L., Singlet oxygen photogeneration and 2,4,6-TCP photodegradation at Pt/TiO_2 under visible light illumination. *Rsc Advances* **2012,** *2* (32), 12378-12383.
23. Vijayan, B. K.; Dimitrijevic, N. M.; Wu, J.; Gray, K. A., The Effects of Pt Doping on the Structure and Visible Light Photoactivity of Titania Nanotubes. *The Journal of Physical Chemistry C* **2010,** *114* (49), 21262-21269.
24. Bamwenda, G. R.; Tsubota, S.; Nakamura, T.; Haruta, M., Photoassisted hydrogen production from a water-ethanol solution: a comparison of activities of Au:TiO_2 and Pt:TiO_2. *Journal of Photochemistry and Photobiology A: Chemistry* **1995,** *89* (2), 177-189.
25. Ding, X.; An, T.; Li, G.; Zhang, S.; Chen, J.; Yuan, J.; Zhao, H.; Chen, H.; Sheng, G.; Fu, J., Preparation and characterization of hydrophobic TiO2 pillared clay: The effect of acid hydrolysis catalyst and doped Pt amount on photocatalytic activity. *Journal of Colloid and Interface Science* **2008,** *320* (2), 501-507.
26. van Ommen, J. R.; Goulas, A., Atomic layer deposition on particulate materials. *Materials Today Chemistry* **2019,** *14*, 100183.
27. Beetstra, R.; Lafont, U.; Nijenhuis, J.; Kelder, E. M.; van Ommen, J. R., Atmospheric Pressure Process for Coating Particles Using Atomic Layer Deposition. *Chemical Vapor Deposition* **2009,** *15* (7-9), 227-233.
28. Kroeze, J. E.; Savenije, T. J.; Warman, J. M., Electrodeless Determination of the Trap Density, Decay Kinetics, and Charge Separation Efficiency of Dye-Sensitized Nanocrystalline TiO_2. *Journal of the American Chemical Society* **2004,** *126* (24), 7608-7618.
29. Lee, J.; Choi, W., Photocatalytic Reactivity of Surface Platinized TiO_2: Substrate Specificity and the Effect of Pt Oxidation State. *The Journal of Physical Chemistry B* **2005,** *109* (15), 7399-7406.
30. Wang, P.; Cheng, M.; Zhang, Z., On different photodecomposition behaviors of rhodamine B on laponite and montmorillonite clay under visible light irradiation. *Journal of Saudi Chemical Society* **2014,** *18* (4), 308-316.
31. K, A.; B.M, J. A., TiO_2-Pt composite photocatalyst for photodegradation and chemical reduction of recalcitrant organic pollutants. *Journal of Environmental Chemical Engineering* **2018,** *6* (5), 5720-5731.
32. Zhou, Y.; King, D. M.; Liang, X.; Li, J.; Weimer, A. W., Optimal preparation of Pt/TiO_2 photocatalysts using atomic layer deposition. *Applied Catalysis B: Environmental* **2010,** *101* (1), 54-60.
33. Siuzdak, K.; Sawczak, M.; Klein, M.; Nowaczyk, G.; Jurga, S.; Cenian, A., Preparation of platinum modified titanium dioxide nanoparticles with the use of laser ablation in water. *Physical Chemistry Chemical Physics* **2014,** *16* (29), 15199-15206.
34. Mehrotra, K.; Yablonsky, G. S.; Ray, A. K., Kinetic Studies of Photocatalytic Degradation in a TiO_2 Slurry System: Distinguishing Working Regimes and Determining Rate Dependences. *Ind. Eng. Chem. Res.* **2003,** *42* (11), 2273-2281.
35. Bumajdad, A.; Madkour, M., Understanding the superior photocatalytic activity of noble metals modified titania under UV and visible light irradiation. *Phys Chem Chem Phys* **2014,** *16* (16), 7146-58.
36. Carneiro, J. T.; Savenije, T. J.; Moulijn, J. A.; Mul, G., The effect of Au on TiO2 catalyzed selective photocatalytic oxidation of cyclohexane. *Journal of Photochemistry and Photobiology A: Chemistry* **2011,** *217* (2), 326-332.
37. Kmetyko, A.; Mogyorosi, K.; Gerse, V.; Konya, Z.; Pusztai, P.; Dombi, A.; Hernadi, K., Photocatalytic H(2) Production Using Pt-TiO_2 in the Presence of Oxalic Acid: Influence of the Noble Metal Size and the Carrier Gas Flow Rate. *Materials (Basel)* **2014,** *7* (10), 7022-7038.
38. Dessal, C.; Martínez, L.; Maheu, C.; Len, T.; Morfin, F.; Rousset, J. L.; Puzenat, E.; Afanasiev, P.; Aouine, M.; Soler, L.; Llorca, J.; Piccolo, L., Influence of Pt particle size and reaction phase on the photocatalytic performances of ultradispersed Pt/TiO_2 catalysts for hydrogen evolution. *Journal of Catalysis* **2019,** *375*, 155-163.
39. Xu, S.; Kim, Y.; Park, J.; Higgins, D.; Shen, S.-J.; Schindler, P.; Thian, D.; Provine, J.; Torgersen, J.; Graf, T.; Schladt, T. D.; Orazov, M.; Liu, B. H.; Jaramillo, T. F.; Prinz, F. B., Extending the limits of Pt/C catalysts with passivation-gas-incorporated atomic layer deposition. *Nature Catalysis* **2018,** *1* (8), 624-630.
40. Wang, D.; Liu, Z.-P.; Yang, W.-M., Revealing the Size Effect of Platinum Cocatalyst for Photocatalytic Hydrogen Evolution on TiO_2 Support: A DFT Study. *ACS Catalysis* **2018,** *8* (8), 7270-7278.

Atmospheric pressure atomic layer deposition of ultralow-loading Cu_2O nanoclusters on TiO_2 nanoparticles for enhanced photocatalytic removal of organic pollutants

3

This work presents a gas-phase approach for the synthesis of Cu_2O/TiO_2 powder-based photocatalysts using atomic layer deposition (ALD). The process was carried out in a fluidized bed reactor working at atmospheric pressure using (trimethylvinylsilyl)-hexafluoroacetylacetonate copper(I) as Cu-precursor and water vapor as oxidizer. With this technique, ultrasmall Cu_2O clusters with an average diameter of 1.3 – 1.5 nm and narrow particle size distribution were successfully deposited onto P25 TiO_2 nanopowder. The self-saturating chemical reactions between the Cu-precursor and H_2O vapor and the linear growth of ALD were achieved, allowing us to control the loading of Cu_2O on the TiO_2 surface. The photocatalytic performance of Cu_2O/TiO_2 photocatalysts was tested by the degradation of organic dyes, including Rhodamine B (RhB), methyl orange (MO) and methylene blue (MB). We found that with a Cu loading of 0.4 at.%, Cu_2O/TiO_2 exhibited excellent photocatalytic activity, which was 120 %, 150 %, and 70 % higher than the photocatalytic activity of P25 TiO_2 in the degradation of RhB, MO, and MB, respectively. The photocatalytic reaction mechanism was further investigated for the degradation of RhB, revealing the dominating role of holes, which contributed to both direct surface oxidation and indirect oxidation (i.e., via the formation of hydroxyl radicals). The results obtained from our work provide a fast, feasible, and scalable process to deposit ultrasmall Cu_2O clusters in a highly controlled fashion for engineering the surface of TiO_2 powder-based materials.

Under review in Journal of Alloys and Compounds

Dominik Benz[†], Y-Nhi T. Nguyen[‡], Thanh-Hiep T. Le[‡], Thanh-Lieu T. Le[‡], J. Ruud van Ommen[†], Hao Van Bui[‖,¶*]

3.1. INTRODUCTION

Owing to its excellent photocatalytic activity, high chemical stability, low cost, and nontoxicity, titanium dioxide (TiO_2) is the most popular photocatalyst that has been used in many environmental and energy applications, such as air purification, water treatment, hydrogen production, and photovoltaics.[1-7] Among various TiO_2 nanomaterials, the commercial Evonik P25 TiO_2 nanopowder commonly exhibits the highest photocatalytic efficiency.[8] The key factor that enables the superior catalytic performance of P25 is the charge transfer at the interfaces between the interconnected rutile and anatase particles [8-9], which are the main components of P25 TiO_2. Accordingly, P25 TiO_2 is composed of nanosized anatase (ca. 70 – 85 %) and rutile crystallites and a small fraction of amorphous TiO_2.[9-11] Due to the different band alignments between anatase and rutile, the interconnection between the anatase and the rutile nanoparticles facilitates the electron transfer from anatase to rutile [12], which enhances the charge separation and consequently improves the photocatalytic efficiency.[8-9, 12-14] Nevertheless, despite its superior catalytic activity, the rapid recombination of photogenerated charge is still a major issue of P25 TiO_2 photocatalyst.[10, 15-17]

Various strategies have been developed for reducing the charge recombination in TiO_2, such as surface treatment and doping,[11, 18-22] hydrothermal treatment for improving the interconnection of TiO_2 nanoparticles and crystallization of the amorphous portion,[8, 13, 23] and surface engineering by coupling with a metallic or semiconducting material.[24-33] In the last case, noble metals, such as Pt, Pd, Au, and Ag have commonly been the materials of choice.[25-27, 30-32, 34-37] On the one hand, by virtue of their excellent catalytic activities, noble metals can act as co-catalysts when coupling with TiO_2, resulting in a synergic effect that enhances of photocatalytic performance.[31, 36-37] On the other hand, as the Fermi levels of noble metals are commonly lower than the conduction band of TiO_2, noble metals can act as electron sinks that facilitate the electron transfer from TiO_2. This increases the charge separation, which further improves the photocatalytic efficiency.[38-39] However, the high cost is a limiting factor that hinders their practical applications. Therefore, semiconducting metal oxides (SMOs), such as CuO, Fe_2O_3, and WO_3, which have been demonstrated as excellent alternative engineering materials for reducing charge recombination in TiO_2, are nowadays more attractive.[28-29, 33, 40-41] The coupling of an SMO and TiO_2 promotes the photogenerated charge transfers at the interface, which is governed by the band alignment between TiO_2 and the SMO. For instance, in CuO/TiO_2 photocatalysts, as the conduction band of CuO is lower than that of TiO_2, under UV irradiation, electrons are driven to migrate from TiO_2 to CuO, thereby increasing the lifetime of holes in TiO_2.[29] This mechanism was also applied for the charge transfer in Fe_2O_3/TiO_2 photocatalysts.[28] However, in a WO_3/TiO_2 photocatalyst, as both the conduction band and the valance band of WO_3 are lower than those of TiO_2, respectively, a double-charge transfer can take place, in which electrons migrate from TiO_2 to WO_3 while holes migrate in the opposite

direction.[42] The charge transfers between the two semiconductors result in photocatalytic enhancement.

Cuprous oxide (Cu_2O) is among the metal oxides that have been used to improve the photocatalytic performance of TiO_2.[43-45] It is a p-type semiconductor whose conduction band is much higher than that of TiO_2 and many other semiconductors.[46] As a consequence, the coupling of Cu_2O and TiO_2 can generate a type-II heterostructure, which allows different charge transfer mechanisms between the two materials.[46-47] In particular, two main charge transfer mechanisms have been observed in Cu_2O/TiO_2 photocatalysts. The first mechanism is related to the double-charge transfer between the two semiconductors.[46] According to this mechanism, as Cu_2O is a p-type semiconductor, while TiO_2 is an n-type semiconductor, the coupling of Cu_2O and TiO_2 results in the formation of a p–n junction that creates a built-in electric field. This electric field promotes the electron transfer from Cu_2O to TiO_2 due to the higher conduction band of Cu_2O (i.e., more negative) with respect to that of TiO_2, while holes are driven to migrate in the opposite direction.[17, 43, 48] The other mechanism is related to the recombination between electrons in the conduction band of TiO_2 and holes in the valance band of Cu_2O [46, 49], which is commonly known as the Z-scheme mechanism.[50-51] Both mechanisms reduce the charge recombination in bulk TiO_2, which consequently improves the photocatalytic performance. Importantly, the Z-scheme charge transfer between Cu_2O and TiO_2 can protect the Cu_2O from photocorrosion.[46, 52] Therefore, Cu_2O/TiO_2 photocatalysts have attracted great attention for applications in energy conversion and photocatalysis.[17, 43, 45, 48, 53-56]

Up to date, Cu_2O/TiO_2 photocatalysts have been mostly synthesized by wet-chemistry methods, such as precipitation,[43, 55] sol-gel,[56] chemical batch deposition,[57] solvothermal,[58] impregnation,[59] solvent reduction,[54, 60] and electrochemical.[61] Despite their great advantages of simplicity, low-cost, and the ability to develop various nanostructures, wet-chemistry methods inherently contain several drawbacks. On the one hand, the use of large amounts of chemicals and solvents for the synthesis is not favorable for large-scale production due to environmental issues. On the other hand, wet-chemistry is usually time-consuming due to the requirements of post-processing and treatment of the products, such as washing, drying, and annealing, which can take from several hours to tens of hours.[46, 54, 58-60] Moreover, wet-chemistry methods may encounter difficulties in controlling the loading, size, and composition of the deposited materials due to their strong dependence on experimental conditions, such as precursor concentration, reaction time and temperature, concentration and types of solvents, etc.[62] Therefore, developing a synthesis process that can tackle the disadvantages of wet-chemistry methods is essentially needed. To this end, atomic layer deposition (ALD) has emerged as an excellent candidate, which has been applied for depositing a number of materials such as Ni, Co, Pt, Pd, Al_2O_3, and SiO_2 on powder- and particle-based substrates.[26-27, 63-68] This is a solvent-free, gas-phase deposition technique, in which the substrate is exposed to the precursors sequentially and separately. As a consequence, the chemical reactions only take place on the substrate surface, and importantly, reactions are self-limiting, which are independent of

precursor concentration, reaction time, and temperature.[69-70] Therefore, ALD allows controlling the amount of deposited materials at the atomic level.[71]

Here, we present an ALD approach for the first time to synthesize multigram-scale Cu_2O/TiO_2 powder-based photocatalysts in a fast, solution-free, and controllable manner. The process was carried out in a fluidized bed reactor (FBR) operating at atmospheric pressure using (trimethylvinylsilyl)-hexafluoroacetylacetonate copper(I) (Cu(I)(hfac) (TMVS)) as the precursor and water vapor as the oxidizer. This enabled the growth of ultrasmall Cu_2O clusters with diameters in the range 1.3 – 1.5 nm, and a narrow particle size distribution on TiO_2 nanoparticles. We demonstrate that the self-limiting characteristics and linear growth of Cu_2O ALD were achieved, which allowed us to tailor the loading of Cu_2O in a controllable fashion. The photocatalytic activity of Cu_2O/TiO_2 photocatalysts was investigated by the photodegradation of organic dyes, including Rhodamine B (RhB), methyl orange (MO) and methylene blue (MB). We found that with a Cu loading of 0.4 %, the photocatalytic activity of Cu_2O/TiO_2 was significantly enhanced, which was 120 %, 150 %, and 70 % higher than that of pristine TiO_2 in the degradation of RhB, MO and MB, respectively. The photocatalytic reaction mechanism was further investigated for the degradation of RhB, revealing the dominating role of holes, which contributed to both direct surface oxidation and indirect oxidation (i.e., via the formation of hydroxyl radicals). Our approach provides a rapid, feasible, and scalable process to deposit ultrasmall Cu_2O clusters in a highly controlled fashion for engineering the surface of TiO_2 powder-based materials.

3.2. EXPERIMENTAL SECTION

P25 TiO_2 powder (mean diameter of 21 nm and specific surface area of 54 m^2g^{-1}) was purchased from Evonik Industries (Hanau, Germany). Cu(I)(hfac)(TMVS) contained in a stainless steel bubbler was purchased from ADVANCED TECH. & IND. CO., LTD. Rhodamine B (RhB), methanol, potassium chlorate ($KClO_3$), dimethyl sulfoxide (DMSO), and ethylenediaminetetraacetic acid (EDTA) were acquired from Sigma Aldrich and used without further purification.

The deposition was carried out in a fluidized bed reactor operating at atmospheric pressure, as described elsewhere.[72] In brief, the reactor consisted of a quartz glass column (diameter of 26 mm and height of 500 mm) placed on a vertical vibration table (Paja 40/40-24) to assist the fluidization of the nanoparticles. The reactor was heated by an IR lamp; the temperature inside the reactor was measured by a type-K thermocouple, which was connected to a PID controller to maintain the reactor temperature at a constant value.

Cu_2O was deposited using Cu(I)(hfac)(TMVS) as the precursor and H_2O as the oxidizer. The Cu-precursor bubbler was maintained at 60 °C, whereas the H_2O bubbler was kept at room temperature. The deposition temperature was 250 °C. During the deposition, a temperature variation of ±10 °C was observed. Pressurized nitrogen

(99.999 vol.%) was used as the carrier gas. For a typical ALD process with 1.3 g TiO_2 powder, a N_2 flow of 0.50 L min^{-1} was introduced from the bottom of the glass column to fluidize the powder, which was supported by a microporous distributor. For the study on the self-limiting characteristics of Cu_2O ALD, the exposure time for Cu(I)(hfac)(TMVS) was varied from 2.5 min to 30 min, whereas the exposure time for H_2O was varied from 2.5 min to 10 min. A purge of N_2 for 5 min was introduced in between the precursor doses to remove the reaction by-products and the residual precursors.

The crystal structure of the Cu_2O/TiO_2 powder was studied by X-ray diffraction (XRD) technique. XRD patterns were obtained by a PANalytical X-pert Pro diffractometer with Cu Kα radiation, secondary flat crystal monochromator, and X'celerator RTMS Detector system. The Cu concentration of the deposited Cu_2O was determined by ICP-OES technique. For each measurement, approximately 30 mg of sample was destructed in a solution consisting of 4.5 ml 30 % HCl, 1.5 ml 65 % HNO_3 and 0.2 ml 40 % HF using a microwave. The destruction time in the microwave was 60 min. After the destruction, the samples were diluted to 50 ml with MQ and analyzed with ICP-OES 5300DV.

TEM micrographs of the samples were acquired using a JEOL JEM1400 transmission electron microscope operating at a voltage of 120 kV and a current density of 50 pA cm^{-2}. As-deposited Cu_2O/TiO_2 nanoparticles were suspended in ethanol and transferred to Quantifoil TEM grids (Cu, 3.05 mm in diameter).

X-ray photoelectron spectra (XPS) were recorded on a ThermoFisher K-Alpha system using Al Kα radiation with a photon energy of 1486.7 eV. The powder samples were immobilized on Carbon tape before loading into the XPS chamber. Scans were acquired using a 400 μm spot size, 55 eV pass energy, and 0.1 eV/step with charge neutralization. The peaks positions were analyze calibrating the C 1s peak at 284.8 eV. The background was subtracted using ThermoAvantage software, applying a "smart" type background subtraction.

The photocatalytic activity of the Cu_2O/TiO_2 catalysts was investigated via the degradation of RhB solution under UV-light irradiation. For each test, 10 mg of the catalyst was dispersed in 80 ml aqueous RhB solution (10 mg L^{-1}) contained in a 200-ml glass beaker (diameter of 8 cm). To reach the adsorption-desorption equilibrium, the solution was stirred in the dark for 30 min. Thereafter, the suspension was exposed to UV-radiation generated by a mercury lamp (25 W, 620 lux at the surface of the reactor) for different exposure times. The suspension was then centrifuged to separate the solid catalyst from the solution. Finally, the solution was analyzed by UV-visible spectroscopy using a Jenway's 6800 double beam spectrophotometer to determine the residual concentration of the RhB in solution. The catalytic activity was analyzed by the first-order kinetics where the slope of $\ln(c_t/c_0)$ vs time gives the kinetic constant. For studying the role of charge carrier in the photodegradation of RhB, $KClO_3$, DMSO, and EDTA were used as the electron, hole,

and hydroxyl radical scavenger, respectively, which was added to the solid-dye suspension prior to the UV-irradiation.

3.3. RESULTS AND DISCUSSION

3.3.1. Surface morphology, composition, and structure

ALD of Cu_2O using Cu(I)(hfac)(TMVS) and H_2O was previously reported by Muñoz-Rojas et al.,[73] demonstrating that the process carried out at atmospheric pressure enabled the deposition of stoichiometric Cu_2O thin films on glass substrates at temperatures from 150 to 300 °C. Although the initial stage of the growth was not studied, the granular surface of the films observed by SEM suggests that the growth of Cu_2O starts with the formation of 3D islands. Here, our ALD in an FBR at 250 °C enabled the growth of ultrasmall clusters on the surface of TiO_2 nanoparticles. Fig. 3.1a shows the TEM image of the Cu_2O/TiO_2 nanoparticles with a Cu atomic concentration of 0.4 %. The Cu_2O particle size distribution (PSD) is shown in the inset of the TEM image. A narrow PSD with an average diameter of 1.3 ± 0.4 nm was obtained, which increased to 1.5 ± 0.4 nm for the Cu_2O/TiO_2 with a Cu atomic concentration of 1.7 % (Fig. 3.1b). XPS analysis confirms the Cu_2O phase, which is indicated by the two peaks at a binding energy of 932.6 and 952.6 eV (Fig. 3.1c). These two peaks represent the doublet states $Cu2p_{3/2}$ and $Cu2p_{1/2}$ of Cu2p core level of Cu_2O. The symmetric shape of the peaks and the absence of the satellite peaks at approximately 943 eV suggests the absence of CuO phase.

Moreover, compared to the XRD pattern of pristine TiO_2, the XRD patterns of Cu_2O/TiO_2 exhibit additional peaks at 36.0° and 43.2°, which are ascribed to the (111) and (200) planes of cubic Cu_2O phase, respectively, whereas no diffraction peak of CuO phase was found. We note that the positions of Cu_2O diffraction peaks exhibited a slight shift with respect to the standard peak positions of Cu_2O (JCPDS 05–0667). This is due to the effect of particle size on the XRD pattern, which is observed for particles with sizes below 5 nm.[74] According to the recent research by Vorontsov et al., this effect is caused by the interference fringes and is not taken into account when considering XRD patterns in standard software. As a consequence, significant shifts up to a few degrees in the XRD patterns can be observed. Nevertheless, this does not rule out the contribution of the distortions and microstrain of the crystalline structure.

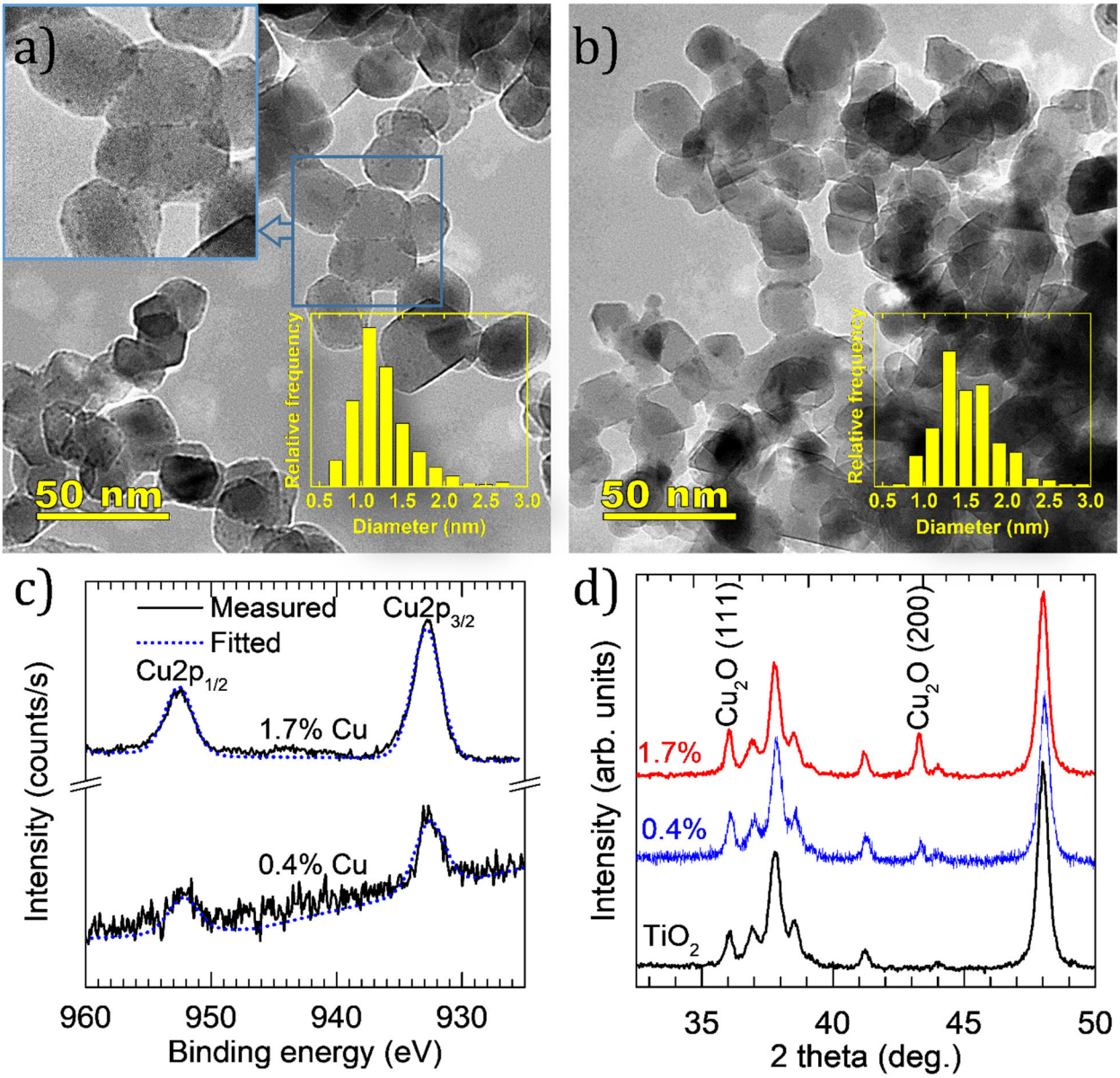

Figure 3.1: TEM images of Cu_2O ultrasmall clusters with the average diameter in the range of 1.3 – 1.5 nm (the smaller and darker dots) on TiO_2 nanoparticles with Cu concentration of 0.4 % (a) and 1.7 % (b), and the corresponding XPS spectra of Cu2p core-level (c). Their XRD patterns are shown in (d), which includes the XRD pattern of P25 TiO_2 as the reference.

The self-limiting characteristics of Cu_2O ALD were investigated by varying the dose time of the precursors. We note that, in a conventional ALD process, the dose time usually ranges from milliseconds to seconds since the materials are commonly deposited on flat substrates, i.e., with a small surface area. Here, the deposition was carried out on P25 TiO_2 nanopowder with a specific surface area of about 54 m^2g^{-1}, each of which was performed on 1.5 g of the material. As a consequence, the dose time was in the range of minutes. Our preliminary experiments showed that, for H_2O exposure, an increase of dose time from 5 min to 10 min did not result in any significant change in the Cu concentration. Therefore, a fixed H_2O dose time of 10 min was

employed to investigate the influence of Cu-precursor dose time, which was varied from 2.5 to 30 min, as demonstrated in Fig. 3.2a. In this figure, each data point represents the Cu concentration obtained after 10 ALD cycles. The results demonstrated that the Cu concentration increased rapidly when the Cu-precursor dose time increased from 2.5 min to 15 min. Thereafter, a further increase of dose time up to 30 min only resulted in a small increase in Cu concentration (i.e., from 4.6 % to 4.8 %). This indicates a saturation that represents the self-limiting characteristic of ALD. Furthermore, in the saturating regime (i.e., Cu-precursor dose time of 15 min and H_2O dose time of 10 min), Cu concentration increased linearly with the number of ALD cycles (Fig. 3.2b). This linear relationship, in conjunction with the self-limiting characteristics, reflects the ALD growth mode of Cu_2O, which allows tailoring of the Cu concentration by varying the number of ALD cycles.

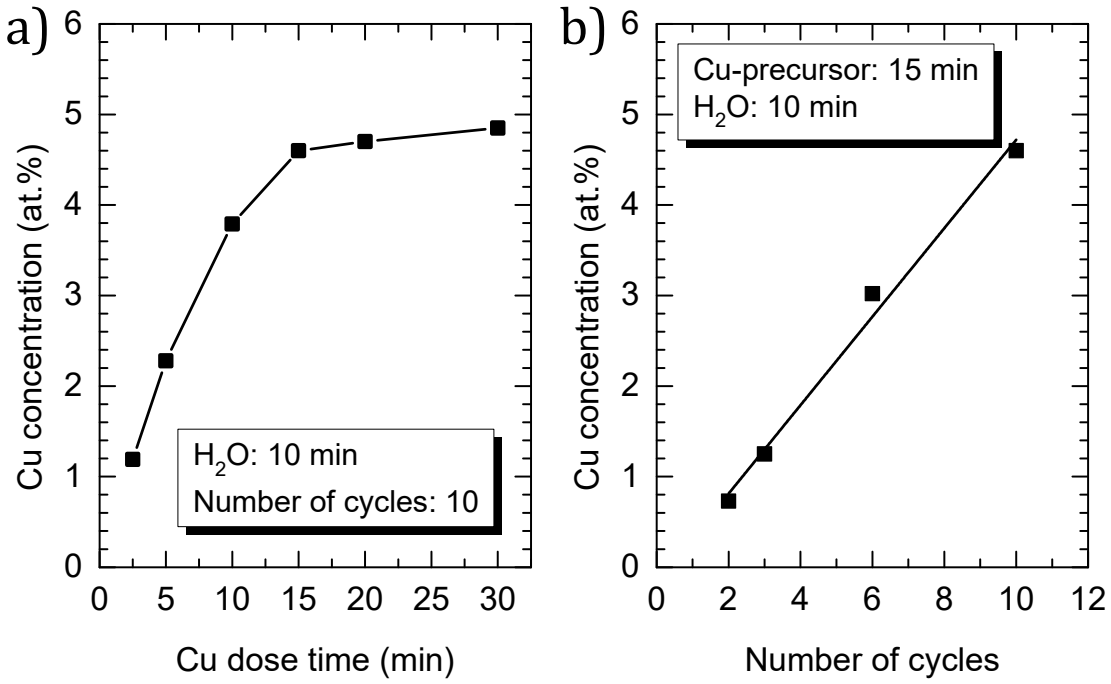

Figure 3.2: Cu concentration as a function of Cu(I)(hfac)(TMVS) dose time at a fixed H_2O dose time of 10 min (a), and Cu concentration as a function of the number of ALD cycles with the Cu-precursor and H_2O dose times of 15 min and 10 min, respectively (b).

3.3.2. Photocatalytic performance of Cu_2O/TiO_2 photocatalysts

RhB was used as a model pollutant for investigating the photocatalytic performance of the photocatalysts. Prior to the irradiation, the RhB/photocatalyst suspension was stirred continuously in the dark until the adsorption/desorption equilibrium was achieved, which was found in the range of 10 – 15 min (Fig. S3.1). During this stage, we observed that surface modification by Cu_2O slightly enhanced the adsorption of the dye molecules on the catalyst surface (ca. 5 – 7 %, Fig. S3.1). However, under the UV

irradiation, a small amount of Cu_2O could significantly alter the degradation rate of the organic pollutant, as demonstrated in Fig. 3.3a. Particularly, for the pristine TiO_2, 90 % of the RhB was degraded after 30 min of irradiation. With the presence of Cu_2O at a Cu atomic percentage of 0.4 %, the degradation time was significantly reduced (i.e., 10 min). From the kinetic plots presented in Fig. 3.3b, which were derived from the degradation curves (Fig. 3.3a),[75] the apparent first-order kinetic constants (i.e., K_{app}) that represent the degradation rate of RhB were determined and plotted in Fig. 3.3c. It was found that the degradation rate obtained for the catalyst with 0.4 % Cu was more than twofold higher than that for the pristine P25 TiO_2 (i.e., 0.123 and 0.055 min^{-1}, respectively). With increasing the Cu concentration, the degradation rate continuously decreased. For the Cu_2O/TiO_2 with 1.2 % Cu, the degradation rate was nearly identical to that of the pristine TiO_2, whereas, at a higher concentration, the photocatalytic activity was lower. The decreasing photocatalytic performance with increasing Cu_2O concentration could be due to the light-shielding effect, in which the presence of Cu_2O on the surface screens the light absorption of TiO_2.[57] We emphasize that ALD of Cu_2O on TiO_2 with 0.4 % Cu requires only 1 ALD cycle and the process carried out in a fluidized bed reactor allows to perform the deposition on multigram TiO_2 powder. Moreover, the obtained product does not need any post-treatment process such as washing, drying or annealing that is commonly required in wet-chemistry methods.[33, 46, 54, 58-60] Therefore, our technique provides a fast, scalable, and efficient route for TiO_2 surface modification to improve photocatalytic performance.

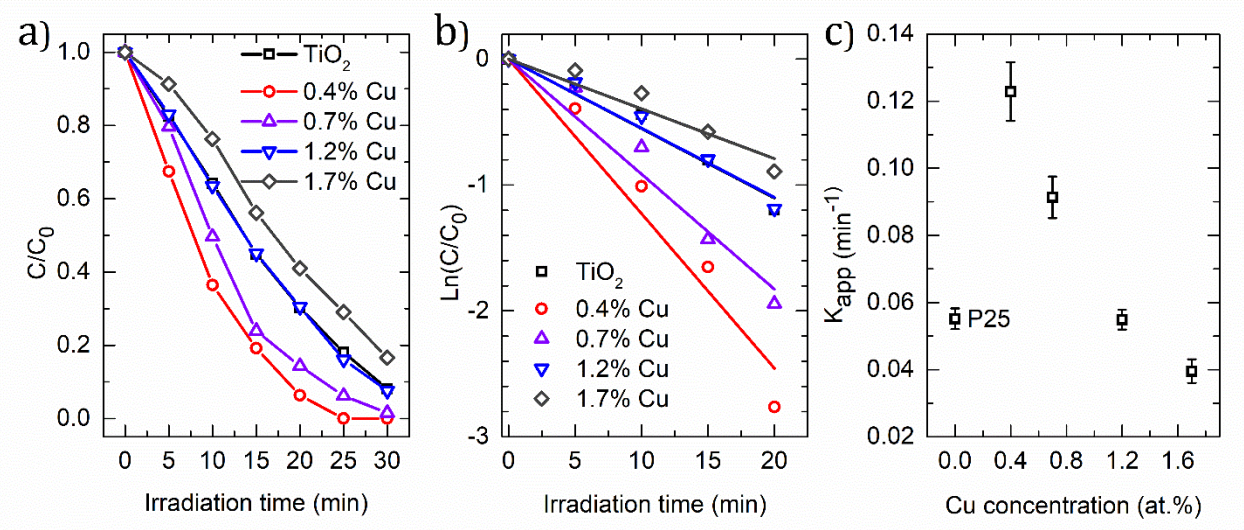

Figure 3.3: Photodegradation of RhB by P25 TiO_2 and Cu_2O/TiO_2 photocatalysts as a function of irradiation time (a) and the corresponding kinetic plots (b), from which the first-order kinetic constants were determined and plotted (c).

The improved photocatalytic performance by depositing Cu_2O was also observed for the photodegradation of methyl orange (MO) and methylene blue (MB). Fig. 3.4a demonstrates the degradation of MO and MB by pristine TiO_2 (the closed symbols)

and Cu_2O/TiO_2 with 0.4 % Cu (the open symbols). For comparison, the degradation of RhB (the dotted curves) is also included. The results show that the degradation of MO was enhanced 2.5 times, whereas an enhancement of 1.7 times was achieved for the degradation of MB (Fig. 3.4b). This further confirms the excellent photocatalytic properties of Cu_2O/TiO_2 over TiO_2.

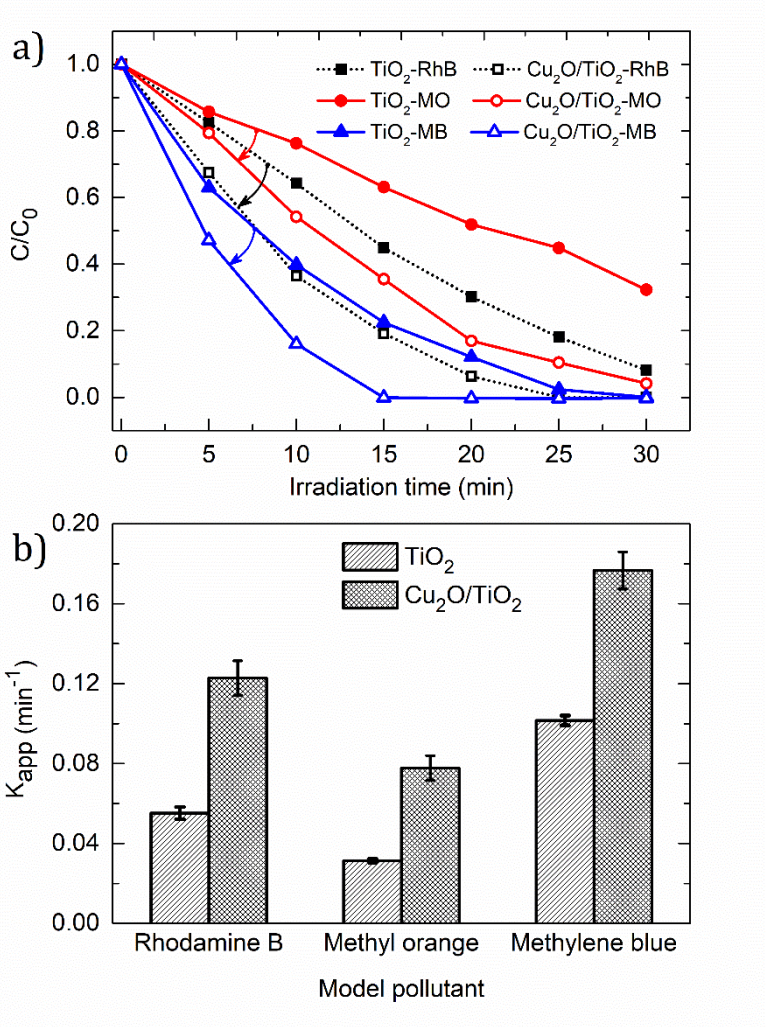

Figure 3.4: Degradation of MO and MB by pristine TiO_2 and Cu_2O/TiO_2 (0.4 % Cu) photocatalysts (a) and the corresponding degradation rate constants (b). The data for RhB degradation are included for comparison. The arrows in (a) show the change of the photodegradation curves from the TiO_2 to the Cu_2O/TiO_2.

3.3.3. Roles of holes in the photodegradation of RhB by Cu_2O/TiO_2 photocatalyst

It has been demonstrated that the photodegradation of organic pollutants by TiO_2-based photocatalysts commonly proceeds via two routes: direct surface oxidation and OH* radical oxidation (i.e., indirect oxidation).[76-80] The direct oxidation occurs when an

organic molecule strongly interacts with the catalyst surface and absorbs the photogenerated holes that eventually leads to the hydrolysis.[76, 79] The indirect oxidation is caused by OH* radicals that are generated by the oxidation of H_2O. Many studies have proved that the degradation of organic pollutants is mainly meditated by OH* radicals.[81] Nevertheless, other studies have also shown a significant contribution of the direct surface oxidation.[82] In this work, the roles of photogenerated carriers were investigated by using scavengers, i.e., EDTA for holes[82] and $KClO_3$ for electrons.[83] We found that the presence of electron scavenger $KClO_3$ enhanced the degradation of RhB (K_{app} increased from 0.122 to 0.219 min^{-1}), while the presence of hole scavenger EDTA significantly diminished the degradation (K_{app} decreased from 0.122 to 0.006 min^{-1}) (Fig. 3.5). This emphasizes the prominent role of holes in the photocatalytic reaction. Since holes can facilitate both direct oxidation and indirect oxidation (i.e., via OH* radical generation), their role was further elucidated by using other scavengers: DMSO and methanol. It has been demonstrated that DMSO scavenges OH* radicals but not holes,[82, 84] while methanol can scavenge both holes and OH* radicals.[82, 85] Therefore, using these scavengers, the contribution of direct oxidation (i.e., directly caused by holes) and indirect oxidation (i.e., caused by OH*) can be evaluated. The results show that when both holes and OH* radicals were scavenged, virtually no degradation was observed (K_{app} = 0.003 min^{-1}). When only OH* radicals were scavenged, the degradation was considerably diminished (K_{app} = 0.052 min^{-1}). This suggests that direct oxidation contributes considerably to the degradation of RhB. We note that when the concentration of DMSO was increased from 0.05 to 0.2 mmol, no significant change of the degradation was found (Fig. S3.2). In addition, the self-degradation and the degradation of RhB caused by the scavengers under UV irradiation (i.e., without catalysts) were inconsiderable (Fig. S3.3). Therefore, we conclude that the degradation of RhB by the Cu_2O/TiO_2 photocatalysts was caused by both direct surface oxidation and indirect oxidation.

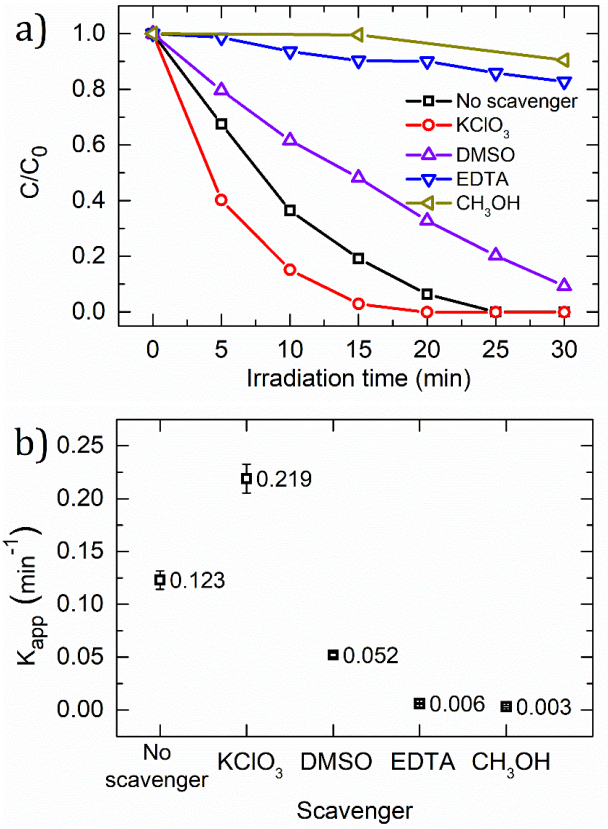

Figure 3.5*:* Influence of scavengers on the photodegradation of RhB by Cu_2O/TiO_2 (0.4 % Cu) photocatalysts (a): $KClO_3$ as electron scavenger, EDTA as hole scavenger, DMSO as OH* radical scavenger, and CH_3OH as both OH* radical and hole scavenger; the K_{app} values were determined from the corresponding degradation curves and plotted (b).

3.4. CONCLUSION

In conclusion, we have demonstrated ALD of Cu_2O using Cu(I)(hfac)(TMVS) and water at 250 °C, which was carried out in a fluidized bed reactor operating at atmospheric pressure. This provided a fast, scalable, and efficient route for TiO_2 surface modification to improve photocatalytic performance. The technique enabled the deposition of ultrasmall Cu_2O clusters with a low loading (i.e., 0.4 % for 1 ALD cycle), a narrow particle size distribution and an average size in the range of 1.3 – 1.5 nm on P25 TiO_2 nanoparticles. The self-limiting characteristics and the linear growth of ALD were achieved, which allowed us to control the amount of Cu_2O deposited on TiO_2 by varying the number of ALD cycles. At a Cu concentration of 0.4 %, the photocatalytic performance of TiO_2 was significantly enhanced, i.e., 2.2 times for RhB, 2.5 times for MO, and 1.7 times for MB. With increasing Cu concentration, the photocatalytic activity decreased; at a Cu concentration of 1.7 %, the photocatalytic activity of Cu_2O/TiO_2 was lower than that of pristine TiO_2. The roles of carriers were studied by investigating the influence of photogenerated carriers and radical scavengers on the degradation of RhB. It was found that both the direct surface oxidation and indirect oxidation by OH* radicals contributed significantly to the photodegradation.

APPENDIX

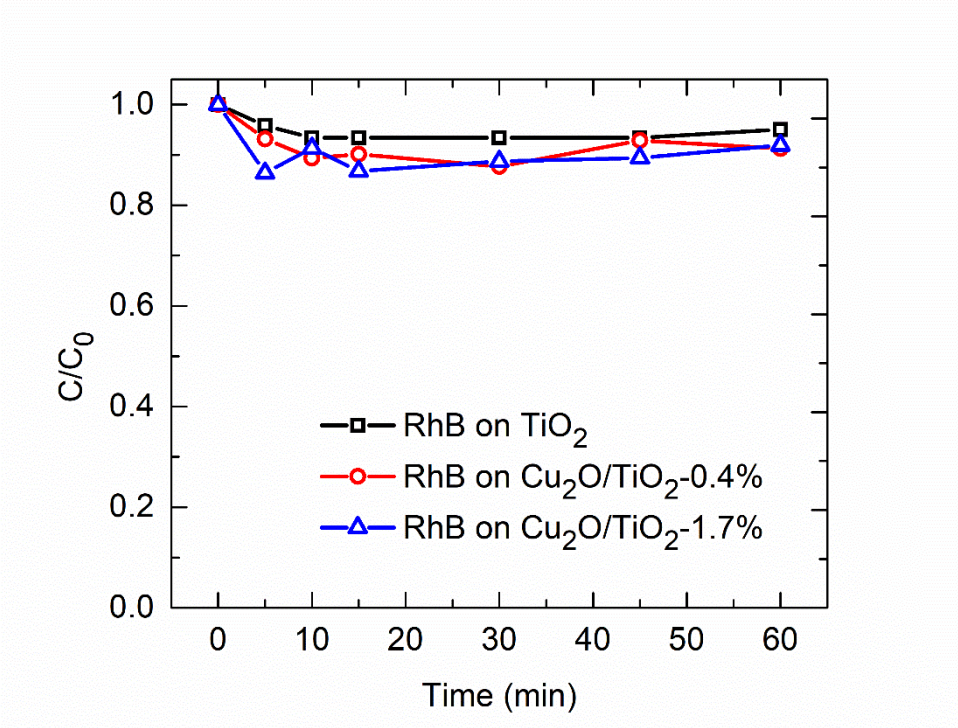

Figure S3.1: Adsorption of RhB on the surface of TiO_2 and Cu_2O/TiO_2 under no irradiation condition (in the dark). The results indicated that the adsorption/desorption equilibrium was obtained after 15 min and the presence of Cu_2O slightly enhanced the adsorption of RhB (ca. 5–7 %).

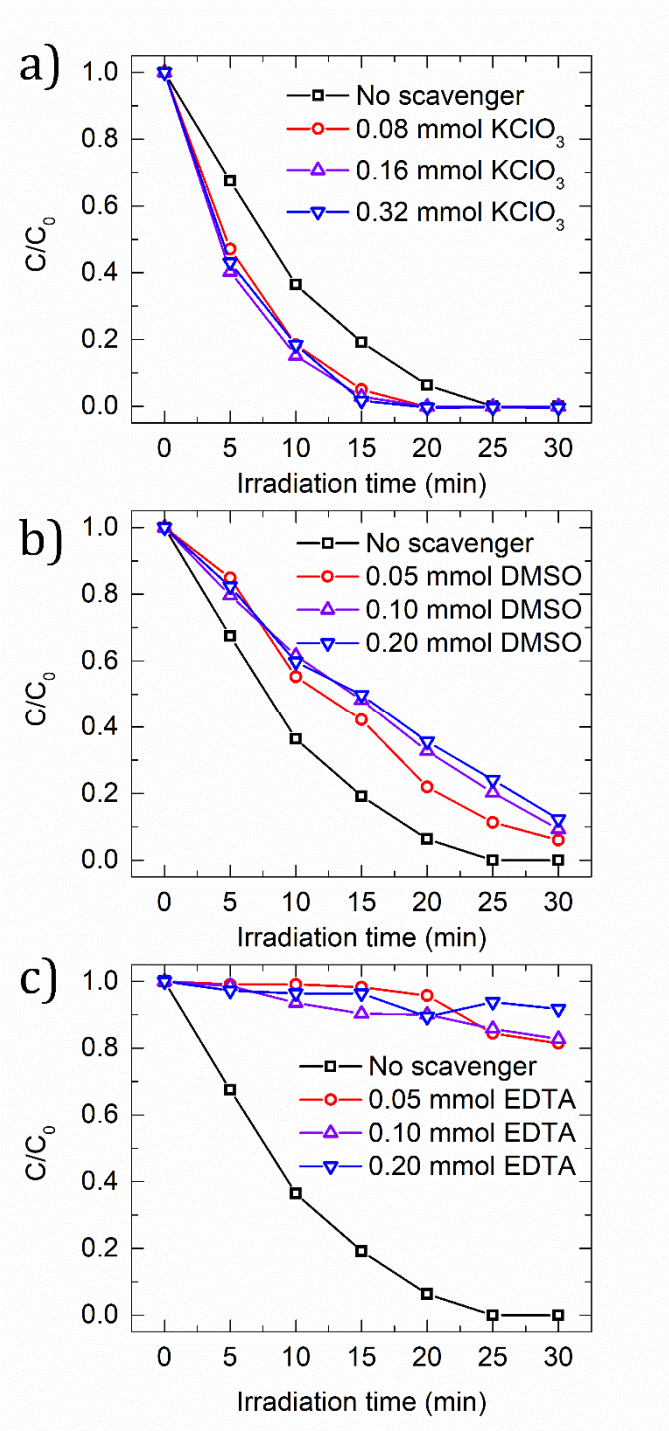

Figure S3.2: Degradation of RhB by Cu_2O/TiO_2 photocatalyst with Cu concentration of 0.4 at.% in the presence of scavengers with different concentrations: $KClO_3$ (a), DMSO (b) and EDTA (c).

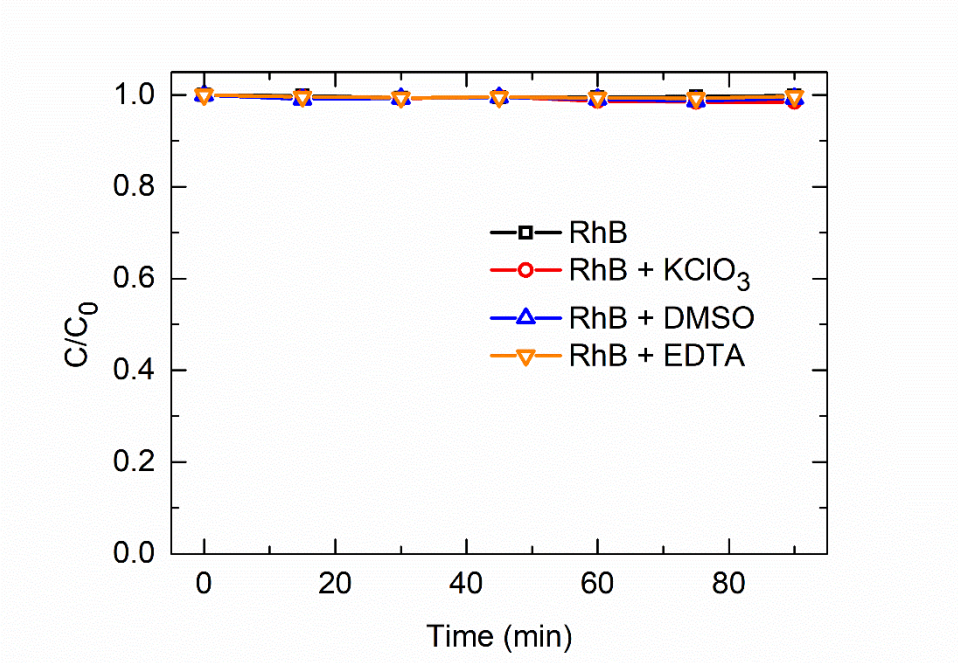

Figure S3.3: Self-degradation curves of RhB (i.e., without catalysts) under UV-irradiation with or without the presence of scavengers. The results indicated the inconsiderable degradation of RhB after 90 min of irradiation.

REFERENCES

1. Fujishima, A.; Zhang, X.; Tryk, D., TiO_2 photocatalysis and related surface phenomena. *Surface Science Reports* **2008,** *63* (12), 515-582.
2. Nakata, K.; Fujishima, A., TiO_2 photocatalysis: Design and applications. *Journal of Photochemistry and Photobiology C: Photochemistry Reviews* **2012,** *13* (3), 169-189.
3. Chiarello, G. L.; Dozzi, M. V.; Selli, E., TiO_2-based materials for photocatalytic hydrogen production. *Journal of Energy Chemistry* **2017,** *26* (2), 250-258.
4. Ge, M.; Cai, J.; Iocozzia, J.; Cao, C.; Huang, J.; Zhang, X.; Shen, J.; Wang, S.; Zhang, S.; Zhang, K.-Q.; Lai, Y.; Lin, Z., A review of TiO_2 nanostructured catalysts for sustainable H_2 generation. *International Journal of Hydrogen Energy* **2017,** *42* (12), 8418-8449.
5. Xing, Z.; Zhang, J.; Cui, J.; Yin, J.; Zhao, T.; Kuang, J.; Xiu, Z.; Wan, N.; Zhou, W., Recent advances in floating TiO_2-based photocatalysts for environmental application. *Applied Catalysis B: Environmental* **2018,** *225*, 452-467.
6. Byrne, C.; Subramanian, G.; Pillai, S. C., Recent advances in photocatalysis for environmental applications. *Journal of Environmental Chemical Engineering* **2018,** *6* (3), 3531-3555.
7. Hagfeldt, A.; Boschloo, G.; Sun, L.; Kloo, L.; Pettersson, H., Dye-Sensitized Solar Cells. *Chemical Reviews* **2010,** *110*, 6595–6663.
8. Ide, Y.; Inami, N.; Hattori, H.; Saito, K.; Sohmiya, M.; Tsunoji, N.; Komaguchi, K.; Sano, T.; Bando, Y.; Golberg, D.; Sugahara, Y., Remarkable Charge Separation and Photocatalytic Efficiency Enhancement through Interconnection of TiO_2 Nanoparticles by Hydrothermal Treatment. *Angew Chem Int Ed Engl* **2016,** *55* (11), 3600-5.
9. Ohtani, B.; Prieto-Mahaney, O. O.; Li, D.; Abe, R., What is Degussa (Evonik) P25? Crystalline composition analysis, reconstruction from isolated pure particles and photocatalytic activity test. *Journal of Photochemistry and Photobiology A: Chemistry* **2010,** *216* (2-3), 179-182.
10. Jiang, X.; Manawan, M.; Feng, T.; Qian, R.; Zhao, T.; Zhou, G.; Kong, F.; Wang, Q.; Dai, S.; Pan, J. H., Anatase and rutile in evonik aeroxide P25: Heterojunctioned or individual nanoparticles? *Catalysis Today* **2018,** *300*, 12-17.
11. Qin, X.; Jing, L.; Tian, G.; Qu, Y.; Feng, Y., Enhanced photocatalytic activity for degrading Rhodamine B solution of commercial Degussa P25 TiO_2 and its mechanisms. *J Hazard Mater* **2009,** *172* (2-3), 1168-74.
12. Shen, S.; Wang, X.; Chen, T.; Feng, Z.; Li, C., Transfer of Photoinduced Electrons in Anatase–Rutile TiO_2 Determined by Time-Resolved Mid-Infrared Spectroscopy. *The Journal of Physical Chemistry C* **2014,** *118* (24), 12661-12668.
13. Shingai, D.; Ide, Y.; Sohn, W. Y.; Katayama, K., Photoexcited charge carrier dynamics of interconnected TiO_2 nanoparticles: evidence of enhancement of charge separation at anatase-rutile particle interfaces. *Phys Chem Chem Phys* **2018,** *20* (5), 3484-3489.
14. Hurum, D. C.; Agrios, A. G.; Gray, K. A.; Rajh, T.; Thurnauer, M. C., Explaining the Enhanced Photocatalytic Activity of Degussa P25 Mixed-Phase TiO_2 Using EPR. *Journal of Physical Chemistry B* **2003,** *107*, 4545-4549.
15. Hurum, D. C.; Gray, K. A.; Rajh, T.; Thurnauer, M. C., Recombination Pathways in the Degussa P25 Formulation of TiO_2: Surface versus Lattice Mechanisms. *Journal of Physical Chemistry B* **2005,** *109*, 977-980.
16. Gao, W.; Lu, J.; Zhang, S.; Zhang, X.; Wang, Z.; Qin, W.; Wang, J.; Zhou, W.; Liu, H.; Sang, Y., Suppressing Photoinduced Charge Recombination via the Lorentz Force in a Photocatalytic System. *Adv Sci (Weinh)* **2019,** *6* (18), 1901244.
17. Li, G.; Huang, J.; Chen, J.; Deng, Z.; Huang, Q.; Liu, Z.; Guo, W.; Cao, R., Highly Active Photocatalyst of Cu_2O/TiO_2 Octahedron for Hydrogen Generation. *ACS Omega* **2019,** *4* (2), 3392-3397.
18. Du, P.; Bueno-López, A.; Verbaas, M.; Almeida, A. R.; Makkee, M.; Moulijn, J. A.; Mul, G., The effect of surface OH-population on the photocatalytic activity of rare earth-doped P25-TiO_2 in methylene blue degradation. *Journal of Catalysis* **2008,** *260* (1), 75-80.
19. Zhou, J.; Takeuchi, M.; Ray, A. K.; Anpo, M.; Zhao, X. S., Enhancement of photocatalytic activity of P25 TiO_2 by vanadium-ion implantation under visible light irradiation. *J Colloid Interface Sci* **2007,** *311* (2), 497-501.
20. Khoa Le, T.; Flahaut, D.; Martinez, H.; Hung Nguyen, H. K.; Xuan Huynh, T. K., Study of the effects of surface modification by thermal shock method on photocatalytic activity of TiO_2 P25. *Applied Catalysis B: Environmental* **2015,** *165*, 260-268.

21. Nawawi, W. I.; Nawi, M. A., Carbon coated nitrogen doped P25 for the photocatalytic removal of organic pollutants under solar and low energy visible light irradiations. *Journal of Molecular Catalysis A: Chemical* **2014,** *383-384*, 83-93.
22. Milosevic, I.; Jayaprakash, A.; Greenwood, B.; van Driel, B.; Rtimi, S.; Bowen, P., Synergistic Effect of Fluorinated and N Doped TiO_2 Nanoparticles Leading to Different Microstructure and Enhanced Photocatalytic Bacterial Inactivation. *Nanomaterials (Basel)* **2017,** *7* (11).
23. Al-Attafi, K.; Nattestad, A.; Wu, Q.; Ide, Y.; Yamauchi, Y.; Dou, S. X.; Kim, J. H., The effect of amorphous TiO_2 in P25 on dye-sensitized solar cell performance. *Chem Commun (Camb)* **2018,** *54* (4), 381-384.
24. Park, H.; Park, Y.; Kim, W.; Choi, W., Surface modification of TiO_2 photocatalyst for environmental applications. *Journal of Photochemistry and Photobiology C: Photochemistry Reviews* **2013,** *15*, 1-20.
25. Lee, J.; Park, H.; Choi, W., Selective Photocatalytic Oxidation of NH_3 to N_2 on Platinized TiO_2 in Water. *Environmental Science & Technology* **2002,** *36*, 5462-5468.
26. Zhou, Y.; King, D. M.; Liang, X.; Li, J.; Weimer, A. W., Optimal preparation of Pt/TiO_2 photocatalysts using atomic layer deposition. *Applied Catalysis B: Environmental* **2010,** *101* (1-2), 54-60.
27. Goulas, A.; Ruud van Ommen, J., Atomic layer deposition of platinum clusters on titania nanoparticles at atmospheric pressure. *Journal of Materials Chemistry A* **2013,** *1* (15), 4647.
28. Moniz, S. J.; Shevlin, S. A.; An, X.; Guo, Z. X.; Tang, J., Fe_2O_3-TiO_2 nanocomposites for enhanced charge separation and photocatalytic activity. *Chemistry: A European Journal* **2014,** *20* (47), 15571-9.
29. Moniz, S. J. A.; Tang, J., Charge Transfer and Photocatalytic Activity in CuO/TiO_2 Nanoparticle Heterojunctions Synthesised through a Rapid, One-Pot, Microwave Solvothermal Route. *ChemCatChem* **2015,** *7* (11), 1659-1667.
30. An, X.; Liu, H.; Qu, J.; Moniz, S. J. A.; Tang, J., Photocatalytic mineralisation of herbicide 2,4,5-trichlorophenoxyacetic acid: enhanced performance by triple junction $Cu–TiO_2–Cu_2O$ and the underlying reaction mechanism. *New Journal of Chemistry* **2015,** *39* (1), 314-320.
31. Zhai, Q.; Xie, S.; Fan, W.; Zhang, Q.; Wang, Y.; Deng, W.; Wang, Y., Photocatalytic conversion of carbon dioxide with water into methane: platinum and copper(I) oxide co-catalysts with a core-shell structure. *Angew Chem Int Ed Engl* **2013,** *52* (22), 5776-9.
32. Hai, Z.; Kolli, N. E.; Uribe, D. B.; Beaunier, P.; Jose-Yacaman, M.; Vigneron, J.; Etcheberry, A.; Sorgues, S.; Colbeau-Justin, C.; Chen, J.; Remita, H., Modification of TiO_2 by Bimetallic Au-Cu Nanoparticles for Wastewater Treatment. *J Mater Chem A Mater* **2013,** *1* (36), 10829-10835.
33. Méndez-Medrano, M. G.; Kowalska, E.; Lehoux, A.; Herissan, A.; Ohtani, B.; Bahena, D.; Briois, V.; Colbeau-Justin, C.; Rodríguez-López, J. L.; Remita, H., Surface Modification of TiO_2 with Ag Nanoparticles and CuO Nanoclusters for Application in Photocatalysis. *The Journal of Physical Chemistry C* **2016,** *120* (9), 5143-5154.
34. Lee, J.; Choi, W.; Yoon, J., Photocatalytic Degradation of N-Nitrosodimethylamine: Mechanism, Product Distribution, and TiO_2 Surface Modification. *Energy & Environmental Science* **2005,** *39*, 6800-6807.
35. Ryu, J.; Choi, W., Effects of TiO_2 Surface Modifications on Photocatalytic Oxidation of Arsenite: The Role of Superoxides. *Energy & Environmental Science* **2004,** *38*, 2928-2933.
36. Tada, H.; Ishida, T.; Takao, A.; Ito, S., Drastic Enhancement of TiO_2-Photocatalyzed Reduction of Nitrobenzene by Loading Ag Clusters. *Languir* **2004,** *20*, 7898-7900.
37. Kozlova, E. A.; Vorontsov, A. V., Noble metal and sulfuric acid modified TiO_2 photocatalysts: Mineralization of organophosphorous compounds. *Applied Catalysis B: Environmental* **2006,** *63* (1-2), 114-123.
38. Zhong, J. B.; Lu, Y.; Jiang, W. D.; Meng, Q. M.; He, X. Y.; Li, J. Z.; Chen, Y. Q., Characterization and photocatalytic property of Pd/TiO_2 with the oxidation of gaseous benzene. *J Hazard Mater* **2009,** *168* (2-3), 1632-5.
39. Wang, W. N.; An, W. J.; Ramalingam, B.; Mukherjee, S.; Niedzwiedzki, D. M.; Gangopadhyay, S.; Biswas, P., Size and structure matter: enhanced CO_2 photoreduction efficiency by size-resolved ultrafine Pt nanoparticles on TiO_2 single crystals. *J Am Chem Soc* **2012,** *134* (27), 11276-81.
40. He, Y.; Ford, M. E.; Zhu, M.; Liu, Q.; Wu, Z.; Wachs, I. E., Selective catalytic reduction of NO by NH_3 with WO_3-TiO_2 catalysts: Influence of catalyst synthesis method. *Applied Catalysis B: Environmental* **2016,** *188*, 123-133.
41. Tae Kwon, Y.; Yong Song, K.; In Lee, W.; Jin Choi, G.; Rag Do, Y., Photocatalytic Behavior of WO_3-Loaded TiO_2 in an Oxidation Reaction. *Journal of Catalysis* **2000,** *191* (1), 192-199.

42. Khan, H.; Rigamonti, M. G.; Boffito, D. C., Enhanced photocatalytic activity of Pt-TiO_2/WO_3 hybrid material with energy storage ability. *Applied Catalysis B: Environmental* **2019,** *252*, 77-85.
43. Huang, L.; Peng, F.; Wang, H.; Yu, H.; Li, Z., Preparation and characterization of Cu_2O/TiO_2 nano–nano heterostructure photocatalysts. *Catalysis Communications* **2009,** *10* (14), 1839-1843.
44. Bessekhouad, Y.; Robert, D.; Weber, J. V., Photocatalytic activity of Cu_2O/TiO_2, Bi_2O_3/TiO_2 and $ZnMn_2O_4$/TiO_2 heterojunctions. *Catalysis Today* **2005,** *101* (3-4), 315-321.
45. Xu, Y.-h.; Liang, D.-h.; Liu, M.-l.; Liu, D.-z., Preparation and characterization of Cu_2O–TiO_2: Efficient photocatalytic degradation of methylene blue. *Materials Research Bulletin* **2008,** *43* (12), 3474-3482.
46. Aguirre, M. E.; Zhou, R.; Eugene, A. J.; Guzman, M. I.; Grela, M. A., Cu_2O/TiO_2 heterostructures for CO_2 reduction through a direct Z-scheme: Protecting Cu_2O from photocorrosion. *Applied Catalysis B: Environmental* **2017,** *217*, 485-493.
47. Wang, Y.; Wang, Q.; Zhan, X.; Wang, F.; Safdar, M.; He, J., Visible light driven type II heterostructures and their enhanced photocatalysis properties: a review. *Nanoscale* **2013,** *5* (18), 8326-39.
48. Wang, J.; Ji, G.; Liu, Y.; Gondal, M. A.; Chang, X., Cu_2O/TiO_2 heterostructure nanotube arrays prepared by an electrodeposition method exhibiting enhanced photocatalytic activity for CO_2 reduction to methanol. *Catalysis Communications* **2014,** *46*, 17-21.
49. Janczarek, M.; Endo, M.; Zhang, D.; Wang, K.; Kowalska, E., Enhanced Photocatalytic and Antimicrobial Performance of Cuprous Oxide/Titania: The Effect of Titania Matrix. *Materials (Basel)* **2018,** *11* (11).
50. Zhou, P.; Yu, J.; Jaroniec, M., All-Solid-State Z-Scheme Photocatalytic Systems. *Advanced Materials* **2014,** *26* (29), 4920-4935.
51. Wang, M.; Sun, L.; Lin, Z.; Cai, J.; Xie, K.; Lin, C., p–n Heterojunction photoelectrodes composed of Cu_2O-loaded TiO_2 nanotube arrays with enhanced photoelectrochemical and photoelectrocatalytic activities. *Energy & Environmental Science* **2013,** *6* (4), 1211.
52. Lalitha, K.; Sadanandam, G.; Kumari, V. D.; Subrahmanyam, M.; Sreedhar, B.; Hebalkar, N. Y., Highly Stabilized and Finely Dispersed Cu_2O/TiO_2: A Promising Visible Sensitive Photocatalyst for Continuous Production of Hydrogen from Glycerol-Water Mixtures. *Journal of Physical Chemistry C* **2010,** *114*, 22181–22189.
53. Wang, Y.; Tao, J.; Wang, X.; Wang, Z.; Zhang, M.; He, G.; Sun, Z., A unique Cu_2O/TiO_2 nanocomposite with enhanced photocatalytic performance under visible light irradiation. *Ceramics International* **2017,** *43* (6), 4866-4872.
54. An, X.; Liu, H.; Qu, J.; Moniz, S. J. A.; Tang, J., Photocatalytic mineralisation of herbicide 2,4,5-trichlorophenoxyacetic acid: enhanced performance by triple junction Cu–TiO_2–Cu_2O and the underlying reaction mechanism. *New J. Chem.* **2015,** *39* (1), 314-320.
55. Niu, F.; Jiang, Y.; Song, W., In situ loading of Cu2O nanoparticles on a hydroxyl group rich TiO_2 precursor as an excellent catalyst for the Ullmann reaction. *Nano Research* **2010,** *3* (11), 757-763.
56. Zhao, K.; Zhao, S.; Qi, J.; Yin, H.; Gao, C.; Khattak, A. M.; Wu, Y.; Iqbal, A.; Wu, L.; Gao, Y.; Yu, R.; Tang, Z., Cu_2O clusters grown on TiO_2 nanoplates as efficient photocatalysts for hydrogen generation. *Inorganic Chemistry Frontiers* **2016,** *3* (4), 488-493.
57. Cheng, W.-Y.; Yu, T.-H.; Chao, K.-J.; Lu, S.-Y., Cu_2O-Decorated Mesoporous TiO_2 Beads as a Highly Efficient Photocatalyst for Hydrogen Production. *ChemCatChem* **2014,** *6* (1), 293-300.
58. Xi, Z.; Li, C.; Zhang, L.; Xing, M.; Zhang, J., Synergistic effect of Cu_2O/TiO_2 heterostructure nanoparticle and its high H_2 evolution activity. *International Journal of Hydrogen Energy* **2014,** *39* (12), 6345-6353.
59. Praveen Kumar, D.; Lakshmana Reddy, N.; Mamatha Kumari, M.; Srinivas, B.; Durga Kumari, V.; Sreedhar, B.; Roddatis, V.; Bondarchuk, O.; Karthik, M.; Neppolian, B.; Shankar, M. V., Cu_2O-sensitized TiO_2 nanorods with nanocavities for highly efficient photocatalytic hydrogen production under solar irradiation. *Solar Energy Materials and Solar Cells* **2015,** *136*, 157-166.
60. Adamu, H.; McCue, A. J.; Taylor, R. S. F.; Manyar, H. G.; Anderson, J. A., Simultaneous photocatalytic removal of nitrate and oxalic acid over Cu_2O/TiO_2 and Cu_2O/TiO_2-AC composites. *Applied Catalysis B: Environmental* **2017,** *217*, 181-191.
61. Li, J., Preparation of highly photocatalytic active nano-size TiO_2/Cu_2O particle composites with a novel electrochemical method. *Electrochemistry Communications* **2004,** *6* (9), 940-943.
62. Nikam, A. V.; Prasad, B. L. V.; Kulkarni, A. A., Wet chemical synthesis of metal oxide nanoparticles: a review. *CrystEngComm* **2018,** *20* (35), 5091-5107.

63. Guo, J.; Van Bui, H.; Valdesueiro, D.; Yuan, S.; Liang, B.; van Ommen, J. R., Suppressing the Photocatalytic Activity of TiO_2 Nanoparticles by Extremely Thin Al_2O_3 Films Grown by Gas-Phase Deposition at Ambient Conditions. *Nanomaterials (Basel)* **2018,** *8* (2).
64. Van Bui, H.; Grillo, F.; Kulkarni, S. S.; Bevaart, R.; Van Thang, N.; van der Linden, B.; Moulijn, J. A.; Makkee, M.; Kreutzer, M. T.; van Ommen, J. R., Low-temperature atomic layer deposition delivers more active and stable Pt-based catalysts. *Nanoscale* **2017,** *9* (30), 10802-10810.
65. Liang, X.; Barrett, K. S.; Jiang, Y. B.; Weimer, A. W., Rapid silica atomic layer deposition on large quantities of cohesive nanoparticles. *ACS Appl Mater Interfaces* **2010,** *2* (8), 2248-53.
66. Liang, X.; Lyon, L. B.; Jiang, Y.-B.; Weimer, A. W., Scalable synthesis of palladium nanoparticle catalysts by atomic layer deposition. *Journal of Nanoparticle Research* **2012,** *14* (6).
67. Lindblad, M.; Lindfors, L. P.; Suntola, T., Preparation of Ni/Al_2O_3 catalysts from vapor phase by atomic layer epitaxy. *Catalysis Letters* **1994,** *27*, 323-336.
68. Rautiainen, A.; Lindblad, M.; Backman, L. B.; Puurunen, R. L., Preparation of silica-supported cobalt catalysts through chemisorption of cobalt(ii) and cobalt(iii) acetylacetonate. *Physical Chemistry Chemical Physics* **2002,** *4* (11), 2466-2472.
69. Puurunen, R. L., Surface chemistry of atomic layer deposition: A case study for the trimethylaluminum/water process. *Journal of Applied Physics* **2005,** *97* (12), 121301.
70. Leskela, M.; Ritala, M., Atomic layer deposition chemistry: recent developments and future challenges. *Angew Chem Int Ed Engl* **2003,** *42* (45), 5548-54.
71. Van Bui, H.; Grillo, F.; van Ommen, J. R., Atomic and molecular layer deposition: off the beaten track. *Chem Commun (Camb)* **2016,** *53* (1), 45-71.
72. Beetstra, R.; Lafont, U.; Nijenhuis, J.; Kelder, E. M.; van Ommen, J. R., Atmospheric Pressure Process for Coating Particles Using Atomic Layer Deposition. *Chemical Vapor Deposition* **2009,** *15* (7-9), 227-233.
73. Muñoz-Rojas, D.; Jordan, M.; Yeoh, C.; Marin, A. T.; Kursumovic, A.; Dunlop, L. A.; Iza, D. C.; Chen, A.; Wang, H.; MacManus Driscoll, J. L., Growth of ~5 $cm^2V^{-1}s^{-1}$ mobility, p-type Copper(I) oxide (Cu_2O) films by fast atmospheric atomic layer deposition (AALD) at 225°C and below. *AIP Advances* **2012,** *2* (4), 042179.
74. Vorontsov, A. V.; Tsybulya, S. V., Influence of Nanoparticles Size on XRD Patterns for Small Monodisperse Nanoparticles of Cu^0 and TiO_2 Anatase. *Industrial & Engineering Chemistry Research* **2018,** *57* (7), 2526-2536.
75. Guo, J.; Yuan, S.; Yu, Y.; van Ommen, J. R.; Van Bui, H.; Liang, B., Room-temperature pulsed CVD-grown SiO_2 protective layer on TiO_2 particles for photocatalytic activity suppression. *RSC Advances* **2017,** *7* (8), 4547-4554.
76. Zhuang, J.; Dai, W.; Tian, Q.; Li, Z.; Xie, L.; Wang, J.; Liu, P.; Shi, X.; Wang, D., Photocatalytic degradation of RhB over TiO_2 bilayer films: effect of defects and their location. *Langmuir* **2010,** *26* (12), 9686-94.
77. Amine-Khodja, A.; Boulkamh, A.; Richard, C., Phototransformation of metobromuron in the presence of TiO_2. *Applied Catalysis B: Environmental* **2005,** *59* (3-4), 147-154.
78. Henderson, M. A., A surface science perspective on TiO_2 photocatalysis. *Surface Science Reports* **2011,** *66* (6-7), 185-297.
79. Nosaka, Y.; Nosaka, A. Y., Generation and Detection of Reactive Oxygen Species in Photocatalysis. *Chem Rev* **2017,** *117* (17), 11302-11336.
80. Zhao, D.; Chen, C.; Wang, Y.; Ji, H.; Ma, W.; Zang, L.; Zhao, J., Surface Modification of TiO_2 by Phosphate- Effect on Photocatalytic Activity and Mechanism Implication. *Journal of Physical Chemistry C* **2008,** *112*, 5993-6001.
81. Nosaka, Y.; Nosaka, A., Understanding Hydroxyl Radical (•OH) Generation Processes in Photocatalysis. *ACS Energy Letters* **2016,** *1* (2), 356-359.
82. Lin, X. H.; Miao, Y.; Li, S. F. Y., Location of photocatalytic oxidation processes on anatase titanium dioxide. *Catalysis Science & Technology* **2017,** *7* (2), 441-451.
83. Syoufian, A.; Nakashima, K., Degradation of methylene blue in aqueous dispersion of hollow titania photocatalyst: study of reaction enhancement by various electron scavengers. *J Colloid Interface Sci* **2008,** *317* (2), 507-12.
84. Eberhardt, M. K.; Colina, R., The reaction of OH radicals with dimethyl sulfoxide. A comparative study of Fenton's reagent and the radiolysis of aqueous dimethyl sulfoxide solutions. *The Journal of Organic Chemistry* **1988,** *53*, 1071-1074.
85. Marugán, J.; Hufschmidt, D.; López-Muñoz, M.-J.; Selzer, V.; Bahnemann, D., Photonic efficiency for methanol photooxidation and hydroxyl radical generation on silica-supported TiO_2 photocatalysts. *Applied Catalysis B: Environmental* **2006,** *62* (3-4), 201-207.

4

Tuning the photocatalytic activity of TiO_2 nanoparticles by ultrathin SiO_2 films grown by low-temperature atmospheric pressure atomic layer deposition

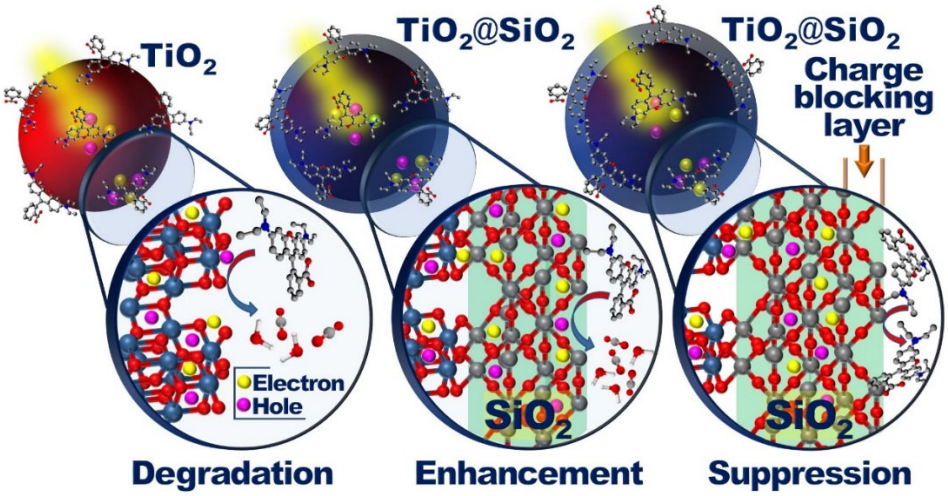

This work demonstrates a feasible and efficient route for the synthesis of noble-metal free TiO_2-based photocatalysts with an enhanced activity and tunable photocatalytic properties. We employed atomic layer deposition to deposit ultrathin SiO_2 layers on P25 TiO_2 nanoparticles, which was carried out in a fluidized bed reactor working at atmospheric pressure using $SiCl_4$ and H_2O as precursors. This enabled the deposition of SiO_2 at 100 °C with the ability to control the thickness at the sub-nanometer level. We observed that by controlling the thickness of the SiO_2 in a very narrow range, i.e., below 2 nm, the photocatalytic activity of TiO_2 could be strongly enhanced or significantly diminished. Namely, an enhancement was obtained for the SiO_2 with a thickness of below 1.4 nm, in which the layer with a thickness of about 0.7 nm exhibited the highest photocatalytic activity, whereas, above 1.4 nm, the photocatalytic activity was significantly attenuated.

Published in Applied Surface Science

Jing Guo, Dominik Benz, Thao-Trang Doan Nguyen, Phuc-Huy Nguyen, Thanh-Lieu Thi Le, Damiano La Zara, Bin Liang, H. T. (Bert) Hintzen, J. Ruud van Ommen, and Hao Van Bui

4.1. INTRODUCTION

For a few decades, since Fujishima and Honda discovered the photocatalytic splitting of water on TiO_2 electrodes [1], enormous efforts have been devoted to the development of TiO_2 photocatalysis. Owing to its excellent photocatalytic properties, high structural and chemical stabilities, low environmental impact, abundance in nature, and especially its suitable flat band potential for various redox reactions, TiO_2 has been widely used in various applications in environmental and energy-related fields, such as air purification, water treatment and hydrogen production. [2-7] However, due to its large bandgap (i.e., ~3.2 eV), TiO_2 does not harvest efficiently sunlight that provides the highest photon flux in the visible and infrared regions. [8] In addition, the rapid recombination of photogenerated electrons and holes is a limiting factor in achieving high photocatalytic efficiencies [6, 9]. Therefore, to improve light harvesting and to reduce charge recombination, electronic structure and surface properties of TiO_2 are usually modified.

The electronic modification of TiO_2 is commonly realized by doping the host material with other elements to form energy levels in the bandgap of TiO_2. [3, 10-13] This consequently reduces the bandgap and enables the absorption of photons with lower energies. [6, 14-17] In contrast, surface modification commonly promotes the charge transfer between the TiO_2 and the deposited materials, which can reduce the charge recombination [14]. In this case, the surface of TiO_2 is engineered by coupling with a thin film or nanoclusters of other materials. [18-31] Due to their high catalytic activities, noble metals are most popularly used. [19-21, 32-33] In addition to promoting the electron transfer due to their lower Fermi levels with respect to the conduction band of TiO_2 [34-36], noble metals can also act as co-catalysts, providing further catalytic enhancement. [14] For instance, the surface modification of TiO_2 nanoparticles by Pt nanoclusters could significantly improve the photocatalytic activity of TiO_2 toward the degradation of Acid Blue 9. [37] Enhancement of photocatalytic performance was also observed for the TiO_2 modified with nanoclusters of Au, Ag, and Cu.[22-25] Nevertheless, the use of noble metal may reduce the stability of the catalysts due to the oxidation at the metal/TiO_2 interface when exposed to UV-irradiation. This can create electron-hole recombination centers that affect the photocatalytic efficiency. [38] In addition, due to their high cost, the use of noble metals is not desirable. Therefore, the surface modification of TiO_2 by metal oxides such as CuO, Cu_2O, Fe_2O_3, CeO_2, MnO_2, and MgO has recently been more attractive. [26-31]

Given its large bandgap (~9 eV), silicon dioxide (SiO_2) is an excellent dielectric that has been a key material in the microelectronic industry. [39] The good electrically insulating nature of SiO_2 also makes it the material of choice for mitigating the photocatalytic activity of TiO_2. [40-43] This is due to the fact that a thin SiO_2 layer can effectively block the transport of photogenerated electrons and holes to the catalyst surface, diminishing the photocatalytic reactions. [40] Nevertheless, many studies have also shown that the coupling with SiO_2 can enhance the photocatalytic activity of TiO_2,

which has been utilized in various applications such as degradation of organic pollutants and bacteria, and CO_2 capture. [44-60] Generally, the enhancement or suppression of photocatalytic activity strongly depends on the concentration (i.e., in the case of TiO_2-SiO_2 mixture) or the thickness (i.e., in the case of TiO_2/SiO_2 core/shell structure) of SiO_2. For example, for the TiO_2/SiO_2 core/shell structure, a thin layer of SiO_2 with a thickness of about 1–2 nm can effectively diminish the photocatalytic activity of TiO_2. [43, 61] Therefore, in order to achieve an enhancement, a thinner layer is needed. This requires a synthesis method that allows controlling the thickness of the coating layer at the sub-nanometer level. In this regard, atomic layer deposition (ALD) is an excellent candidate. This is a gas-phase deposition technique that allows controlling the amount of deposited material down to the atomic scale, which has been utilized for the deposition of various materials. [62-63]

In this work, we employ ALD to deposit ultrathin SiO_2 films on P25 TiO_2 nanoparticles to realize a TiO_2/SiO_2 core/shell structure and investigate their photocatalytic properties. The SiO_2 ALD is carried out in a fluidized bed reactor (FBR) operating at atmospheric pressure, using silicon tetrachloride ($SiCl_4$) as the precursor and H_2O as the co-reactant. We demonstrate that this ALD process enables the deposition of SiO_2 at 100 °C. This deposition temperature is significantly lower than the typical temperature range (i.e., 300–420 °C) for conventional SiO_2 ALD using $SiCl_4$ and H_2O. [64-66] Using ALD, we are able to control the thickness of the SiO_2 at the sub-nanometer level, which allows studying its influence on the photocatalytic activity of the TiO_2/SiO_2 photocatalysts. It is found that enhancement is obtained for the SiO_2 coating with a thickness of below 1.4 nm, in which the layer with a thickness of about 0.7 Å exhibits the highest photocatalytic activity. Above 1.4 nm, the photocatalytic activity is significantly attenuated. As a consequence, by varying the thickness of the SiO_2 coating in a very narrow range, i.e., below 2 nm, the photocatalytic activity of TiO_2 can be altered from enhancement to suppression, providing a feasible and efficient route to tune the photocatalytic activity of TiO_2 without the use of noble metals.

4.2. EXPERIMENTAL SECTION

4.2.1. Preparation of TiO_2/SiO_2 core/shell photocatalysts

The deposition of SiO_2 on TiO_2 nanoparticles was carried out in a fluidized bed reactor (FBR) operating at atmospheric pressure, as described elsewhere. [67] Degussa P25 TiO_2 (mean diameter of 21 nm and specific surface area of 54 m^2g^{-1}) was purchased from Evonik Industries (Hanau, Germany). Silicon tetrachloride ($SiCl_4$) contained in a stainless steel bubbler was provided by Akzo Nobel HPMO (Amersfoort, the Netherlands). Pressurized nitrogen (99.999 vol.%) was used as the carrier gas. For

each experiment, 1.5 g of powder was used. The powder is fluidized by an N_2 gas flow of 0.5 L min^{-1}, which was introduced through the distributor plate placed at the bottom of the glass column. An ALD cycle consisted of alternating exposures of the TiO_2 powder to $SiCl_4$ vapor (1 min), followed by an N_2 purging step (3 min), the deionized water vapor (3 min), and finally an N_2 purging of 8 min. The deposition temperature was set at 100 °C. During the deposition, a temperature variation of ±5 °C was observed.

4.1.1. Characterization

The morphology of the TiO_2/SiO_2 particles was characterized by transmission electron microscopy (TEM) using a JEOL JEM1400 transmission electron microscope. X-ray photoelectron spectroscopy (XPS) was employed to investigate elemental compositions and bonding states of the TiO_2/SiO_2 catalysts using a ThermoFisher K-Alpha system (photon energy of 1486.7 eV). The peak positions were calibrated by using the C 1*s* peak at 284.8 eV as the reference.

The atomic concentration of the deposited SiO_2 was determined using instrumental neutron activation analysis (INAA). For each measurement, 100 mg powder was loaded into high purity polyethylene capsules. The samples and a reference sample were irradiated at a constant neutron flux. All reactors used for neutron activation employed uranium fission, which provides a neutron flux (kinetic energy less than 0.5 eV) in the order of 10^{12} cm $^{-2}s^{-1}$. Upon irradiation, a neutron can be absorbed by the target nucleus (i.e., Si), forming a radioactive nucleus. The nuclear decay of the radioactive nuclei produces Gamma rays, which can be detected by the INAA detectors, from which the Si loading was determined.

The specific surface area (SSA) of the powder was determined by the BET method using a Micromeritics Tristar II at 77 K. For each measurement, 160 mg of the powder was used. All the samples were annealed in N_2 at 150 °C for 16 hours prior to the measurements. Data analysis was performed using Microactive software V3.02. The BET SSA was determined by fitting of the data points in the P/P_0 = 0.05–0.225 region.

The photodegradation of Rhodamine B (RhB) in aqueous solution was used to evaluate the photocatalytic activity of the TiO_2/SiO_2 photocatalysts. In each experiment, 10 mg of the catalyst was added to 80 mL RhB solution (RhB concentration of 10 mg L^{-1}) contained in a 200-ml glass beaker (diameter of 8 cm). The suspension was continuously stirred in the dark for 30 min to obtain the adsorption/desorption equilibrium, which was then exposed to UV-radiation generated by a mercury lamp (25 W, 620 lux at the reactor surface) for different exposure times. After separating the solid catalyst by centrifuging, the solution was analyzed by UV-visible spectroscopy using a Jenway's 6800 double beam spectrophotometer to determine the RhB residual concentration.

4.2. RESULTS AND DISCUSSION

4.2.1. Morphology, structure and elemental composition of the TiO_2/SiO_2 photocatalysts

The reactions between $SiCl_4$ and H_2O in ALD of SiO_2 are based on the ligand exchange between the functional groups, i.e., –Cl and –OH, on the surface, which requires a relatively high temperature, typically in the range of 300–420 °C. [64-66] For lower deposition temperatures, the presence of a catalyst, such as ammonia (NH_3) or pyridine (C_5H_5N), is commonly needed. [68-69] Nevertheless, the $SiCl_4/H_2O$ ALD process carried out in a fluidized bed reactor operating at atmospheric pressure in this work enabled the growth of SiO_2 at 100 °C, which is significantly lower than the deposition temperature reported in the literature. [64-66] Previous research demonstrated that high partial pressure of the reactants plays a crucial role and enables deposition at lower temperature. [70] TEM images presented in Figs. 4.1a–d demonstrate the deposition of TiO_2/SiO_2 nanoparticles with a core/shell structure. From the TEM images, the thickness of the SiO_2 layer is determined, whereas the Si atomic concentration (Si at. %) is measured by INAA. The plots of SiO_2 thickness and Si at.% as a function of the number of ALD cycles exhibit a linear dependence (Fig. 4.1e) that represents the linear-growth regime of ALD. [71] In this regime, a growth-per-cycle (GPC) of approximately 0.5 Å is obtained, which is slightly lower than the GPC of the SiO_2 ALD reported in the literature (i.e., 0.7–1.1 Å). [64-65] In addition, the small variation of the GPC obtained for different $SiCl_4$ exposure times (i.e., from 5s to 120 s) shown in Fig. 4.1f reflects the self-saturating behavior of ALD. [71] This self-limiting behavior, in combination with the linear growth, provides the ability to control the thickness of the SiO_2 layer at the sub-nanometer level by controlling the number of cycles. This allows us to investigate the influence of the SiO_2 thickness at the ultrathin regime (i.e., < 2 nm) on the photocatalytic activity of TiO_2.

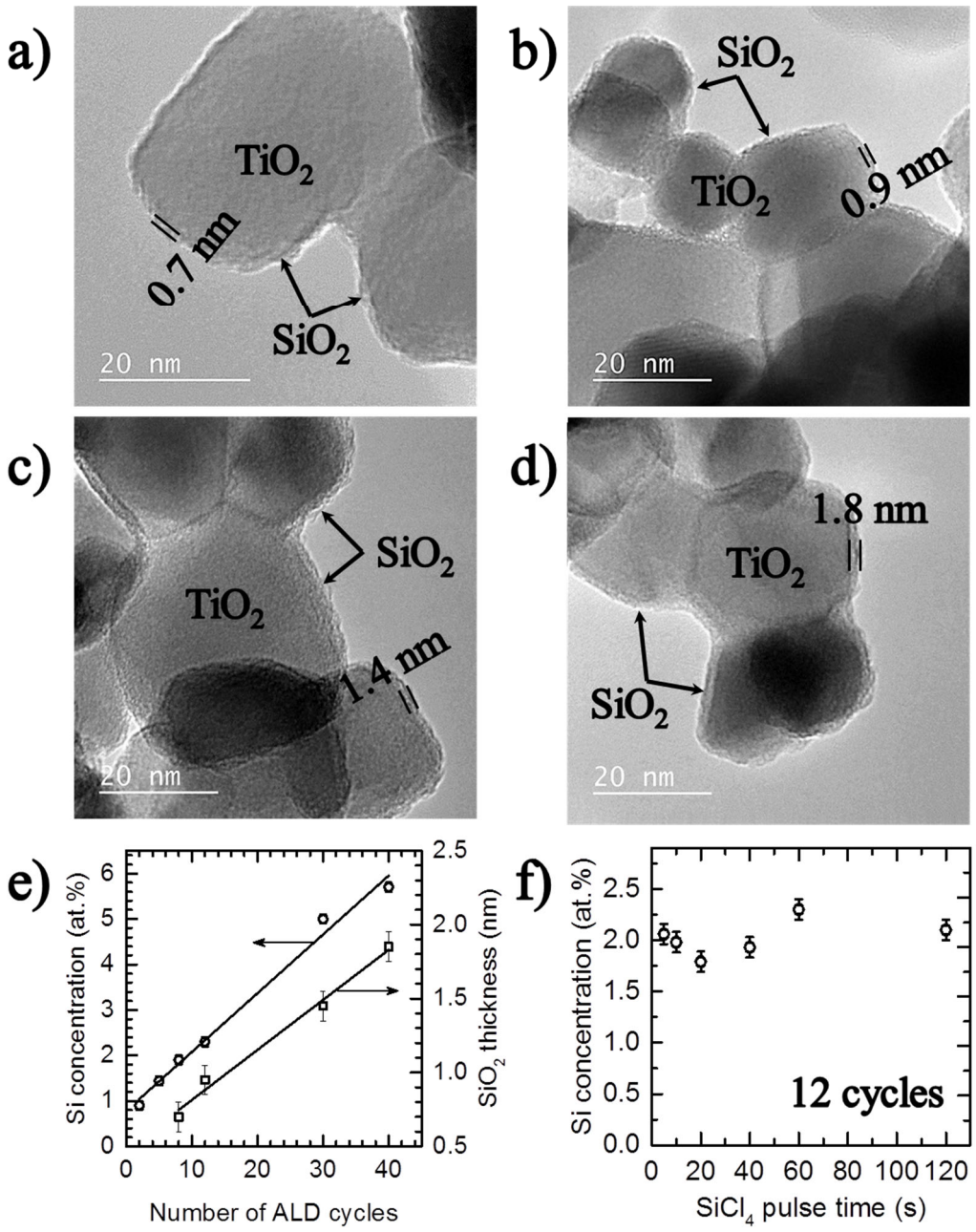

Figure 4.1: TEM images of TiO2 nanoparticles coated with SiO2 films grown at 100 °C for 8 cycles (a), 12 cycles (b), 30 cycles (c) and 40 cycles (d). The SiO2 film thickness (□) and the Si atomic concentration (○) as a function of the number of cycles are plotted in (e). The plot in (f) shows the Si atomic concentration obtained for 12 ALD cycles in which the SiCl4 pulse time is varied from 5 to 120 s while the pulse time of H2O vapor is fixed at 300 s.

The specific surface area (SSA) of the TiO_2 powders before and after coating with SiO_2 is determined by BET method. An SSA of 54.5 $m^2\,g^{-1}$ is obtained for the uncoated P25 TiO_2, which is consistent with the SSA value provided by the supplier. No considerable change is observed for the total SSA obtained for the TiO_2 powder coated with SiO_2 for different numbers of ALD cycles, as shown in Fig. 4.2 (the squares).

However, using the T-method [72], the analysis of the isothermal curves reveals the presence of micropores in the SiO_2 films whose volume and SSA increase with the number of cycles (Fig. 4.2, the stars and the triangles). The external SSA of the powders is determined from the total SSA and the SSA of the micropores, showing a slight decrease with increasing the number of ALD cycles (Fig. 4.2, the circles). This decrease is attributed to the increase in particle size caused by the SiO_2 coating layer.

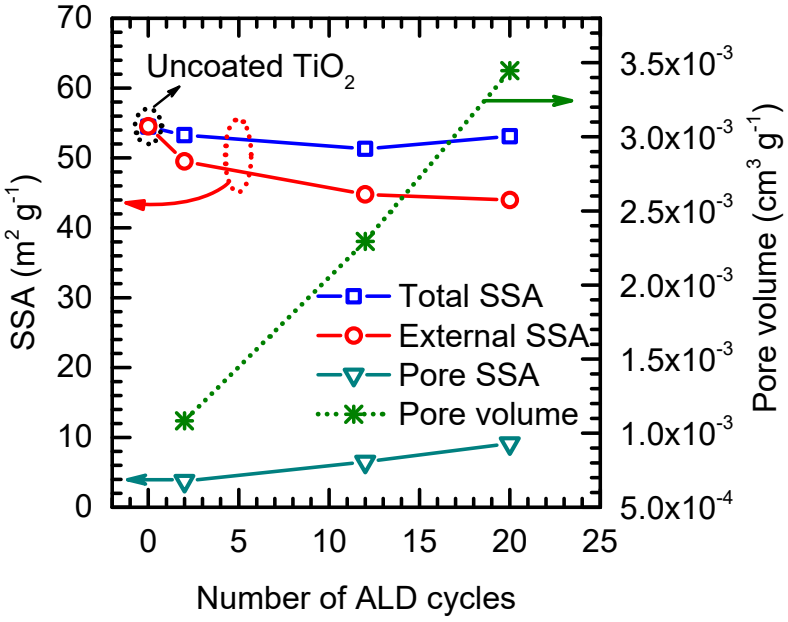

Figure 4.2: The total SSA (□), micropore SSA (▽), micropore volume (✳) and external SSA (○) of the TiO_2 powder coated with SiO2 for different numbers of ALD cycles as determined by BET.

The results obtained from the XRD characterization show the amorphous state of the SiO_2 films, even after annealing at 500 °C for 16 hours (Fig. S4.1, *Supporting Information*). The XPS spectra of the C 1s, Ti 2p, O 1s and Si 2p core-levels of the uncoated TiO_2 and TiO_2/SiO_2 are presented in Fig. 4.3. We note that in order to eliminate the influence of the peak shift due to charging effects, the peak positions are calibrated by referencing the C–C peak of the C 1s to the binding energy (BE) of 284.8 eV (Fig. 4.3a). [47] For the uncoated TiO_2, the two peaks at BE = 464.2 eV (Ti $2p_{1/2}$) and BE = 458.6 eV (Ti $2p_{3/2}$) in the top spectrum of Fig. 4.3b reflect a doublet state of Ti(IV) 2p that arises from the spin-orbit coupling. These two peaks in conjunction with the peak at BE = 529.7 eV of O 1s (Fig. 4.3c, the top spectrum) represent the Ti–O bond of TiO_2 (hereafter designated as O_{-Ti}). [47, 73-74] The peak at BE = 457.4 eV in the Ti 2p top spectrum (Fig. 4.3b) could represent the Ti $2p_{3/2}$ of the Ti(III) compounds (e.g., Ti_2O_3, oxygen vacancies, etc.) [74], whereas the broad peak at 532.0 eV in the O 1s top spectrum (Fig. 4.3c) is attributed to the chemisorbed hydroxyl groups (i.e., OH groups) on the surface [54]. The presence of these OH groups is confirmed by the FTIR spectra (Fig. S4.2, *Appendix).*

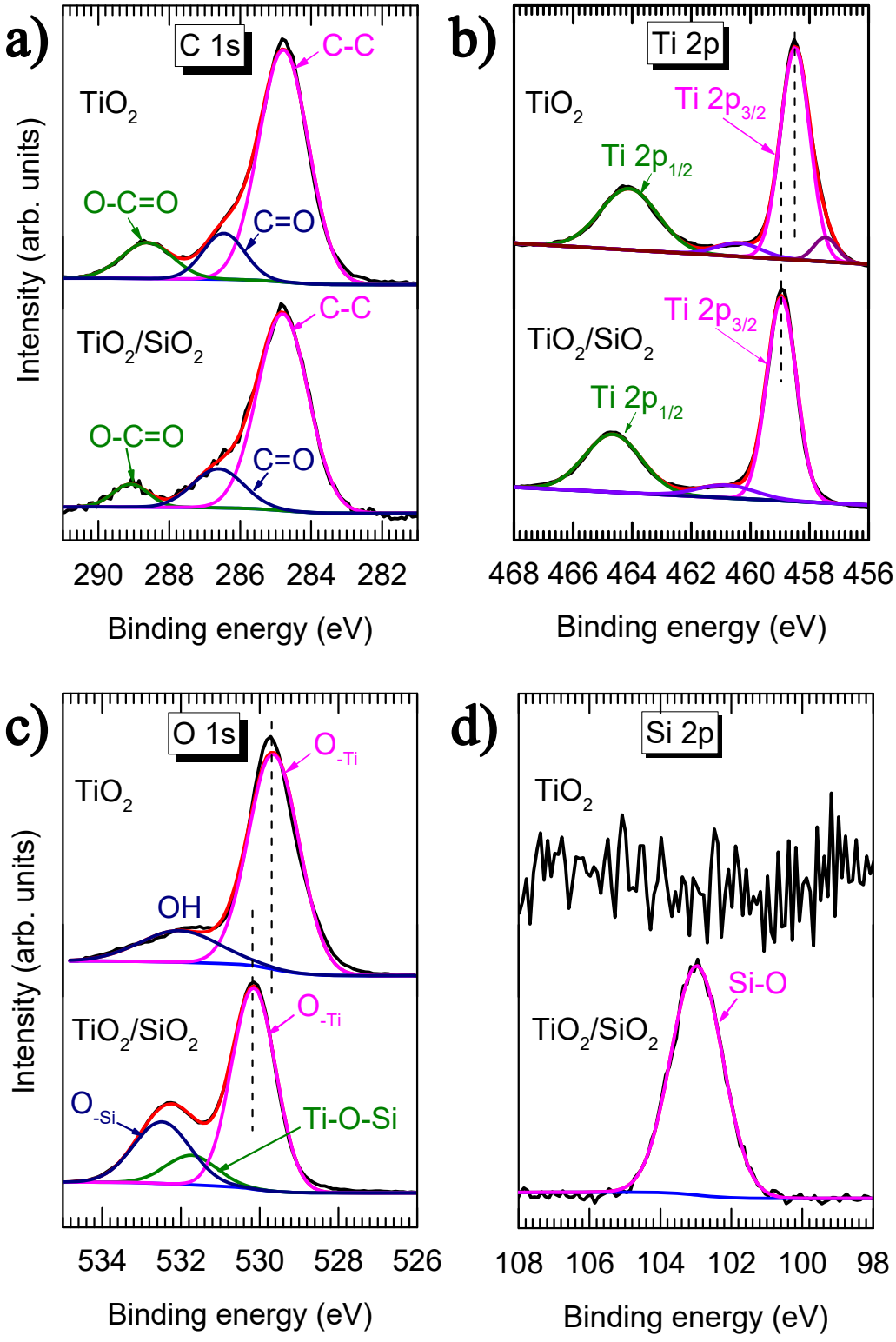

Figure 4.3: Core-level XPS spectra of C 1s (a), Ti 2p (b), O 1s (c) and Si 2p (d) of the uncoated TiO2 (top spectra) and TiO2 coated with SiO2 for 12 ALD cycles (bottom spectra).

For TiO_2/SiO_2, the peak at BE = 532.4 eV (O 1s, Fig. 4.3c) and the peak at BE = 103.0 eV (Si 2p, Fig. 4.3d) represent the Si–O bond (hereafter designated as O_{-Si}). [75-76] The binding energy difference between the Si 2p and the O 1s of the O_{-Si}

bond is 429.4 eV, which is consistent with the binding energy difference of the Si–O bond of SiO_2 (i.e., 429.3–429.4 eV). [75-76]

Furthermore, after coating with SiO_2, the Ti 2p and O 1s peaks of the O–Ti bond exhibit remarkable shifts (i.e., 0.4 eV for Ti 2p and 0.5 eV for O 1s) toward the higher binding energy (Fig. 4.3b and Fig. 4.3c). This shift is evidence of the formation of Ti–O–Si linkages at the interface between TiO_2 and SiO_2 and arises from the difference in electron negativity between Si (1.90), Ti (1.56) and O (3.44) [47, 77]. The presence of the linkages is also indicated by the peak at 531.8 eV in the O 1s spectrum (Fig. 4.3c). [78-79] The XPS analyses confirm the presence of SiO_2, which is additionally supported by the FTIR spectra (Fig. S4.2, *Supporting Information)*.

4.2.2. Photocatalytic properties of the TiO_2/SiO_2 core/shell nanoparticles

The adsorption of RhB on the photocatalysts before UV-irradiation was examined by monitoring the change of RhB concentration while stirring the catalyst/RhB aqueous mixture in the dark. This study was carried out for the uncoated TiO_2 and the TiO_2 coated with SiO_2 for 2 and 12 ALD cycles; the results are presented in Fig. 4.4a. Analogous behavior is observed for all samples, which shows a rapid decrease of the RhB concentration in the first 10 min caused by the adsorption of RhB on the surface of TiO_2. Thereafter, no considerable change of the RhB concentration is observed, indicating that the adsorption-desorption equilibrium has been established. The similar adsorption of RhB on TiO_2 and the SiO_2-coated TiO_2 suggests that the adsorption of RhB molecules is not enhanced by the SiO_2 layer, which is in contrast with the results reported in the pioneering work of Anderson and Bard, in which an enhanced adsorption of the organic molecules on the catalyst surface due to SiO_2 was observed [45, 80]. However, the SiO_2 layer strongly alters the photodegradation of RhB under UV-light irradiation, as shown in Fig. 4.4b. Particularly, for the uncoated TiO_2, approximately 90% of the RhB is degraded after 30 min irradiation. For the TiO_2/SiO_2, the photodegradation exhibits a strong dependence on the thickness of the SiO_2 coating layer, which can be estimated by the kinetics of the photodegradation reaction described by equation: [81]

$$\ln(C_0/C) = k_{app} \cdot t, \text{ or } C = C_0 \cdot \exp(-k_{app} \cdot t) \quad (1)$$

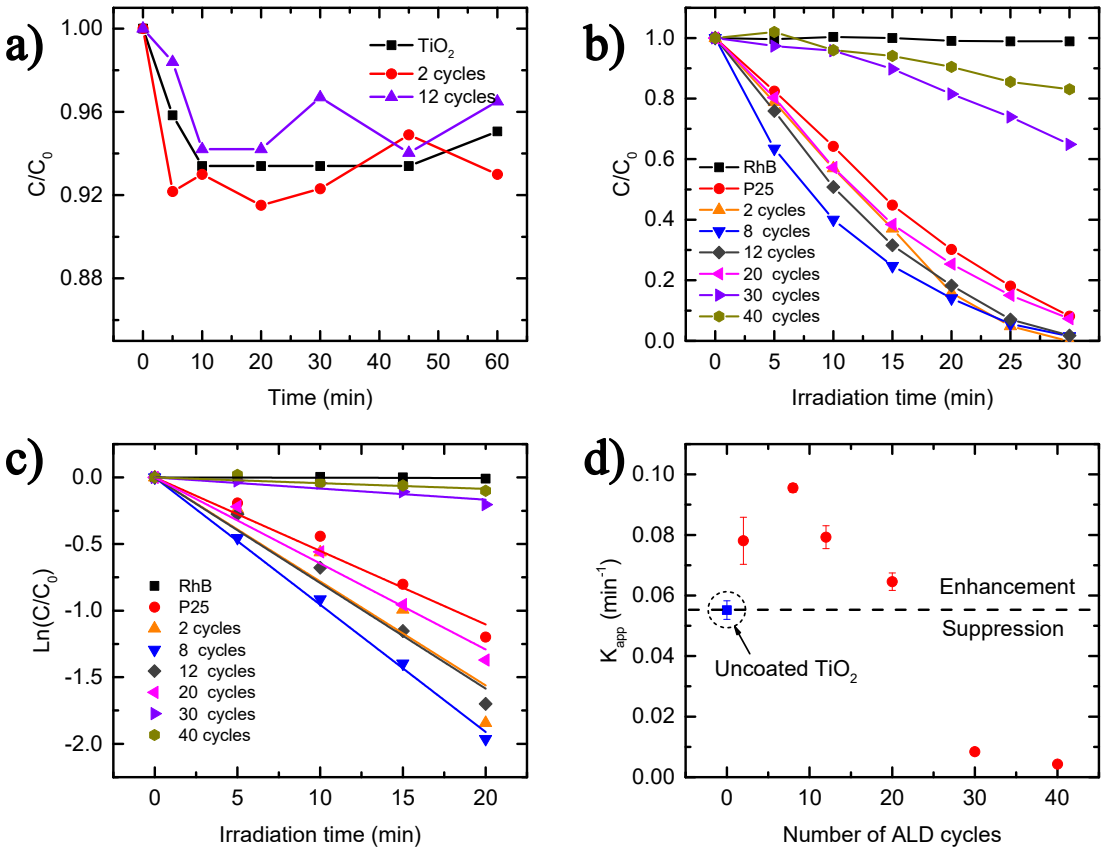

Figure 4.4: Adsorption behavior of RhB on the uncoated TiO2 and the TiO2 coated with SiO2 for 2 and 12 ALD cycles (a), the degradation of RhB as a function of irradiation time (b) and the corresponding kinetic plots (c), from which the first-order kinetic c

where k_{app} represents the degradation rate, which is commonly referred as the apparent first-order kinetic constant. The plots $ln(C_0/C)$ vs. t are shown in Fig. 4.4c, from which the k_{app} values are determined and plotted in Fig. 4.4d. For the uncoated TiO_2, a k_{app} of 55.2×10^{-3} min^{-1} is obtained. The coating of TiO_2 by SiO_2 initially results in an increase of k_{app} with increasing the number of ALD cycles, reaches the maximum value of 95.6 $\times10^{-3}$ min^{-1} at 8 ALD cycles, which is corresponding to a SiO_2 film thickness of about 0.7 nm (Fig. 4.1a). Hereafter, k_{app} gradually decreases to 64.6×10^{-3} min^{-1} for 20 ALD cycles, which is slightly higher than the k_{app} obtained for the uncoated TiO_2. A further increase of the number of cycles to 30 and 40 results in a rapid drop of k_{app} to 8.4×10^{-3} min^{-1} and 4.3×10^{-3} min^{-1}, respectively. The low k_{app} values achieved for 30 and 40 ALD cycles, which correspond to the SiO_2 thickness of 1.4 and 1.8 nm (Figs. 4.1c-d), respectively, indicate that the photocatalytic activity of TiO_2 is strongly suppressed. Furthermore, photocatalytic tests under visible light showed no catalytic activity, indicating that self-sensitation plays a negligible role in the photocatalytic mechanism and the degradation of RhB is purely based on the photocatalytic activity of the modified P25 particles.

The results show that by varying the thickness of the SiO_2 layer, the photocatalytic activity of TiO_2 can be tuned. In particular, an enhancement can be achieved by coating the TiO_2 with a SiO_2 layer thinner than 1.4 nm, in which a layer of 0.7 nm provides the highest photocatalytic activity. For SiO_2 layers thicker than 1.4 nm, the photocatalytic activity of TiO_2 is significantly diminished. It can be seen that the photocatalytic activity of TiO_2/SiO_2 powders is highly sensitive to the thickness of the SiO_2 layer. A small variation of the thickness in a very narrow range (i.e., below 2 nm) may entirely alter the photocatalytic property of the material from enhancement to suppression. As a consequence, tuning the catalytic activity of TiO_2 by SiO_2 requires precise control of the coating thickness. This can be a major challenge to conventional synthesis techniques such as sol-gel and hydrothermal. However, as demonstrated, the ALD process reported in the present work has shown great advantages in controlling the thickness of SiO_2 down to the sub-nanometer level, providing the ability to tailor the photocatalytic properties of TiO_2 for various applications. For instance, whereas the enhanced activity is highly desirable for photocatalysis, the suppression is of great interest for the applications of TiO_2 in pigment, paint, and cosmetic industries. [7, 82]

4.3. CONCLUSIONS

In conclusion, ALD using $SiCl_4$ and H_2O carried out in a fluidized bed reactor operating at atmospheric pressure enables the deposition of SiO_2 on P25 TiO_2 nanoparticles at 100 °C, which is significantly lower than the deposition temperature in conventional ALD processes. The linear-growth regime with a growth-per-cycle of 0.5 Å is achieved, and the self-limiting characteristic of the SiO_2 ALD is demonstrated. It is found that the photocatalytic activity of SiO_2-coated TiO_2 particles is strongly dependent on the thickness of the SiO_2 layer, which takes place in a very narrow thickness range, i.e., below 2 nm. Particularly, a SiO_2 layer below 1.4 nm can significantly enhance the photocatalytic activity of TiO_2, in which the highest enhancement is obtained at a thickness of about 0.7 nm. SiO_2 layers above 1.4 nm strongly diminish the photocatalytic activity. As a consequence, by controlling the thickness of SiO_2 coating at the sub-nanometer level, the photocatalytic property of TiO_2 is tuned from an enhancement to a suppression. Therefore, our work has demonstrated a feasible and efficient route not only for the synthesis of noble-metal free TiO_2-based photocatalysts with enhanced activity but also for tuning the photocatalytic properties. Moreover, the low-temperature ALD process is a valuable asset that can enable the application of SiO_2 coating on temperature-sensitive materials such as polymers and organic materials.

APPENDIX

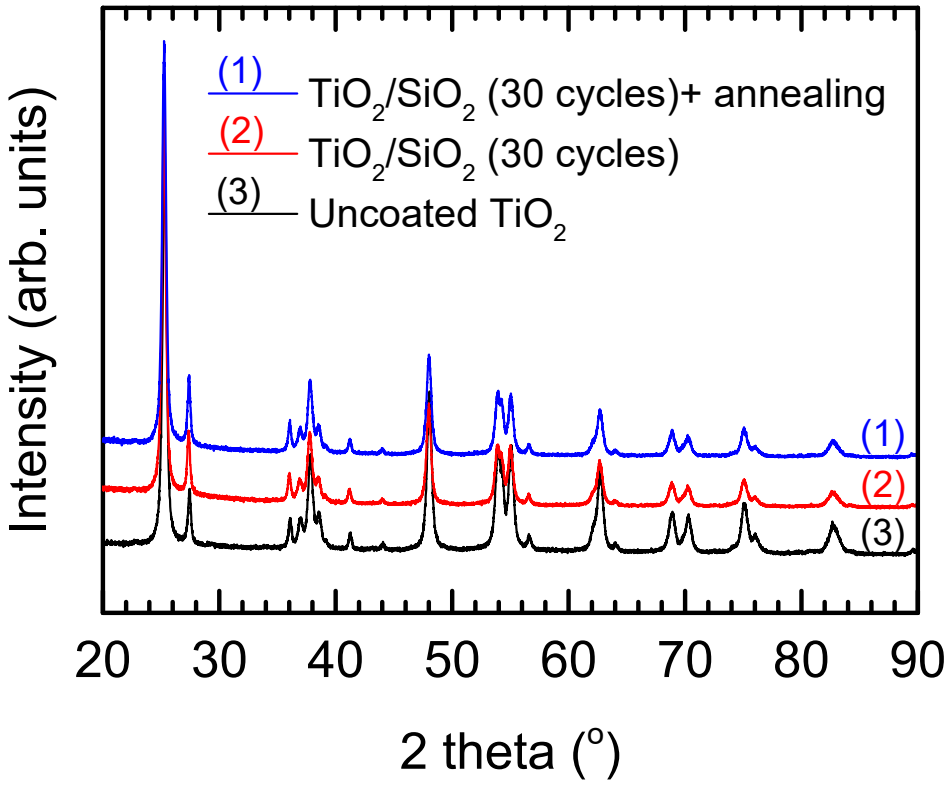

Figure S4.1: XRD patterns of the initial TiO2 powder (3), the TiO_2 coated with SiO2 for 30 ALD cycles before (2) and after (1) annealing at 500 °C for 16 hours in air. The results show that the XRD peaks of the P25 TiO_2 are unaffected after coating with SiO_2, even after the annealing. This suggests the amorphous state of the SiO_2 layer. The measurements were carried using a PANalytical X-pert Pro diffractometer with Cu Kα radiation.

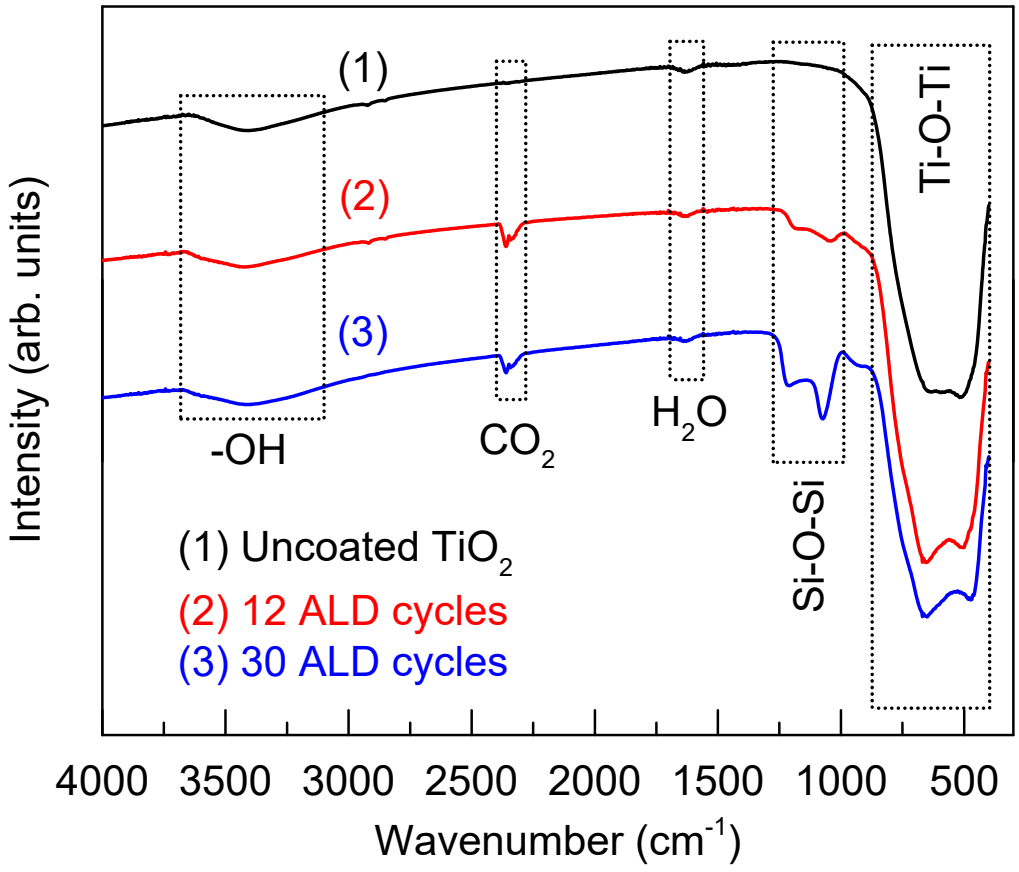

Figure S4.2: FTIR spectra of the uncoated TiO2 (1), TiO_2 coated with SiO2 for 12 ALD cycles (2) and 30 ALD cycles (3). The spectra show the presence of hydroxyl groups and physisorbed water for both uncoated and SiO_2-coated TiO_2 in the spectral ranges of 3100–3600 cm^{-1} and 1550–1700 cm^{-1}, respectively. The peaks in the spectral range of 2280–2400 cm^{-1} represent the adsorbed CO_2, which is only observed for the TiO2/SiO2. The peaks in the spectral range of 980–1275 cm^{-1} represent the Si–O–Si bonds, which are not observed for the uncoated TiO_2. This is evidence of the presence of SiO_2 on the surface of TiO_2.

REFERENCES

1. Fujishima, A.; Honda, K., Electrochemical photolysis of water at a semiconductor electrode. *Nature* **1972,** *238*, 37-38.
2. Nakata, K.; Fujishima, A., TiO_2 photocatalysis: Design and applications. *Journal of Photochemistry and Photobiology C: Photochemistry Reviews* **2012,** *13* (3), 169-189.
3. Devi, L. G.; Kavitha, R., A review on non metal ion doped titania for the photocatalytic degradation of organic pollutants under UV/solar light: Role of photogenerated charge carrier dynamics in enhancing the activity. *Applied Catalysis B: Environmental* **2013,** *140-141*, 559-587.
4. Ganguly, P.; Byrne, C.; Breen, A.; Pillai, S. C., Antimicrobial activity of photocatalysts: Fundamentals, mechanisms, kinetics and recent advances. *Applied Catalysis B: Environmental* **2018,** *225*, 51-75.
5. Fujishima, A.; Zhang, X.; Tryk, D., TiO_2 photocatalysis and related surface phenomena. *Surface Science Reports* **2008,** *63* (12), 515-582.
6. Schneider, J.; Matsuoka, M.; Takeuchi, M.; Zhang, J.; Horiuchi, Y.; Anpo, M.; Bahnemann, D. W., Understanding TiO_2 photocatalysis: Mechanisms and materials. *Chemical Reviews* **2014,** *114* (19), 9919-86.
7. Chen, X.; Mao, S. S., Titanium dioxide nanomaterials: Synthesis, properties, modifications, and applications. *Chemical Reviews* **2007,** *107*, 2891−2959.
8. Kumar, S. G.; Devi, L. G., Review on modified TiO_2 photocatalysis under UV/visible light: Selected results and related mechanisms on interfacial charge carrier transfer dynamics. *Journal of Physcal Chemistry A* **2011,** *115* (46), 13211-41.
9. Ohtani, B., Titania photocatalysis beyond recombination: A critical review. *Catalysts* **2013,** *3* (4), 942-953.
10. Chang, S.-m.; Liu, W.-s., The roles of surface-doped metal ions (V, Mn, Fe, Cu, Ce, and W) in the interfacial behavior of TiO_2 photocatalysts. *Applied Catalysis B: Environmental* **2014,** *156-157*, 466-475.
11. Elbanna, O.; Zhang, P.; Fujitsuka, M.; Majima, T., Facile preparation of nitrogen and fluorine codoped TiO_2 mesocrystal with visible light photocatalytic activity. *Applied Catalysis B: Environmental* **2016,** *192*, 80-87.
12. Giannakas, A. E.; Antonopoulou, M.; Daikopoulos, C.; Deligiannakis, Y.; Konstantinou, I., Characterization and catalytic performance of B-doped, B–N co-doped and B–N–F tri-doped TiO_2 towards simultaneous Cr(VI) reduction and benzoic acid oxidation. *Applied Catalysis B: Environmental* **2016,** *184*, 44-54.
13. Inturi, S. N. R.; Boningari, T.; Suidan, M.; Smirniotis, P. G., Visible-light-induced photodegradation of gas phase acetonitrile using aerosol-made transition metal (V, Cr, Fe, Co, Mn, Mo, Ni, Cu, Y, Ce, and Zr) doped TiO_2. *Applied Catalysis B: Environmental* **2014,** *144*, 333-342.
14. Park, H.; Park, Y.; Kim, W.; Choi, W., Surface modification of TiO_2 photocatalyst for environmental applications. *Journal of Photochemistry and Photobiology C: Photochemistry Reviews* **2013,** *15*, 1-20.
15. Asahi, R.; Morikawa, T.; Ohwaki, T.; Aoki, K.; Taga, Y., Visible-light photocatalysis in nitrogen-doped titanium oxides. *Science* **2001,** *293*, 269-271.
16. Asahi, R.; Morikawa, T.; Irie, H.; Ohwaki, T., Nitrogen-doped titanium dioxide as visible-light-sensitive photocatalyst: designs, developments, and prospects. *Chemical Reviews* **2014,** *114* (19), 9824-52.
17. Sun, M.; Zhang, X.; Li, J.; Cui, X.; Sun, D.; Lin, Y., Thermal formation of silicon-doped TiO_2 thin films with enhanced visible light photoelectrochemical response. *Electrochemistry Communications* **2012,** *16* (1), 26-29.
18. Méndez-Medrano, M. G.; Kowalska, E.; Lehoux, A.; Herissan, A.; Ohtani, B.; Bahena, D.; Briois, V.; Colbeau-Justin, C.; Rodríguez-López, J. L.; Remita, H., Surface modification of TiO_2 with Ag nanoparticles and CuO nanoclusters for application in photocatalysis. *The Journal of Physical Chemistry C* **2016,** *120* (9), 5143-5154.
19. Prakash, J.; Sun, S.; Swart, H. C.; Gupta, R. K., Noble metals-TiO_2 nanocomposites: From fundamental mechanisms to photocatalysis, surface enhanced Raman scattering and antibacterial applications. *Applied Materials Today* **2018,** *11*, 82-135.
20. Wei, Z.; Janczarek, M.; Endo, M.; Wang, K.; Balčytis, A.; Nitta, A.; Méndez-Medrano, M. G.; Colbeau-Justin, C.; Juodkazis, S.; Ohtani, B.; Kowalska, E., Noble metal-modified faceted

anatase titania photocatalysts: Octahedron versus decahedron. *Applied Catalysis B: Environmental* **2018,** *237*, 574-587.
21. Tahir, M.; Tahir, B.; Amin, N. A. S., Synergistic effect in plasmonic Au/Ag alloy NPs co-coated TiO_2 NWs toward visible-light enhanced CO_2 photoreduction to fuels. *Applied Catalysis B: Environmental* **2017,** *204*, 548-560.
22. Méndez-Medrano, M. G.; Kowalska, E.; Lehoux, A.; Herissan, A.; Ohtani, B.; Rau, S.; Colbeau-Justin, C.; Rodríguez-López, J. L.; Remita, H., Surface modification of TiO_2 with Au nanoclusters for efficient water treatment and hydrogen generation under visible light. *The Journal of Physical Chemistry C* **2016,** *120* (43), 25010-25022.
23. Tahir, M., Synergistic effect in MMT-dispersed Au/TiO_2 monolithic nanocatalyst for plasmon-absorption and metallic interband transitions dynamic CO_2 photo-reduction to CO. *Applied Catalysis B: Environmental* **2017,** *219*, 329-343.
24. Wang, T.; Wei, J.; Shi, H.; Zhou, M.; Zhang, Y.; Chen, Q.; Zhang, Z., Preparation of electrospun Ag/TiO_2 nanotubes with enhanced photocatalytic activity based on water/oil phase separation. *Physica E: Low-dimensional Systems and Nanostructures* **2017,** *86*, 103-110.
25. Kumar, M. K.; Bhavani, K.; Naresh, G.; Srinivas, B.; Venugopal, A., Plasmonic resonance nature of Ag-Cu/TiO_2 photocatalyst under solar and artificial light: Synthesis, characterization and evaluation of H_2O splitting activity. *Applied Catalysis B: Environmental* **2016,** *199*, 282-291.
26. Wang, Y.; Zhao, J.; Wang, T.; Li, Y.; Li, X.; Yin, J.; Wang, C., CO_2 photoreduction with H_2O vapor on highly dispersed CeO_2/TiO_2 catalysts: Surface species and their reactivity. *Journal of Catalysis* **2016,** *337*, 293-302.
27. Stucchi, M.; Boffito, D. C.; Pargoletti, E.; Cerrato, G.; Bianchi, C. L.; Cappelletti, G., Nano-MnO_2 decoration of TiO_2 microparticles to promote gaseous ethanol visible photoremoval. *Nanomaterials (Basel)* **2018,** *8* (9).
28. Xie, S.; Wang, Y.; Zhang, Q.; Deng, W.; Wang, Y., MgO- and Pt-promoted TiO_2 as an efficient photocatalyst for the preferential reduction of carbon dioxide in the presence of water. *ACS Catalysis* **2014,** *4* (10), 3644-3653.
29. Moniz, S. J.; Shevlin, S. A.; An, X.; Guo, Z. X.; Tang, J., Fe_2O_3 -TiO_2 nanocomposites for enhanced charge separation and photocatalytic activity. *Chemistry-A European Journal* **2014,** *20* (47), 15571-9.
30. Tsui, L.-k.; Zangari, G., Modification of TiO_2 nanotubes by Cu_2O for photoelectrochemical, photocatalytic, and photovoltaic devices. *Electrochimica Acta* **2014,** *128*, 341-348.
31. Zhao, K.; Zhao, S.; Qi, J.; Yin, H.; Gao, C.; Khattak, A. M.; Wu, Y.; Iqbal, A.; Wu, L.; Gao, Y.; Yu, R.; Tang, Z., Cu_2O clusters grown on TiO_2 nanoplates as efficient photocatalysts for hydrogen generation. *Inorganic Chemistry Frontiers* **2016,** *3* (4), 488-493.
32. Collado, L.; Reynal, A.; Coronado, J. M.; Serrano, D. P.; Durrant, J. R.; de la Peña O'Shea, V. A., Effect of Au surface plasmon nanoparticles on the selective CO_2 photoreduction to CH_4. *Applied Catalysis B: Environmental* **2015,** *178*, 177-185.
33. Dozzi, M. V.; Chiarello, G. L.; Pedroni, M.; Livraghi, S.; Giamello, E.; Selli, E., High photocatalytic hydrogen production on Cu(II) pre-grafted Pt/TiO_2. *Applied Catalysis B: Environmental* **2017,** *209*, 417-428.
34. Xie, S.; Wang, Y.; Zhang, Q.; Fan, W.; Deng, W.; Wang, Y., Photocatalytic reduction of CO_2 with H_2O: Significant enhancement of the activity of Pt-TiO_2 in CH_4 formation by addition of MgO. *Chemical Communications* **2013,** *49* (24), 2451-3.
35. Jakob, M.; Levanon, H.; Kamat, P. V., Charge distribution between UV-Irradiated TiO_2 and gold nanoparticles: Determination of shift in the Fermi level. *Nano Letters* **2003,** *3*, 353–358.
36. Subramanian, V.; Wolf, E. E.; Kamat, P. V., Catalysis with TiO_2/gold nanocomposites. Effect of metal particle size on the fermi level equilibration. *Journal of the American Chemical Society* **2004,** *126*, 4943-4950.
37. van Ommen, J. R.; Kooijman, D.; de Niet, M.; Talebi, M.; Goulas, A., Continuous production of nanostructured particles using spatial atomic layer deposition. *Journal of Vacuum Science and Technology A* **2015,** *33*, 021513.
38. Subramanian, V.; Wolf, E.; Kamat, P. V., Semiconductor−metal composite nanostructures. To what extent do metal nanoparticles improve the photocatalytic activity of TiO_2 films. *Journal of Physical Chemistry B* **2001,** *105*, 11439-11446.
39. Nicollian, E. H.; Brews, J. R., MOS (metal oxide semiconductor) physics and technology. *JOHN WILEY & SON* **1982**.
40. Guo, J.; Yuan, S.; Yu, Y.; van Ommen, J. R.; Van Bui, H.; Liang, B., Room-temperature pulsed CVD-grown SiO_2 protective layer on TiO_2 particles for photocatalytic activity suppression. *RSC Advances* **2017,** *7* (8), 4547-4554.

41. Lee, H. S.; Koo, S. M.; Yoo, J. W., TiO_2-SiO_2 nanoparticles for suppressing photocatalytic activities and improving hydrophilicity. *Journal of Ceramic Processing Research* **2012,** *13*, S300-S303.
42. Liang, X.; Barrett, K. S.; Jiang, Y. B.; Weimer, A. W., Rapid silica atomic layer deposition on large quantities of cohesive nanoparticles. *ACS Applied Materials & Interfaces* **2010,** *2* (8), 2248-53.
43. King, D. M.; Liang, X.; Burton, B. B.; Kamal Akhtar, M.; Weimer, A. W., Passivation of pigment-grade TiO_2 particles by nanothick atomic layer deposited SiO_2 films. *Nanotechnology* **2008,** *19* (25), 255604.
44. Šuligoj, A.; Štangar, U. L.; Ristić, A.; Mazaj, M.; Verhovšek, D.; Tušar, N. N., TiO_2–SiO_2 films from organic-free colloidal TiO_2 anatase nanoparticles as photocatalyst for removal of volatile organic compounds from indoor air. *Applied Catalysis B: Environmental* **2016,** *184*, 119-131.
45. Anderson, C.; Bard, A. J., An improved photocatalyst of TiO_2/SiO_2 prepared by a sol-gel synthesis. *Journal of Physical Chemistry* **1995,** *99*, 9882-9885.
46. Levchuk, I.; Kralova, M.; Rueda-Márquez, J. J.; Moreno-Andrés, J.; Gutiérrez-Alfaro, S.; Dzik, P.; Parola, S.; Sillanpää, M.; Vahala, R.; Manzano, M. A., Antimicrobial activity of printed composite TiO_2/SiO_2 and TiO_2/SiO_2/Au thin films under UVA-LED and natural solar radiation. *Applied Catalysis B: Environmental* **2018,** *239*, 609-618.
47. Li, G.; Liu, F.; Zhang, Z., Enhanced photocatalytic activity of silica-embedded TiO_2 hollow microspheres prepared by one-pot approach. *Journal of Alloys and Compounds* **2010,** *493* (1-2), L1-L7.
48. Aguado, J.; Vangrieken, R.; Lopezmunoz, M.; Marugan, J., A comprehensive study of the synthesis, characterization and activity of TiO_2 and mixed TiO_2/SiO_2 photocatalysts. *Applied Catalysis A: General* **2006,** *312*, 202-212.
49. Malinowska, B.; Walendziewski, J.; Robert, D.; Weber, J. V.; Stolarski, M., The study of photocatalytic activities of titania and titania–silica aerogels. *Applied Catalysis B: Environmental* **2003,** *46* (3), 441-451.
50. Jafry, H. R.; Liga, M. V.; Li, Q.; Barron, A. R., Simple route to enhanced photocatalytic activity of P25 titanium dioxide nanoparticles by silica addition. *Environmental Science and Technology* **2011,** *45* (4), 1563-8.
51. Yaparatne, S.; Tripp, C. P.; Amirbahman, A., Photodegradation of taste and odor compounds in water in the presence of immobilized TiO_2-SiO_2 photocatalysts. *Journal of Hazardous Materials* **2018,** *346*, 208-217.
52. Harraz, F. A.; Abdel-Salam, O. E.; Mostafa, A. A.; Mohamed, R. M.; Hanafy, M., Rapid synthesis of titania–silica nanoparticles photocatalyst by a modified sol–gel method for cyanide degradation and heavy metals removal. *Journal of Alloys and Compounds* **2013,** *551*, 1-7.
53. Liga, M. V.; Maguire-Boyle, S. J.; Jafry, H. R.; Barron, A. R.; Li, Q., Silica decorated TiO_2 for virus inactivation in drinking water--simple synthesis method and mechanisms of enhanced inactivation kinetics. *Environmental Science and Technology* **2013,** *47* (12), 6463-70.
54. Yuan, L.; Han, C.; Pagliaro, M.; Xu, Y.-J., Origin of enhancing the photocatalytic performance of TiO_2 for artificial photoreduction of CO_2 through a SiO_2 coating strategy. *The Journal of Physical Chemistry C* **2015,** *120* (1), 265-273.
55. Kang, C.; Jing, L.; Guo, T.; Cui, H.; Zhou, J.; Fu, H., Mesoporous SiO_2-modified nanocrystalline TiO_2 with high anatase thermal stability and large surface area as efficient photocatalyst. *Journal of Physical Chemistry C* **2009,** *113*, 1006–1013.
56. Li, G.; Gray, K. A., The solid–solid interface: Explaining the high and unique photocatalytic reactivity of TiO2-based nanocomposite materials. *Chemical Physics* **2007,** *339* (1–3), 173-187.
57. Pinho, L.; Mosquera, M. J., Photocatalytic activity of TiO_2–SiO_2 nanocomposites applied to buildings: Influence of particle size and loading. *Applied Catalysis B: Environmental* **2013,** *134-135*, 205-221.
58. Yu, Y.; Zhu, M.; Liang, W.; Rhodes, S.; Fang, J., Synthesis of silica–titania composite aerogel beads for the removal of Rhodamine B in water. *RSC Advances* **2015,** *5* (89), 72437-72443.
59. Li, Z.; Hou, B.; Xu, Y.; Wu, D.; Sun, Y., Hydrothermal synthesis, characterization, and photocatalytic performance of silica-modified titanium dioxide nanoparticles. *Journal of Colloid and Interface Science* **2005,** *288* (1), 149-54.
60. Gao, X.; EWachs, I., Titania–silica as catalysts - molecular structural characteristics and physico-chemical properties. *Catalysis Today* **1999,** *51*, 233-254.
61. Simpson, D. J.; Thilagam, A.; Cavallaro, G. P.; Kaplun, G.; Gerson, A. R., SiO_2 coated pure and doped titania pigments- low temperature CVD deposition and quantum chemical study. *Physical Chemistry Chemical Physics* **2011,** *13*, 21132-21138.

62. Van Bui, H.; Grillo, F.; van Ommen, J. R., Atomic and molecular layer deposition: off the beaten track. *Chemical Communications* **2017,** *53* (1), 45-71.
63. Miikkulainen, V.; Leskela, M.; Ritala, M.; Puurunen, L., Crystallinity of inorganic films grown by atomic layer deposition: Overview and general trends. *Journal of Applied Physics* **2013,** *113*, 021301.
64. Ferguson, J. D.; Weimer, A. W.; George, S. M., Atomic layer deposition of SiO_2 films on BN particles using sequential surface reactions. *Chemistry of Materials* **2000,** *12*, 3472–3480.
65. Sneh, O.; Wise, M. L.; Ott, A. W.; Okada, L. A.; George, S. M., Atomic layer growth of SiO_2 on Si(100) using $SiCl_4$ and H_2O in a binary reaction sequence. *Surface Science* **1995,** *334*, 135-152.
66. Kang, J. K.; Musgrave, C. B., Mechanism of atomic layer deposition of SiO_2 on the silicon (100)-2×1 surface using $SiCl_4$ and H_2O as precursors. *Journal of Applied Physics* **2002,** *91* (5), 3408-3414.
67. Guo, J.; Van Bui, H.; Valdesueiro, D.; Yuan, S.; Liang, B.; van Ommen, J. R., Suppressing the photocatalytic activity of TiO_2 nanoparticles by extremely thin Al_2O_3 films grown by gas-phase deposition at ambient conditions. *Nanomaterials* **2018,** *8* (2).
68. Klaus, J. W.; George, S. M., SiO_2 chemical vapor deposition at room temperature using $SiCl_4$ and H_2O with an NH_3 catalyst. *Journal of The Electrochemical Society* **2000,** *147*, 2658-2664.
69. Du, Y.; Du, X.; George, S. M., SiO_2 film growth at low temperatures by catalyzed atomic layer deposition in a viscous flow reactor. *Thin Solid Films* **2005,** *491* (1-2), 43-53.
70. Van Bui, H.; Grillo, F.; Kulkarni, S. S.; Bevaart, R.; Van Thang, N.; van der Linden, B.; Moulijn, J. A.; Makkee, M.; Kreutzer, M. T.; van Ommen, J. R., Low-temperature atomic layer deposition delivers more active and stable Pt-based catalysts. *Nanoscale* **2017,** *9* (30), 10802-10810.
71. George, S. M., Atomic layer deposition: An overview. *Chemical Reviews* **2010,** *110*, 111-131.
72. de Boer, J. H.; Lippens, B. C.; Linsen, B. G.; Broekhoff, J. C. P.; van den Heuvel, A.; Osinga, T., J., The t-curve of multimolecular N_2-adsorption. *Journal of Colloid and Interfac Science* **1966,** *21*, 405-414.
73. Jun, J.; Dhayal, M.; Shin, J.-H.; Kim, J.-C.; Getoff, N., Surface properties and photoactivity of TiO_2 treated with electron beam. *Radiation Physics and Chemistry* **2006,** *75* (5), 583-589.
74. Biesinger, M. C.; Lau, L. W. M.; Gerson, A. R.; Smart, R. S. C., Resolving surface chemical states in XPS analysis of first row transition metals, oxides and hydroxides: Sc, Ti, V, Cu and Zn. *Applied Surface Science* **2010,** *257* (3), 887-898.
75. Sasahara, A.; Pang, C. L.; Tomitori, M., Atomic scale analysis of ultrathin SiO_2 films prepared on TiO_2(100) surfaces. *Journal of Physcal Chemistry C* **2010,** *114*, 20189–20194.
76. Chao, S. S.; Takagi, Y.; Lucovsky, G.; Pai, P.; C., C. R.; Tyler, J. E.; Keem, J. E., Chemical states study of Si in SiOx films grown by PECVD. *Applied Surface Science* **1986,** *26*, 575-583.
77. Xu, Y.-h.; Zeng, Z.-x., The preparation, characterization, and photocatalytic activities of Ce-TiO_2/SiO_2. *Journal of Molecular Catalysis A: Chemical* **2008,** *279* (1), 77-81.
78. Ren, S.; Zhao, X.; Zhao, L.; Yuan, M.; Yu, Y.; Guo, Y.; Wang, Z., Preparation of porous TiO_2/silica composites without any surfactants. *Journal of Solid State Chemistry* **2009,** *182* (2), 312-316.
79. Zhang, H.; Luo, X.; Xu, J.; Xiang, B.; Yu, D., Synthesis of TiO_2/SiO_2 core/shell nanocable arrays. *Journal of physical Chemistry B* **2004,** *108*, 14866–14869.
80. Anderson, C.; Bard, A. J., Improved photocatalytic activity and characterization of mixed TiO_2/SiO_2 and TiO_2/Al_2O_3 materials. *Journal of Physical Chemistry B* **1997,** *101*, 2611-2616.
81. Wang, S.; Teng, F.; Zhao, Y., Effect of the molecular structure and surface charge of a bismuth catalyst on the adsorption and photocatalytic degradation of dye mixtures. *RSC Advances* **2015,** *5*, 76588-76598.
82. Auffan, M.; Pedeutour, M.; Rose, J.; Masion, A.; Ziarelli, F.; Borschneck, D.; Chaneac, C.; Botta, C.; Chaurand, P.; Labille, J.; Bottero, J.-Y., Structural degradation at the surface of a TiO_2-based nanomaterial used in cosmetics. *Environmental Science and Technology* **2010,** *44*, 2689–2694.

5

Mechanistic insight into the improved photocatalytic degradation of dyes using TiO_2 (P25) nanoparticles with an ultrathin SiO_2 coating

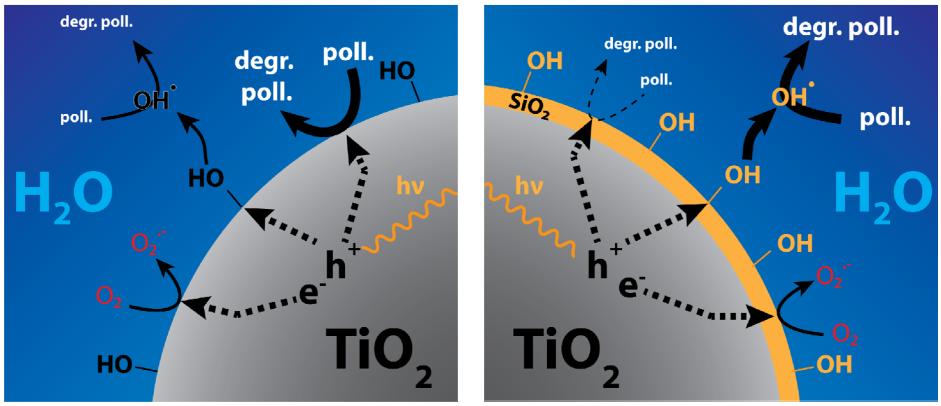

The photocatalytic mechanism of TiO_2 (P25) nanoparticles coated with SiO_2 (SiO_2:P25) layers by atomic layer deposition has been studied. The formation of thin SiO_2 layers on P25 not only gives a photocatalytic improvement for the degradation of Rhodamine B (3.6–fold) and Acid Blue 9 (3–fold) but also changes the mechanism from direct oxidation of the pollutant at the surface of TiO_2 (P25) *to a predominantly OH radical based degradation of the pollutants using SiO_2:*TiO_2(P25)*. SiO_2 layers on TiO_2 improve the generation of OH radicals due to the more acidic Si–OH groups in combination with the facilitated charge separation at the TiO_2–SiO_2 interface. The degradation of differently charged dyes on the SiO_2:*TiO_2(P25) *surface demonstrates the independence of the adsorption properties on the photocatalytic improvement. Simultaneous degradation of two dyes demonstrated the advantage of SiO_2:*TiO_2 (P25) *being less selective and, therefore, may be better suited for general water purification.*

In Preparation

Dominik Benz, Hao Van Bui, Hubertus T. Hintzen, Michiel T. Kreutzer, and J. Ruud van Ommen

5.1. INTRODUCTION

Photocatalysis undoubtedly has excellent potential for chemistry with several environmental applications, such as air purification and water cleaning. Since the first paper by Fujishima and Honda [1] almost 50 years ago, substantial progress has been made. However, further significant steps are required to come to the broad implementation of this technology. For the commonly used photocatalyst TiO_2, numerous studies have investigated the photocatalytic mechanism. [2-11] However, improved photocatalysts based on modifications of TiO_2 are often still lacking a clear description of the photocatalytic mechanism. This hampers the rational design of high-performance photocatalysts, where the combination of multiple materials could lead to significant activity improvement.

The photocatalytic activity is commonly improved by incorporating heteroatoms either in bulk or adding materials onto the surface, which enhances one or more properties important for photocatalysis. In heterogeneous photocatalysis for water treatment four different steps are essential for a reaction: 1) adsorption of reactants to the surface, 2) light absorption of the catalyst leading to excitation of an electron from the valence band (VB) to the conduction band (CB) 3) redox reactions of the reactants (pollutant, H_2O or O_2) on the surface to directly degrade pollutants or generate reactive oxygen species (ROS) and 4) desorption of the reactant from the surface. Upon light absorption with an energy higher than the bandgap, an electron (e^-) is excited to the conduction band, leaving a hole (h^+) back in the valence band. Excited electrons are able to reduce the dissolved O_2 in the water to a superoxide radical O_2^{*-}, further reacting to OH^* radicals, and subsequently attacking and degrading the pollutant. Moreover, holes in the VB are either able to oxidize the pollutant directly or react with water to form hydroxyl radicals OH^*, which subsequently attack the pollutant. [12-13] In order to improve the performance of a photocatalyst, different strategies can be applied to optimize the properties involved in each step: 1) Increase the adsorption of the reactants to reduce mass transfer limitations, 2) absorb more light to generate more charge carriers or utilize the light better by preventing electron-hole recombination, 3) improve the formation of reactive oxygen species (OH^*, O_2^{*-}) to degrade pollutants faster, and 4) enhance the desorption of products to prevent surface poisoning. [14-15]

Photocatalysts containing both SiO_2 and TiO_2 were investigated widely in recent research. However, SiO_2 was mostly used as a substrate were TiO_2 was deposited onto since it is believed that SiO_2 due to its electronic properties will block the photocatalytic activity. [16-20] Reports indicate that by using SiO_2 as a substrate, the adsorption of pollutants is increased due to a change in the surface charge/zeta potential leading to an improvement in the photocatalytic activity. [16-17] Only recently, studies of core/shell particles with TiO_2 and SiO_2 have elaborated on the photocatalytic activity of degrading organic pollutants. [21-25] Very thin layers of SiO_2 on TiO_2 are needed to observe an improvement in the photocatalytic activity. The reasons for the enhancement are ascribed to enhanced adsorption [21-22, 26] and better charge transfer/ improved charge separation [27-29] or better desorption of the degradation products. [23-24]

However, an overall understanding with a clear insight into the predominant photocatalytic reaction pathway is still lacking.

In this chapter, we elucidate the photocatalytic mechanism of SiO_2 coated TiO_2 (P25) by evaluating the fundamental steps in photocatalysis for TiO_2 (P25) compared to SiO_2:TiO_2(P25). Applying the finding from our previous research [30] where atomic layer deposition allowed us to build up SiO_2 layer by layer due to its characteristic alternating gas phase exposures of metal precursor and oxidizer, resulting in a photocatalytic improvement for SiO_2 on TiO_2 (P25), the thus obtained materials will serve us to clarify the predominant photocatalytic pathways. By comparison of the degradation behavior of two oppositely charged pollutants, we elaborate on the importance of adsorption on the surface. Sacrificial agents and simultaneous degradation of two oppositely charged dye molecules gave insight into predominant photocatalytic pathways for the radical generation. For this purpose, we employ atomic layer deposition (ALD) to deposit ultra-thin layers of SiO_2 onto TiO_2 (P25) particles to obtain a model catalyst where we are able to investigate the photocatalytic mechanism in detail. This will open up the door for further developments of novel multi-component materials, where different functionalities linked to subsequent mechanisms steps could be added to further improve the catalytic activity.

5.2. EXPERIMENTAL SECTION

5.2.1. Materials synthesis

TiO_2 (P25) nanoparticles (mean diameter ~21 nm, specific surface area of ~54 m^2g^{-1} measured by BET) were purchased from Evonik Industries (Hanau, Germany). The powder was sieved prior to the ALD experiments with a 250 µm sieve to break or exclude larger agglomerates.
Silicon tetrachloride ($SiCl_4$) was purchased from Sigma-Aldrich and stored in a stainless steel bubbler for mounting into the ALD setup.
Acid Blue 9 (AB9), Rhodamine B (RhB), Methanol, and DMSO were purchased from Sigma Aldrich and were used without further purification.
Silicon dioxide was deposited on the P25 particles on a homebuilt ALD setup in a fluidized bed under atmospheric pressure based on a setup described elsewhere. [31-32] In brief, the P25 powder was placed in a quartz glass column (diameter 26 mm, height 500 mm), which was then placed on a vertical vibration table (Paja 40/40-24) to assist fluidization. SiO_2 layers were deposited using $SiCl_4$ and H_2O as precursors, which both were kept at room temperature in stainless steel bubblers. The reactor was heated to 100 °C by an IR lamp, and a temperature feedback controller was placed inside the powder bed throughout the deposition process. Different SiO_2 loadings were produced by applying up to 40 cycles using 30 s $SiCl_4$ exposure and a 30 s water pulse. The precursors were carried to the reactor by a flow of nitrogen (0.5 L/min) and the pulses

were separated by purging steps of nitrogen for 3 min and 8 min, respectively. Afterward, the samples were calcined at 500 °C for 2h in air in a Neytech Vulcan Benchtop furnace.

5.2.2. Materials characterization

For the ICP-OES analysis, approximately 30 mg of sample was destructed in 4.5 ml 30 % HCl + 1.5 ml 65 % HNO_3 + 0.2 ml 40% HF acid mixture using a microwave. The destruction time in the microwave was 60 min. After the destruction, the samples were diluted to 50 ml with Milli-Q and analyzed with ICP-OES 5300DV. For Ti analysis, the samples were also diluted 20 times.

TEM micrographs were acquired from a JEOL JEM1400 transmission electron microscope at 120 kV. As-deposited TiO_2-SiO_2 nanoparticles were suspended in ethanol and transferred to Cu transmission electron microscopy grids (3.05 mm in diameter, Quantifoil).

X-ray photoelectron spectra (XPS) were recorded on a ThermoFisher K-Alpha system using Al Kα radiation with a photon energy of 1486.7 eV. The powder samples were immobilized on copper tape before loading into the XPS chamber. Scans were acquired using a 400 μm spot size, 55 eV pass energy, and 0.1 eV/step with charge neutralization. The peak positions were analyzed by calibrating the C 1s peak at 285 eV. The background was subtracted using ThermoAvantage software, applying a *SMART* type background subtraction.

UV/Vis diffuse reflectance spectra (DRS) were recorded on a Lamda 900 spectrophotometer recording the reflectance of the samples from an incident wavelength of 250 nm to 600 nm. The bandgap was obtained using the corresponding Tauc plot.

Zeta-potential measurements were executed on a Malvern Zetasizer Nano. The zeta-potential was measured in a solution of Rhodamine B (12 mg/l_{aq}) and Acid Blue 9 (16 mg/l_{aq}) with a catalyst concentration of 1 g/l. Prior to the measurement, the sample was stirred for 15 min, dispersed with a Sonotrode (Dr. Hielscher GmbH) for 1 min, followed by 15 min stirring. After equilibrating for 5 min, the sample was measured at 25 °C. For error analysis, each dispersion was measured three times.

Diffuse reflectance infrared Fourier transform spectra (DRIFTS) were recorded on a Thermo Nicolet Nexus IR with the OMNIC software. The sample was heated and measured at 150 °C to reduce the influence of adsorbed water. KBr served as a background and was subtracted for each sample.

5.2.3. Photocatalytic testing

Photocatalytic testing was performed in a 100 ml cylindrical glass container (irradiation surface 11.3 cm^2) with a 30 ml solution of Acid Blue 9 (16 mg/l, 20 µmol/l in deionized water) or Rhodamine B (12 mg/l, 25 µmol/l in deionized water) and 30 mg of catalyst powder. The test was executed in an Atlas SunTest XXL solar simulator equipped with 3 Xenon lamps (45 W/m^2) to ensure homogeneous light distribution and simulating the sun's spectrum in both the UV and visible light range. [33] Multiple samples were irradiated simultaneously on a stirring plate (700 rpm) with multiple spots. The powder was dispersed by sonicating the dispersion with the powder for 10 min. Additionally, the dispersion was stirred in the dark for another 20 min in order to reach the adsorption-desorption equilibrium. 1 ml samples were taken after distinct times of irradiation and were then centrifuged, and the supernatant liquid was then analyzed using a UV/Vis spectrometer (Hach-Lange DR5000). The absorption was measured at 629 nm and 554 nm, which are the maxima for Acid Blue 9 and RhB, respectively, from which the dye concentration C was deduced. According to first-order kinetics, $\ln(C_0/C_t)$ was plotted vs. decomposition time and the slope of the linear regression represents the kinetic constant. Tests with sacrificial agents were executed in the same manner adding 175 µl (82 mmol/l) of DMSO or 100 µl (82 mmol/l) methanol to the solution.

5

5.3. RESULTS AND DISCUSSION

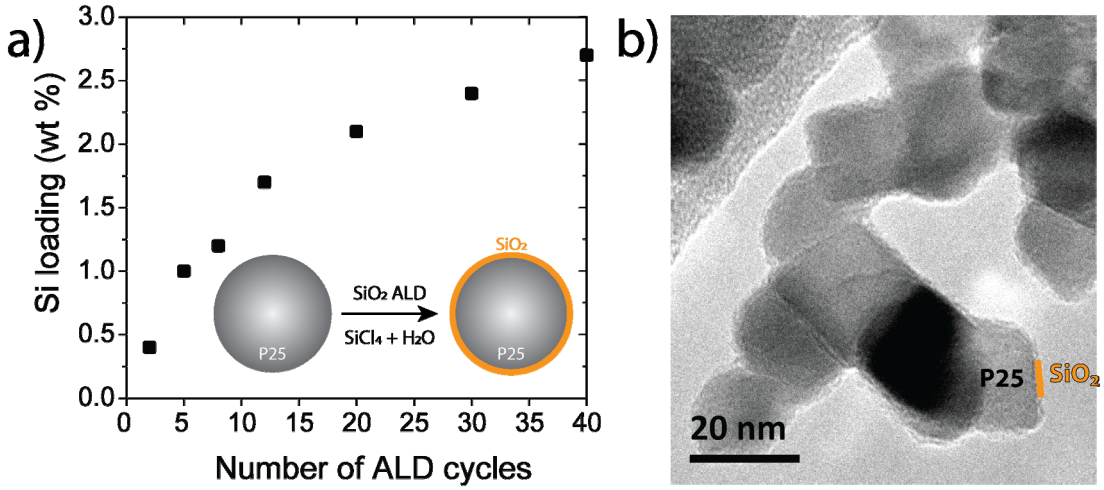

Figure 5.1: a) Loading of Si (wt %) vs. the number of ALD cycles; b) TEM image of SiO_2:TiO_2(P25) (1.7 wt % Si), layers of SiO_2 of around 1 nm thickness decorate the surface of P25 particles.

SiO_2 layers were deposited on P25 using atomic layer deposition. With this technique, we deposited SiO_2 up to 2.7 wt % Si (Fig. 5.1a) in a very conformal manner (Fig. 5.1b) where the Si loading (wt %) increases with the number of ALD cycles (Fig. 5.1a). The

higher growth per cycle for a low number of cycles arises from the better reactivity of $SiCl_4$ with the TiO_2 surface. The deposition could be proven by TEM, which exhibits a layer of SiO_2 around the P25 particle (Fig. 5.1b). Despite that in the TEM pictures, layer formation for high loadings can be clearly observed, the detection of ultrathin layers of SiO_2 for samples with very low loading remains difficult due to the resolution limit of the TEM. Moreover, a low number of cycles might cause porous or even incomplete coatings leaving the TiO_2 surface exposed to the environment. Additionally, for samples with a low number of $SiCl_4/H_2O$, XPS analysis reveals extensive contamination with Cl due to the incomplete reaction of $SiCl_2$ with water (Fig. S5.1). Post-annealing in air at 500 °C converted residual SiO_xCl_{4-2x} into SiO_2, as demonstrated by XPS (Fig. S5.2), eliminating the contamination arising from the deposition process. XRD revealed that P25 keeps its mixed crystalline anatase/rutile phase after annealing in air and that SiO_2 remained amorphous on the surface of TiO_2 (P25). [30] The photocatalytic degradation of both RhB and AB9 displays a major improvement with the deposition of SiO_2 layers onto P25 (Fig. S5.5, Fig. 5.2, RhB: 3.5-fold improvement for annealed 1.7 wt % SiO_2:TiO_2(P25), AB9: 3-fold improvement for annealed 1.7 wt % SiO_2:TiO_2(P25)). Moreover, while the post-treatment only insignificantly influences the photocatalytic activity of P25, it strongly influences the performance of SiO_2:TiO_2(P25). The Cl contamination has a significant negative impact on the photocatalytic activity with especially Acid Blue 9 (AB9) strongly adsorbing on the surface of the low loaded Si samples (Fig. S5.3). These chlorides in solution may arise from the reaction of water with the residual Cl in SiO_xCl_{4-2x} layer. Chloride contamination in solution results in a strong increase in the zeta potential of SiO_2. [34] This results in a more positive zeta potential, strongly increasing the adsorption of the negatively charge AB9 molecules. Additionally, chloride ions have been found capable of scavenging holes, leading to a decrease in photocatalytic activity. [35-36] This demonstrates that a pure SiO_2 layer is highly beneficial for photocatalytic improvement. Therefore, for the subsequent experiments, the annealed samples have been used.

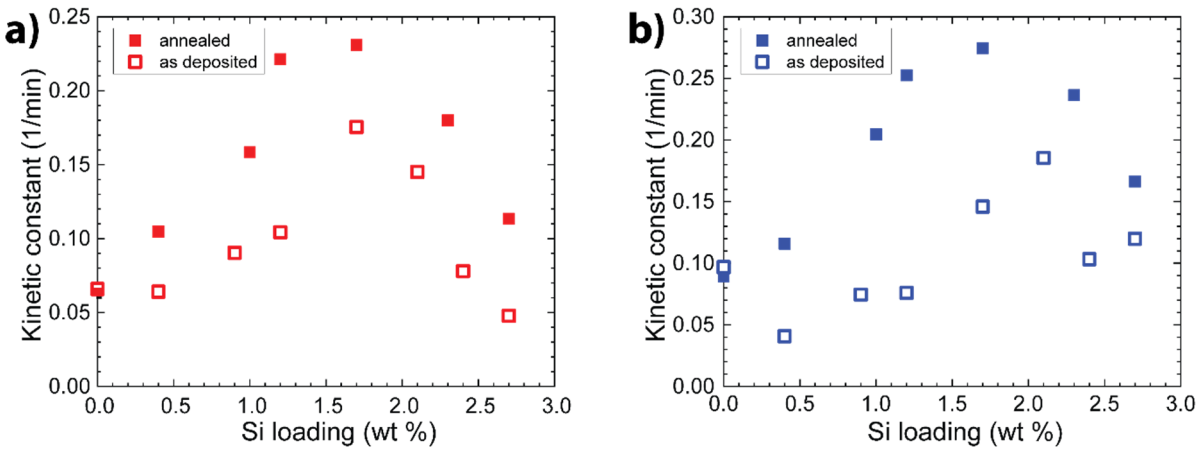

Figure 5.2: Kinetic constant for the photocatalytic degradation of a) RhB and b) AB9 using various loadings of Si, lighter shades represent the as-deposited samples.

Our previous research demonstrated a twofold enhancement for the degradation of Rhodamine B (RhB) with a loading of 1.9 wt % Si, followed by a total suppression of the photocatalytic activity for higher loadings (> 5 wt % Si). [30] Silicon dioxide – as an electric insulator with a bandgap of 9 eV – is not expected to have photocatalytic properties using the sun spectrum, due to insufficient photon energy to generate excited electrons and holes. This lack of charge transport in intrinsic SiO_2 explains the trend towards total suppression of the photocatalytic activity for higher loadings where the SiO_2 approaches the properties of pure SiO_2 as intrinsically photocatalytic inactive material. Higher loadings leading to thicker coatings additionally hinder the pollutants from reaching the active TiO_2 surface and blocking electron transport from the TiO_2 to the surface. [37] This explains the photocatalytic suppression of thick SiO_2 layers on P25. However, the reason for the photocatalytic enhancement due to an ultrathin SiO_2 layer on P25 particles and the predominant degradation pathways are still unresolved. We will now look at the activity increase for very low loadings using different tools to investigate the photocatalytic mechanism of a thin SiO_2 layer on P25 nanoparticles.

It is well known that SiO_2 surfaces have more acidic OH groups than TiO_2, which will result in a more negative zeta potential: the points of zero charge are about 3 [38] and 6 [39], respectively. Figure 5.3a shows the zeta potential for different loadings of SiO_2 on P25. It should be noted that the zeta potential was measured in the dye solutions to imitate the conditions used in the photocatalytic experiments. Uncoated P25 has a slightly positive zeta potential of 0-15 mV dependent on the dye in the solution. Upon deposition of SiO_2, the zeta potential decreases to approximately -40 mV for the samples with the highest SiO_2 loading, clearly indicating not only a change in the value but also a change from positive to negative values. This is a result of the difference of the isoelectric point (IEP) of SiO_2 (IEP = 3) versus TiO_2 (IEP = 6). [18, 40] The zeta potential of the powders dispersed in the solution of AB9 is generally more negative than in a solution of RhB (Fig. 5.2a), indicating that AB9, as a negatively charged dye, adsorbs strongly on the surface decreasing the effective intrinsic positive charge of the P25 particles. The change of zeta-potential upon deposition of SiO_2 on P25 particles is expected to lead to a difference in the adsorption behavior of RhB – a positively charged dye. Upon deposition of SiO_2, the adsorption-desorption equilibrium of AB9 trends to negligible adsorption whereas for RhB, an increase of adsorption and thus decrease in concentration is observed for higher loadings. (Fig. 5.3b).

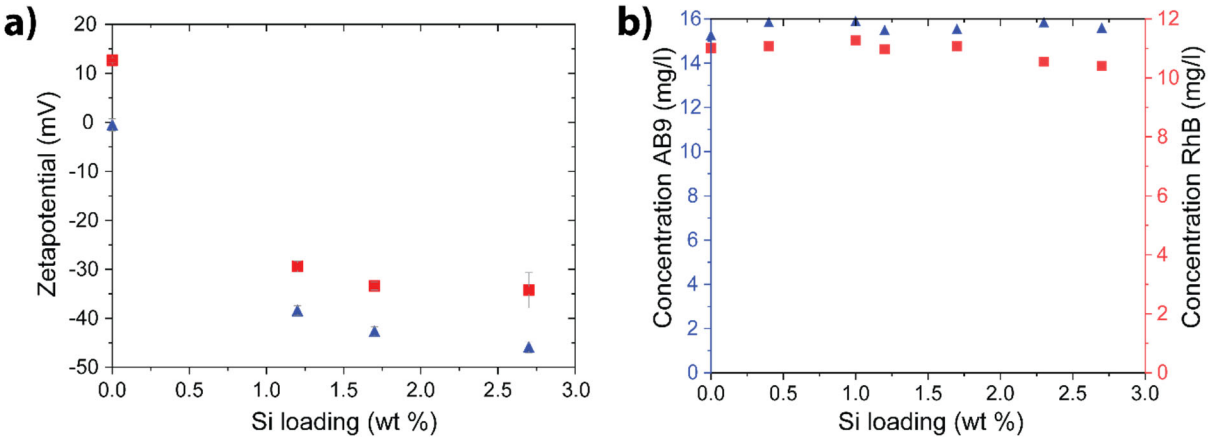

Figure 5.3: a) Zeta potential vs. SiO_2 loading (blue data points represent zeta potential in AB9 solution and red data points in RhB solution) b) Remaining concentration of AB9 (blue triangles) and RhB (red squares) after reaching the adsorption-desorption equilibrium. The initial concentration for AB9 and RhB was 16 mg/l and 12 mg/l, respectively.

Although negligible adsorption of AB9 on the surface of SiO_2 according to the results showing in Fig. 5.3b, we still can observe an improvement in the photocatalytic activity (2.5 times enhancement at 1.7 wt % Si). This demonstrates that eventual adsorption of reactants may play an insignificant role on the photocatalytic activity of SiO_2:TiO_2(P25).

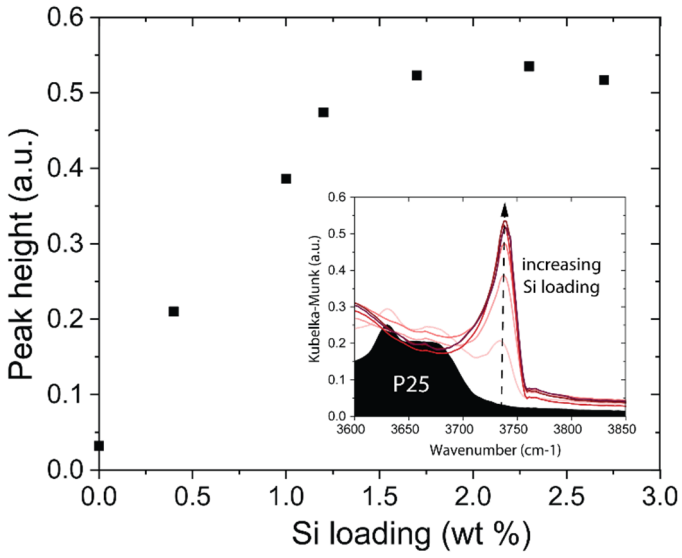

Figure 5.4: Peak height of Si-OH signal in DRIFTS spectra for samples with various Si loading; Inset: DRIFTS spectrum of different loadings of SiO_2 on P25 in the characteristic range for surface OH groups.

Surface OH groups have been shown to have an important role on the photocatalytic activity of TiO_2. [41] DRIFTS analysis provides insight into the quantity and type of

OH groups on the surface. The number of acidic surface OH groups on the SiO_2 surface (3740 cm^{-1}) increases with the Si loading reaching a plateau at 1.7 wt % Si. While for 0.4 wt % Si, the Ti-OH peaks (3600 – 3700 cm^{-1}) are still clearly visible, indicating only partial coverage of SiO_2 on P25, the Ti–OH peaks become less pronounced with increasing Si loading. These more acidic OH groups on the silica surface promote the generation of OH radicals. [42] The trend in the number of OH groups strongly correlates with the improvement of the photocatalytic activity for low loadings until 1.7 wt% Si demonstrating the influence of OH groups on the photocatalytic activity. Moreover, the stagnant number of OH groups for higher Si loadings combined with the insulating properties would, therefore, result in the observed optimal loading for SiO_2 on TiO_2 for the photocatalytic degradation.

In order to check the reaction pathways scavenging agents can be utilized to block specific pathways to find which contribution dominates in the photocatalytic degradation. Organic pollutants are generally degraded via three pathways [35, 43]: 1) direct oxidation by reaction with hole, and 2) decomposition by reaction with OH radicals, generated via h^+_{VB}, or 3) using the excited e^- in the conduction band to facilitate the O_2 reduction followed by OH radical formation (Fig. 5.5b).

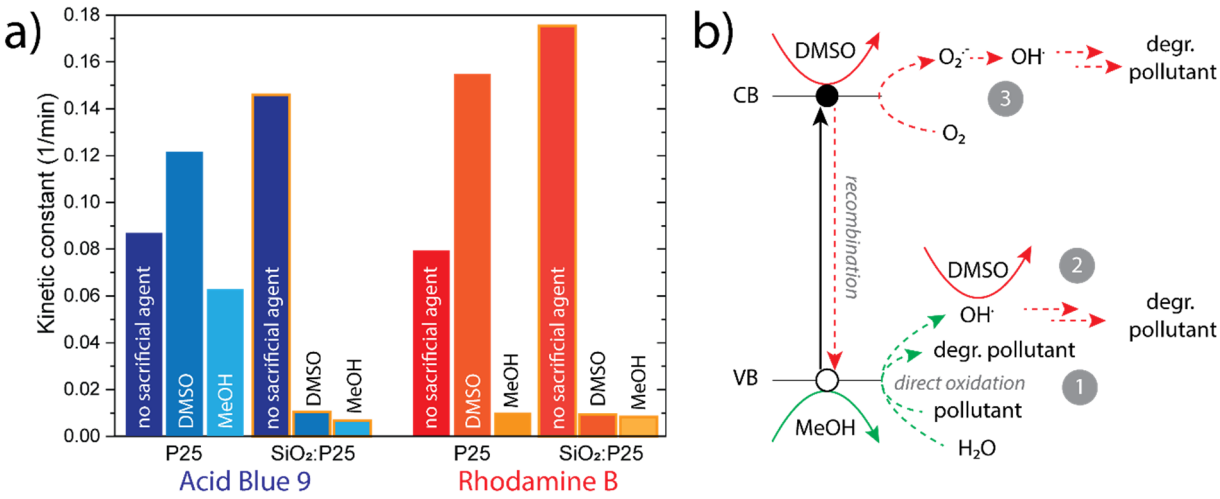

Figure 5.5: a) Kinetic constants for photocatalytic degradation of RhB or AB9 using DMSO (as CB electron scavenger and OH radical scavenger) or MeOH (as hole scavenger) for P25 and SiO_2:TiO_2(P25) (1.7 wt % Si). b) Schematic reaction pathways showing the influence of sacrificial agents DMSO and MeOH, dashed lines represent the reaction pathways that are prevented by the addition of sacrificial agents.

The addition of DMSO in large excess (scavenger/pollutant, mol/mol) to the suspension with P25, to ensure the prevalent reaction with the scavenger instead of the pollutant, surprisingly promotes the photocatalytic degradation of both AB9 and RhB. Even though DMSO used in photocatalytic studies is well known as OH radical scavenger [9, 44-46], these properties would only explain a decrease in the photocatalytic activity. Unfortunately, a detailed comparison of the experimental conditions with other

studies on P25 remains difficult due to the lack of information on the process conditions and scavenger concentration in many publications. However, other studies in the field of biology report DMSO as an acceptor for electrons to be reduced to dimethylsulfide. [47-48] DMSO is, therefore, not only able to scavenge OH radicals but also might react with the CB electrons. In the case of P25, this would thus result in the observed increase in the photocatalytic activity since the scavenging of the CB electrons will lead to suppression of charge recombination, allowing more VB holes to react with the pollutant directly. The results lead to the conclusion that by adding DMSO, the degradation of the pollutant only can be achieved by direct oxidation. This also indicates that degradation via OH radicals is not very effective for P25. When adding MeOH – a hole scavenger [49] – in both cases (AB9 and RhB) for P25, the photocatalytic activity drops. In the case of RhB, the degradation is strongly hindered. This demonstrates, on the one hand, that MeOH blocks the degradation pathways via the VB but also that the degradation pathway via the CB is not a dominant pathway for dye degradation using P25. These results suggest that the primary contributing mechanism is direct oxidation of the pollutant, which advocates that the adsorption of pollutants is an essential step for the photocatalytic degradation using P25. For the degradation of AB9, MeOH decreases the activity only slightly. AB9 and MeOH are in competition for the adsorption on the surface because of the negative charge of AB9 which is attracted by the positively charged TiO_2 surface, which leads to the degradation of AB9 whereas RhB (with its positive charge, negligibly adsorbed on the TiO_2 surface) seems to remain unreacted. Although these results indicate that direct oxidation dominates the degradation pathway of dyes, the degradation of RhB suggests that direct oxidation is not the exclusive mechanism, but the generation of ROS (i.e OH^*, O_2^{-*}) is still a possible pathway, yet less pronounced.

In the case of SiO_2:TiO_2(P25), DMSO reduces the photocatalytic activity to a very low value. As stated earlier, DMSO blocks not only the degradation via OH radicals generated via the VB but also the CB pathways by scavenging the CB electrons. Therefore, only degradation via direct oxidation would still be accessible. However, very little activity is observed, which poses that direct oxidation is not very pronounced for dye degradation using SiO_2:TiO_2(P25). Adding MeOH decreases the activity to the same extent as DMSO. This implies that also CB pathways are not the predominant degradation pathways since the VB pathways are blocked for dye degradation. These findings suggest that the OH radicals generated via the VB pathway on the SiO_2 surface are the dominant species for dye degradation using SiO_2:TiO_2(P25). The OH radicals will be formed on the SiO_2 surface diffusing then into the solution. [42]

SiO_2 layers are often used as anti-reflection layers, decreasing the scattered light from the coated particles. [50-51] However, this effect is, although present, in this case, not very pronounced according to the light absorption measurements (Fig. S5.4), due to the fact that the SiO_2 layer is ultrathin. The bandgap slightly shifts to larger values upon deposition of SiO_2 on the surface of P25 nanoparticles (Fig. S5.4), indicating that with higher Si loading negatively influences the light absorption. Previous research proposed that thin layers of SiO_2, despite the insulating properties of pure SiO_2, not

only allow the hole transfer to the surface by a tunneling effect due to a very thin coating of SiO_2 but also improve the charge separation due to the formation of a space charge layer as a consequence of Si-O-Ti interlinkages at the SiO_2-TiO_2 interface. [27, 52-53] The loading with low amounts of SiO_2 gives rise to incomplete coverage of the TiO_2 particles leaving the TiO_2 surface exposed to the environment. The excited electrons will, therefore, be able to react on the accessible TiO_2 surface facilitating a definitive charge separation. [22] Overall, the efficient charge separation followed by electron consumption at the TiO_2 surface and simultaneous hole transfer to the SiO_2 surface inducing the subsequent reaction with the more acidic Si–OH groups will then result in the increased formation of OH radicals. However, not only is the activity increased, but also the mechanism has changed compared to P25, i.e. thin SiO_2 layers on TiO_2 change the contribution of the different pathways from direct oxidation (P25) to degradation via OH radicals (SiO_2:TiO_2(P25)).

Additionally, testing the photocatalytic behavior of both materials – P25 and SiO_2:TiO_2(P25) – by the simultaneous degradation of AB9 and RhB gives insight into the selectivity and degradation behavior towards these pollutants.

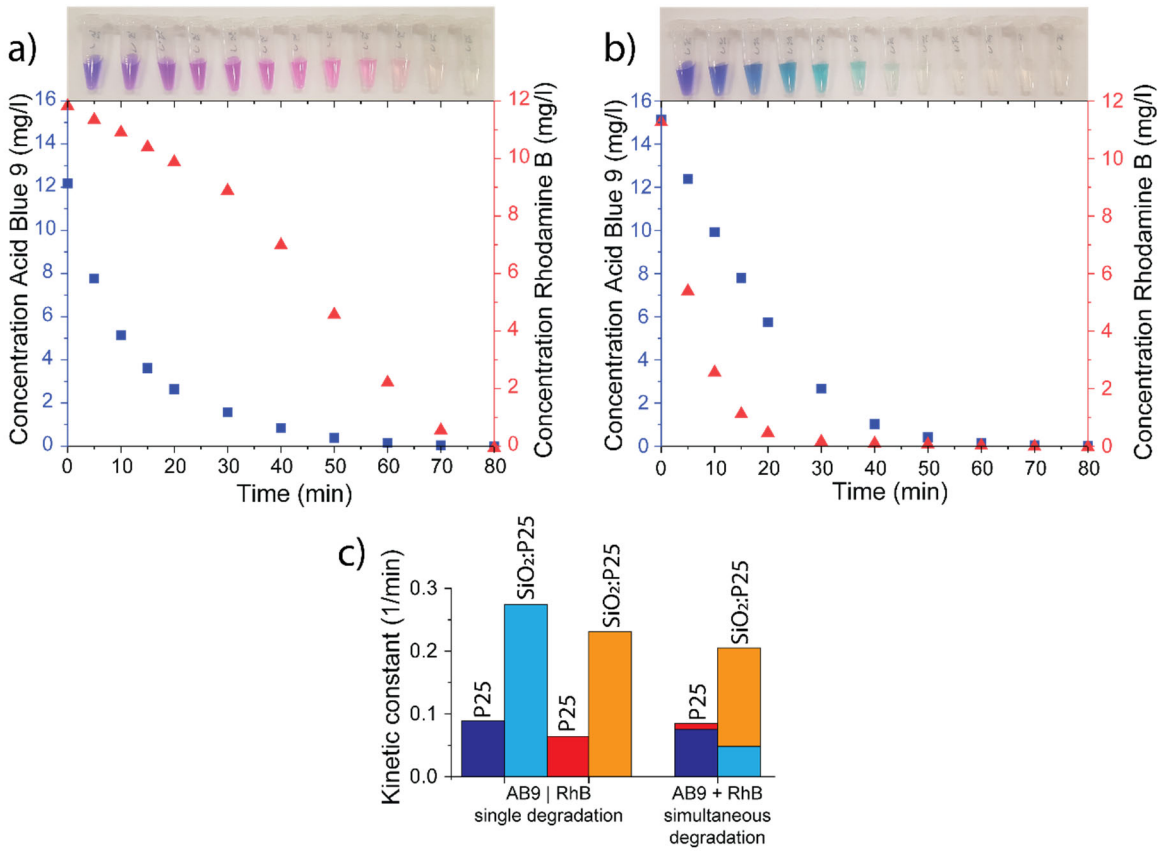

Figure 5.7: Simultaneous degradation of AB9 (blue squares) and RhB (red triangles) using a) P25 and b) SiO_2:TiO_2(P25) (1.7 wt % Si); c) first-order kinetic constants (0-20 min) for degradation of single compounds and simultaneous degradation of AB9 and RhB, the kinetic constants for simultaneous degradation are stacked

Table 5.1: Kinetic constants for the degradation of AB9, RhB (single), and RhB+AB9 (combined) using P25 and SiO_2:TiO_2(P25) (1.7 wt % Si). The kinetic constants were fitted from 0 to 20 min according to 1st order kinetics

Kinetic constant (min^{-1})	Acid Blue 9		Rhodamine B	
	Single	*Combined*	*Single*	*Combined*
P25	0.087 ± 0.001	0.079 ± 0.002	0.066 ± 0.001	0.009 ± 0.001
SiO_2:TiO_2(P25)	0.263 ± 0.006	0.046 ± 0.001	0.230 ± 0.003	0.154 ± 0.002

Following the color of the reaction solution by eye already gives a first indication for different degradation kinetics (Fig. 5.7a, b). While for P25, the red color (RhB) remains longer in solution, SiO_2:TiO_2(P25) maintains the blue color (AB9) for longer, indicating a quicker degradation of AB9 and RhB for P25 and SiO_2:TiO_2(P25), respectively. Moreover, SiO_2:TiO_2(P25) decolorizes the solution overall faster than uncoated P25, which proves the superiority of SiO_2:TiO_2(P25) over uncoated P25. In detail, P25 degrades AB9 faster than RhB showing first-order kinetics similar to the degradation of only AB9 in the solution (Fig. 5.7c, dark blue bars). On the other hand, the degradation of RhB is obstructed in the beginning when the concentration of AB9 is still high, only accelerating starting from 30 min when a low concentration of AB9 remains in the solution. This obstruction changes the kinetics of the degradation of RhB from 1st order kinetics, according to the Langmuir-Hinshelwood mechanism, over the whole range of reaction time, to two distinct time regimes, one which has limited adsorption due to the competition with AB9 (0-30 min) and the following (30-80 min), where the low AB9 concertation interferes less with the degradation of RhB. Noting that the direct dye oxidation is the dominant degradation mechanism, negatively charged AB9 adsorbed on the positive TiO_2 surface will impede RhB from getting access to reactive oxygen species and subsequently being degraded. Only after the concentration of AB9 on the surface has decreased sufficiently, RhB may reach the proximity of the TiO_2 to be attacked by radical species or ROS may be able to diffuse to the RhB molecules in solution additionally demonstrating the importance of adsorption on the surface advocating that the direct oxidation pathway is prevalent for P25. The similar speed of degradation for AB9 in the single degradation and combined degradation substantiates this pathway (Fig. 5.7c, Table 3.1).

For SiO_2:TiO_2(P25), in addition to faster degradation of RhB over AB9 in the dye mixture, the 1st order reaction mechanism remains valid for both individual dye degradations. With the positive charge, RhB prevails over AB9 for the competitive attraction to the negatively charged SiO_2 surface where the reactive oxygen species are formed, which explains the faster degradation of RhB (50 min) versus AB9 (70 min) as displayed in Figure 5.7b. In contrast to P25, both dyes are, however, degraded truly simultaneously in 1st order kinetics. Additionally, in all cases the degradation of the dye was complete since photocatalytic powder did not show any remaining coloring after

separation from the reaction solution. Comparing the kinetic constants with only a single dye in solution, the degradation proceeds overall slower, whereas the summation of the kinetic constants gives about equal values as for the individual degradation (Table 3.1). This indicates that both dyes are reached by degradation species simultaneously. This insight is in agreement with our previous finding that for SiO_2:TiO_2(P25), OH radicals are the predominant degradation pathway rather than direct oxidation on the surface. OH radicals – generated on the surface – can diffuse to a certain extent into the solution making the direct adsorption of the pollutant less relevant for the photocatalytic degradation. Considering this mechanism, the addition of both the individual kinetic constants for the combined degradation should add up to the kinetic constant obtained from the single dye degradation. However, the added kinetic constant is slightly lower than the kinetic constant of the single dyes. This behavior is already well observed in the literature that for higher pollutant concentrations, the kinetic constant decreases due to mass transport limitations. [2, 35]

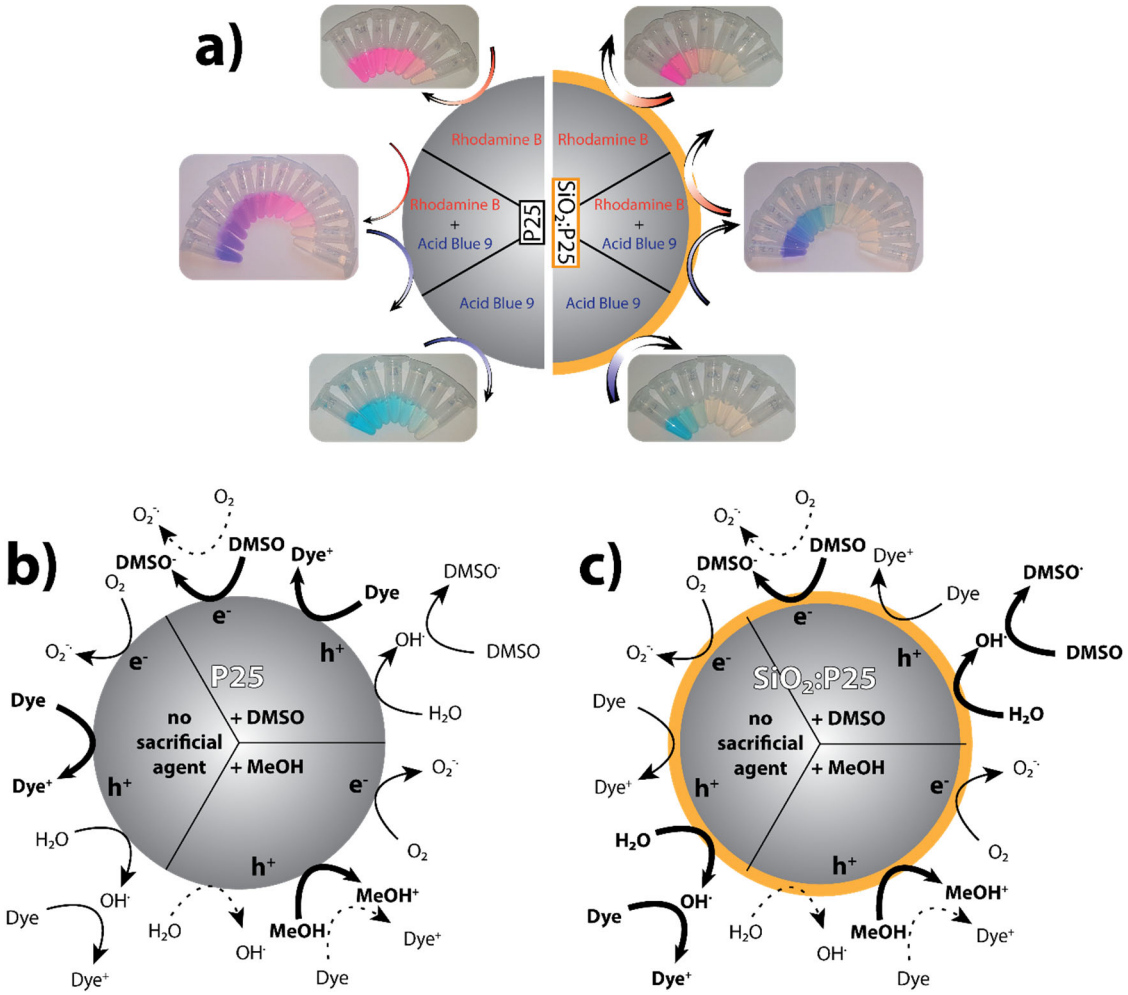

Figure 5.8: a) Scheme of the degradation of RhB, RhB + AB9, AB9 using P25 and SiO_2:TiO_2(P25), thickness of arrows represent the photocatalytic activity, pictures display the real samples taken after distinct time intervals; Photocatalytic mechanisms for b) P25 and c) SiO_2:TiO_2(P25) using no sacrificial agent, DMSO or MeOH; predominant reaction pathways are marked with thick arrows, pathways blocked by the sacrificial agent are displayed in dashed lines.

From the studies with sacrificial agents and the simultaneous degradation of two dyes, we can summarize that the P25 main, yet, not exclusive mechanism is direct oxidation for degrading organic pollutants, which can be concluded by the preferred degradation of the adsorbed pollutant. On the other hand, for SiO_2:TiO_2(P25), the simultaneous degradation of both dyes proves the preferred degradation via OH radicals, where direct contact with the surface is less important. OH radicals can diffuse to a certain extent into the solution to also oxidize molecules which are not directly adsorbed on the surface. Therefore, apart from the general improvement of SiO_2:TiO_2(P25) over P25 due to the easier OH radical generation from the Si–OH groups SiO_2:TiO_2(P25) degrades organic dyes less selectively. Although this lower selectivity might be disadvantageous for degradation of a defined effluent from a production site, the goal to clean water from an undefined water source requires unselective degradation of all organic matter to obtain good water quality. Clarifying the photocatalytic mechanism for SiO_2:TiO_2(P25) and applying this knowledge on the different degradation mechanisms opens doors to further developments where specific properties can be fine-tuned in catalyst development. Several modifications with different materials might, e.g., with atomic layer deposition, be able to improve individual pathways for radical generation and manufacture, therefore an overall better photocatalyst.

5.4. CONCLUSION

We have shown that thin layers of SiO_2 onto P25 can enhance the photocatalytic activity for the degradation of dyes independent on the charge of the pollutant. This indicates that the change of the surface charge by the deposition of SiO_2 layers on P25 only has little influence on the improved photocatalytic activity. The surface charge of SiO_2-coated TiO_2 (negative) versus uncoated TiO_2 (positive) changes only the preference of which pollutant will be degraded first when both are to be degraded simultaneously. But for independent dye degradation experiments, SiO_2:TiO_2(P25) shows superior photocatalytic activity, which can be ascribed to the more acidic OH groups on the surface introduced by the SiO_2 coating and the enhanced electron-hole separation due to the Ti–O–Si linkages at the TiO_2–SiO_2 interface as proposed in the literature. Using DMSO and MeOH as sacrificial agents, we have shown the difference in photocatalytic behavior of P25 and SiO_2:TiO_2(P25). From these experiments, it can be concluded that P25 prevalently degrades organic pollutants via direct oxidation by reaction with holes, whereas SiO_2:TiO_2(P25)mainly enhances the OH radical formation from reaction with holes, which is then responsible for pollutant degradation.

APPENDIX

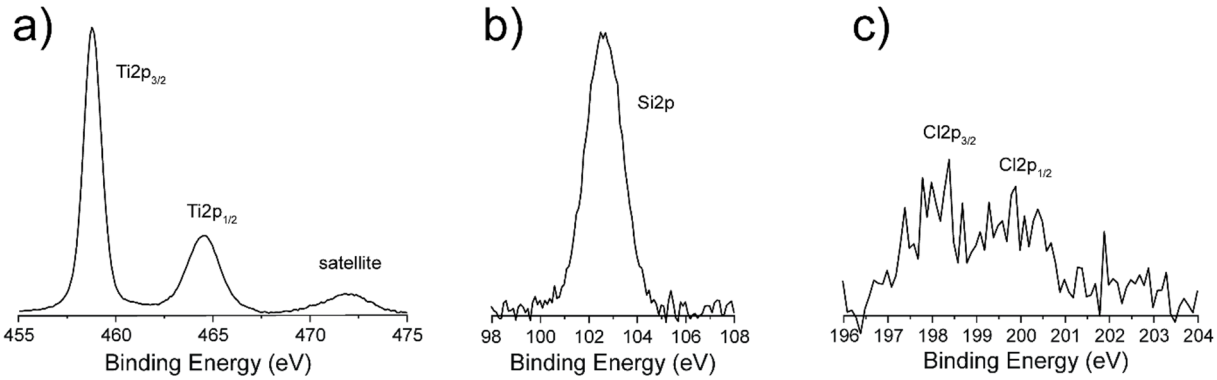

Figure S5.1: HRXPS spectra of SiO_2:P25 (1.7 wt % Si) a) HRXPS Ti spectrum, b) HRXPS Si spectrum, c) HRXPS Cl spectrum

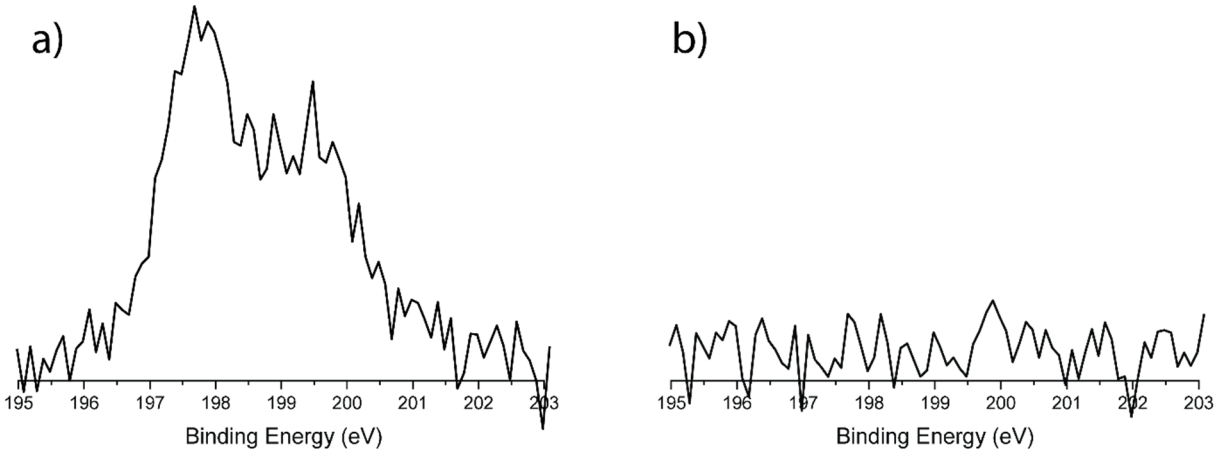

Figure S5.2: XPS Cl spectrum a) before and b) after annealing of low loaded SiO_2:P25 (0.4 wt% Si)

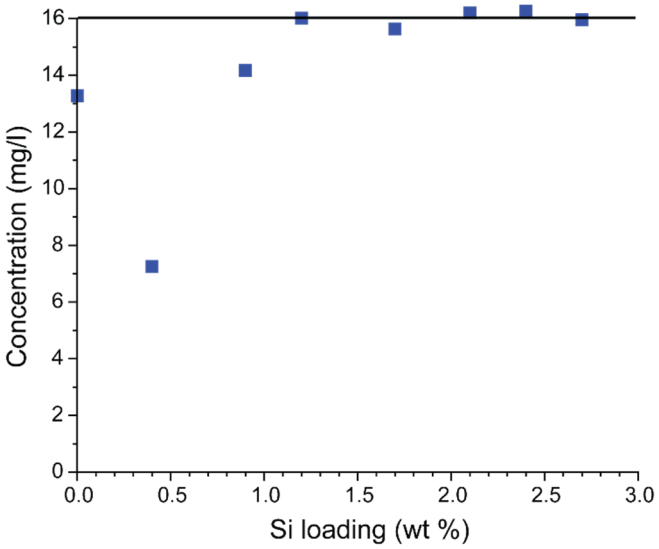

Figure S5.3: Remaining concentration of AB9 in the solution after reaching the adsorption-desorption equilibrium for samples without post-annealing in air

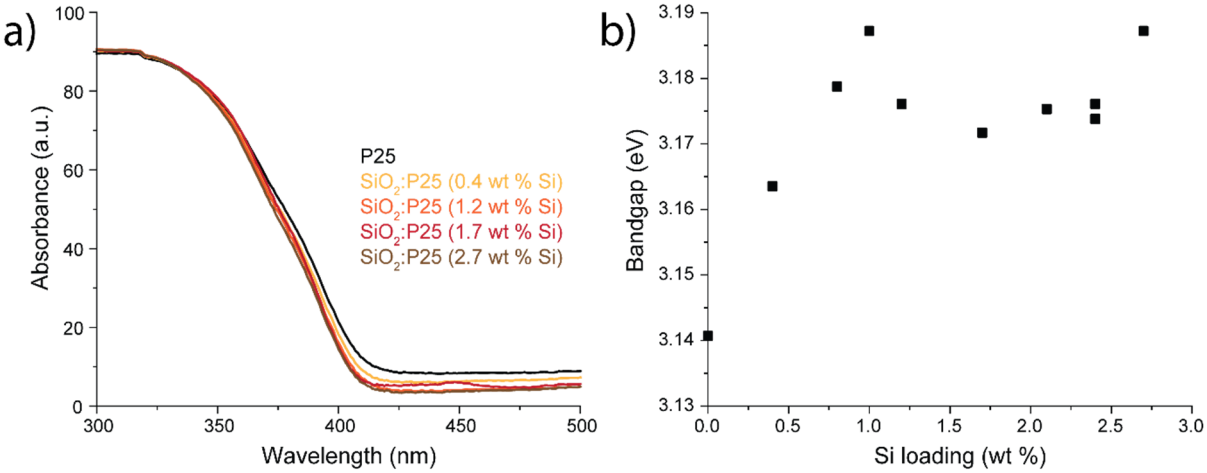

Figure S5.4: a) UV/Vis DRS for different loaded SiO_2:P25 catalysts, b) Bandgap of the SiO_2:P25 materials with different loadings calculated via the Tauc method form UV/Vis DRS spectra

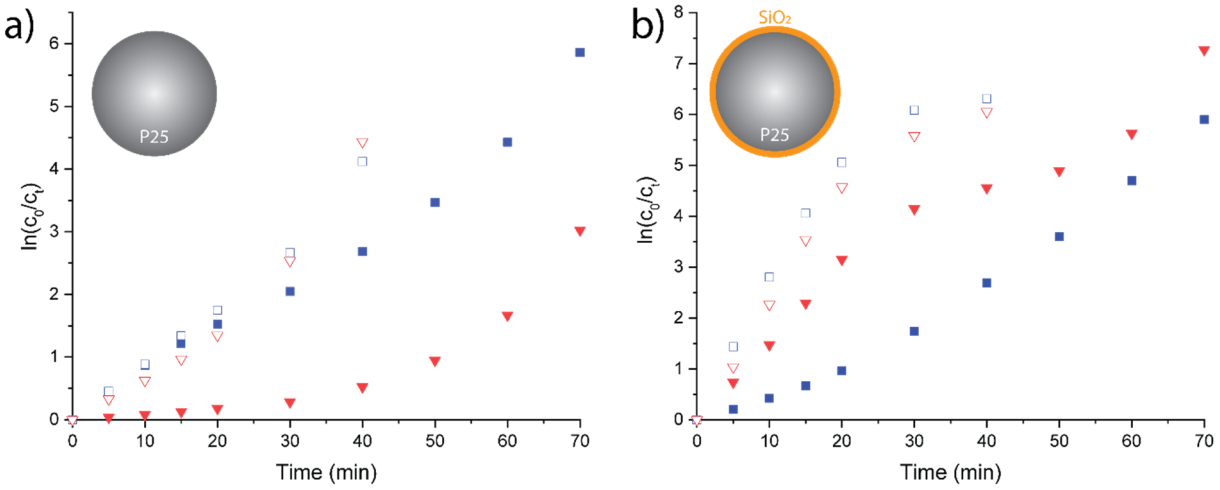

Figure S5.5: Plot of the $\ln(c_0/c_t)$ vs. the time for the degradation of Acid Blue 9 (blue square) and Rhodamine B (red triangles) for single compound degradation (empty symbols) and simultaneous degradation (filled symbols), a) P25 b) SiO_2:P25

REFERENCES

1. Fujishima, A.; Honda, K., Electrochemical Photolysis of Water at a Semiconductor Electrode. *Nature* **1972,** *238* (5358), 37-38.
2. Reza, K. M.; Kurny, A. S. W.; Gulshan, F., Parameters affecting the photocatalytic degradation of dyes using TiO2: a review. *Applied Water Science* **2015,** *7* (4), 1569-1578.
3. Carp, O.; Huisman, C. L.; Reller, A., Photoinduced reactivity of titanium dioxide. *Progress in Solid State Chemistry* **2004,** *32* (1–2), 33-177.
4. Trawiński, J.; Skibiński, R., Rapid degradation of clozapine by heterogeneous photocatalysis. Comparison with direct photolysis, kinetics, identification of transformation products and scavenger study. *Science of The Total Environment* **2019,** *665*, 557-567.
5. Fujishima, A.; Rao, T. N.; Tryk, D. A., Titanium dioxide photocatalysis. *Journal of Photochemistry and Photobiology C: Photochemistry Reviews* **2000,** *1* (1), 1-21.
6. Nosaka, Y.; Nosaka, A., Understanding Hydroxyl Radical (•OH) Generation Processes in Photocatalysis. *ACS Energy Letters* **2016,** *1* (2), 356-359.
7. Zhang, J.; Nosaka, Y., Mechanism of the OH Radical Generation in Photocatalysis with TiO_2 of Different Crystalline Types. *The Journal of Physical Chemistry C* **2014,** *118* (20), 10824-10832.
8. Levchuk, I.; Guillard, C.; Dappozze, F.; Parola, S.; Leonard, D.; Sillanpaa, M., Photocatalytic activity of TiO_2 films immobilized on aluminum foam by atomic layer deposition technique. *J. Photochem. Photobiol. A-Chem.* **2016,** *328*, 16-23.
9. Lin, X. H.; Miao, Y.; Li, S. F. Y., Location of photocatalytic oxidation processes on anatase titanium dioxide. *Catalysis Science & Technology* **2017,** *7* (2), 441-451.
10. Mortazavian, S.; Saber, A.; James, D. E., Optimization of Photocatalytic Degradation of Acid Blue 113 and Acid Red 88 Textile Dyes in a UV-C/TiO2 Suspension System: Application of Response Surface Methodology (RSM). *Catalysts* **2019,** *9* (4).
11. Motegh, M.; Cen, J.; Appel, P. W.; van Ommen, J. R.; Kreutzer, M. T., Photocatalytic-reactor efficiencies and simplified expressions to assess their relevance in kinetic experiments. *Chemical Engineering Journal* **2012,** *207-208*, 607-615.
12. Dong, S.; Feng, J.; Fan, M.; Pi, Y.; Hu, L.; Han, X.; Liu, M.; Sun, J.; Sun, J., Recent developments in heterogeneous photocatalytic water treatment using visible light-responsive photocatalysts: a review. *Rsc Advances* **2015,** *5* (19), 14610-14630.
13. Hoffmann, M. R.; Martin, S. T.; Choi, W.; Bahnemann, D. W., Environmental Applications of Semiconductor Photocatalysis. *Chemical Reviews* **1995,** *95* (1), 69-96.
14. Lee, K.; Yoon, H.; Ahn, C.; Park, J.; Jeon, S., Strategies to improve the photocatalytic activity of TiO2: 3D nanostructuring and heterostructuring with graphitic carbon nanomaterials. *Nanoscale* **2019,** *11* (15), 7025-7040.
15. Gaya, U. I., Origin of the Activity of Semiconductor Photocatalysts. In *Heterogeneous Photocatalysis Using Inorganic Semiconductor Solids*, Springer Netherlands: Dordrecht, 2014; pp 91-135.
16. Ullah, S.; Ferreira-Neto, E. P.; Pasa, A. A.; Alcântara, C. C. J.; Acuña, J. J. S.; Bilmes, S. A.; Martínez Ricci, M. L.; Landers, R.; Fermino, T. Z.; Rodrigues-Filho, U. P., Enhanced photocatalytic properties of core@shell SiO_2@TiO_2 nanoparticles. *Applied Catalysis B: Environmental* **2015,** *179*, 333-343.
17. Williams, P. A.; Ireland, C. P.; King, P. J.; Chater, P. A.; Boldrin, P.; Palgrave, R. G.; Claridge, J. B.; Darwent, J. R.; Chalker, P. R.; Rosseinsky, M. J., Atomic layer deposition of anatase TiO2 coating on silica particles: growth, characterization and evaluation as photocatalysts for methyl orange degradation and hydrogen production. *Journal of Materials Chemistry* **2012,** *22* (38), 20203-20209.
18. Ekka, B.; Sahu, M. K.; Patel, R. K.; Dash, P., Titania coated silica nanocomposite prepared via encapsulation method for the degradation of Safranin-O dye from aqueous solution: Optimization using statistical design. *Water Resources and Industry* **2016**.
19. Risa, K.; Naoki, S.; Makoto, O., Controlled Photocatalytic Ability of Titanium Dioxide Particle by Coating with Nanoporous Silica. *Chemistry Letters* **2008,** *37* (1), 76-77.
20. Kim, B.; Yang, I.; Jung, J. C.; Lee, T. S.; Yeom, B., Titania nanoparticle-loaded mesoporous silica synthesized through layer-by-layer assembly for the photodegradation of sodium dodecylbenzenesulfonate. *Applied Surface Science* **2019,** *490*, 38-46.
21. Grover, I. S.; Prajapat, R. C.; Singh, S.; Pal, B., SiO2-coated pure anatase TiO_2 catalysts for enhanced photo-oxidation of naphthalene and anthracene. *Particuology* **2017,** *34*, 156-161.

22. Giesriegl, A.; Blaschke, J.; Naghdi, S.; Eder, D., Rate-Limiting Steps of Dye Degradation over Titania-Silica Core-Shell Photocatalysts. *Catalysts* **2019,** *9* (7).
23. Nussbaum, M.; Paz, Y., Ultra-thin SiO_2 layers on TiO_2: improved photocatalysis by enhancing products' desorption. *Physical Chemistry Chemical Physics* **2012,** *14* (10), 3392-3399.
24. Oguma, J.; Kakuma, Y.; Nishikawa, M.; Nosaka, Y., Effects of Silica-Coating on the Photoinduced Hole Formation and Decomposition Activity of Titanium Dioxide Photocatalysts Under UV Irradiation. *Catalysis Letters* **2012,** *142* (12), 1474-1481.
25. Ide, Y.; Koike, Y.; Ogawa, M., Molecular selective photocatalysis by TiO_2/nanoporous silica core/shell particulates. *Journal of Colloid and Interface Science* **2011,** *358* (1), 245-251.
26. Anderson, C.; Bard, A. J., An Improved Photocatalyst of TiO_2/SiO_2 Prepared by a Sol-Gel Synthesis. *The Journal of Physical Chemistry* **1995,** *99* (24), 9882-9885.
27. Yuan, L.; Han, C.; Pagliaro, M.; Xu, Y.-J., Origin of Enhancing the Photocatalytic Performance of TiO_2 for Artificial Photoreduction of CO_2 through a SiO_2 Coating Strategy. *The Journal of Physical Chemistry C* **2016,** *120* (1), 265-273.
28. Gong, Y.; Wang, D. P.; Wu, R.; Gazi, S.; Soo, H. S.; Sritharan, T.; Chen, Z., New insights into the photocatalytic activity of 3-D core–shell P25@silica nanocomposites: impact of mesoporous coating. *Dalton Transactions* **2017,** *46* (15), 4994-5002.
29. Hu, S.; Li, F.; Fan, Z., Preparation of SiO_2-Coated TiO_2 Composite Materials with Enhanced Photocatalytic Activity Under UV Light. *Bulletin of the Korean Chemical Society* **2012,** *33* (6), 1895-1899.
30. Guo, J.; Benz, D.; Nguyen, T.-T. D.; Nguyen, P.-H.; Thi Le, T.-L.; La Zara, D.; Liang, B.; Hintzen, H. T.; van Ommen, J. R.; Bui, H. V., Tuning the Photocatalytic Activity of TiO_2 Nanoparticles by Ultrathin SiO_2 Films Grown by Low-Temperature Atmospheric Pressure Atomic Layer Deposition. *Applied Surface Science* **2019,** *[Under review]*.
31. Beetstra, R.; Lafont, U.; Nijenhuis, J.; Kelder, E. M.; van Ommen, J. R., Atmospheric Pressure Process for Coating Particles Using Atomic Layer Deposition. *Chemical Vapor Deposition* **2009,** *15* (7-9), 227-233.
32. van Ommen, J. R.; Goulas, A., Atomic layer deposition on particulate materials. *Materials Today Chemistry* **2019,** *14*, 100183.
33. Doekhi-Bennani, Y. Photoelectrocatalysis in water treatment. PhD Thesis, Delft University of Technology, Delft, 2017.
34. Kosmulski, M., Positive Electrokinetic Charge of Silica in the Presence of Chlorides. *Journal of Colloid and Interface Science* **1998,** *208* (2), 543-545.
35. Ahmed, S.; Rasul, M. G.; Martens, W. N.; Brown, R.; Hashib, M. A., Advances in Heterogeneous Photocatalytic Degradation of Phenols and Dyes in Wastewater: A Review. *Water, Air, & Soil Pollution* **2010,** *215* (1-4), 3-29.
36. Sökmen, M.; Özkan, A., Decolourising textile wastewater with modified titania: the effects of inorganic anions on the photocatalysis. *Journal of Photochemistry and Photobiology A: Chemistry* **2002,** *147* (1), 77-81.
37. El-Toni, A. M.; Yin, S.; Sato, T., Control of silica shell thickness and microporosity of titania-silica core-shell type nanoparticles to depress the photocatalytic activity of titania. *J Colloid Interface Sci* **2006,** *300* (1), 123-30.
38. Cloarec, J. P.; Chevalier, C.; Genest, J.; Beauvais, J.; Chamas, H.; Chevolot, Y.; Baron, T.; Souifi, A., pH driven addressing of silicon nanowires onto Si_3N_4/SiO_2 micro-patterned surfaces. *Nanotechnology* **2016,** *27* (29), 295602.
39. Zeng, M., Influence of TiO2Surface Properties on Water Pollution Treatment and Photocatalytic Activity. *Bulletin of the Korean Chemical Society* **2013,** *34* (3), 953-956.
40. Konecoglu, G.; Safak, T.; Kalpakli, Y.; Akgun, M., Photocatalytic degradation of textile dye CI Basic Yellow 28 wastewater by Degussa P25 based TiO_2. *Advances in environmental research* **2015,** *4* (1), 25-38.
41. Simonsen, M. E.; Li, Z.; Søgaard, E. G., Influence of the OH groups on the photocatalytic activity and photoinduced hydrophilicity of microwave assisted sol–gel TiO_2 film. *Applied Surface Science* **2009,** *255* (18), 8054-8062.
42. Narayanasamy, J.; Kubicki, J. D., Mechanism of Hydroxyl Radical Generation from a Silica Surface: Molecular Orbital Calculations. *The Journal of Physical Chemistry B* **2005,** *109* (46), 21796-21807.
43. Gaya, U. I., Principles of Heterogeneous Photocatalysis. In *Heterogeneous Photocatalysis Using Inorganic Semiconductor Solids*, Springer Netherlands: Dordrecht, 2014; pp 1-41.

44. Lopes, O. F.; Carvalho, K. T. G.; Macedo, G. K.; de Mendonça, V. R.; Avansi, W.; Ribeiro, C., Synthesis of $BiVO_4$via oxidant peroxo-method: insights into the photocatalytic performance and degradation mechanism of pollutants. *New Journal of Chemistry* **2015,** *39* (8), 6231-6237.
45. Panganamala, R. V.; Sharma, H. M.; Heikkila, R. E.; Geer, J. C.; Cornwell, D. G., Role of hydroxyl radical scavengers dimethyl sulfoxide, alcohols and methional in the inhibition of prostaglandin biosynthesis. *Prostaglandins* **1976,** *11* (4), 599-607.
46. Yoshimura, Y.; Inomata, T.; Nakazawa, H.; Kubo, H.; Yamaguchi, F.; Ariga, T., Evaluation of Free Radical Scavenging Activities of Antioxidants with an H_2O_2/NaOH/DMSO System by Electron Spin Resonance. *Journal of Agricultural and Food Chemistry* **1999,** *47* (11), 4653-4656.
47. Zinder, S. H.; Brock, T. D., Dimethyl sulfoxide as an electron acceptor for anaerobic growth. *Archives of Microbiology* **1978,** *116* (1), 35-40.
48. Beliaev, A. S.; Klingeman, D. M.; Klappenbach, J. A.; Wu, L.; Romine, M. F.; Tiedje, J. M.; Nealson, K. H.; Fredrickson, J. K.; Zhou, J., Global Transcriptome Analysis of Shewanella oneidensis MR-1 Exposed to Different Terminal Electron Acceptors. *Journal of Bacteriology* **2005,** *187* (20), 7138-7145.
49. Puangpetch, T.; Sreethawong, T.; Yoshikawa, S.; Chavadej, S., Hydrogen production from photocatalytic water splitting over mesoporous-assembled $SrTiO_3$ nanocrystal-based photocatalysts. *Journal of Molecular Catalysis A: Chemical* **2009,** *312* (1), 97-106.
50. Prado, R.; Beobide, G.; Marcaide, A.; Goikoetxea, J.; Aranzabe, A., Development of multifunctional sol–gel coatings: Anti-reflection coatings with enhanced self-cleaning capacity. *Solar Energy Materials and Solar Cells* **2010,** *94* (6), 1081-1088.
51. Lari, N.; Ahangarani, S.; Shanaghi, A., Preparation of nanostructure silica antireflective coatings by using sol–gel method. *Optik* **2015,** *126* (24), 5363-5367.
52. Miyashita, K.; Kuroda, S.-i.; Sumita, T.; Ubukata, T.; Kubota, H., Spectrum Response of the Vacuum-Deposited SiO_2/TiO_2 Multilyaer Film with Improved Photo-Catalytic Activity. *Journal of Materials Science Letters* **2001,** *20*, 2137-2140.
53. Guan, K.; Xu, H.; Lu, B. J., Hydrophilic property of SiO_2-TiO_2 overlayer films and TiO_2/SiO_2 mixing films. *Transactions of Nonferrous Metals Society of China (English Edition)* **2004,** *14*, 251-254.

6

ALD designed multi-component photocatalyst Pt:SiO_2:TiO_2 (P25) particles with improved activity for pollutant degradation

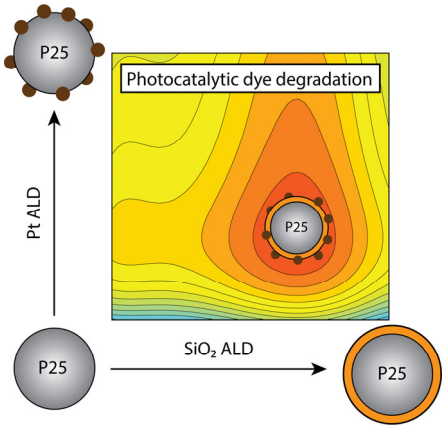

Photocatalysts for water cleaning typically lack efficiency for practical applications. Here we present a bi-modified (Pt:SiO_2:TiO_2 (P25)) material that was developed using knowledge of working mechanisms of mono-modified catalysts combined with the abilities of Atomic Layer Deposition (ALD). The deposition of ultrathin SiO_2 layers on TiO_2 nanoparticles, applying ALD in a fluidized bed reactor, demonstrated in earlier studies their beneficial effects for the photocatalytic degradation of organic pollutants due to more acidic surface Si–OH groups which benefit the hydroxyl radical generation. Furthermore, our investigation on the role of Pt on TiO_2(P25) as an improved photocatalyst demonstrated that oxygen adsorbed on the Pt particles reacts to superoxide radicals as an important factor for the catalytic improvement. Having recognized that the two independent materials, SiO_2:TiO_2(P25) and Pt:TiO_2(P25), have different mechanisms improving the photocatalytic activity provided the opportunity to combine these two materials into a bi-modified material, where we deposited SiO_2 onto TiO_2(P25) followed by deposition of nanoclusters of Pt. The resulting Pt:SiO_2:TiO_2(P25) nanopowder exceeded the dye degradation performance of both the individual SiO_2:TiO_2(P25) (1.5 fold) and Pt:TiO_2(P25) (four-fold) catalysts by six-fold as compared to TiO_2 (P25). This approach shows that by understanding the individual materials' behavior and using ALD as an appropriate deposition technique, new materials can be designed, further improving the photocatalytic activity and moving one step closer to implementation. We demonstrate that ALD is an attractive tech-nology to synthesize the catalysts developed by this approach in a precise and scalable way.

Published in Nanomaterials

Dominik Benz, Hubertus T. Hintzen, Hao Van Bui, Michiel T. Kreutzer, and J. Ruud van Ommen

6.1. INTRODUCTION

Titania (TiO_2) was first discovered as an active photocatalyst almost half a century ago [1] and still serves as a widely used benchmark for the development of new photocatalytic materials or as a substrate material to improve their photocatalytic properties. [2-4] The photocatalytic performance combined with affordable price, stability, and non-toxicity are a few reasons for this success in scientific publications. However, its implementation in real applications, despite these advantages, is hampered by poor sunlight utilization, due to a large bandgap, and charge recombination resulting in insufficient efficiency. [5-7] Improving TiO_2 by incorporating several elements into the lattice (bulk modification) or depositing different materials onto the surface (surface modification) has been extensively explored ever since. [8-13] This includes modifications with both noble metals and metal oxide for the improvement in: 1) reactant adsorption and reactivity by surface modification, 2) light absorption by bandgap modification, 3) charge utilization by modification of the band levels. These three approaches are dominantly targeted to develop a better catalyst. On the other hand, especially improvements in the rates and mechanisms of radical generation are often underestimated since they are often attributed to the improved light absorption or reduced charge recombination. However, it has been shown that surface modifications, which lead to a different type and amount of terminal OH groups, result in an increased OH radical generation. [14] Factors such as adsorption of the reactants for the ROS formation have been demonstrated to play a crucial role in the enhancement of the photocatalytic activity. [15-17] Overall, the photocatalytic mechanism gives four different points to tackle for making improved materials: [18-19]

1) Adsorption of reactants
2) Creation of charge carriers by light absorption
3) Charge carrier separation
4) Degradation reactions, along:
    a) Conduction band pathway via superoxide radicals (converting into hydroxyl radicals)
    b) Valence band pathway via direct oxidation
    c) Valence band pathway via hydroxyl radicals

While earlier material development focused more on the enhancement using single modifications on active materials, recently, multicomponent systems have received more attention. [20-25] However, most works on multicomponent materials focus on combining materials where components improve the processability of the catalyst for their implementation in future reactors (i.e., dispersion, separation using magnets). [21, 26] Multicomponent materials containing iron oxide as a core material, due to its magnetic properties, are good examples of materials improving both the processability and activity of a catalyst to enhance separation from the liquid after the reaction. [21, 24] Another approach is to modify the surface of an already photocatalytic material with a coating to change the deposition properties of the subsequently added co-catalyst i.e., increasing control of the particle size by modifying the surface or

preventing the agglomeration of deposited nanoclusters of the surface by a cover layer. [27-30] However, the manipulation of physical properties such as increased surface area, the addition of magnetic properties, or a beneficial layer to improve the dispersion of co-catalyst particles [31-32] is more straightforward than modifying the photocatalytic mechanisms themselves. The question arises whether multiple components, each enhancing the photocatalytic process, can be combined to reach higher enhancement than each component individually.

The approach of combining materials to make a more complex and improved structure can be tackled utilizing the advantages of atomic layer deposition. This technology allows to precisely control the deposition of various materials onto a surface. The advantages of confined scalable bottom-up building up of multicomponent catalyst materials could lead to the development of improved photocatalysts. However, building up multicomponent catalysts requires detailed knowledge of the photocatalytic working principles of the base materials as well as the building blocks and their interaction.

Surface deposited Pt on TiO_2 (P25) is a well-developed catalyst and has shown superior activity for the photocatalytic degradation of various organic pollutants. [33-34] Pt enhances the photocatalytic activity of TiO_2(P25) for dye degradation by acting as an adsorption surface for O_2 suppressing charge carrier recombination by facilitating improved radical generation via the conduction pathway in the presence of dissolved O_2. [15, 35] Our previous findings for the role of an ultrathin SiO_2 coating on TiO_2(P25) nanoparticles demonstrated an improved photocatalytic activity due to the improved generation of OH radicals at the SiO_2 surface from the more efficiently separated holes on the SiO_2 surface by the more acidic Si-OH surface groups [14, 17], which is different from TiO_2(P25) as well as Pt:TiO_2(P25). From this detailed analysis of the photocatalytic mechanisms, the question arises whether the advantages of these bi-material composites, Pt:TiO_2(P25) and SiO_2:TiO_2(P25), can be combined in a tri-material composite resulting in a further improved photocatalyst for dye degradation. Here, we demonstrate that catalyst development following the design principles of combining characteristics that are improving individual aspects of the photocatalytic reaction pathways can lead to superior photocatalysts by taking advantage of the controllability of the deposition using ALD.

6.2. EXPERIMENTAL SECTION

6.2.1. Synthesis

TiO_2 nanoparticles (P25, mean diameter ~21 nm, specific surface area of ~54 $m^2\ g^{-1}$ measured by BET) was purchased from Evonik Industries (Hanau, Germany). Silicon tetrachloride ($SiCl_4$) and trimethyl(methylcyclopentadienyl)platinum(IV) ($MeCpPtMe_3$) were purchased from AlfaAesar (Karlsruhe, Germany) and Strem Chemicals (Bischheim, France), respectively. Both chemicals were stored in a stainless steel

bubbler for mounting into the ALD setup. Acid Blue 9 (Brilliant Blue FCF) and sodium polyphosphate were purchased from SigmaAldrich (Zwijndrecht, The Netherlands) and used without further purification. Pt:SiO_2:TiO_2(P25) was synthesized via a two-step deposition process:

1) SiO_2 was deposited on TiO_2(P25) on a homebuilt ALD setup in a fluidized bed under atmospheric pressure, as described in detail elsewhere. [36-37] In brief, 5 g of the TiO_2(P25) powder was put in a quartz glass column (diameter 26 mm, height 500 mm), which was then placed on a vertical vibration table (Paja 40/40-24, Oosterhout, The Netherlands) to assist fluidization. The powder was sieved prior to the ALD experiments with a mesh size of 250 µm to break or exclude larger agglomerates. SiO2 layers were deposited using $SiCl_4$ and H_2O as precursors, which were both kept at room temperature in stainless steel bubblers. The reactor was heated to 100 °C throughout the deposition process using an IR lamp. For different SiO_2 loadings, up to 40 cycles were applied using an exposure time of 30 s $SiCl_4$ and a 3 min H_2O pulse. Purging steps of nitrogen for 3 min and 8 min, respectively, separated the precursor pulses.

2) The SiO_2:TiO_2(P25)powder was split into 1.5 g batches, which were then used for the deposition of Pt clusters on the SiO_2:TiO_2(P25)surface using $MeCpPtMe_3$and O_2 as precursors. The Pt precursor was stored in stainless steel bubblers and held at 70 °C. For those experiments, one ALD cycle was performed using exposure times for the Pt precursor ranging from 20 sec to 5 min. The O_2 exposure was set to 5 min, and both precursor exposures were separated using purge steps of 5 min with N_2, respectively. Afterward the coated powders were treated under an atmosphere of 5 % H_2 in N_2 (v/v) in a fixed bed reactor. The temperature was ramped up from room temperature to 200 °C with a rate of 2 °C/min and then was held constant for 5 min after which the powder was allowed to cool to room temperature.

6.2.2. Characterization

For the ICP-OES analysis, approximately 30 mg of sample was digested in a mixture of 4.5 mL 30% HCl, 1.5 mL 65% HNO_3, and 0.2 mL 40% HF using a microwave for 60 min. After the digestion, the samples were diluted to 50 mL with MilliQ water, and the weight percentage (wt. %) of Pt, Si, and Ti were analyzed with a Perkin Elmer ICP-OES 5300DV (Waltham, MA, USA) system. The samples were also diluted 20 times for the analysis of the Ti concentration.

TEM micrographs were acquired from a JEOL JEM1400 transmission electron microscope (Akishima, Japan) at 120 kV. As-deposited Pt:SiO_2:TiO_2(P25) nanoparticles were suspended in ethanol and transferred to Cu transmission electron microscopy grids (3.05 mm in diameter, Quantifoil, Großlöbichau, Germany).

X-ray photoelectron spectra (XPS) were recorded on a ThermoFisher K-Alpha (Blijswik, The Netherlands) system using Al Kα radiation with a photon energy of 1486.7 eV. A sufficient amount of powders was immobilized on copper tape before loading into the XPS chamber. Survey scans were acquired using a 400 µm spot size, 55 eV pass energy, and 0.1 eV/step with charge neutralization. The peak positions were calibrated by referencing the C 1s peak to 284.8 eV and previous background subtraction using the Thermo Avantage software (v5.985, accessed on 19 Feb 2019).

6.2.3. Photocatalytic testing

The photocatalytic activity was evaluated in a 100 ml glass bottle (irradiation surface 11.3 cm^2) with a 30 ml solution of Acid Blue 9 (16 mg/l in deionized water) and 30 mg of catalyst powder. Sodium polyphosphate (0.3 ml, 100 g/l in water) was added to aid the dispersion of the powder. [38] The powder was dispersed by sonicating the solution with the powder for 10 min. Additionally, the dispersion was stirred in the dark for another 20 min in order to reach the dye-adsorption-desorption equilibrium. The test was executed in open air in an Atlas SunTest XXL solar simulator equipped with three Xenon lamps (45 W/m^2) [39] to ensure homogeneous light distribution simulating the sun's spectrum in both the UV and visible light range. Multiple samples were irradiated on a multiple stirring plate (700 rpm). Samples of 1 ml were taken after distinct times of irradiation, were then centrifuged, and the dye concentration in the supernatant liquid was determined using a UV/Vis spectrometer (Hach-Lange DR5000). The absorption was measured at 629 nm, which represents the maximum absorption for Acid Blue 9. According to 1st order kinetics, $\ln(C_0/C_t)$ was plotted vs. time, and the slope of the linear regression represents the kinetic constant.

6.3. RESULTS & DISCUSSION

Previously, we have reported on the mechanisms of SiO_2:TiO_2(P25) [16-17] and Pt:TiO_2(P25) [35] for the photocatalytic degradation of organic pollutants. With an optimum loading of 1.7 wt. % Si we concluded that for TiO_2 (P25), a very thin SiO_2 layer combined improve charge separation with an increased OH radical formation due to more acidic surface OH groups at the SiO_2 surface leading to a higher degradation rate of organic pollutants in water. Too thick an SiO_2 layer shields off the TiO_2 and drastically reduces the photocatalytic activity. For Pt:TiO_2(P25), the role of dissolved O_2 in combination with the enhanced charge separation turned out to be crucial for the enhancement of the photocatalytic activity. Pt acts as a recombination center and reduces the photocatalytic activity if the electrons cannot be harvested adequately in case no O_2 is present or the Pt loading is too high. This gave rise to the improved behavior for Pt:TiO_2(P25) samples with an optimal Pt loading of 0.34 wt. %. Higher loadings decreased the photocatalytic activity even to lower values than intrinsic

TiO_2(P25) (>2 wt % Pt). In earlier research, SiO_2 layers often have been used to encapsulate Pt nanoclusters on the surface of TiO_2 to improve the Pt nanoparticle dispersion by preventing noble metal cluster agglomeration, improving the catalytic performance. [31-32, 40] According to our previous results, it would be more advantageous to keep Pt clusters exposed on the surface by the deposition of SiO_2 followed by Pt, since both materials, Pt and SiO_2, are crucial for the generation of radicals on the surface. The overcoating of Pt with SiO_2 would reduce the effect of Pt adsorbing O_2 and possibly even give a worse photocatalyst due to the charge recombination property of the Pt nanoclusters in case the lack of access to O_2 prevents the harvest of electrons. Therefore, for the material design, we chose to coat first the TiO2 (P25) nanoparticles with SiO_2 and subsequently deposit Pt onto the SiO_2:TiO2(P25)substrate (Figure 6.1a). Despite the spatial separation of the Pt clusters from TiO_2, electrons may still be able to transfer to the Pt clusters as for the SiO_2:TiO_2(P25) catalyst excited electrons may still reach through the ultrathin SiO_2 layer to be harvested. [16-17] For low Si loadings the layer may be porous and incomplete which would also give the chance for a reaction of the electrons directly on the TiO_2 surface. By applying 2 to 40 ALD cycles of $SiCl_4$ and H_2O the loading evolved from 0.4 to 2.7 wt % Si in a conformal manner (Figure 6.1a). Afterward, Pt was deposited onto SiO_2:TiO_2(P25) in various loadings by using different pulse times (20 s to 5 min) for $MeCpPtMe_3$ and O_2 as a counter reactant (Figure 6.1b). In order to reach the required very low Pt loadings the pulse time was in the undersaturation regime resulting in a dependency of the pulse time versus Pt loading rather the commonly used cycle number. Using this approach, we could precisely tune the loadings for both the SiO_2 coating and the Pt clusters.

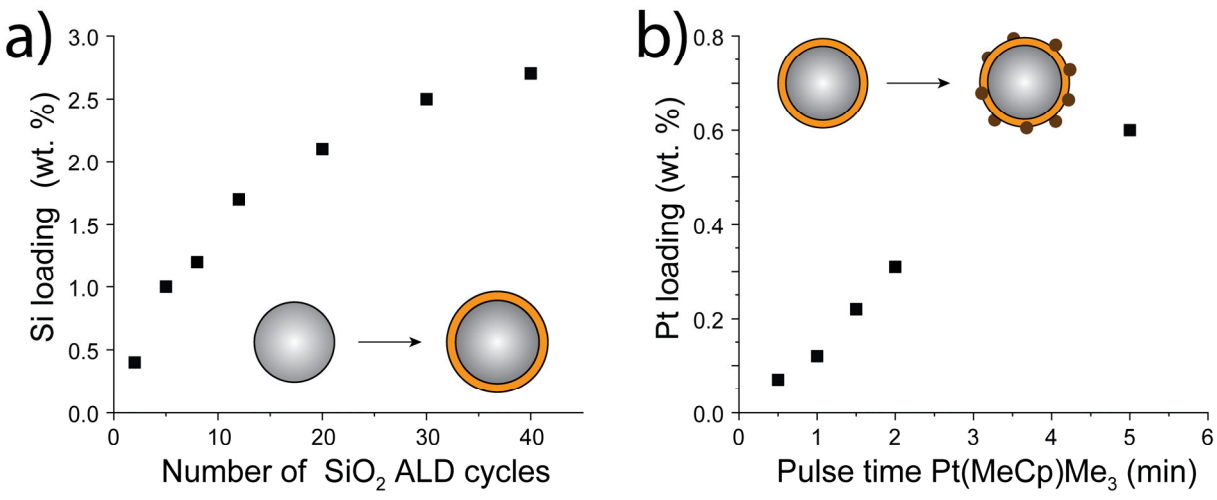

Figure 6.1: a) Development of the Si loading with the number of applied SiO_2 ALD cycles on bare TiO_2 (P25) particles, b) Development of the Pt loading with the Pt precursor pulse time ($MeCpPtMe_3$) on SiO_2 overcoated TiO_2 (P25) particles (2.1 ± 0.2 wt. % Si).

This design of experiments gives a matrix of various combinations of SiO_2 and Pt loadings onto P25 nanoparticles. Analyzing the morphology with TEM revealed the growth of SiO_2 as conformal sub-nanometer layers layers with various loading (Figure 6.2a) onto P25 and the Pt clusters (1–2 nm) deposited onto the SiO_2 layers in the second step (Figure 6.2b, Figure 6.S1). This is in agreement with our previous studies that show the growth of layers of SiO_2 due to the high affinity towards the TiO_2 surface. [16] On the other hand, the high surface energy of Pt results in the expected island growth on the surface of SiO_2, resulting in similar behavior as the deposition of Pt clusters on P25 itself. [41] Due to the very minute addition of material on the P25 particles TEM pictures confirms an unchanged particle size of Pt:SiO_2:TiO_2(P25) particles compared to pristine P25 of about 30 nm (Figure 6.2b). For lower loaded SiO_2 samples, the layers are not clearly visible due to resolution limitations of the TEM. It is expected that for a low number of cycles, the SiO_2 layer may be incomplete, and the TiO_2 surface is still exposed. XPS confirmed the deposition of both materials, SiO_2 and Pt (Figure 6.2c–e). From the high-resolution spectra, we can identify the characteristic peaks for each element – Ti, Si, and Pt. For the range between 450 eV and 475 eV, the characteristic Ti(IV) peaks for TiO_2 can be observed at binding energies of 458.68 eV (Ti $2p_{3/2}$) and 464.34 eV (Ti $2p_{1/2}$). The Si 2p peak characteristic for SiO_2 arises at 102.36 eV. After deconvolution of the Pt HR-XPS spectrum, three peaks arise where the peaks at 70.90 eV and 74.01 eV can be fitted to Pt(0) $4f_{7/2}$ and Pt(0) $4f_{5/2}$ respectively correlating them to the metallic Pt species, and at a binding energy of 76.06 eV, a satellite peak from the Ti 3s peak arises. XRD studies on TiO_2(P25) after modification with SiO_2 and Pt using ALD showed no change in the TiO_2 crystal structure featuring anatase and rutile phase typical for the mixed phase P25 nanoparticles (Figure S6.3). The modified TiO_2 (P25) showed a peak at 46.6° indicating the Pt(200) facet. However, other facets of Pt were not observable. Due to the only minute changes, i.e., ultra-thin layers of SiO_2 on the surface of TiO_2 XRD features of SiO_2 remain undetected. UV/Vis absorbance spectra (measured with DRS) show that the addition of neither SiO_2 layers nor Pt clusters leads to a significant change in the bandgap of the modified catalysts (Figure S6.4). The deposition of Pt clusters leads (for both TiO_2(P25) itself as well as SiO_2:TiO_2(P25)) to strong absorption throughout the visible spectrum caused by the metallic particles on the surface of the catalysts. Previous studies on the effect of the BET surface area of the single modified materials SiO_2:TiO_2(P25) (54 m^2/g) [16] and Pt:TiO_2(P25) (55 m^2/g) [35] demonstrated that a minute additions of SiO_2 and Pt are not significantly affecting the BET surface area compared to pure TiO_2 (P25) (55 m^2/g). Therefore we expect a similar BET surface area for the bi-modified Pt:SiO_2:TiO_2(P25) photocatalyst. Furthermore, the adsorption of Acid Blue 9 on the surface of the prepared catalysts after reaching the adsorption-desorption equilibrium did not change significantly upon modification of TiO_2(P25) (Figure S6.5)

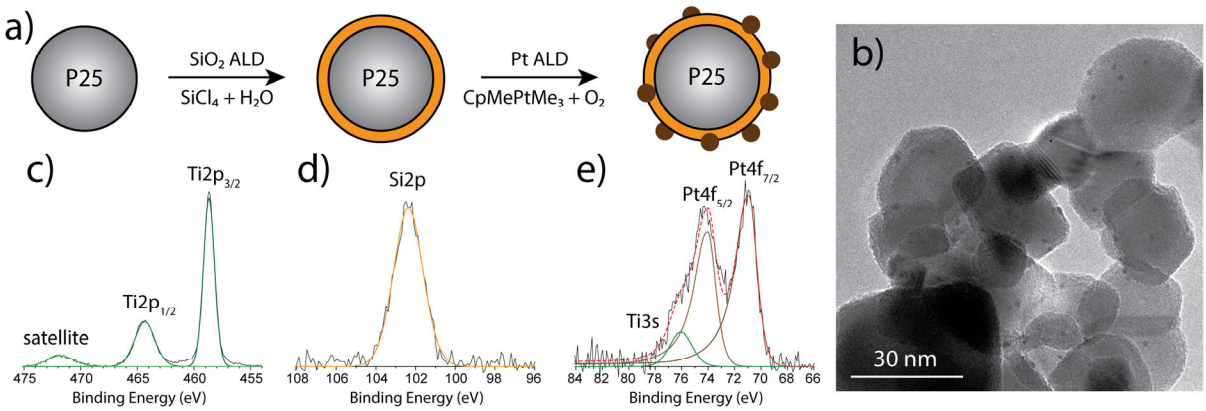

Figure 6.2: a) Deposition scheme for the material development of Pt:SiO_2:TiO_2(P25), b) TEM picture of Pt:SiO_2:TiO_2(P25) (1 wt. % Si, 1.23 wt. % Pt), grey large particle are TiO_2(P25) particles, SiO_2 layer around TiO_2(P25) particles can be observed, dark spots indicate Pt nanoclusters, c) Ti HRXPS spectrum with typical TiO_2 features, d) Si HRXPS spectrum, single peak represents SiO_2 (orange), e) Pt HRXPS spectrum, doublet peak represents Pt metal (brown), single peak represents Ti satellite peak (green).

In order to investigate the photocatalytic performance of the combined material (Pt:SiO_2:TiO_2(P25)), it is compared to the original material (TiO_2(P25)) and the single-modified materials – Pt:TiO_2(P25) and SiO_2:TiO_2(P25). First, the photocatalytic degradation for those individual compounds is investigated to benchmark the measurements. As compared to TiO_2(P25), the optimal Pt loading of about 0.34 wt. % gives a 4-fold increase in the activity of Pt:TiO_2(P25) for the photocatalytic degradation of AB9 (Figure 6.3a) while SiO_2:TiO_2(P25) shows a 1.5-fold increased photocatalytic activity with an optimal loading of about 1.2 wt. % Si (Figure 6.3b). In our previous research, an optimal loading of about 1.8 wt. % Si was reported, which is in line with the results in this paper. [17]

In Figure 6.3, we show the photocatalytic degradation of Acid Blue 9 for different coated Pt:SiO_2:TiO_2(P25) samples with various SiO_2 and Pt loading in order to find the optimum loading. We can identify an optimal behavior in the range of 1.5–2.2 wt. % Si and around 0.3 - 0.4 wt. % Pt (Figure 6.3c). This range is also covering the ranges of individual catalysts SiO_2:TiO_2(P25)and Pt:TiO_2(P25) perform in an optimal way. The best performing catalyst of the Pt:SiO_2:TiO_2(P25) series (1.9 wt. % Si, 0.60 wt. % Pt) degrades AB9 about six times better than P25. Evidently, the combination of Pt nanoparticles onto sub-nanometer layers of SiO_2 coated on P25 particles results in an improved photocatalytic material. Although the best performing catalyst with 0.60 wt. % Pt is slightly outside the range of the optimal loading (Table 6.1, Figure S6.2) for Pt:TiO_2(P25) mono-modified (0.34 wt. %), the fitting of the data (2D polynomial model) reveals that the optimal loading for the mono-modified materials Pt:TiO_2(P25) and SiO_2:TiO_2(P25) coincides with the optimal loadings for these mono-modified catalysts. This indicates that there is limited interaction between the improvement mechanisms of depositing SiO_2 and Pt onto P25. In this context it may be speculated that the growth of Pt on the SiO_2 coating may positively influence particle

size distribution due to a change in surface energy. However, a study on the detailed evolution of the particle size distribution of Pt clusters on different surfaces would be outside of the scope of this study yet important for further research.

On the one hand, a sub-nanometer SiO_2 layer on TiO_2 (P25) particles improves the OH radical generation at the SiO_2 surface from the holes generated in the VB. On the other hand, Pt clusters facilitate effective electron-hole-pair separation by using the TiO_2 CB electrons as reducing agents to generate superoxide radicals ($O_2^{-\cdot}$) from dissolved O_2. Combining both materials, SiO_2 and Pt, with TiO_2(P25) increases the photocatalytic activity by increasing mainly the radical generation.

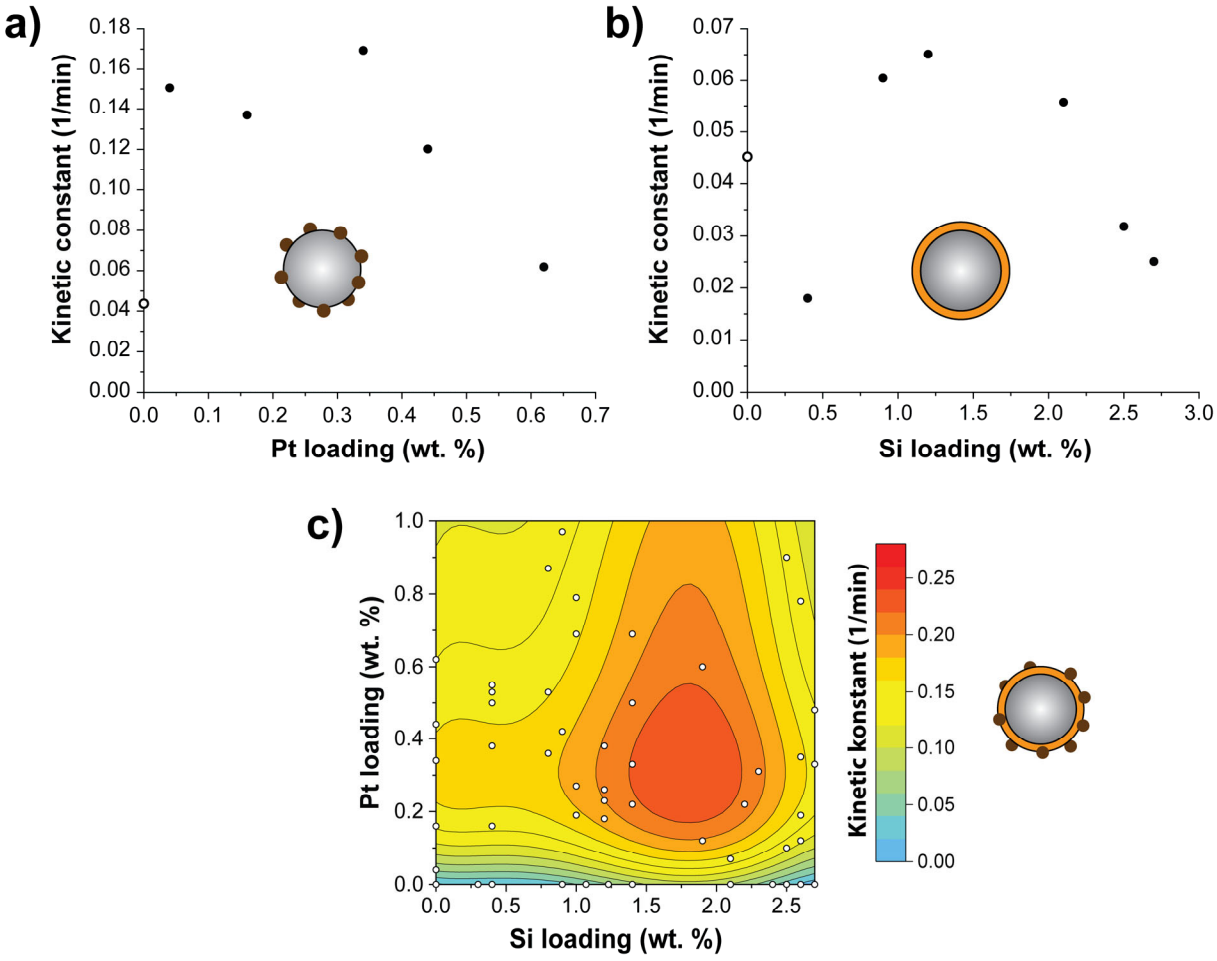

Figure 6.3: Kinetic constant for degradation of AB9 a) with different loadings of Pt on TiO2(P25), b) with different loadings of SiO_2 on TiO2(P25), c) combined Pt:SiO_2:TiO_2(P25)material with different loadings of Pt and SiO_2 for the degradation of AB9 (fitted)

Table 6.1: Kinetic constants for the best performing photocatalysts for the mono-modified and bi-modified TiO_2-catalysts. Kinetic constants are calculated form pseudo 1st order kinetics.

	TiO_2(P25)	Pt:TiO_2(P25)	SiO_2:TiO_2(P25)	Pt:SiO_2:TiO_2(P25)
Optimal loading	-	0.34 wt. % (Pt)	1.2 wt. % (Si)	0.6 wt. % (Pt), 1.9 wt. % (Si)
Kinetic constant (min^{-1})	0.044	0.169	0.065	0.267
Improvement ratio	1	3.84	1.48	6.07

The current study does not show any serious deactivation of the photocatalyst during the use of the photocatalyst. Nevertheless, a detailed analysis of the long-term reusability will be required for the implementation in future reactors for water treatment and is recommended to be subject to follow-up research. Applying the same strategy followed in this research to improve the photocatalytic activity using a base material with increased light absorption could further increase the overall performance. For example, N-doping has been shown to reduce the bandgap of titania, increasing the light absorption in the visible light regime. [42-43] Adding another material on the surface is, on the other hand, not recommended. This would probably lead to coverage of the photocatalytic relevant surface groups reducing the reactive oxygen species generation. Furthermore, the modification of TiO_2 by layer/nanocluster combination using cheaper materials as replacement for e.g., Pt may result in both efficient and cheaper catalysts. In our experiments we were able to coat powder of up to 5 g (~270 m^2 surface area) using atomic layer deposition in a fluidized bed. This technique provides therefore a great opportunity to scale up the preparation of multicomponent catalysts.

6.4. CONCLUSION

This work shows that by the smart combination of different materials onto TiO_2(P25), better photocatalyst can be engineered using the excellent precision of ALD in a fluidized bed. As a successful example we designed a Pt:SiO_2:TiO_2(P25) material with improved photocatalytic properties by depositing Pt clusters on SiO_2 coated TiO_2(P25). The choice of the coating materials Pt and SiO_2 was based on our previous detailed analysis of the photocatalytic mechanism of both SiO_2:TiO_2(P25) and Pt:TiO_2(P25). ALD provided the opportunity to precisely control the loading of SiO_2 and Pt, resulting in a matrix of various loaded Pt:SiO_2:TiO_2(P25) surface modified nanoparticles. We showed that this material accelerates the photocatalytic degradation rate of Acid Blue 9 by a factor 6, which is superior to both SiO_2:TiO_2(P25) (1.5×) and Pt:TiO_2(P25) (4×).

APPENDIX

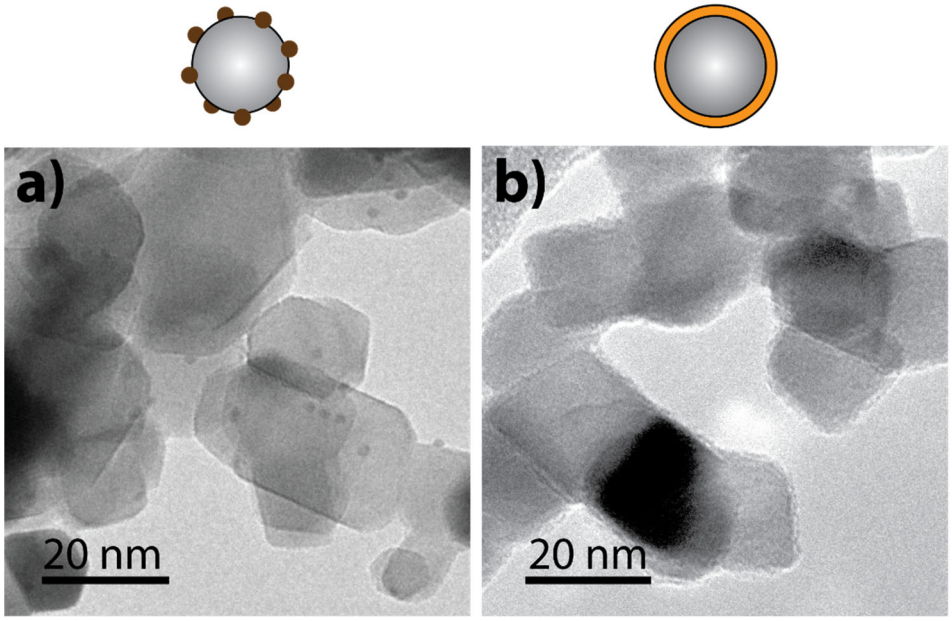

Figure S6.1: TEM pictures of mono modified catalysts; a) Pt:TiO_2(P25) (0.34 wt. % Pt), b) SiO_2:TiO_2(P25) (1.7 wt. % Si)

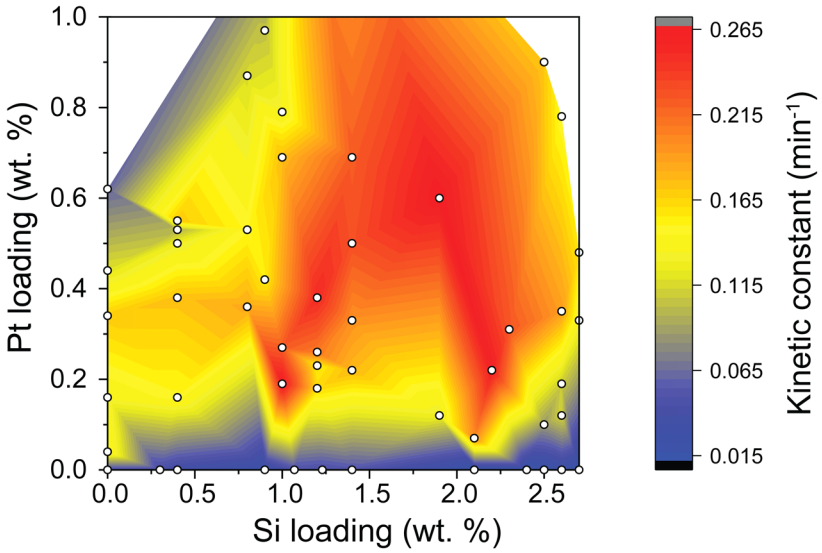

Figure S6.2: Contour plot for the unfitted photocatalytic activity degrading Acid Blue 9 with the multi-component material Pt:SiO_2:TiO_2(P25)

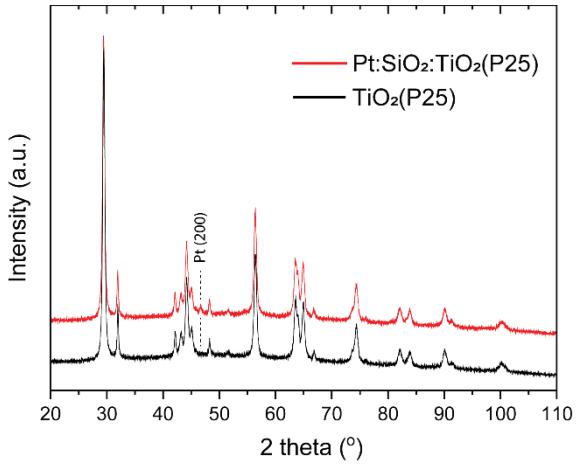

Figure S6.3. XRD pattern of bare TiO_2(P25) (black) and Pt:SiO_2:TiO_2(P25) (red) with the characteristic phase composition for anatase/rutile mixed phase TiO_2(P25) nanopowder.

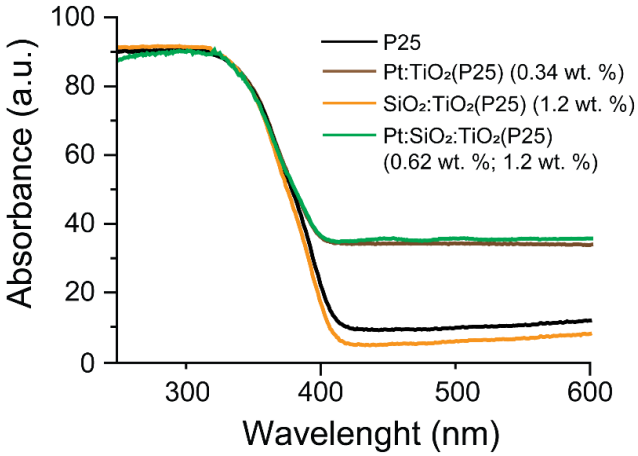

Figure S6.4. UV/Vis DRS spectra of the deposited catalysts with TiO_2 (P25) as a reference (black), SiO_2:TiO_2(P25) (orange), Pt: TiO_2(P25) (brown), Pt:SiO_2: TiO_2(P25) (green).

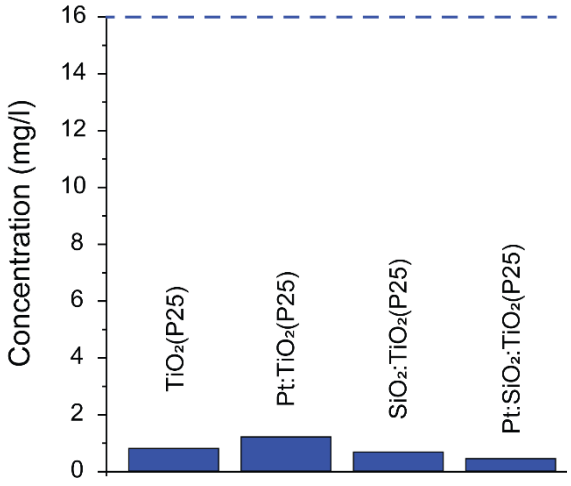

Figure S6.5. Adsorbed Acid Blue 9 on the catalyst surface after reaching the adsorption desorption equilibrium. The dashed line represents the original concentration of Acid Blue 9 in the solution as described in the Experimental section.

REFERENCES

1. Fujishima, A.; Honda, K., Electrochemical Photolysis of Water at a Semiconductor Electrode. *Nature* **1972,** *238* (5358), 37-38.
2. Pastrana-Martínez, L. M.; Morales-Torres, S.; Carabineiro, S. A. C.; Buijnsters, J. G.; Figueiredo, J. L.; Silva, A. M. T.; Faria, J. L., Photocatalytic activity of functionalized nanodiamond-TiO2 composites towards water pollutants degradation under UV/Vis irradiation. *Applied Surface Science* **2018,** *458*, 839-848.
3. Driessen, M. D.; Grassian, V. H., Photooxidation of Trichloroethylene on Pt/TiO_2. *The Journal of Physical Chemistry B* **1998,** *102* (8), 1418-1423.
4. Wang, M.; Sun, L.; Lin, Z.; Cai, J.; Xie, K.; Lin, C., p–n Heterojunction photoelectrodes composed of Cu_2O-loaded TiO_2 nanotube arrays with enhanced photoelectrochemical and photoelectrocatalytic activities. *Energy & Environmental Science* **2013,** *6* (4), 1211.
5. Ahmed, S.; Rasul, M. G.; Martens, W. N.; Brown, R.; Hashib, M. A., Advances in Heterogeneous Photocatalytic Degradation of Phenols and Dyes in Wastewater: A Review. *Water, Air, & Soil Pollution* **2010,** *215* (1-4), 3-29.
6. Pelaez, M.; Nolan, N. T.; Pillai, S. C.; Seery, M. K.; Falaras, P.; Kontos, A. G.; Dunlop, P. S. M.; Hamilton, J. W. J.; Byrne, J. A.; O'Shea, K.; Entezari, M. H.; Dionysiou, D. D., A review on the visible light active titanium dioxide photocatalysts for environmental applications. *Applied Catalysis B-Environmental* **2012,** *125*, 331-349.
7. Anwer, H.; Mahmood, A.; Lee, J.; Kim, K.-H.; Park, J.-W.; Yip, A. C. K., Photocatalysts for degradation of dyes in industrial effluents: Opportunities and challenges. *Nano Research* **2019,** *12* (5), 955-972.
8. Carneiro, J. T.; Savenije, T. J.; Moulijn, J. A.; Mul, G., The effect of Au on TiO2 catalyzed selective photocatalytic oxidation of cyclohexane. *Journal of Photochemistry and Photobiology A: Chemistry* **2011,** *217* (2), 326-332.
9. Lim, T. H.; Jeong, S. M.; Kim, S. D.; Gyenis, J., Degradation characteristics of NO by photocatalysis with TiO_2 and CuO/TiO_2. *Reaction Kinetics and Catalysis Letters* **2000,** *71* (2), 223-229.
10. Lei, M.; Wang, N.; Zhu, L. H.; Zhou, Q. L.; Nie, G.; Tang, H. Q., Photocatalytic reductive degradation of polybrominated diphenyl ethers on CuO/TiO_2 nanocomposites: A mechanism based on the switching of photocatalytic reduction potential being controlled by the valence state of copper. *Applied Catalysis B-Environmental* **2016,** *182*, 414-423.
11. Gong, Y.; Wang, D. P.; Wu, R.; Gazi, S.; Soo, H. S.; Sritharan, T.; Chen, Z., New insights into the photocatalytic activity of 3-D core–shell P25@silica nanocomposites: impact of mesoporous coating. *Dalton Transactions* **2017,** *46* (15), 4994-5002.
12. Tsukamoto, D.; Shiraishi, Y.; Sugano, Y.; Ichikawa, S.; Tanaka, S.; Hirai, T., Gold Nanoparticles Located at the Interface of Anatase/Rutile TiO_2 Particles as Active Plasmonic Photocatalysts for Aerobic Oxidation. *J. Am. Chem. Soc.* **2012,** *134* (14), 6309--6315.
13. Zhou, Y.; King, D. M.; Liang, X.; Li, J.; Weimer, A. W., Optimal preparation of Pt/TiO_2 photocatalysts using atomic layer deposition. *Applied Catalysis B: Environmental* **2010,** *101* (1-2), 54-60.
14. Simonsen, M. E.; Li, Z.; Søgaard, E. G., Influence of the OH groups on the photocatalytic activity and photoinduced hydrophilicity of microwave assisted sol–gel TiO_2 film. *Applied Surface Science* **2009,** *255* (18), 8054-8062.
15. Muhich, C. L.; Zhou, Y.; Holder, A. M.; Weimer, A. W.; Musgrave, C. B., Effect of Surface Deposited Pt on the Photoactivity of TiO_2. *The Journal of Physical Chemistry C* **2012,** *116* (18), 10138-10149.
16. Guo, J.; Benz, D.; Doan Nguyen, T.-T.; Nguyen, P.-H.; Thi Le, T.-L.; Nguyen, H.-H.; La Zara, D.; Liang, B.; Hintzen, H. T.; van Ommen, J. R.; Van Bui, H., Tuning the photocatalytic activity of TiO_2 nanoparticles by ultrathin SiO_2 films grown by low-temperature atmospheric pressure atomic layer deposition. *Applied Surface Science* **2020,** *530*, 147244.
17. Benz, D.; Bui, H. V.; Hintzen, H. T.; Kreutzer, M. T.; Van Ommen, J. R., Mechanistic insight into the improved photocatalytic degradation of dyes using TiO_2 (P25) nanoparticles with an ultrathin SiO_2 coating. **2020,** *in preparation*.
18. Gaya, U. I., *Heterogeneous Photocatalysis Using Inorganic Semiconductor Solids*. Springer: 2014.
19. Linsebigler, A. L.; Lu, G.; Yates, J. T., Photocatalysis on TiO_2 Surfaces: Principles, Mechanisms, and Selected Results. *Chemical Reviews* **1995,** *95* (3), 735-758.

20. Zhang, A.-Y.; Wang, W.-K.; Pei, D.-N.; Yu, H.-Q., Degradation of refractory pollutants under solar light irradiation by a robust and self-protected ZnO/CdS/TiO_2 hybrid photocatalyst. *Water Research* **2016,** *92*, 78-86.
21. Yu, X.; Liu, S.; Yu, J., Superparamagnetic γ-Fe_2O_3@SiO_2@TiO_2 composite microspheres with superior photocatalytic properties. *Applied Catalysis B: Environmental* **2011,** *104* (1), 12-20.
22. Zhang, F.; Liu, W.; Liu, Y.; Wang, J.; Ji, G., Fabrication and enhanced photocatalytic properties of Pt@SiO_2@TiO_2 composites by surface plasma resonance from Pt nanoparticles. *Journal of Nanoparticle Research* **2015,** *17* (2), 62.
23. Li, S.; Cai, J.; Wu, X.; Liu, B.; Chen, Q.; Li, Y.; Zheng, F., TiO_2@Pt@CeO_2 nanocomposite as a bifunctional catalyst for enhancing photo-reduction of Cr (VI) and photo-oxidation of benzyl alcohol. *Journal of Hazardous Materials* **2018,** *346*, 52-61.
24. Deng, X.; Li, S., Vapor phase synthesis of 2,3,6-trimethylphenol from m-cresol and methanol with Fe_2O_3-SiO_2-CuO catalyst. *Catalysis Communications* **2018,** *111*, 100-103.
25. Wang, J. C.; Kondrat, S. A.; Wang, Y. Y.; Brett, G. L.; Giles, C.; Bartley, J. K.; Lu, L.; Liu, Q.; Kiely, C. J.; Hutchings, G. J., Au-Pd Nanoparticles Dispersed on Composite Titania/Graphene Oxide-Supports as a Highly Active Oxidation Catalyst. *Acs Catalysis* **2015,** *5* (6), 3575-3587.
26. Liu, S.; Guo, M.-X.; Shao, F.; Peng, Y.-H.; Bian, S.-W., Water-dispersible and magnetically recoverable Fe_3O_4/Pd@nitrogen-doped carbon composite catalysts for the catalytic reduction of 4-nitrophenol. *RSC Advances* **2016,** *6* (80), 76128-76131.
27. Cheng, N.; Banis, M. N.; Liu, J.; Riese, A.; Li, X.; Li, R.; Ye, S.; Knights, S.; Sun, X., Extremely Stable Platinum Nanoparticles Encapsulated in a Zirconia Nanocage by Area-Selective Atomic Layer Deposition for the Oxygen Reduction Reaction. *Advanced Materials* **2015,** *27* (2), 277-281.
28. Dai, Y.; Zhu, M.; Wang, X.; Wu, Y.; Huang, C.; Fu, W.; Meng, X.; Sun, Y., Visible-light promoted catalytic activity of dumbbell-like Au nanorods supported on graphene/TiO_2 sheets towards hydrogenation reaction. *Nanotechnology* **2018,** *29* (24), 245703.
29. Bo, Z.; Ahn, S.; Ardagh, M. A.; Schweitzer, N. M.; Canlas, C. P.; Farha, O. K.; Notestein, J. M., Synthesis and stabilization of small Pt nanoparticles on TiO_2 partially masked by SiO_2. *Applied Catalysis A: General* **2018,** *551*, 122-128.
30. Song, Z.; Wang, B.; Cheng, N.; Yang, L.; Banham, D.; Li, R.; Ye, S.; Sun, X., Atomic layer deposited tantalum oxide to anchor Pt/C for a highly stable catalyst in PEMFCs. *Journal of Materials Chemistry A* **2017,** *5* (20), 9760-9767.
31. Wan, C.; Cheng, D.-g.; Chen, F.; Zhan, X., Fabrication of CeO_2 nanotube supported Pt catalyst encapsulated with silica for high and stable performance. *Chemical Communications* **2015,** *51* (48), 9785-9788.
32. Zhao, E. W.; Maligal-Ganesh, R.; Mentink-Vigier, F.; Zhao, T. Y.; Du, Y.; Pei, Y.; Huang, W.; Bowers, C. R., Atomic-Scale Structure of Mesoporous Silica-Encapsulated Pt and PtSn Nanoparticles Revealed by Dynamic Nuclear Polarization-Enhanced 29Si MAS NMR Spectroscopy. *The Journal of Physical Chemistry C* **2019,** *123* (12), 7299-7307.
33. Sadeghi, M.; Liu, W.; Zhang, T. G.; Stavropoulos, P.; Levy, B., Role of Photoinduced Charge Carrier Separation Distance in Heterogeneous Photocatalysis: Oxidative Degradation of CH_3OH Vapor in Contact with Pt/TiO_2 and Cofumed TiO_2−Fe_2O_3. *The Journal of Physical Chemistry* **1996,** *100* (50), 19466-19474.
34. Chen, J.-J.; Wang, W.-K.; Li, W.-W.; Pei, D.-N.; Yu, H.-Q., Roles of Crystal Surface in Pt-Loaded Titania for Photocatalytic Conversion of Organic Pollutants: A First-Principle Theoretical Calculation. *ACS Applied Materials & Interfaces* **2015,** *7* (23), 12671-12678.
35. Benz, D.; Felter, K. M.; Köser, J.; Thöming, J.; Mul, G.; Grozema, F. C.; Hintzen, H. T.; Kreutzer, M. T.; van Ommen, J. R., Assessing the Role of Pt Clusters on TiO_2 (P25) on the Photocatalytic Degradation of Acid Blue 9 and Rhodamine B. *The Journal of Physical Chemistry C* **2020,** *124* (15), 8269-8278.
36. Beetstra, R.; Lafont, U.; Nijenhuis, J.; Kelder, E. M.; van Ommen, J. R., Atmospheric Pressure Process for Coating Particles Using Atomic Layer Deposition. *Chemical Vapor Deposition* **2009,** *15* (7-9), 227-233.
37. van Ommen, J. R.; Goulas, A., Atomic layer deposition on particulate materials. *Materials Today Chemistry* **2019,** *14*, 100183.
38. van Driel, B. A.; Kooyman, P. J.; van den Berg, K. J.; Schmidt-Ott, A.; Dik, J., A quick assessment of the photocatalytic activity of TiO_2 pigments — From lab to conservation studio! *Microchemical Journal* **2016,** *126*, 162-171.
39. Doekhi-Bennani, Y. Photoelectrocatalysis in water treatment. PhD Thesis, Delft University of Technology, Delft, 2017.

40. Shan, J.; Lei, Z.; Wu, W.; Tan, Y.; Cheng, N.; Sun, X., Highly Active and Durable Ultrasmall Pd Nanocatalyst Encapsulated in Ultrathin Silica Layers by Selective Deposition for Formic Acid Oxidation. *ACS Applied Materials & Interfaces* **2019**.
41. Faust, M.; Enders, M.; Gao, K.; Reichenbach, L.; Muller, T.; Gerlinger, W.; Sachweh, B.; Kasper, G.; Bruns, M.; Bräse, S.; Seipenbusch, M., Synthesis of Pt/SiO_2 Catalyst Nanoparticles from a Continuous Aerosol Process using Novel Cyclo-octadienylplatinum Precursors. *Chemical Vapor Deposition* **2013,** *19* (7-8-9), 274-283.
42. Gao, B.; Ma, Y.; Cao, Y.; Yang, W.; Yao, J., Great Enhancement of Photocatalytic Activity of Nitrogen-Doped Titania by Coupling with Tungsten Oxide. *The Journal of Physical Chemistry B* **2006,** *110* (29), 14391-14397.
43. Zhang, J.; Wu, Y.; Xing, M.; Leghari, S. A. K.; Sajjad, S., Development of modified N doped TiO_2 photocatalyst with metals, nonmetals and metal oxides. *Energy & Environmental Science* **2010,** *3* (6), 715-726.

7

Thermal Atomic Layer Deposition of Gold Nanoparticles: Controlled Growth and Size Selection for Photocatalysis

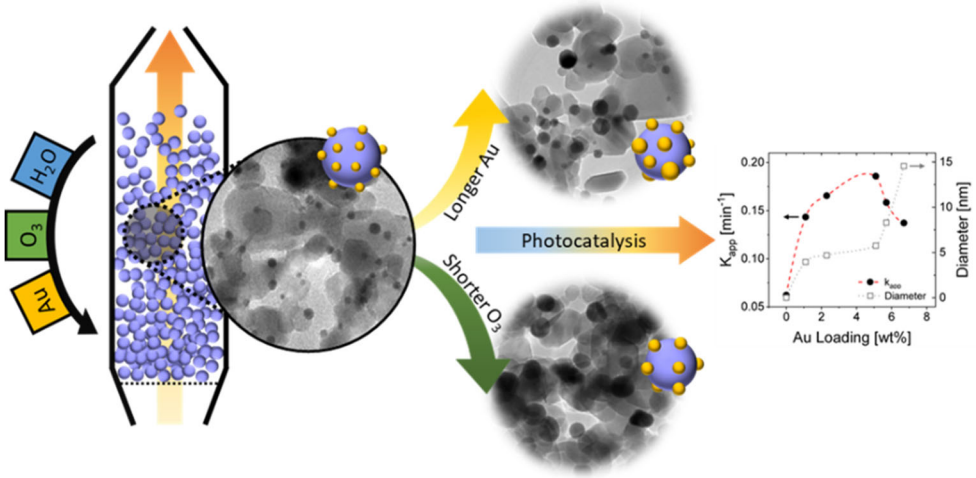

Gold nanoparticles have been extensively studied for their applications in catalysis. For Au nanoparticles to be catalytically active, controlling the particle size is crucial. Here we present a low temperature (105 °C) thermal atomic layer deposition approach for depositing gold nanoparticles on TiO_2 with controlled size and loading using trimethylphosphino-trimethylgold (III) and two co-reactants (ozone and water) in a fluidized bed reactor. We show that the exposure time of the precursors is a variable that can be used to decouple the Au particle size from the Au loading. Longer exposures of ozone narrow the particle size distribution while longer exposures of water broaden it. By studying the photocatalytic activity of Au/TiO_2 nanocomposites we show how the ability to control particle size and loading independently can be used not only to enhance performance but also to investigate structure-property relationships. This study provides insights into the mechanism underlying formation and evolution of Au nanoparticles via a vapor phase technique, which eliminates the shortcomings of conventional liquid-base processes.

Published in *Nanoscale*

Fatemeh S. M. Hashemi, Fabio Grillo, Vikram R. Ravikumar, Dominik Benz, Ankit Shekhar, Matthew B. E. Griffiths, Seán T. Barry, and J. Ruud van Ommen

7.1. INTRODUCTION

Gold was long thought to be far less catalytically active than other transition metals. Yet studies in the late 80s showed that Au nanoparticles supported on metal oxides such as TiO_2 exhibits an extraordinary high activity towards various catalytic oxidation and reduction reactions, such as low-temperature combustion, partial oxidation of hydrocarbons, hydrogenation of unsaturated hydrocarbons, and reduction of nitrogen oxides. [1-10] The catalytic properties of Au nanoparticles originate from quantum, electronic, and geometric finite-size effects, and are therefore strongly related to the particle size. [10-11] For example, Au nanoparticles supported on TiO_2 exhibit a high activity towards the oxidation of CO only when their size is within an optimal range of 2-3 nm [10]. Furthermore, Au nanoparticles can extend the absorption of TiO_2 in the visible range to an extent that depends on their size thanks to plasmon resonance, that is, the resonant oscillation of free electrons induced by incident light. [12-13] While the sensitivity of the structure-property relationship of Au nanoparticles can add a new dimension to the design of catalysts, it also poses a challenge. This is because practical applications often require large amounts of material, and fabricating supported nanoparticles with a controlled size in a scalable fashion remains challenging. [14-16]

Conventional techniques for the synthesis of supported Au nanoparticles typically rely on liquid-phase processes. [17-19] However, the practical applicability of these methods is limited by a number of shortcomings: high levels of impurities in the final product arising from residual solvents, poor control over the composition and the size distribution in large batches, and high sensitivity to operating conditions. [20] These factors can significantly affect the lifetime, activity, selectivity, and stability of the catalyst. [15, 21] Thus, an alternative solvent-free, controllable, and scalable method is highly desired.

Atomic layer deposition (ALD) is a vapor-phase deposition technique that is emerging as a promising method for the synthesis of supported nanoparticles as it boasts high precursor utilization efficiency, low degree of contamination of the final product, and an excellent degree of control over both the metal loading and the particle size. [16, 22-28] While there exist over seventy ALD processes for the deposition of noble metals, only limited success with regards to Au has been reported. [1] Two successful studies on ALD of Au include a plasma process at 120 °C using (trimethylphosphino)-trimethylgold(III) as metal precursor; and a thermal process at 180 °C, with dimethylgold(III)(diethylthiocarbamato) as metal precursor. [29-30] In both studies, the deposition was carried out on flat substrates under vacuum conditions. While such processes are certainly promising for a number of applications, plasma and vacuum processes are not readily scalable to large quantities of high-surface-area supports, which are relevant for catalytic applications. [16]

In this work, we demonstrate a synthesis method for scalable fabrication of supported Au nanoparticles on TiO_2 via thermal atmospheric-pressure ALD. This ALD process

uses trimethylphosphino-trimethyl gold (III) as the metal precursor, and ozone and water as counter reactants, at low temperatures (105 °C). We show that it is possible to control the broadness of the particle size distribution while retaining a given metal loading by tuning the exposure of the counter reactants. Interestingly, ozone and water have opposing effects on the size distribution: long ozone exposures narrow the size distribution, whereas long water exposures broaden it. Finally, by leveraging our independent control over loading and particle size, we explore the structure sensitivity of the Au/TiO_2 nanocomposites against the photocatalytic decomposition of a model dye. In doing so, we show a threefold enhancement in the photocatalytic activity of commercial titania P25. By boasting an independent control over particle size and metal loading, our thermal atmospheric-pressure ALD process can open new possibilities for the application of supported Au nanoparticle in large scale catalytic processes.

7.2. EXPERIMENTAL SECTION

7.2.1. Material Deposition

Aeroxide P25 titanium oxide particles from Evonik industries with a mean diameter of 32.7 nm, a specific area of 52.4 m^2/g were used as the support material for the deposition of Au. The nanoparticles were treated with oxygen (99.999 vol%) for 10 min followed by nitrogen (99.999 vol%) for 10 min at 105 °C before the Au ALD experiments. The deposition experiments were carried out in a custom-built vibration-assisted fluidized bed ALD reactor operating at atmospheric pressure described elsewhere. [31] The ALD reaction chamber was a 25 mm I.D. glass column into which 2 g of titania P25 NPs were loaded for each ALD run. The metal precursor bubbler and the line connecting the bubbler to the reactor were heated to 85 °C and 95 °C, respectively. An infra-red lamp was used to heat and maintain the reactor at 105 °C. Trimethylphosphino-trimethyl gold (III) was synthesized as described previously. [29]

7.2.2. Materials Characterization

To determine Au and P loading (wt%) on powders, Inductively Coupled Plasma Optical Emission Spectrometry (ICP-OES) analyses were performed in Perkin-Elmer Optima 5300DV Optical emission spectrometer. About 25 to 50 mg of samples were used for each ICP-OES measurement.

X-ray Photoelectron Spectroscopy (XPS) samples were analyzed in a Thermo Scientific K-Alpha X-ray spectrometer. The X-ray source was a monochromatic AlKa source with a beam energy of 1486.7 eV and a spot size of 400 µm. The obtained Au 4f, P 2p, O 1s, C 1s, and Ti 2p spectra were processed in CasaXPS.

Diffuse Reflectance Infrared Fourier-Transform Spectroscopy (DRIFTS) measurements were made using a NICOLET 8700 spectrometer in diffuse reflectance mode with a range of 500-4000 cm-1 (128 scans).

For Transmission Electron Microscopy (TEM) measurements, the NPs were suspended in a droplet of ethanol, which was then cast on a copper TEM grid. The TEM micrographs were obtained by a JEOL JEM 1400TEM operating at 120 kV. Number based particle size distributions were obtained from image analysis of the micrographs. The projected area of each particle (A_{p_i}) was measured manually using ImageJ. Then the equivalent particle diameter was estimated as $d_{p_i} = \sqrt{4A_{p_i}/\pi}$ for ~100-600 NPs from 15 to 40 micrographs taken at different locations of the TEM grid and at different magnifications. The measured diameters are displayed as binned scatter plots and box-and-whisker diagrams. In the scatter plots, all the measured diameters are grouped into bins whose width and height indicate different size ranges and their relative frequency, respectively. The box-and-whisker diagrams represent different statistical descriptors of the populations: the whiskers indicate the minimum and maximum observed diameter, the lower and upper side of the box indicate the first to the third quartile of the population, respectively, and the diamond inside the box indicates the mean diameter.

Diffuse Reflectance-Ultraviolet/Visible Spectroscopy (DRS) measurements were performed on a Perkin-Elmer Lambda 900 spectrometer in diffuse reflectance mode at a range of 250 to 800 nm using an integration sphere. Barium sulfate (BaSO4) was used as a blank standard.

The photocatalytic tests were performed on organic Rhodamine B dye. First, 30 mg of catalyst material was dispersed into a solution of Rhodamine B (30 ml, 16 mg/l, in DI water). Then Sodium polyphosphate (0.33 ml, 100 g/l in DI water) was added to improve the dispersion of the particles. The dispersion was sonicated for 10 min and stirred in the dark for 20 min to reach the adsorption-desorption equilibrium. Then the samples were top-illuminated in an Atlas SUNTEST XXL equipped with three Xenon lights to ensure homogeneous light distribution (45 W/m^2) simulating the sun's spectrum in both the UV and visible light range. [32] The reactor (irradiation surface 11.3 cm^2) was cooled using a water bath at 20 °C while the dispersion was continuously stirred during the test using a magnetic stirrer at 700 rpm. After distinct time intervals, samples of 1 ml were taken, centrifuged, and the light absorption at 629 nm was measured using a HACH LANGE DR5000 UV/Vis Spectrometer to follow the degradation of Rhodamine B by time. The kinetic constant was calculated using the 1st order kinetics.

7.3. RESULTS AND DISCUSSION

As described by Griffiths et al., trimethylphosphino-trimethyl gold(III) vapor pressure follows a Antoine equation (ln(p) = 0.059T − 1.65). For titania nanoparticles with the surface area of 50 cm^2/g, a long Au dosage time (+60 min) is required to saturate the titania surface groups. Thus for demonstrating the saturation behavior of this precursor, we only perform 1 ALD cycle. To achieve the thermal ALD of Au on gram-scale batches of high-surface-area powders, we adapted the plasma process reported by Griffiths et al., which consists of ABC cycles comprising the sequence of pulses: Au precursor/oxygen plasma/water. In our process, the oxygen plasma step is replaced by exposure to 1 bar of ozone. The effect of the exposure to ozone and water is studied by performing more cycles (3 to 9) where short exposures of the Au precursor were used. As we will discuss below, within the cycle range explored here (1-9), the deposition process results in the formation of nanoparticles rather than films. In particular, we show that both the Au loading and the size distribution of the nanoparticles can be controlled even when running the chemisorption of the Au precursor in a sub-saturation regime.

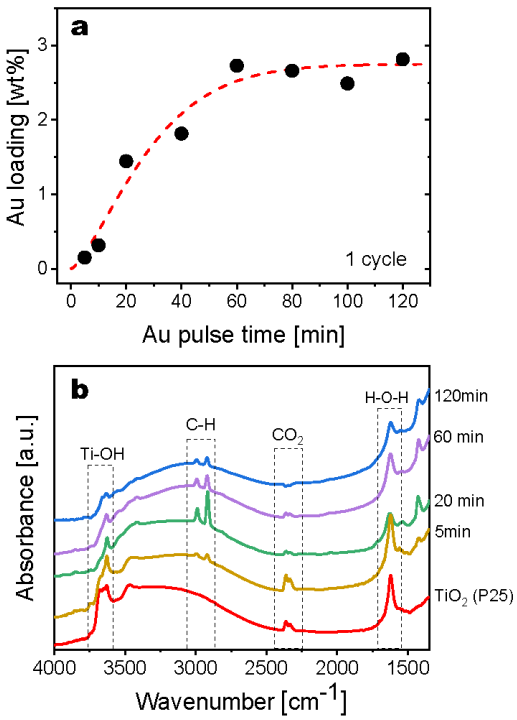

Figure 7.1: Self-limiting behavior of the Au precursor chemisorption. (a) Evolution of the Au loading on TiO_2 nanoparticles after one cycle with increasing exposure time. The ozone and water exposure times were: 10 min and 30 secs, respectively, and the reactor temperature was kept at 105 °C (The dashed red line is drawn to guide the eye). (b) FTIR spectra acquired at 120 °C on the Au/TiO_2 nanocomposites obtained after 1 ALD cycle with different Au precursor exposure times.

The self-limiting behavior of the precursor chemisorption was probed by measuring the Au loading (wt%) on the TiO_2 nanopowders after exposure times in the range of 5-150 min. The Au loading was measured with ICP-OES (Fig 7.1a). For all saturation experiments, ozone and water exposures were kept at 10 min and 30 secs, respectively. The Au loading progressively increases up to exposure times of about 60 min, after which it plateaus and remains virtually constant at around 2.7 wt% within a time window of about one hour, i.e. for a total exposure of 120 min. This demonstrates the self-limiting nature of the deposition process. Upon prolonging the exposure time up to 150 min, well past the minimum saturation time, higher Au loadings were observed (Supporting info Fig 7.1). At such long exposures, it is not surprising that parasitic Chemical vapor deposition (CVD) components might manifest themselves. In fact, although precursor is known to decompose at about 120 °C and the bulk temperature of the reactor is kept constant at 105 °C, after the surface reactions have terminated unreacted precursor can still be expected to decompose at a very slow rate, which over long time scales (~30 min) can add up to noticeable amounts of precursor being decomposed. Furthermore, local hot spots occurring sporadically across the reactors can also contribute to a small CVD component. Nonetheless, a self-limiting deposition is retained over a broad time window (~1 hour), attesting the robustness of this ALD process. Furthermore, a loading of 2.7 wt% after one cycle corresponds to a growth per cycle of~1.6 Au atoms/nm^2 and thus to ~0.1 Au(111) monolayer (1.387 × 1015 atoms/cm^2). [33] The deposition of less than a monolayer per cycle further attests to the ALD-nature of the precursor chemisorption on TiO_2 [34].

A detailed analysis of the TiO_2 surface functional groups by FTIR measurements reveals an interesting trend in the evolution of surface functional groups. Upon longer Au precursor exposures, the Ti-OH peak decreases while a -CH peak emerges. Furthermore, the H-O-H bending peak related to adsorbed water also decreases with an increase in the Au precursor exposure (Fig 7.1b).

To gain further insights into the growth process, we repeated the saturation experiments by performing 5 ALD cycles. This allowed us to study the aggregation of the as-deposited Au atoms into nanoparticles in more detail, as lower cycle numbers result in nanoparticles too small to be observed with TEM. In particular, we studied the evolution of the loading and the size distribution of the nanoparticles by exposing the TiO_2 nanopowders to the Au precursor for pulse times in the range of 5-40 min (i.e., sub-saturating doses). Similar to the saturation experiments, we kept the ozone and water exposures at 10 min and 30 sec, respectively (Fig 7.2).

Image analysis of TEM micrographs together with elemental analysis shows that an increase in Au loading with increasing Au precursor exposure time is accompanied by a higher degree of metal aggregation, as attested by the increase in particle size, the broadening of the size distribution, and the decreased number of particles (Fig 7.2). This points to the fact that sintering mechanisms, such as nanoparticle diffusion and coalescence or Ostwald ripening, play an important role during the growth process. [22, 35] This is not surprising because the high surface energy of noble metals

typically translates into a poor wetting of metal oxide surfaces, and in particular of titania. [36-39] In fact, increasing the Au precursor exposure time from 5 to 40 min results in the formation of fewer but larger particles, as the average diameter grows from ~4 nm to ~ 15 nm, while the span of the size distribution (the difference between the maximum and the minimum observed diameter) grows from ~5 to ~21 nm (Fig 7.2a and c).

Diffuse Reflectance-Ultraviolet/Visible Spectroscopy (DRS) was employed to characterize the absorption properties of Au nanoparticles at different Au precursor dose times (Fig 7.2d). The absorption spectra show the emergence and evolution of the Plasmon resonance as the Au precursor dosage time is increased. With the growth of larger particles at higher loadings of Au, the absorption band narrows, the plasmon resonance shifts to lower wavelengths (from 576 to 536 nm), and the intensity of the plasmon resonance wavelength increases from 0.2 to 1.7 (Fig 7.2d). For Au nanoparticles smaller than 20 nm, the blue shift and narrowing of the absorption are attributed to the increase in particle size. [40-42] The intensification of the absorption is correlated with the increase in Au loading and particle size. [12, 43] The DRS results, therefore, confirm the quantum confinement effects emerging in the ALD-grown nanoparticles and demonstrates the ability to tune them.

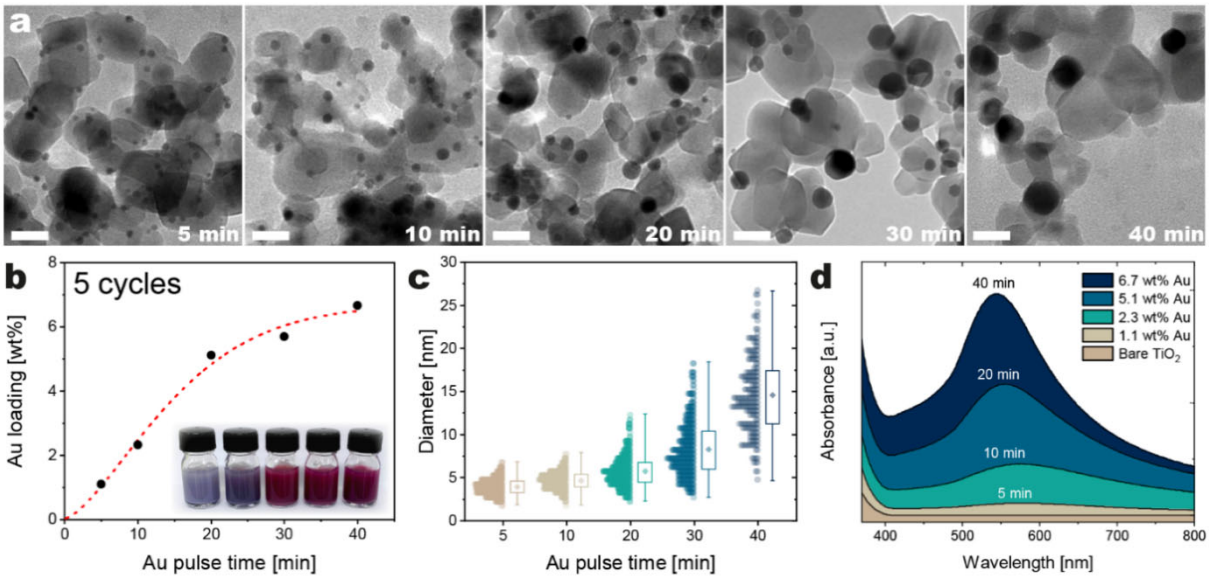

Figure 7.2: Evolution of the morphology, Au loading, and absorbance in the visible spectrum of the Au/TiO_2 obtained after 5 cycles with different precursor exposure times. (a) TEM micrographs of the Au/TiO_2 nanocomposites (scale bar 20 nm), (b) ICP results Au loading as the Au exposure time increases with corresponding photos of colloidal suspensions of the Au/TiO_2 nanocomposites (The dashed red line is drawn to guide the eye), (c) size distribution of the ALD-grown Au nanoparticles, (d) absorbance of the Au/TiO_2 nanocomposites as obtained via DRS measurements.

As synthesizing nanoparticles with an average size below 10 nm is essential for the catalytic applications of Au/TiO_2 nanocomposites, we focused on tuning the size distribution and the Au loading by tuning the exposures of the counter reactants while

using short Au precursor exposures. First, we studied the effect of varying the ozone exposure from 30 s to 10 min, while keeping the precursor and water exposure time constant at 10 min and 30 secs, respectively. The elemental analysis confirms that the Au loading on P25 nanoparticles is virtually unaffected by varying the ozone exposure over such a time window (Fig 7.3b). Nonetheless, the ozone exposure time has a dramatic effect on the size distribution of the ALD-grown nanoparticles, in that both the average size and the width of the size distribution are drastically reduced from 9.35 nm (std. dev. of 3.3 nm) to 4.68 nm (std. dev. of 1.0 nm) when the ozone exposure time is increased from 0.5 to 10 min (Fig 7.3a and d). Furthermore, the long tail that is observed at shorter ozone exposures gradually disappears with increasing exposure times. The fact that the loading is virtually unaffected by increasing ozone exposures, while the size distribution varies dramatically, suggests that the ozone changes the chemical affinity between Au and titania, and thus its degree of wetting and propensity to aggregate. XPS results confirm that the ozone affects the chemistry of the deposited Au as a significant decrease in Au (III) fraction is observed as the ozone exposure is increased (Fig 7.3c). Since ozone participates in the combustion reactions of the organic ligands remaining after the precursor chemisorption, an exposure to ozone is expected to promote the reduction of the deposited Au. At the same time, prolonged ozone exposures may also induce the formation of a thin oxide layer on the surface of the nanoparticles that promote their stability. [38, 44-45]

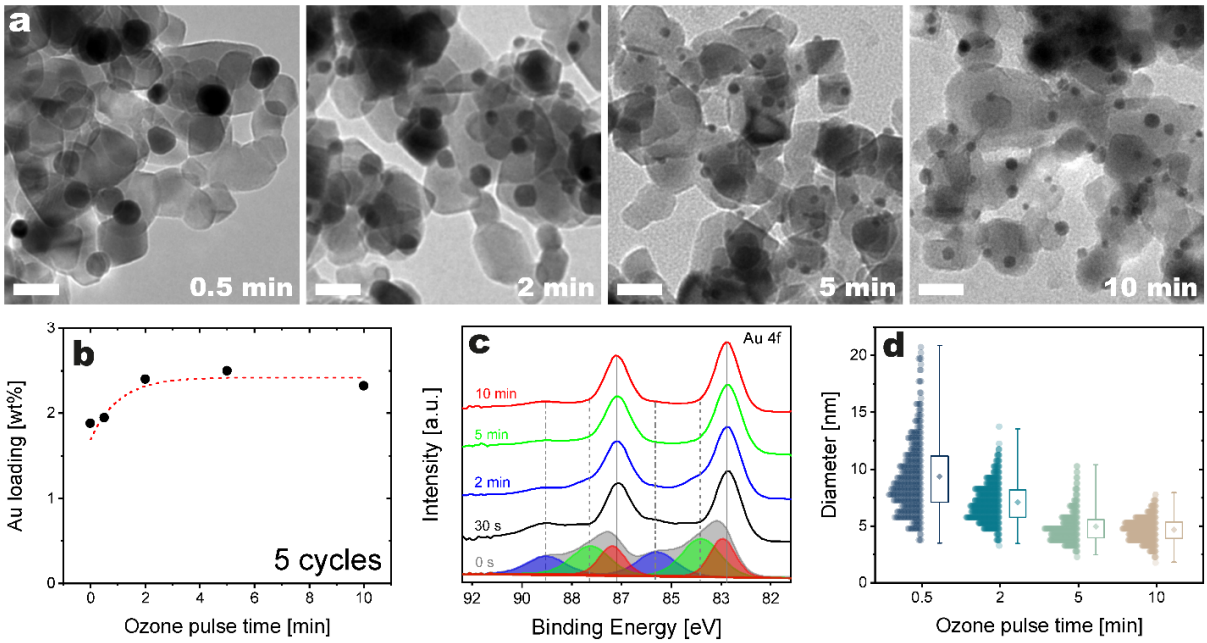

Figure 7.3: Evolution of the morphology, Au loading, and chemical state of the Au/TiO_2 nanocomposites obtained after 5 cycles with different ozone exposure times. (a) TEM micrographs of the Au/TiO_2 nanocomposites (scale bar: 20 nm), (b) evolution of the Au loading with the ozone exposure time (The dashed red line is drawn to guide the eye), (c) evolution of the chemical state of the ALD-grown Au as captured by the Au 4f region of XPS spectra. [Fitted peaks in 0 s ozone curve show different oxidation states of Au (red Au(0), green Au(I) and blue Au(III)), (d) evolution of the size distribution of the ALD-grown Au nanoparticles with increasing ozone exposure times.

Next, the effect of water exposure was studied by keeping Au and ozone exposure at 10 min and varying the water exposure from 0 to 2 min. An analysis of the elemental composition by XPS and ICP shows no appreciable changes in the loading of Au on titania nanoparticles upon longer water exposures (Fig 7.4e, Supporting info Fig 7.2). Nonetheless, longer water exposures broaden the size distribution of the Au nanoparticles (Fig 7.4 a-d and f). These results suggest that water promotes surface mobility, and thus the propensity of adatoms and nanoparticles to diffuse and coalesce, while not affecting the amount of precursor that can chemisorb in every cycle.

Griffiths et al. performed a ternary Au ALD process on Si wafers using water as the second counter reactant to eliminate the phosphorus impurity. [29] Water would react with the phosphorous impurities producing phosphoric acid, which more readily desorbs from the growth surface. However, in our case, ICP-OES and XPS show no changes in the phosphorous content upon increasing the water exposure time (supporting info Fig 7.2). The ineffectiveness of water exposure in removing P can be attributed to the differences in the ALD environment and support material used here compared to the study by Griffiths et al. When the ALD process is performed in vacuum and on flat substrates with a surface area of ~cm^2, several seconds of water exposure suffice to hydrolyze the phosphorus to phosphoric acid and purge the latter from the reactor. However, in our experiments, the high surface area of the powders (~100 m^2) and the use of atmospheric pressure might hinder the removal of phosphorous. In fact, the removal of low-vapor-pressure substances, such as phosphoric acid, can be particularly slow in powders compared with flat substrates because of two phenomena: (1) capillary condensation, and (2) the fact that molecules that desorb from one particle can adsorb onto other particles before they can escape from the reactor. [46] In particular, the latter is exacerbated by operating the reactor at relatively high pressure compared with the vacuum reactors used by Griffiths et al. [29] The effective removal of phosphorus in the form of phosphoric acid would probably require much longer water exposures, which would be cumbersome as they tend to disrupt the fluidization behavior of the powders. Hence, the fabrication of phosphorus-free Au/TiO_2 nanocomposites via fluidized bed reactors operating at atmospheric pressure might require more aggressive treatments.

Next, the effect of varying the number of ALD cycles was studied using the following sequence of Au-O_3-H_2O exposure times: 10 min-10 min-30 sec. A 10 min nitrogen purge was applied after each precursor/co-reactant exposure. The Au loading shows linear evolution with the number of cycles in the range of 1-9 cycles (Fig 7.5 a). Increasing the number of cycles results in a slight increase in the average diameter of the ALD-grown nanoparticles, while the span of size distribution remains relatively constant (Fig 7.5 a-c and e). This is not surprising because a precursor exposure time of 10 min translates into a growth per cycle of only ~0.26 at/nm^2, which is 0.02 Au(111) ML. As a result, increasing the number of cycles from 3 to 9 would result in a total increase of ~1.6 at/nm^2, which in itself cannot result in an appreciable change in particle size. Hence, this clearly illustrates how the use of long ozone exposures in conjunction with short precursor exposures mitigates nanoparticle sintering in each

ALD cycle, and thus lends itself to the fine-tuning of the size of the ALD-grown nanoparticles down to the sub-nanometer level.

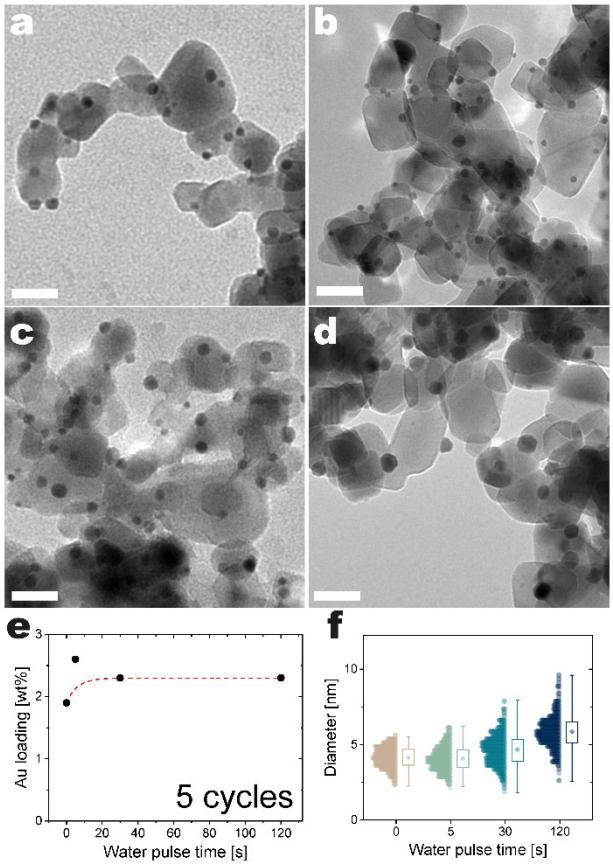

Figure 7.4: Evolution of the morphology and Au loading of the Au/TiO_2 nanocomposites obtained after 5 cycles with different water exposure times. (a-d) TEM micrographs of the Au/TiO_2 nanocomposites (scale bar 20 nm), (e) evolution of the Au loading (The dashed red line is drawn to guide the eye), (f) size distribution of the ALD-grown Au nanoparticles at different water exposure times.

The plasmon resonance peak measured from the samples with a varying number of cycles shifts towards lower wavelengths (578 to 544 nm) as the number of Au ALD cycles increases (Fig 7.5f). A stronger and narrower absorption band is also observed as a result of increasing Au loading upon increasing the number of cycles. As the Au particle size variation from the 3 cycles to 5 cycles experiments is less than one nanometer (4.5 to 4.7 nm), the detected shift in the resonance peak wavelength is almost negligible (~ 8 nm shift). On the other hand, the Au loading has a 40% increase from 3 to 5 cycles. This substantial change in the Au loading explains the enhanced resonance intensity and narrowing down of the plasmon resonance peak.

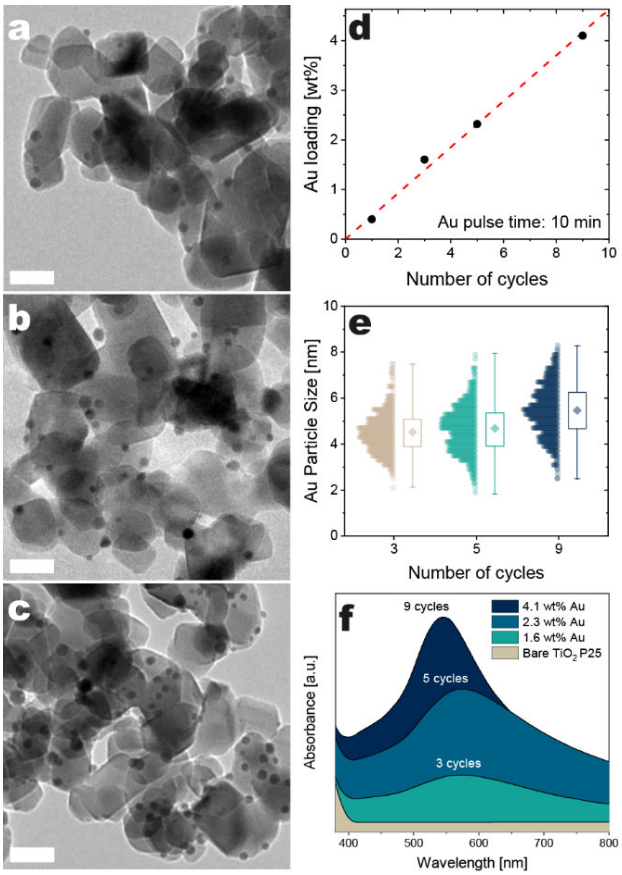

Figure 7.5: Effect of varying the number of cycles using long ozone exposures and short precursor exposures. (a-c) TEM micrographs of the Au/TiO_2 nanocomposites (scale bar 20 nm), (d) evolution of the Au loading with the number of cycles (The dashed red line is drawn to guide the eye), (e) Size distribution of the ALD-grown Au nanoparticles (f) Absorbance of the Au/TiO_2 nanocomposites as obtained via DRS measurements.

To further demonstrate the ability of our process to control the size distribution of the ALD-grown nanoparticles at a given Au loading, we tested the photocatalytic activity of the Au/TiO_2 nanocomposites towards the degradation of a model dye: Rhodamine B. Incorporating titania with Au nanoparticles has been reported to increase its photocatalytic activity towards various reactions, including the oxidation of organic molecules and water splitting. [12, 47-50] Several mechanisms have been proposed in the literature to explain such an enhancement. For example, Au nanoparticles can extend the absorption of titania in the visible region because of plasmon resonance, and they can mediate surface charge recombination rates. In general, the effect of Au nanoparticles varies across different reactions and strongly depends on both the loading and the particle size. Although understanding the exact mechanism behind the enhanced photocatalytic activity of Au/TiO_2 towards the decomposition of Rhodamine B is beyond the scope of this work, we do show how the precision of our process can be used to decouple the effect of loading and particle size, and thus lead to optimal photocatalysts.

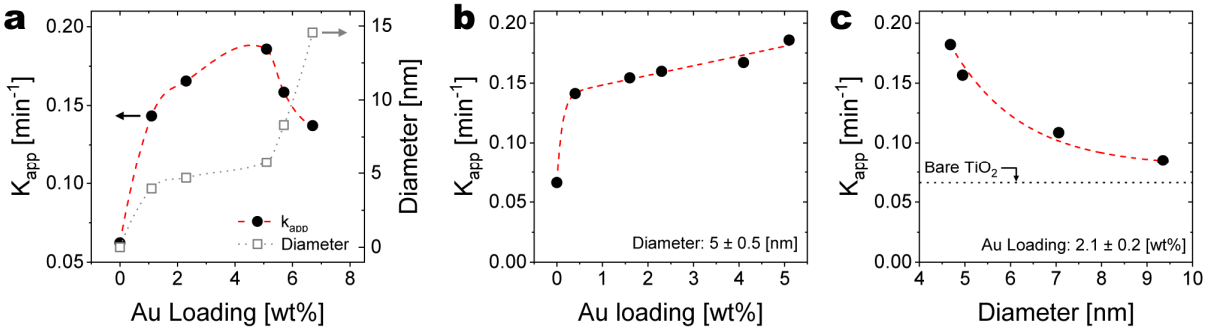

Figure 7.6: Photocatalytic activity of the Au/TiO_2 nanocomposites towards the decomposition of Rhodamine B with (a) varying both Au loading and particle size, (b) fixed particle size (5 nm) and varying Au loading, (c) fixed Au loading (2%) and increasing particle size.

First, we tested the photocatalytic activity of the nanocomposites obtained after five cycles using five different precursor exposures (Fig 7.6a), which translate into Au loadings that vary in the range ~1-7 wt% and particle sizes in the range ~5-15 nm. On these samples, the Au loading and the particle size are not decoupled as higher loadings correspond to larger particle sizes. As shown in Figure 7.6a, higher loadings, and thus larger particle sizes have a non-monotonic effect on the photocatalytic activity of the nanocomposites, as quantified in terms of the apparent rate constant (k_{app}) extracted from the decay over time of the Rhodamine B concentration upon illumination (Supporting info Fig 7.3). The rate constant increases threefold upon increasing the Au loading to ~5 wt% compared with bare TiO_2. Yet increasing the loading further sees a gradual drop in k_{app} . Although a maximum exists, loading and particle size are coupled and so it is not clear whether this trend is to be attributed to the loading or the particle size. This exemplifies one of the common problems encountered in fundamental studies into the catalytic activity of nanostructured materials.

To illustrate how our process can be used to gain insights into the structure-dependent properties of Au/TiO_2 nanocomposites, we studied the photocatalytic activity of samples obtained by decoupling the Au loading from the particle size. Figure 7.6b shows that for a given particle size (5 nm), k_{app} increases roughly linearly with the Au loading in the range ~0.5-5 wt%. On the other hand, Figure 7.6c shows that at a given loading (~2.1 wt%), k_{app} rapidly decreases with increasing particle size (in the range ~4-10 nm), and approaches the value obtained for the control case with bare TiO_2 for a particle size around 10 nm and larger. A similar trend was reported in the seminal work by Haruta [9], where they show that the catalytic activity of Au nanoparticles towards CO oxidation rapidly decreases with increasing particle size, and virtually vanishes beyond 10 nm.

7.4. CONCLUSION

We demonstrated ALD of Au on gram-scale batches of titania nanopowders using a thermal process employing a fluidized bed reactor operated at atmospheric pressure. We performed ALD at the relatively low temperature of 105 °C using trimethylphosphino-trimethyl gold (III) as the metal precursor and ozone and water as co-reactants. This process leads to the formation of supported Au nanoparticles, with the number of cycles controlling the Au loading. We found that by varying the exposure time of the co-reactants, it is possible to control the broadness of the size distribution of the Au nanoparticles independently from the Au loading. In particular, ozone and water exposures have opposite effects: long ozone exposures suppress nanoparticle sintering and thus result in narrow size distributions, whereas long water exposures lead to broad ones. By leveraging the ability of the process to control the particle size at given loading, we could explore the structure-property relationship of the ALD-grown Au/TiO_2 in the photocatalytic degradation of Rhodamine B. We could achieve up to a threefold increase in the photocatalytic activity of titania by increasing the Au loading in the range 0-5 wt% while maintaining a constant nanoparticle size of ~5 nm. Conversely, increasing the nanoparticle size from 5 to 9 nm at the given loading of ~2.1 wt% resulted in a decrease of the photocatalytic activity, which gradually approached that of bare TiO_2. This process opens new avenues not only for the scalable fabrication of Au/TiO_2 nanocomposites, but also for investigating the structure-property relationship of supported Au nanoparticles.

APPENDIX

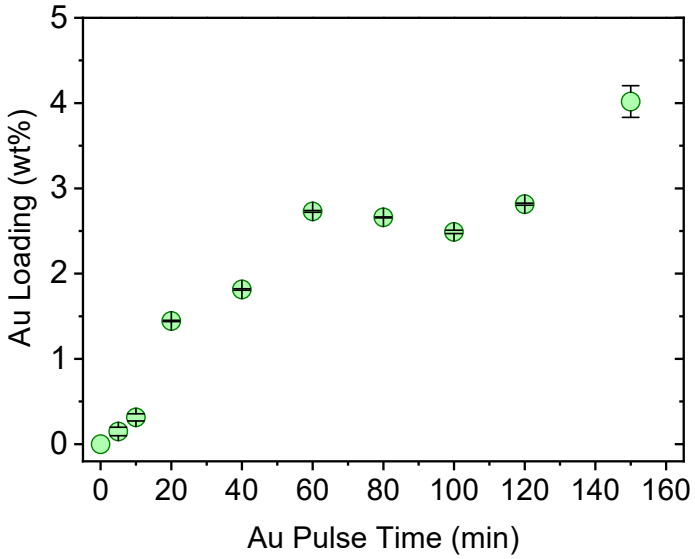

Figure S7.7: ICP measurements, Au loading on TiO_2 nanoparticles as a function of Au precursor exposure time for 1 ALD cycle

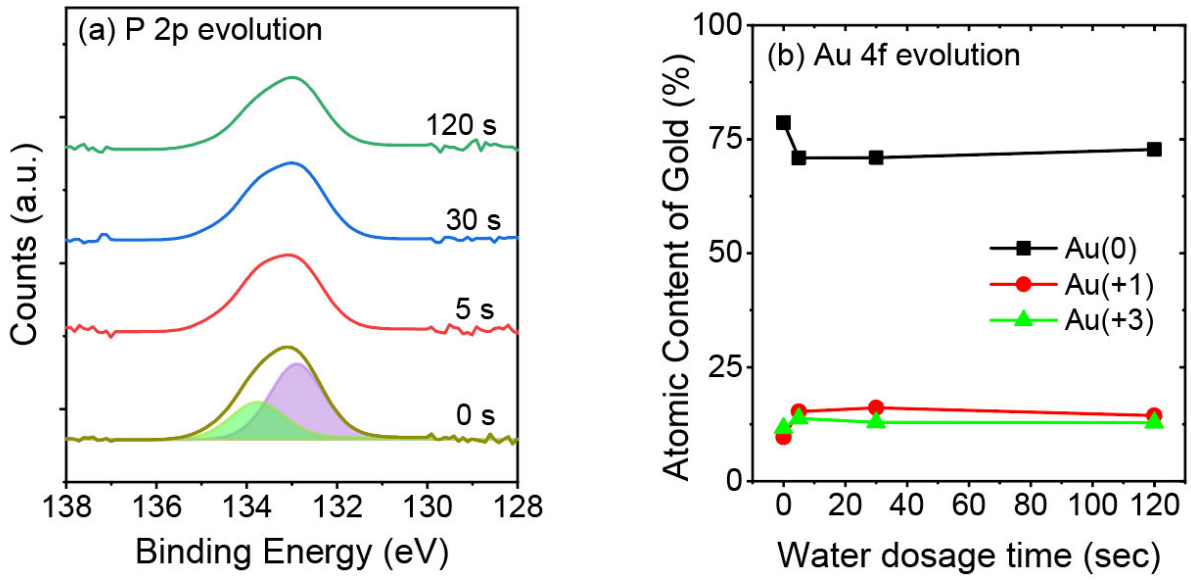

Figure S7.2: effects of increasing water dosage time on the P and Au composition of the nanoparticles. (a) XPS evolution of P2p peak (purple: high binding energy peak, green: low binding energy peak) (b) XPS evolution of Au 4f oxidation states

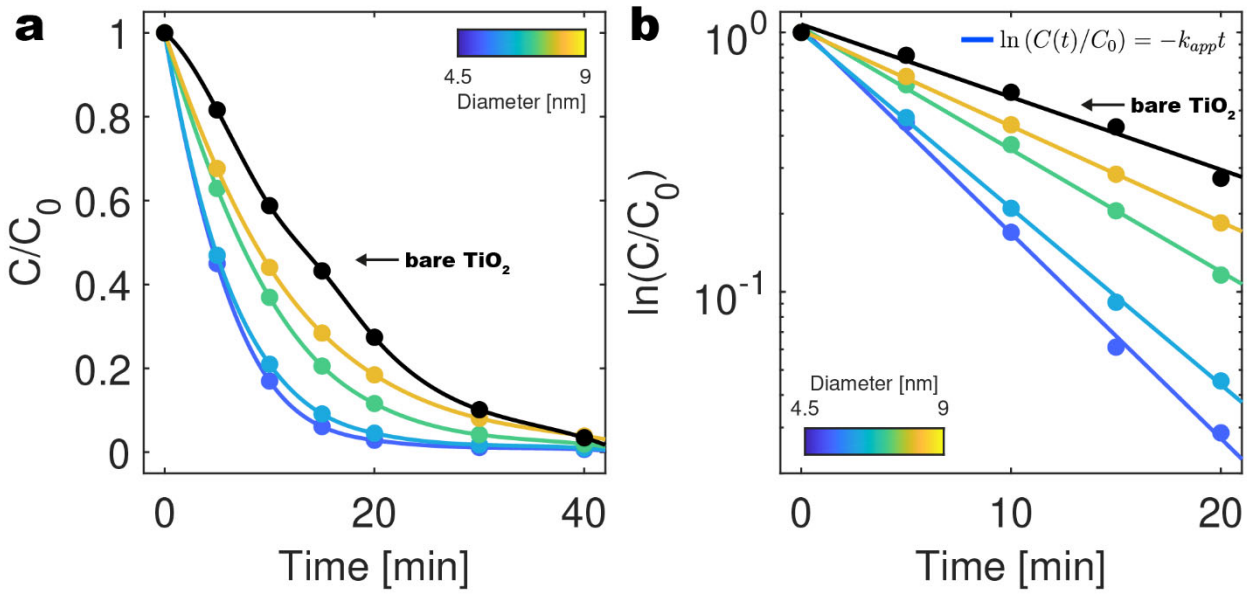

Figure S7.3: Changes in the concentration of RhB solution containing the TiO_2 and Au/TiO_2 nanoparticles as the Au nanoparticle size increases (a) C/C_0 versus illumination time (b) $\ln(C/C_0)$ versus illumination time. The reported k_{app} value for each sample is calculated from the slope of each curve in this graph.

REFERENCES

1. Hämäläinen, J.; Ritala, M.; Leskelä, M., Atomic Layer Deposition of Noble Metals and Their Oxides. *Chemistry of Materials* **2014,** *26* (1), 786-801.
2. Hosseini, M.; Barakat, T.; Cousin, R.; Aboukais, A.; Su, B. L.; De Weireld, G.; Siffert, S., Catalytic performance of core-shell and alloy Pd-Au nanoparticles for total oxidation of VOC: The effect of metal deposition. *Applied Catalysis B: Environmental* **2012,** *111*, 218-224.
3. Hosseini, M.; Siffert, S.; Tidahy, H. L.; Cousin, R.; Lamonier, J. F.; Aboukais, A.; Vantomme, A.; Roussel, M.; Su, B. L., Promotional effect of gold added to palladium supported on a new mesoporous TiO_2 for total oxidation of volatile organic compounds. *Catalysis Today* **2007,** *122* (3-4), 391-396.
4. Barakat, T.; Rooke, J. C.; Franco, M.; Cousin, R.; Lamonier, J.-F.; Giraudon, J.-M.; Su, B.-L.; Siffert, S., Pd- and/or Au-Loaded Nb- and V-Doped Macro-Mesoporous TiO_2 Supports as Catalysts for the Total Oxidation of VOCs. *European Journal of Inorganic Chemistry* **2012,** *2012* (16), 2812--2818.
5. Moreau, F.; Bond, G. C.; Taylor, A. O., Gold on titania catalysts for the oxidation of carbon monoxide: control of pH during preparation with various gold contents. *Journal of Catalysis* **2005,** *231* (1), 105--114.
6. Corma, A.; Serna, P.; García, H., Gold Catalysts Open a New General Chemoselective Route to Synthesize Oximes by Hydrogenation of α,β-Unsaturated Nitrocompounds with H_2. *Journal of the American Chemical Society* **2007,** *129* (20), 6358-6359.
7. Dollinger, A.; Stolch, L.; Luo, Y.; Beck, M.; Strobel, C. H.; Hagner, M.; Dilger, S.; Bein, M.; Polarz, S.; Gantefoer, G. F.; Kim, Y.-D.; Proch, S., Size-selected gold clusters on porous titania as the most "gold-efficient" heterogeneous catalysts. *Phys. Chem. Chem. Phys.* **2014,** *16*, 11017-11023.
8. Haruta, M.; Yamada, N.; Kobayashi, T.; Iijima, S., Gold catalysts prepared by coprecipitation for low-temperature oxidation of hydrogen and of carbon monoxide. *Journal of Catalysis* **1989,** *115* (2), 301-309.
9. Haruta, M., Size- and support-dependency in the catalysis of gold. *Catalysis Today* **1997,** *36* (1), 153-166.
10. Valden, M.; Lai, X.; Goodman, D. W., Onset of catalytic activity of gold clusters on titania with the appearance of nonmetallic properties. *Science* **1998,** *281* (5383), 1647-1650.
11. Li, L.; Larsen, A. H.; Romero, N. A.; Morozov, V. A.; Glinsvad, C.; Abild-Pedersen, F.; Greeley, J.; Jacobsen, K. W.; Norskov, J. K., Investigation of Catalytic Finite-Size-Effects of Platinum Metal Clusters. *J Phys Chem Lett* **2013,** *4* (1), 222-226.
12. Tsukamoto, D.; Shiraishi, Y.; Sugano, Y.; Ichikawa, S.; Tanaka, S.; Hirai, T., Gold Nanoparticles Located at the Interface of Anatase/Rutile TiO_2 Particles as Active Plasmonic Photocatalysts for Aerobic Oxidation. *J. Am. Chem. Soc.* **2012,** *134* (14), 6309--6315.
13. Jain, P. K.; Huang, X.; El-Sayed, I. H.; El-Sayed, M. A., Noble Metals on the Nanoscale: Optical and Photothermal Properties and Some Applications in Imaging, Sensing, Biology, and Medicine. *Accounts of Chemical Research* **2008,** *41* (12), 1578-1586.
14. Cargnello, M., Colloidal Nanocrystals as Building Blocks for Well-Defined Heterogeneous Catalysts. *Chemistry of Materials* **2019,** *31* (3), 576-596.
15. Roldan Cuenya, B.; Behafarid, F., Nanocatalysis: size- and shape-dependent chemisorption and catalytic reactivity. *Surface Science Reports* **2015,** *70* (2), 135-187.
16. Van Bui, H.; Grillo, F.; van Ommen, J. R., Atomic and molecular layer deposition: off the beaten track. *Chem. Commun.* **2017,** *53*, 45-71.
17. Zang, L.; Macyk, W.; Lange, C.; Maier, W. F.; Antonius, C.; Meissner, D.; Kisch, H., Visible-Light Detoxification and Charge Generation by Transition Metal Chloride Modified Titania. *Chemistry – A European Journal* **2000,** *6* (2), 379--384.
18. Amaniampong, P. N.; Li, K.; Jia, X.; Wang, B.; Borgna, A.; Yang, Y., Titania-Supported Gold Nanoparticles as Efficient Catalysts for the Oxidation of Cellobiose to Organic Acids in Aqueous Medium. *ChemCatChem* **2014,** *6* (7), 2105--2114.
19. Li, D.; McCann, J. T.; Gratt, M.; Xia, Y., Photocatalytic deposition of gold nanoparticles on electrospun nanofibers of titania. *Chemical Physics Letters* **2004,** *394* (4), 387--391.
20. O'Neill, B. J.; Jackson, D. H. K.; Lee, J.; Canlas, C.; Stair, P. C.; Marshall, C. L.; Elam, J. W.; Kuech, T. F.; Dumesic, J. A.; Huber, G. W., Catalyst Design with Atomic Layer Deposition. *ACS Catalysis* **2015,** *5* (3), 1804-1825.

21. Mondloch, J. E.; Bayram, E.; Finke, R. G., A review of the kinetics and mechanisms of formation of supported-nanoparticle heterogeneous catalysts. *Journal of Molecular Catalysis A: Chemical* **2012,** *355*, 1-38.
22. Grillo, F.; Van Bui, H.; Moulijn, J. A.; Kreutzer, M. T.; van Ommen, J. R., Understanding and Controlling the Aggregative Growth of Platinum Nanoparticles in Atomic Layer Deposition: An Avenue to Size Selection. *The Journal of Physical Chemistry Letters* **2017,** *8* (5), 975-983.
23. Grillo, F.; Kreutzer, M. T.; van Ommen, J. R., Modeling the precursor utilization in atomic layer deposition on nanostructured materials in fluidized bed reactors. *Chemical Engineering Journal* **2015,** *268*, 384-398.
24. George, S. M., Atomic Layer Deposition: An Overview. *Chemical Reviews* **2010,** *110* (1), 111-131.
25. Grillo, F.; Van Bui, H.; La Zara, D.; Aarnink, A. A. I.; Kovalgin, A. Y.; Kooyman, P.; Kreutzer, M. T.; van Ommen, J. R., From Single Atoms to Nanoparticles: Autocatalysis and Metal Aggregation in Atomic Layer Deposition of Pt on TiO_2 Nanopowder. *Small* **2018,** *14* (23).
26. Van Bui, H.; Grillo, F.; Kulkarni, S. S.; Bevaart, R.; Van Thang, N.; van der Linden, B.; Moulijn, J. A.; Makkee, M.; Kreutzer, M. T.; van Ommen, J. R., Low-temperature atomic layer deposition delivers more active and stable Pt-based catalysts. *Nanoscale* **2017,** *9* (30), 10802-10810.
27. Dendooven, J.; Ramachandran, R. K.; Solano, E.; Kurttepeli, M.; Geerts, L.; Heremans, G.; Rongé, J.; Minjauw, M. M.; Dobbelaere, T.; Devloo-Casier, K.; Martens, J. A.; Vantomme, A.; Bals, S.; Portale, G.; Coati, A.; Detavernier, C., Independent tuning of size and coverage of supported Pt nanoparticles using atomic layer deposition. *Nature Communications* **2017,** *8* (1).
28. Mackus, A. J. M.; Weber, M. J.; Thissen, N. F. W.; Garcia-Alonso, D.; Vervuurt, R. H. J.; Assali, S.; Bol, A. A.; Verheijen, M. A.; Kessels, W. M. M., Atomic layer deposition of Pd and Pt nanoparticles for catalysis: on the mechanisms of nanoparticle formation. *Nanotechnology* **2016,** *27* (3).
29. Griffiths, M. B. E.; Pallister, P. J.; Mandia, D. J.; Barry, S. T., Atomic Layer Deposition of Gold Metal. *Chemistry of Materials* **2016,** *28* (1), 44-46.
30. Mäkelä, M.; Hatanpää, T.; Mizohata, K.; Räisänen, J.; Ritala, M.; Leskelä, M., Thermal Atomic Layer Deposition of Continuous and Highly Conducting Gold Thin Films. *Chemistry of Materials* **2017,** *29* (14), 6130-6136.
31. Goulas, A.; Ruud van Ommen, J., Atomic layer deposition of platinum clusters on titania nanoparticles at atmospheric pressure. *J. Mater. Chem. A* **2013,** *1* (15), 4647--4650.
32. Doekhi-Bennani, Y. Photoelectrocatalysis in water treatment. PhD Thesis, Delft University of Technology, Delft, 2017.
33. Foiles, S. M.; Baskes, M. I.; Daw, M. S., Embedded-atom-method functions for the fcc metals Cu, Ag, Au, Ni, Pd, Pt, and their alloys. *Physical Review B* **1986,** *33* (12), 7983-7991.
34. Puurunen, R. L., Surface chemistry of atomic layer deposition: A case study for the trimethylaluminum/water process. **2005,** *97* (12), 121301.
35. Grillo, F.; Moulijn, J. A.; Kreutzer, M. T.; van Ommen, J. R., Nanoparticle sintering in atomic layer deposition of supported catalysts: Kinetic modeling of the size distribution. *Catalysis Today* **2018,** *316*, 51-61.
36. La Torre, A.; Gimenez-Lopez, M. D.; Fay, M. W.; Rance, G. A.; Solomonsz, W. A.; Chamberlain, T. W.; Brown, P. D.; Khlobystov, A. N., Assembly, Growth, and Catalytic Activity of Gold Nanoparticles in Hollow Carbon Nanofibers. *Acs Nano* **2012,** *6* (3), 2000-2007.
37. Bell, G. R.; Dawson, P. M.; Pandey, P. A.; Wilson, N. R.; Mulheran, P. A., Size-dependent mobility of gold nano-clusters during growth on chemically modified graphene. *Apl Mater* **2014,** *2* (1).
38. Ruckenstein, E., Role of Wetting in Sintering and Redispersion of Supported Metal Crystallites. *Journal of Crystal Growth* **1979,** *47* (5-6), 666-670.
39. Jak, M. J. J.; Konstapel, C.; van Kreuningen, A.; Verhoeven, J.; Frenken, J. W. M., Scanning tunnelling microscopy study of the growth of small palladium particles on TiO2(110). *Surface Science* **2000,** *457* (3), 295-310.
40. Cottancin, E.; Celep, G.; Lermé, J.; Pellarin, M.; Huntzinger, J. R.; Vialle, J. L.; Broyer, M., Optical Properties of Noble Metal Clusters as a Function of the Size: Comparison between Experiments and a Semi-Quantal Theory. *Theoretical Chemistry Accounts* **2006,** *116* (4), 514--523.
41. Fleger, Y.; Rosenbluh, M., Surface Plasmons and Surface Enhanced Raman Spectra of Aggregated and Alloyed Gold-Silver Nanoparticles. 2009; Vol. 2009, p 5.
42. Peng, S.; McMahon, J. M.; Schatz, G. C.; Gray, S. K.; Sun, Y., Reversing the size-dependence of surface plasmon resonances. *Proc Natl Acad Sci USA* **2010,** *107* (33), 14530.

43. Martínez, E. D.; Boissiére, C.; Grosso, D.; Sanchez, C.; Troiani, H.; Soler-Illia, G. J. A. A., Confinement-Induced Growth of Au Nanoparticles Entrapped in Mesoporous TiO_2 Thin Films Evidenced by in Situ Thermo-Ellipsometry. *J. Phys. Chem. C* **2014,** *118* (24), 13137--13151.
44. Solano, E.; Dendooven, J.; Ramachandran, R. K.; Van de Kerckhove, K. V.; Dobbelaere, T.; Hermida-Merino, D.; Detavernier, C., Key role of surface oxidation and reduction processes in the coarsening of Pt nanoparticles. *Nanoscale* **2017,** *9* (35), 13159-13170.
45. Goula, G.; Botzolaki, G.; Osatiashtiani, A.; Parlett, C. M. A.; Kyriakou, G.; Lambert, R. M.; Yentekakis, I. V., Oxidative Thermal Sintering and Redispersion of Rh Nanoparticles on Supports with High Oxygen Ion Lability. *Catalysts* **2019,** *9* (6).
46. Onn, T.; Küngas, R.; Fornasiero, P.; Huang, K.; Gorte, R. J. I., Atomic layer deposition on porous materials: Problems with conventional approaches to catalyst and fuel cell electrode preparation. **2018,** *6* (1), 34.
47. Li, X. Z.; Li, F. B., Study of Au/Au^{3+}-TiO_2 Photocatalysts toward Visible Photooxidation for Water and Wastewater Treatment. *Environmental Science & Technology* **2001,** *35* (11), 2381-2387.
48. Rosseler, O.; Shankar, M. V.; Du, M. K.-L.; Schmidlin, L.; Keller, N.; Keller, V., Solar light photocatalytic hydrogen production from water over Pt and Au/TiO_2(anatase/rutile) photocatalysts: Influence of noble metal and porogen promotion. *Journal of Catalysis* **2010,** *269* (1), 179-190.
49. Paramasivam, I.; Macak, J. M.; Schmuki, P., Photocatalytic activity of TiO_2 nanotube layers loaded with Ag and Au nanoparticles. *Electrochemistry Communications* **2008,** *10* (1), 71-75.
50. Sangpour, P.; Hashemi, F.; Moshfegh, A. Z., Photoenhanced Degradation of Methylene Blue on Cosputtered M:TiO2 (M = Au, Ag, Cu) Nanocomposite Systems: A Comparative Study. *The Journal of Physical Chemistry C* **2010,** *114* (33), 13955-13961.

8

Outlook and conclusions

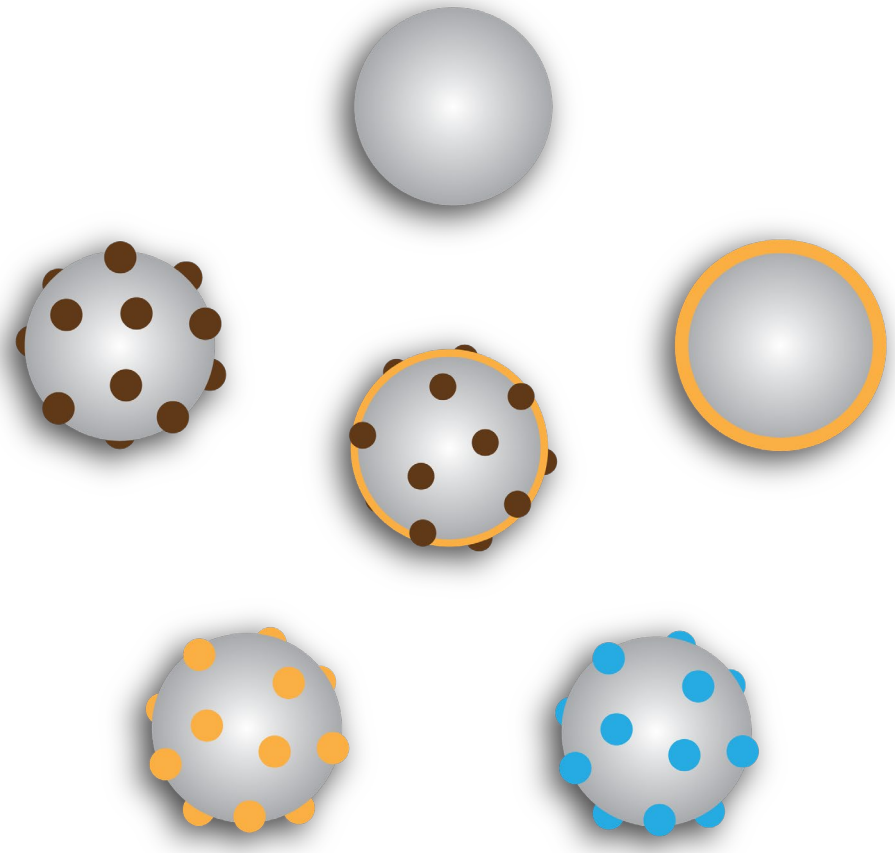

8.1. GENERAL OUTCOME

This thesis focuses on the development of improved photocatalysts to degrade organic pollutants in water. Starting with TiO_2 (P25) particles as photoactive material, we were able to utilize the precise controllability of atomic layer deposition (ALD) using various deposits (Chapter 2: Pt, Chapter 3: Cu_2O, Chapters 4 & 5: SiO_2, Chapter 6: a combination of SiO_2 and Pt, and Chapter 7: Au) increasing the photocatalytic activity. The deposition of Cu_2O clusters and SiO_2 layers on P25, respectively, provided noble metal-free photocatalysts with superior photocatalytic activity. This gives the opportunity to reduce the costs of photocatalysts, while keeping the improvement factor at the same level or even higher than noble metal catalysts such as Pt:TiO_2 (P25) (Table 8.1). Mechanistic studies for SiO_2:TiO_2(P25) revealed the change in the mechanism for P25 from direct oxidation on the surface to a more hydroxyl-based mechanism for the degradation of dyes upon deposition of SiO_2. Furthermore, this change resulted in a different selectivity for the degradation of multiple compounds in the water, which adds complication to the evaluation of different materials that differently perform when it comes to photodegradation of multiple components in a system. Moreover, revealing the working principles of the Pt modified P25 catalyst demonstrates how modifications of a base material can affect the performances of photocatalysts under different atmospheres O_2 and Ar, respectively.

Table 8.1: Cost of the P25 and chemicals used in this thesis to deposit modifications on the surface of TiO_2 (P25) and improve its photocatalytic activity. The cost of the gold deposition could not be calculated, since the precursor is not commercially available.

Catalyst Material	P25	Pt:P25	Cu_2O:P25	SiO_2:P25	Pt:SiO_2:P25	
Precursor	-	$Pt(Me)_3$ CpMe	Cu(hfac) $*SiC_2H_3(Me)_3$	$SiCl_4$	$SiCl_4$	$Pt(Me)_3$ CpMe
Price [€/g]	1.61	254.00	6.89	0.53	0.53	254.00
Molar mass [g/mol]	-	319.3	370.5	169.9	169.9	319.3
Supplier	Sigma Aldrich	Strem Chemicals	Gelest	Sigma Aldrich	Sigma Aldrich	Strem Chemicals
Optimal loading [wt. %]	-	0.36 (Pt)	0.40 (Cu)	1.80 (Si)	1.20 (Si)	0.62 (Pt)
Price catalyst (coating only) [€/kg]	1610.00	3107.27 (1497.27)	1770.81 (160.81)	1668.08 (58.08)	4227.35 (38.72) (2578.63)	
Enhancement factor	1	2 *(Chapter 2)*	2 *(Chapter 3)*	3 *(Chapter 5)*	6 *(Chapter 6)*	
Price / Enh. factor	**1610**	**1554**	**885**	**556**	**705**	

Furthermore, using ALD in a fluidized bed offers the opportunity to produce high-surface-area photocatalyst material (P25: 55 m^2/g) of up to 5 g per batch. More importantly, ALD provides precise tunability of the loading (Chapters 2 to 7) and the cluster size of deposits (especially in Chapter 7). [1] In all of our studies, we find that optimal performance can be achieved with only minute loadings (for layers (SiO_2) and clusters (Pt, Au, and Cu_2O)). This advocates the importance of controllability to develop high-performance catalysts. In case of SiO_2 the layer thickness (1.2 nm optimal thickness) determines the photocatalytic activity, for Pt and Cu_2O modification only very low loadings (0.34 wt. % Pt, 0.4 wt. % Cu) give a further improvement while Au clusters of very defined particle size (5 nm) were most active. These results advocate the advantages ALD provides to the controllable design of optimized photocatalytic materials.

8.2. LIMITATIONS OF THE USED APPROACH AND RECOMMENDATIONS FOR FURTHER IMPROVEMENT

We have shown that ALD has excellent potential in catalyst improvement, especially when very low loadings or layer thicknesses are required. The scalability and depositions under atmospheric pressures are a great benefit for developing this technique further for catalyst manufacturing. However, despite the pure gas-phase deposition, which makes the use of solvents as a source of contamination redundant, ALD deposits often deal with contaminations from precursors, too. For the deposition of SiO_2 layers, we have shown in Chapter 3 how the residual contamination Cl from the $SiCl_4$ precursor can adversely affect the photocatalytic activity. Nevertheless, simple post-treatment could reduce the contamination leading to improved photocatalytic activity. Other than for SiO_2, during ALD of Au in Chapter 7, the P residues seem to be very persistent on the surface, which possibly affect the photocatalytic performance, and further treatment should be explored to remove those supposedly harmful contaminants.

The studies in this thesis were mainly based on the degradation of dye molecules. However, lately, the discussion in literature arises whether the degradation of dye molecules is a suitable experiment to evaluate the photocatalytic activity of newly developed materials also for water purification. [2-3] Due to the capability of absorbing solar light, specific dye molecules themselves may be excited and degrade instantly (self-degradation) or, secondly, inject excited electrons into the catalyst material, which leads to the degradation of the dye molecule. Preliminary photocatalytic tests under visible light for SiO_2:TiO_2(P25) and Cu_2O:TiO_2(P25) showed however, no catalytic activity indicating the absence of the self-sensitization for those catalytic systems. Nevertheless, this issue should be further investigated in follow-up studies. Additionally, the electron injection mechanism may only occur when the dye molecule is able to adsorb on the surface. In our studies, we both checked for self-degradation without a catalyst and we addressed the second issue by testing the degradation of dye

molecules, which have different charges leading to both attractive and repulsive interactions with the catalyst surface. Furthermore, the possibility to diminish the photocatalytic activity under certain conditions (Ar atmosphere, scavenging agents) also shows that the degradation of the dye molecules via self-degradation cannot be the main contribution for the degradation. Additionally, experiments using a light source emitting photons of lower energy than the bandgap of the photocatalyst would further clarify the role of the dye electron injection mechanism. Apart from these issues, in order to further investigate the general photocatalytic activity of the developed materials, as a next step more contaminants (herbicides, pesticides, pharmaceuticals) need to be tested to thrive to implementation of the technology into real life. Especially the simultaneous degradation of multiple pollutants may change the overall efficiency and selectivity of pollutant degradation (Chapter 5).

Even though numerous analysis tools have been developed to investigate the mechanistic pathways in photocatalysis, many techniques do not give a clear solution since the results depend on different parameters. A precise analysis of the influence of different parameters remains challenging and often ambiguous. As we have seen in Chapter 5, the addition of sacrificial agents (DMSO, MeOH) may be helpful in investigating the predominant degradation pathway. However, the apparent role of those molecules in the photocatalytic mechanisms is not entirely resolved. Ideally, mechanistic insight would arise from the deconvolution of different parameter and their individual influence on the photocatalytic activity. Therefore, experimental design and understanding of interaction with different pollutants and especially sacrificial agents need improvement to manifest conclusions. Well understood model systems to test the activity, and in-situ measurements of the radical generation and charge carrier kinetics may help to further understand the underlying principles for specific materials.

Furthermore, the possibilities to evaluate photocatalytic activities and especially compare them still lack so far because of the various ways of testing a photocatalyst. Standardized testing of catalysts in a specific environment (reactors, light spectrum & intensity, irradiation area, atmosphere) would increase the comparability between materials in publications. The goal should be to determine the intrinsic activity of a material per surface area. Using slurry systems to test the activity is the most commonly used and easiest way to measure the photocatalytic activity of a powder photocatalyst. However, two regimes can be chosen to evaluate the activity: high and low catalyst concentration. [4] High catalyst concentration prevents the scattering of incoming light out of the reactor. A photon that is not absorbed but scattered by a catalyst particle is then likely to be absorbed by another catalyst particle in the slurry. However, as a result of the high catalyst concentration in the slurry, the light may only partially penetrate into the slurry, leaving a significant fraction of the particles not irradiated. Furthermore, the effect of agglomeration of particles for high concentration has shown to have a substantial effect on the apparent kinetic constant due to mass transport limitation from the dye solution into the agglomerates. [5] Low catalyst concentration could prevent the mass transport limitation due to limited agglomeration and would make sure all particles are homogenously irradiated. For low concentrations,

a kinetic regime can be reached where the catalyst concentration scales linearly with the activity indicating that mass transfer limitations play only a negligible role anymore. [5] The light scattering properties, i.e. absorption coefficient, on the other hand, of differently modified materials, will become more prevalent at low catalyst concentrations. However, measuring and correlating the scattering index with the kinetic constants would give in this case the intrinsic kinetic constant of materials per surface area. This would not only make the comparison between materials easier but also would give the chance to translate experimental results of the catalyst activity to reactor modeling and reactor design. Additionally, revealing the mechanism of certain modifications could not only lead to better understanding of the working principles but also a smart catalyst design could be persued. Combining materials which modify different parts of the photocatalytic mechanism individually such as the combination of enhanced adsorption with improved surface reactivity would strongly increase the photocatalytic activity of these smartly designed new materials. ALD with its precise controlabillity of material deposition on the surface could play an important role in the specific design of these materials.

After initially evaluating the photocatalytic activity in defined lab environments, the translation to more complex systems with various parameters such as additional ion concentration needs to be taken into account. The problem here is that for different added molecules, the activity does not change similarly for different catalysts. In that regard, the effect of substances such as dispersing agents e.g. sodium polyphosphate, is still unresolved, leading to different activity trends upon addition for i.e., P25 and Pt:TiO_2(P25). This makes it almost impossible to predict the activity of a catalyst in a different environment unless the mechanisms are clearly resolved. In the case of an application for water treatment, this makes the technology unreliable for unknown water sources and negates the technology as applicable for general water treatment. On the other hand, numerous reports have shown progress in the revelation of mechanism and trends in activity in the presence of other pollutants or ions. [6-7] Therefore, evaluating the excellent potential of photocatalysis, especially in an area where conventional treatment technologies reach their limits such as the removal of micropollutants, I would recommend focusing photocatalysis first towards the treatment of special effluents of manufacturing plants or hospitals. In those, the water contamination is more defined and stable and the combination with other treatment technologies is more feasible and affordable. After successful implementation in this area, the next step should then thrive to implementation of photocatalysis to provide clean drinking water from a polluted water source to people in low-resource settings.

REFERENCES

1. Grillo, F.; Van Bui, H.; Moulijn, J. A.; Kreutzer, M. T.; van Ommen, J. R., Understanding and Controlling the Aggregative Growth of Platinum Nanoparticles in Atomic Layer Deposition: An Avenue to Size Selection. *The Journal of Physical Chemistry Letters* **2017,** *8* (5), 975-983.
2. Parrino, F.; Loddo, V.; Augugliaro, V.; Camera-Roda, G.; Palmisano, G.; Palmisano, L.; Yurdakal, S., Heterogeneous photocatalysis: guidelines on experimental setup, catalyst characterization, interpretation, and assessment of reactivity. *Catalysis Reviews* **2019,** *61* (2), 163-213.
3. Shaham-Waldmann, N.; Paz, Y., Away from TiO_2: A critical minireview on the developing of new photocatalysts for degradation of contaminants in water. *Materials Science in Semiconductor Processing* **2016,** *42*, 72-80.
4. Motegh, M.; Cen, J.; Appel, P. W.; van Ommen, J. R.; Kreutzer, M. T., Photocatalytic-reactor efficiencies and simplified expressions to assess their relevance in kinetic experiments. *Chemical Engineering Journal* **2012,** *207-208*, 607-615.
5. Mehrotra, K.; Yablonsky, G. S.; Ray, A. K., Kinetic Studies of Photocatalytic Degradation in a TiO_2 Slurry System: Distinguishing Working Regimes and Determining Rate Dependences. *Ind. Eng. Chem. Res.* **2003,** *42* (11), 2273-2281.
6. Carrier, M.; Perol, N.; Herrmann, J.-M.; Bordes, C.; Horikoshi, S.; Paisse, J. O.; Baudot, R.; Guillard, C., Kinetics and reactional pathway of Imazapyr photocatalytic degradation Influence of pH and metallic ions. *Applied Catalysis B: Environmental* **2006,** *65* (1), 11-20.
7. Kudlek, E.; Dudziak, M.; Bohdziewicz, J., Influence of Inorganic Ions and Organic Substances on the Degradation of Pharmaceutical Compound in Water Matrix. *Water* **2016,** *8* (11).

SAMENVATTING

Fotokatalysatoren gebruiken, anders dan conventionele katalysatoren, licht om een reactie te activeren. Door het absorberen van fotonen raken elektronen geëxciteerd en bereiken ze hogere energietoestanden om een redoxreactie te starten. Dit principe kan gebruikt worden om chemicaliën te produceren zoals waterstof via de reductie van water of om koolstofdioxide om te zetten naar brandstoffen, zoals methaan, methanol en formaldehyde. Naast productie van chemicaliën kan de reductieve/ oxidatieve potentiaal van de geëxciteerde elektronen/gaten gebruikt worden om moleculen af te breken. Dit is vooral handig voor zelfreinigende materialen of het verwijderen van organische moleculen, zoals kleurstoffen, pesticiden of farmaceutica uit afvalwaterstromen. Dit is nuttig omdat toenemende watervervuiling steeds meer de menselijke gezondheid schaadt, met name in ontwikkelingslanden. Ondanks het grote potentieel en uitgebreid onderzoek gedurende de laatste decennia, is de ontwikkeling van goedkope en efficiënte fotokatalysatoren en goed inzicht in van het mechanisme van fotokatalytische degradatie nog steeds niet in zicht; dit zit de vertaling van het laboratorium naar de applicatie in de weg. TiO_2 (P25) is een goedkoop en niet-giftig fotoactief materiaal, maar te inefficiënt voor waterreiniging. Dit proefschrift zal zich focussen op de modificatie van TiO_2 (P25) en op de evaluatie van de fotokatalytische mechanismen. Atoomlaagdepositie (ALD) geeft ons de mogelijkheid om de depositie van vele verschillende materialen exact te kunnen besturen op atomaire schaal, een voordeel dat het ontwerp en de activiteit van de fotokatalysator kan verbeteren.

Ondanks de geavanceerde ontwikkeling van Pt:TiO_2(P25) als een fotokatalysator is het mechanisme van fotokatalytische degradatie nog steeds niet volledig opgehelderd. De deconvolutie van katalytische effecten is cruciaal voor de analyse en evaluatie van het fotokatalyse mechanisme om de mogelijke nadelen te identificeren en deze kennis te gebruiken om katalytische materialen te verbeteren. In Hoofdstuk 2 worden de dominante katalytische parameters een voor een geanalyseerd om de rol van Pt clusters op Pt:TiO_2(P25)-nanodeelties op te helderen voor de degradatie van organische kleurstofmoleculen. Het is ons gelukt om de verbeterde adsorptie van opgelost O_2 op Pt clusters op TiO_2 (P25)-deeltjes te bewijzen, resulterend in verbetering van de fotokatalytische degradatie van organische kleurstofmoleculen. Pt:TiO_2(P25) functioneerde slechter als fotokatalysator in een inerte atmosfeer als gevolg van lading recombinatie en een gebrek aan O_2, wat het belang van correcte werkomstandigheden voor bepaalde katalytische materialen aantoont.

Het gebruiken van metaaloxiden in plaats van edelmetalen in fotokatalysatoren zou de kosten significant kunnen verminderen. De depositie van Cu_2O op TiO_2 (P25), als een goedkoper alternatief voor edelmetalen zoals Pt, kan resulteren in een verbeterde ladingsscheiding door gunstige energiebandposities van Cu_2O in vergelijking tot TiO_2. Het is ons gelukt om Cu_2O nanoclusters te deponeren op het oppervlak van TiO_2 (P25) deeltjes door ALD in een gefluïdiseerd bed te gebruiken (Hoofdstuk 3). Dankzij de zelflimiterende ALD-reacties konden we de hoeveelheid Cu_2O clusters op het oppervlak controleren. Een zeer lage hoeveelheid Cu_2O op TiO_2(P25) (0.4 wt % Cu) vertoonde een dubbele fotokatalytische activiteit voor de degradatie van verschillende kleurstofmoleculen vergeleken met puur P25.

Een nog goedkoper en stabieler materiaal is SiO_2. Ondanks de inactiviteit van SiO_2 voor fotokatalytische reacties, zorgde een ultradunne coating van SiO_2 op P25 voor een toename aan fotokatalytische activiteit van 100% (Hoofstuk 4). Door de exacte dikte van de SiO_2 coating te controleren is het ons gelukt om de fotokatalytische activiteit aan te passen van versterking (<1.2 nm) tot onderdrukking (>1.2 nm) met een optimale activiteit voor een coatingdikte van 0.7 nm. De oorsprong van de katalytische verbetering van SiO_2:TiO_2(P25) deeltjes is getest door twee tegengesteld geladen kleurstofmoleculen te gebruiken om het effect van adsorptie op de fotokatalytische verbetering te onderzoeken. Scavengers onthulden een verandering in het degradatiepad van directe oxidatie (P25) naar hydroxil-radicaal-gebaseerde degradatie als resultaat van de meer zure OH-groepen aan het SiO_2 oppervlak. Dit leidt tot minder selectieve degradatie van meerdere verontreinigingen, wat met name handig is voor de simultane degradatie van meerdere verontreinigingen (Hoofdstuk 5).

Door de verkregen inzichten van Hoofdstuk 2 en 5 te gebruiken hebben we een nieuw fotokatalysator ontwikkeld door een materiaal te synthetiseren met een dun laagje SiO_2 op TiO_2 (P25), gevolgd door de depositie van Pt-clusters met de intentie om de voordelen van beide gedeponeerde materialen in een enkel materiaal te combineren. Pt:SiO_2:TiO_2(P25) toonde een verdere verbetering in de activiteit van de fotokatalytische degradatie van Acid Blue 9 (6x beter dan P25), waarbij de optimale belading van SiO_2 en Pt op P25 op het gecombineerde materiaal vergelijkbaar zijn met de enkelvoudig aangepaste materialen SiO_2:P25 en Pt:P25 (Hoofdstuk 6). Dit toont aan dat de combinatie van meerdere materialen de deur opent naar verdere katalytische verbeteringen door het gebruik van ALD.

Als een alternatief voor Pt kunnen Au-deeltjes voordelige eigenschappen hebben als co-katalysatoren voor de fotokatalytische degradatie van organische verontreinigingen. Wij hebben als eersten in een gefluïdiseerd-bed-ALD-reactor Au-clusters gedeponeerd op TiO_2(P25)-nanodeeltjes bij atmosferische druk (Hoofdstuk 7). Los van zelflimiterend gedrag konden we grootte van de Au-clusters manipuleren door de duur van de oxidator-puls aan te passen. Dit is vooral interessant aangezien het de mogelijkheid geeft om cluster-groottes te varieren terwijl de Au lading constant blijft. De fotokatalytische activiteit voor verschillende Au-cluster-groottes varieerde, wat het belang van controleerbaarheid van zowel lading als ook cluster grootte voor katalytische toepassingen benadrukt.

Atoomlaagdepositie in een gefluïdiseerd bed biedt dus uitstekende controle over oppervlaktemodificaties om de fotokatalytische activiteit van TiO_2(P25)-nanodeeltjes te verbeteren. Dit proefschrift beschrijft verschillende benaderingen om de fotokatalytische activiteit te verhogen zoals de verbetering van de reactantadsorptie voor Pt:P25 (Hoofdstuk 2), de verbetering van de ladingsverdeling voor Cu_2O:P25 (Hoofdstuk 3), en de verbetering van de oppervlakte-reactiviteit voor SiO_2:P25 (Hoofdstuk 4). Verder tonen de resultaten aan dat ALD een zeer veelzijdige techniek is om multicomponent fotokatalysatoren te synthetiseren om zo de fotokatalytische eigenschappen te kunnen afstemmen en de materialen te verbeteren voor toekomstige implementatie.

SUMMARY

Photocatalysts, contrary to conventional catalysts, utilize light to drive a reaction. By absorption of photons, electrons are excited and reach higher states to initiate a redox reaction. This principle can be broadly used to produce chemicals such as hydrogen via the reduction of water or transform carbon dioxide into solar fuels, i.e., methane, methanol, and formaldehyde. Besides chemical production, the reductive/oxidative potential of the excited electrons/holes can be utilized to degrade molecules. This is especially useful for self-cleaning materials or for cleaning waste water streams from molecules such as dyes, pesticides, or pharmaceuticals, as water pollution levels increasingly harm human health, especially in developing countries. Despite the great potential and vast research activities over the last decades, the development of cheap and efficient photocatalysts and especially the evaluation of the mechanism of photocatalytic degradation pathways are still lacking, which hampers the translation from lab to application. TiO_2 (P25) is a cheap and non-toxic photoactive material, yet too inefficient for water cleaning. This thesis focuses on the surface modification of TiO_2 (P25), minimizing various drawbacks of TiO_2 (P25) and on the evaluation of the photocatalytic mechanisms. Atomic layer deposition (ALD) allows us to precisely control the deposition of many different materials at the atomic level, an advantage that could improve the photocatalyst design and optimize the activity.

Despite the mature development of Pt:TiO_2(P25) as a photocatalyst, the mechanism for photocatalytic pollutant degradation is still under discussion. The deconvolution of catalytic effects is crucial for the analysis and evaluation of the photocatalysis mechanism in order to identify drawbacks and use this knowledge to improve catalytic materials. In Chapter 2, the dominant catalytic parameters are evaluated separately to clarify the role of Pt clusters on TiO_2(P25) nanoparticles for the degradation of organic dye molecules. We were able to prove the beneficial role of dissolved O_2 on Pt clusters on P25 particles resulting in the photocatalytic improvement on the degradation of organic dye molecules. Pt:TiO_2(P25) performed worse as a photocatalyst in an inert atmosphere as a consequence of the charge recombination and a lack of O_2, which demonstrates the importance of the correct working environments for certain catalyst materials.

Moving away from photocatalysts containing noble metals to metal oxides would significantly decrease the cost. The deposition of Cu_2O on TiO_2 (P25), as a cheaper alternative to noble metals such as Pt, may result in an enhanced charge separation due to the aligned band positions of Cu_2O compared to TiO_2. We were able to deposit Cu_2O nanoclusters on the surface of TiO_2 (P25) particles using ALD in a fluidized bed (Chapter 3). The self-limiting ALD characteristic allowed us to precisely control the loading of the Cu_2O clusters on the surface. Very low loaded Cu_2O:TiO_2(P25) (0.4 wt % Cu) demonstrated a double photocatalytic activity for the degradation of several dye molecules compared to bare P25.

An even cheaper and more stable material is SiO_2. Despite the catalytic inertness of SiO_2 for photocatalytic reactions, an ultrathin overcoating of SiO_2 layers over P25 increased the photocatalytic activity by 100 % (Chapter 4). By precisely controlling the thickness of the SiO_2 coating, we were able to tune the photocatalytic activity from enhancement (<1.2 nm) to suppression (>1.2 nm) with an optimum activity at a coating thickness of 0.7 nm. Evaluating the origin of the catalytic improvement SiO_2:TiO_2(P25) particles were tested using two differently charged dye molecules to investigate the effect of adsorption on the photocatalytic improvement. Scavenging agents revealed a change of the degradation pathway from direct oxidation (P25) to hydroxyl radical based degradation as a result of the more acidic surface OH groups on the SiO_2 surface. This leads to less selective degradation of multiple pollutants, which is especially useful for the simultaneous degradation of multiple pollutants (Chapter 5).

Using the insights gained in Chapters 2, 4, and 5, we designed a new catalyst material by building up a material with a thin layer of SiO_2 on TiO_2(P25), followed by the deposition of Pt clusters to use both materials' advantages in a single material. Pt:SiO_2:P25 exhibited a further improvement in the activity for the degradation of Acid Blue 9 (6x better than P25), where the optimal loading ranges of SiO_2 and Pt on P25 in the combined material are similar to the mono-modified materials SiO_2:P25 and Pt:P25 (Chapter 6). This demonstrates that the combination of multiple materials opens the door to further catalyst improvement using ALD.

As an alternative to Pt, gold particles may have advantageous properties as cocatalysts for the degradation of organic pollutants. For the first time in a fluidized bed ALD reactor, we deposited gold clusters on TiO_2 (P25) nanoparticles at atmospheric pressure (Chapter 7). Apart from self-limiting behavior, we could control the gold cluster size by modifying the pulse duration of the oxidizer pulse. This is especially interesting since it provides the opportunity to vary cluster size while keeping the Au loading constant. Moreover, the photocatalytic activity varied for different Au cluster sizes, which stresses the importance of controllability over both loading and cluster size for catalytic applications.

It can be concluded that atomic layer deposition in a fluidized bed provides excellent control over surface modifications to improve the photocatalytic activity of TiO_2 (P25) nanoparticles. This thesis demonstrates different approaches to improve the photocatalytic activity such as improving reactant adsorption for Pt:P25 (Chapter 2), improving the charge separation for Cu_2O:P25 (Chapter 3), and improving the surface reactivity for SiO_2:P25 (Chapter 4). Moreover, the results demonstrate that ALD is a very versatile tool to built up multicomponent photocatalysts to further tune and improve the photocatalytic properties in a material needed for future implementation.

ACKNOWLEDGMENTS

Writing this part of my thesis means that I have reached the end of a major chapter in my career. This book should prove that I reached a state where I can defend my work during the last four years and the achievements I accomplished in this process. However, without the contributions of so many different people, specifically my supervisors, collaborators, friends, and family, this book would be just an exotic thought of a young fellow from a small village in the middle of Bavaria. Therefore, I would like to take this opportunity here to express my sincerest gratitude to the people who supported and followed me throughout this journey.

I want to start thanking the person who had a big contribution to me actually coming to Delft and choosing the path of the PhD. Julien, your guidance and supervision during my BSc thesis and MSc thesis inspired me and enormously helped me to develop as a scientist. Your positive attitude and commitment towards students made my time in your group in Erlangen a great pleasure both from a personal and scientific point of view. Your enjoyment of helping and guiding me during my time in Erlangen by a situation where I dropped by your office late afternoon for a short question which turned into a personal two hour lecture about electrochemistry until you remembered that you should finish a proposal due at midnight. I always enjoyed coming back to Erlangen for a visit and observe how great your group is developing. I am delighted that you agreed to be part of my defence committee so that you not only pathed me the way to explore new frontiers here in Delft but also (hopefully) the successful defence of my PhD thesis.

Ruud, thank you for giving me this opportunity to follow the way of a PhD candidate and guiding me until the end. It was a great journey where I learned a lot about executing research independently, and I am very grateful for the opportunities you gave me. I appreciate that you had always an open door for me so I could be sure that in case I need help you will be there to help me overcome the obstacle. Besides the work environment, I appreciate your competitiveness in various fun occasions during our group activities (e.g. karting or the eggrun). Competing against you gave a nice flavour to the whole PhD experience, even though in case of a loss I would need to listen to that story for some time - but that makes the next win even sweeter.

Hao, I would like to thank you for guiding me through the first and final stage of my PhD, and I would like to express my sincere gratitude for giving me the opportunity for a research stay at Phenikaa University in Vietnam. It was one of the highlights during my time as a PhD candidate to experience a completely different environment. Your welcoming attitude and helping hand from booking a taxi to showing me the typical Vietnamese cuisine and finding me local travel guides made my stay an unforgettable experience.

Bert, even though you joined as a supervisor past the halfway mark I can consider your contribution one of the largest. You helped me to look even more critically at my results

and challenged me in situations where I thought I considered it all. Your direct feedback and very valuable comments significantly raised the quality of this thesis.

Michiel, you helped me very much to broaden my horizon in how to execute research. Despite the limited interactions we have had, your feedback was always on point and helped me to look at my results from a different angle. Thank you for hosting the Christmas dinner and summer BBQ, it was always great fun to bring the group together outside of the department walls.

I would also like to thank Prof. Sammy Verbruggen, Prof. Luuk Rietveld and Prof. Bernard Dam for taking the time to evaluate my doctoral thesis and being part of the defence committee and appreciate your feedback to make this thesis stronger.

Besides the scientific part without the help of secretaries in and outside of PPE writing this thesis would have taken quite a bit longer. Elly, Jennifer, and Leslie thanks a lot for taking care of any organizational part of my PhD journey and providing valuable advice in various situations. Caroline, thank you for taking care of sending my samples around the globe and making sure they arrive safely. Karin and Astrid, thank you for making my life easy in booking progress meetings Michiel or numerous signature requests.

Mojgan, you kept the lab running and your calm and caring attitude was infectious. Especially after these days were nothing seemed to work and all experiments (and setups) failed your helping hands made sure we could proceed with success. Aris, your “short” intermezzo at PPE brought the level of lab organization to a new level. Your drive to help people wherever you can and your experience in the ALD world made not only every discussion very fruitful but also super enjoyable. Stefan, whenever it came to a homebuilt part you were the person to get in touch with. Your skills were essential to keep our dear ALD systems operational and updated. Thank you for that. Kristen, thanks for letting me “steal” components from your biolab to keep my experiments going without a delay. Bart, Liliana and Willy, without your skills and knowledge in the field of catalysis engineering I would have struggled way more to get the results I can now present in this thesis. Thank you for letting me expand in your lab and being so helpful in executing experiments and troubleshooting the equipment. Ruben, thank you for your help in the UV/Vis measurements and Armand for introducing me to the experimental opportunities in the Waterlab. Bart, I will remember you always being the firefighter for any Labview issues of our ALD systems. The issues we ran into were numerous and what impressed me was your positive approach to the problems and your continuous will to fix the issues we were presenting to you. Additionally, thanks for making sure that the XPS was up and running as much as possible and therefore providing a smooth operation. Wiel, I can’t recall the number of times I was stuck at the TEM machine/software. Nevertheless, you were always available and provided a speedy solution so I could continue without much delay. Thank you!

Pouyan and Volkert, despite our interaction was mainly based on the journal club, you helped me getting out of my comfort zone to explore new fields of science and discuss

the outcome in vibrant discussions. Gabrie, it is great to see how you interact with the people around you, always trying to find solutions which fit both sides. I really want to thank you your input on my future development both scientifically and personally. Henk, thank you for being part of my supervisory team in the beginning of my PhD. Even though our interaction was unfortunately short – I hope you enjoy your retirement to the fullest – you had a great influence on the development of me and my project in the early stage.

During my time as a PhD student I got the opportunity to collaborate with many different people, who certainly had a big impact on the outcome of this thesis. Thanks to the group of Prof. Rik van Deun at the University of Ghent for hosting me so willingly for the photoluminescence measurements. Prof. Jorg Thöming, thanks for hosting me in your research group in Bremen to learn about DLS measurements, and Jan, I really appreciate your patience and helpfulness in measuring my samples. Ina, thank you for helping me out on the FTIR measurements and your patience in answering all my questions about the possibilities in characterization methods in catalysis engineering. Kevin, your dedication towards collaboration was a blessing for me. Thank you for being so eager and helpful with the TRMC measurements and always having an open door to discuss with me the results.

The supervision of numerous students was always a pleasure for me. Thank you, Alain, Francesco, Jonathan, Mohammed, Mourijn, Egem, Floris, Roel, Sophie, Vanessa, Ankit, and Dylan. I really enjoyed working together with all of you to try to solve the problems we were facing during this research together. I greatly appreciate the work you put in to make this research successful. It was always a pleasure to discuss the results with you, and I was impressed about the different points of views you brought into this project. I wish you all the best for your future and it would be great if I could read some research work from you in the future.

I would like to thank everyone in the Delft Global Initiative. When I heard the first time the plans you had about bringing research to people in need, it really triggered me. It was one of the main reasons to apply to the project about water treatment. The working culture and the pure dedication to make things possible in an area often overlooked was a genuinely inspiring experience. It was great to see how you pushed forward the needs of people who are not as privileged as we are. I am honoured to have been part of that very active community and to see other projects flourish to have a real impact on society. Jennifer and Claire, thank you for putting this program together and allow me to be part of that. Friso and Sophie, thanks for the great lunches and high quality lunch talks which helped me to broaden my horizon and experience many different angles of how we as a society can tackle the severe problems occurring and arising in different parts of the world. But most importantly, I would like to thank all my Delft Global fellows – Anteneh, Camille, Christine, Hendrik, Henry, Juan Carlo, Juan, Merel, Michel, Mona, Nishant, Petra, Pieter, Rachel, Roos, Saqr, Tope, Yask, Mitasha. It took us a while in the beginning to understand what Delft Global Fellow actually means, but we certainly knew from the start that it was something special and we were all proud

to be in there. It was really great to talk and listen to your very diverse research, sharing experiences being jealous of each other's research trips and learning from both defeat and success in the individual research. Keep up the great work you are doing, and I am very much looking forward to the outcome and wish you the best of luck and success in making the world a better place with your research.

Andris and Aswin, I could not have asked for better paranymphs for my doctoral defence, even though the corona crisis might take away this honour. Andris, it was such a great honour to share the Ultimate field with you both at Force Elektro and the National Team, share shelter, then a proper accommodation and so many great experiences and memories around my frisbee career. With you around, I was sure to accomplish great things and to push greater heights outside academia. Your combination of competitiveness and fun gave a great mixture for suffering with fun both on and off the field. The fact that we could discuss for literally hours whether acting or reacting is easier for people and still come to an agreement at 3 am shows how our strong personalities fit so well together. Thank you for sharing the successes with me but especially in defeat for lifting me up and providing with valuable advice. Aswin, there was a time ini the beginning where I thought it would be difficult find a good connection. I am very glad that I was so wrong about my judgement. Having you as an office mate was key to for me to survive the challenging days in the office always being available for a ranting session to release pressure and focus back on the good things. I know I can trust you in making fun both with and of me in good times but, more importantly offer your help in difficult situations. Your wisdom and calmness contributed so much to me standing here to be able to defend my PhD work.

Shaurya, for no person I would like to exchange you as an office mate. Experiencing your enlightenment was such a great experience and helped me so much to look at things from different angles. The fun we created in our office was just on a higher level. I truly think that we both defined new physical laws by being able to pull each other out of the same pit sometimes being stuck in. Me carrying you through the survival run was just a small payback for the carrying you did for me during our time in the office. Maulik, your calm and considerate way of dealing with things impressed me a lot. Seeing you in situations where others would certainly have broken carried me where situations got tight. It was a pleasure to return this favour at the survival run. Kartik, I admired your perseverance in how you approached your PhD project. It was fun to see how you prepared yourself with your spicey food for the challenges of the PhD journey. Damiano, I think I got the best compliment I can receive from an Italian by officially announcing that my homemade pizza is eatable. It was always fun to discuss with you why pineapple on a pizza is a crime, but Nutella is fine on the other hand. I admire your work attitude digging deep into topics not only related to your research but also starting your own investigation on various topics such corona crisis and providing always very valuable information. Samir, your fun attitude was the reviving force in PPE. It was always fun to have you around because there was a certainty that any bad mood was gone in no time. Thanks, Isabell, Zaid and Georg for bringing new spirit into PPE and initiating the restart of Friday drinks to keep a social touch. Ruben, thanks for accepting

my push up challenges and competing with you for the top on the whiteboard and for your help to translate my thesis summary into Dutch. Dayinta, Durgesh, Andrea, David, Fabio, Melvin, thank you for your advice and make me feel at home in the early stage with all the borrels. I also would like to thank all other current and former group members of PPE for being part of my journey here at TU Delft and filled it with memories I will never forget: Alvaro, Yujie, Jing, Fuweng, Feilong, Josette, Erik, Hamid, Saeed, Abtin, Serhii, Afshin, Alessandro, Qian.

Sid and Manas, you brought PPE and TP closer together by seeking those cross-group activities, organizing borrels, and introducing me to Bollywood movie culture. Sid, thanks for being founding father of the “one last drink” at Doerak. Your passion for art impressed me a lot which was a nice change to the pragmatic PhD research. Robert, having you as a German fellow in the office next door was so refreshing. Thanks for your numerous help in the CE lab and it was always fun to trash talk with you to keep the mood up.

I recommend everybody during a PhD to diversify to other areas to accomplish things in a different environment, since it is unavoidable to face stressful, challenging, and disappointing situations. For me playing Ultimate Frisbee with Force Elektro was the ground to recharge, enjoy the sport I love and share the emotions during wins and losses, training in hail and sunshine and working out together. Ravi, Richard, Stidge and Andris it was so great to see how you initiated the reanimation of Force Elektro’s competitiveness. You built the foundation for the future success and I learned a lot as a coach and player from you. Ravi and Ingeborg, I don’t know what I would have done without you, giving me shelter in your house. There are no words to express my appreciation. Hosting movie nights, game nights and just discussing about our most favourite topic – Ultimate Frisbee – was such a help to free my head and refocus. Because of you guys I got the chance for so many new experiences, going to Windmill Windup and play Ultimate Frisbee on a high level. Richard, your passion for Ultimate Frisbee is just unreal. Besides being injured, you completely committed to the club, kept investing time in making people better and showed me not to give up in difficult times. Stidge, your fun competitive attitude such a unique approach I was blessed having experienced. Sharing the field with you was always the pure enjoyment and coaching together helped me develop more different approaches to coaching and leading a team.

The most memorable day in this period was that one day in June 2019 where Force Elektro became Dutch champion for the first time in the club history. I am not going to lie, as we all know the path was far from easy and we almost took a very wrong exit on the way. Nevertheless, we managed to grow together as a team and we showed what team spirit and determination could lead to: Dutch Ultimate Frisbee Champion 2019, Force Elektro. Thank you for sharing this great experience with me: Bert, Camilo, Dani, Georg, Guido, Jasper, Jos, Klaas, Lennart, Leo, Martijn, Max, Mika, Nathan, Patrick, Wouter. Thank you for trusting in me as your coach. I can tell this year I learned the most and it was an honour to be part of that team which defined itself by great team

spirit. FORCE ELEK---TROOOO!!! Thank you to all other Force Elektro members I had the chance to meet during my time in Delft! It was an amazing experience sharing a big part of my time with you!

Viki, thank you for being such an awesome listener. It always a great relief to talk to you about the challenges in- and outside the PhD life. I appreciate all the times you managed to visit, and I feel sorry not having been able to return that favour, yet. Tim and Tomasz, what adventures we have managed to experience. Thanks for the several kitesurfing sessions, the trip to the Sahara and the hike in Iceland with you guys was one of the best hikes in my life. I am certainly looking forward to other adventure trips with you to come. Benjamin, I admire your passion for both science and sports, very much similar how I try to make it the last four years. Thanks for teaching me a bit of biology in our collaboration, I really enjoyed working together with you. I hope we can catch up again for some tennis matches since it was a lot of fun despite me loosing most of the times. Karo, having you as a roommate was such a great time. Your kindness exceeds any scale, so much that it sometimes makes me wonder how a person can possibly that kind.

Claudi, Anne, Chrisi und Lukas, vielen Dank für die unzähligen Skype Sessions. Es war immer erfrischend mit euch in alten Erinnerungen unserer gemeinsamen Zeit in Erlangen zu schwelgen. Sebastian, vielen Dank für die Gastfreundschaft bei meinen Besuchen in Erlangen. Es ist immer wieder schön, an die alte Wirkungsstätte zurückkehren zu können und so herzlich willkommen geheißen zu werden.

Florian und Markus, unsere gemeinsamen Unternehmungen gaben mir immer ein Gefühl des nach Hausekommens. Vielen Dank für die gemeinsamen Bergtouren, Skiurlaube und Spielerunden. Aber am dankbarsten bin ich dafür, dass ich mich auf euch immer verlassen kann und in schwierigen Zeiten wir als Brüder immer zusammenhalten können.

Liebe Mama, lieber Papa, das Beste kommt zum Schluss. Worte zu finden, welchen Verdienst ihr an diesem Erfolg habt, ist fast unmöglich. Ich will es trotzdem versuchen: Oft gratuliert ihr mir für meine Errungenschaften, die ich unabhängig und ohne viel Hilfe erreicht hätte. Ihr habt selten Unrecht, aber in der Hinsicht muss ich euch energisch widersprechen. Alles was ich bis jetzt erreichen konnte, war nur mit eurer Hilfe möglich. Für die Unterstützung, die ich von euch erfahren durfte, über all die Jahre hinweg, in der Schule, and der Universität und während meiner Promotion bin ich euch auf ewig dankbar. Ihr habt immer versucht, mir alle Dinge zu ermöglichen und mir Arbeiten abzunehmen, damit ich mich besser auf die Schule/Uni/Promotion konzentrieren konnte und das ausüben konnte was mir Spaß macht. Ohne eure Hingabe und Unterstützung wäre es mir unmöglich gewesen, so weit in meiner akademischen Laufbahn zu kommen, die jetzt mit dem Doktortitel gekrönt werden wird. Vielen lieben Dank! Ich bin unendlich dankbar und stolz, euch als Eltern zu haben.

thank you vielen Dank dank u paldies

merci ευχαριστώ धन्यवाद grazie

നന്ദി متشكرم dziękuję Ci gracias

teşekkür ederim cảm ơn bạn 谢谢

спасибі

CURRICULUM VITAE

Dominik Benz was born on June 26, 1990 in Roth, Germany. He finished primary education in Obermaessing followed by completing high school in Hilpoltstein in 2010 where he started developing his interests in chemistry choosing this subject as part of his general higher education entrance qualification (Abitur). After serving his civil service in the army base Bogen, he committed 2011 to study Molecular Science at the Friedrich-Alexander University Erlangen-Nuremberg. He completed his BSc program in 2013 focusing on synthetic chemistry for water splitting catalysts and obtained his MSc degree in 2015. During his MSc studies, he was granted an exchange scholarship at the University of Wollongong, Australia, broadening his knowledge on polymer chemistry in the working group of Prof. Dr. Marc in het Panhuis. As his MSc thesis project, he choose to work on buffer layers for thin film solar cells by atomic layer deposition under the guidance of Prof. Dr. Julien Bachmann. In 2016 Dominik joined Prof. Dr. Ruud van Ommen's group in Chemical Engineering at Delft University of Technology to pursue his PhD degree. In the framework of Delft Global Initiative, he was working on the catalyst development by atomic layer deposition for cleaning water using sunlight. During his PhD studies he had the chance for a short research stay at Phenikaa University, Hanoi, Vietnam, to experience first-hand the severe water pollution in surface water.

Dominik took actively part in the Ultimate Frisbee community in Delft and in The Netherlands. Under his guidance as coach of the 1st men team Force Elektro became Dutch National Champion 2019 for the first time in club history. Additionally, he competed with the Dutch National team at the European Ultimate Championships in Gyor, Hungary in 2019.

OUTREACH

Journal papers

1. **Benz, D**.; Felter, K. M.; Köser, J.; Thöming, J.; Mul, G.; Grozema, F. C.; Hintzen, H. T.; Kreutzer, M. T.; van Ommen, J. R., Assessing the Role of Pt Clusters on TiO2 (P25) on the Photocatalytic Degradation of Acid Blue 9 and Rhodamine B. *The Journal of Physical Chemistry C* **2020,** *124* (15), 8269-8278.

2. Guo, J.; **Benz, D.**; Doan Nguyen, T.-T.; Nguyen, P.-H.; Thi Le, T.-L.; La Zara, D.; Liang, B.; Hintzen, H. T.; van Ommen, J. R.; Bui, H. V., Tuning the Photocatalytic Activity of TiO_2 Nanoparticles by Ultrathin SiO2 Films Grown by Low-Temperature Atmospheric Pressure Atomic Layer Deposition. *Applied Surface Science* **2020,** *530*, 147244.

3. **Benz, D.**; Van Bui, H.; Hintzen, H.T.; Kreutzer, M.T.; van Ommen, J.R. Synthesis of a Rationally Designed Multi-Component Photocatalyst Pt:SiO_2:TiO_2(P25) with Improved Activity for Dye Degradation by Atomic Layer Deposition. *Nanomaterials* **2020**, *10*, 1496.

4. **Benz D.**, Nguyen Y-Nhi T., Le Thanh-Hiep T., Le Thanh-Lieu T., van Ommen, J. R.,Bui H. V., Atmospheric-pressure atomic layer deposition of ultralow-loading Cu_2O nanoclusters on TiO_2 nanoparticles for enhanced photocatalytic removal of organic pollutants *The Journal of Alloys and Compounds [Under review]*

5. **Benz, D.**; Bui, H. V.; Hintzen, H. T.; Kreutzer, M. T.; Van Ommen, J. R., Mechanistic insight into the improved photocatalytic degradation of dyes using TiO_2 (P25) nanoparticles with an ultrathin SiO_2 coating. *[in preparation]*.

6. Hashemi, F. S. M.; Grillo, F.; Ravikumar, V. R.; **Benz, D.**; Shekhar, A.; Griffiths, M. B. E.; Barry, S. T.; van Ommen, J. R., Thermal atomic layer deposition of gold nanoparticles: controlled growth and size selection for photocatalysis. *Nanoscale* **2020,** *12* (16), 9005-9013.

7. Martín-Sómer, M.; **Benz, D.**; van Ommen, J.R.; Marugán, J. Multitarget Evaluation of the Photocatalytic Activity of P25-SiO_2 Prepared by Atomic Layer Deposition. *Catalysts* **2020**, *10*, 450.

8. La Zara, D.; Bailey, M. R.; Hagedoorn, P.-L.; **Benz, D.**; Quayle, M. J.; Folestad, S.; van Ommen, J. R., Sub-nanoscale Surface Engineering of TiO_2 Nanoparticles by Molecular Layer Deposition of Poly(ethylene terephthalate) for Suppressing Photoactivity and Enhancing Dispersibility. *ACS Applied Nano Materials* **2020,** *3* (7), 6737-6748.

9. Lehner, B. A. E.; Janssen, V. A. E. C.; Spiesz, E. M.; **Benz, D.**; Brouns, S. J. J.; Meyer, A. S.; van der Zant, H. S. J., Creation of Conductive Graphene Materials by Bacterial Reduction Using Shewanella Oneidensis. *ChemistryOpen* **2019,** *8* (7), 888-895.

Presentations

DPTI event 2016, Rotterdam, The Netherlands (poster)

ICCE 2017, Erlangen, Germany (oral presentation)

Research Exhibition 2017, Delft, The Netherlands

DPTI 2018, Rotterdam, The Netherlands (poster, 2nd poster price)

HERALD Summit 2018, Braga, Portugal (poster)

CHAINS 2018, Veldhoven, The Netherlands (oral presentation)

NCCC 2019, Noordwijk, The Netherlands (oral presentation)

NPM-4 2019, Antwerp, Belgium (oral presentation)

ALD 2019, Seattle, USA (oral presentation)